Microcavity PDMS and Gold Substrates for Supported Lipid Bilayers

Sean Maher B.Sc.

Thesis Submitted for the Degree of Doctor of Philosophy

Supervisor:

Prof. Tia Keyes

School of Chemical Sciences **Feb 2016**

Declaration:

I hereby certify that this material, which I now submit for assessment on the programme of study leading to the award of PhD, is entirely my own work, that I have exercised reasonable care to ensure that the work is original, and does not to the best of my knowledge breach any law of copyright, and has not been taken from the work of others save and to the extent that such work has been cited and acknowledged within the text of my work.

Signed: _____

(Candidate) ID No.: _____

Date: _____

Contents

Declaration: ii
Abbreviations: vii
Acknowledgements: ix

Chapter 1
Literature Survey 1
2.2 Introduction 2
2.3 Components of the Cell Membrane 3
2.3.1 Lipids 3
2.3.2 Membrane Proteins 8
2.3.3 Transport Across the Cell Membranes 10
2.4 Model Lipid Bilayers 12
2.4.1 Lipid Vesicles: 13
2.4.2 Black Lipid Membranes: 14
2.4.3 Supported Lipid Membranes 15
2.4.4 Polymer cushioned lipid bilayers: 20
2.5 Background to Methods used for Fabrication and Characterisation of Supported Lipid Bilayer 26
2.5.1 Langmuir-Blodgett Trough: 26
2.5.2 Confocal Imaging Microscope 29
2.5.3 Fluorescence Correlation Spectroscopy 31
2.5.4 Electrochemical Impedance Spectroscopy 36
2.6 Conclusions 41

Chapter 2
Planar and Microcavity Supported Lipid Bilayerson PDMS Substrates. 42
2.1 Introduction 43
2.2 Experimental 47
2.2.1 Modification of Planar PDMS Surfaces 47
2.2.2 Fabrication of PDMS Substrates for Supported Lipid Bilayers 48
2.2.3 Formation of Phospholipid Bilayers on PDMS Substrates 51
2.2.4 Confocal Microscopy 53
2.2.5 Fluorescence Lifetime Correlation Spectroscopy 53
2.3 Results and Discussion 54

2.3.1 Contact Angle Measurements of Modified Planar PDMS Surface 55
2.3.2 Formation and Mobility of Supported Bilayers on Planar PDMS.....59
2.3.3 Spanning Phospholipid Bilayers on PDMS Micro Cavities 66
2.3.4 Diffusion Studies of Supported Bilayers on PDMS Micro Cavities....72
2.4 Conclusions 74

Chapter 3
Characterization of Suspended Lipid Bilayers on Gold Microcavity Substrates. 75
3.1 Introduction 76
3.2 Experimental 79
3.2.1 Fabrication of Gold Microcavity Substrates 79
3.2.2 Characterisation of Gold Microcavity Substrates by Cyclic Voltammetry 80
3.2.3 Formation of Suspended Lipid Bilayers on Gold Microcavity Substrates.....81
3.2.4 Fluorescence Lifetime Correlation Spectroscopy of Suspended Lipid Bilayers on Gold Microcavity Substrates 81
3.2.5 Incorporation of Ionophores into Microcavity Suspended Lipid Bilayers.....82
3.2.6 Electrochemical Impedance Spectroscopy 83
3.3 Results and Discussion 83
3.3.1 Characterization by Scanning Electron Microscopy.....83
3.3.2 Characterization of Gold Microcavities by Cyclic Voltammetry 86
3.3.3 Selective surface modification of the Arrays:.....89
3.3.4 Diffusional Studies of Suspended Lipid Bilayers on Gold Microcavity Substrates.....92
3.3.5 Characterisation of Suspended Lipid Bilayers by Electrochemical Impedance Spectroscopy. 97
3.3.6 Characterisation of Uniporter Ionophore in Suspended Lipid Bilayers by Electrochemical Impedance Spectroscopy 104
3.3.7 Incorporation of Antiporter, Nigericin, into a Microcavity Supported Lipid Bilayer 110
3.4 Conclusions 116

Chapter 4
A Strategy for Spatiotemporal control of reagent delivery to lipid bilayer. 118
4.1 Introduction 119
4.2 Experimental 122
4.2.1 Materials: 122
4.2.2 Modification of Gold Microcavities 122
4.2.3 Coupling of β-Cyclodextrin to Avidin. 123
4.2.4 Characterisation of Modified Gold Microcavity Substrates by Cyclic Voltammetry 124
4.2.5 Formation of Suspended Lipid Bilayers 125
4.2.6 Electrochemical Impedance Spectroscopy 125
4.3 Results and Discussion 125
4.4 Conclusions 147

Chapter 5
An Investigation into use of Photolithographically Prepared silicon moulds for highly reproducible templating of pore arrays. 149
5.1 Introduction: 150
5.2 Experimental: 153
5.2.1 Materials: 153
5.2.2 Moulding of PDMS using Tyndall Substrates: 154
5.2.3 Stretching of PDMS: 155
5.2.4 Formation of Spanning lipid bilayers over stretched substrates: 157
5.2.5 Scanning Electron Microscopy: 158
5.2.6 Fluorescence Imaging: 158
5.3 Results and Discussion: 158
5.3.1 Characterisation of PDMS Direct from Tyndall Substrates: 158
5.3.2 Fluorescence imaging of lipid bilayers on cavity substrates Direct From Tyndall Substrates 160
5.3.3 Moulds made by Stretching PDMS: 162
5.3.4 PDMS Formed from Epoxy Moulds: 166
2.6.1 169
5.3.5 Fluorescence imaging of lipid bilayers on stretched cavity substrates. 169
5.3.6 Effect of cavity shape on cavity filling: 171
5.4 Conclusion: 174

Chapter 6 Conclusion and Future Work 175
6.1 Conclusion: 176
6.2 Further work 180
6.3 References: 184

Abbreviations:

AC	Alternating Current.
ACF	Auto Correlation Function.
APTES	3-Aminopropyltriethoxysilane.
β-CD	β-Cyclodextrin.
BLM	Black Lipid Membrane.
C	Capacitance.
CA	Contact Angle.
CPE	Constant Phase Element.
CV	Cyclic Voltammetry.
D_L	Lateral Diffusion.
DMPC	1,2-dimyristoyl-*sn*-glycero-3-phosphocholine.
DOPC	1,2-dioleoyl-*sn*-glycero-3-phosphocholine.
DOPE	1,2-dioleoyl-*sn*-glycero-3-phosphoethanolamine.
DOPS	1,2-dioleoyl-sn-glycero-3-phospho-L-serine.
EIS	Electrochemical Impedance Spectroscopy.
Fc	Ferrocene.
FCS	Fluorescence Correlation Spectroscopy.
FLCS	Fluorescence Lifetime Correlation Spectroscopy.
GUV	Giant Unilamular Vesicle
LB	Langmuir-Blodgett.
L_o	Liquid Ordered Phase.
ME	Mercaptoethanol.
MSLB	Microcavity Suspended Lipid Bilayer.
MUV	Multilamellar Vesicles.

PC	Phosphocholine.
PDMS	Polydimethoxysilane.
PEG	Polyethylene Glycol.
PS	Polystyrene Spheres.
R	Resistance.
SA	Streptavidin.
SEM	Scanning Electron Microscope.
SLB	Supported Lipid Bilayer.
SUV	Small Unilamular Vesicle.
t-BLM	Tethered Bilayer Membrane
Z	Total Impedance.
Ω	Ohm.

Acknowledgements:

First and foremost, I'd like to thank Prof. Tia Keyes for her constant support, guidance and encouragement throughout the last few years. I would also like to thank the technical staff of the chemistry department in DCU, who were always there to provide assistance when needed. I would also like to thank Prof. Robert Forster for his assistance and advice on the electrochemistry in this work.

I would like to thank all the members of my research group, past and present, who were always there to help. A special thanks to the postdocs Hajra and Siva who passed on their essential knowledge and experience. I would also like to thank Nabil Mellouky for is assistance in the work presented in chapter 5.

A huge thank you to all my postgraduate friends in DCU especially Brian, Nicky and Leeanne, thank you for all the support and all the good times.

I would like to thank my family for all their support throughout my PhD and my many years in college. Finally I would like to thank my partner Greg for all his support during the final stages of this PhD.

List of Publications and Presentations:

Publications:

- H. Basit, S. Maher, V. Gaul, R.J. Forster, T.E Keyes, *Aqueous-filled polymer microcavity arrays: versatile and stable lipid bilayer platforms offering high lateral mobility to incorporated membrane proteins*, Analyst, 140, 3012-3018.
- S. Maher, H. Basit, R.J. Forster, T.E Keyes, *Micro Cavity Spanning Supported Lipid Bilayers for the Electrochemical Investigation of Ionophore Activity.* In Draft
- S. Maher, H. Basit, R.J. Forster, T.E. Keyes, *Micro Cavity Spanning Supported Lipid Bilayers for the Electrochemical Investigation of Ionophore Activity.* In Draft

Poster Presentations:

- Measuring the Diffusion of Support Lipid Bilayer Films on PDMS**,** Smart Surfaces 2012, Dublin, Ireland, March 2012.
- PDMS Substrates for Support Lipid Bilayer Films, Biophotonics and Imaging Graduate Summer School, Galway, June 2012
- Optimising the Surface Chemistry of PDMS to Support Lipid Bilayer Films, BioPhotonics and Imaging Conference, June 2013.

Abstract:

Microcavity PDMS and Gold Substrates for Supported Lipid Bilayers

Sean Maher BSc

Cell membranes surround all living cells and are comprised of a complex matrix of phospholipids and proteins. The proteins embedded in or bound to the exterior of the membrane are responsible for a wide range of processes, for example cell signalling, and transport of material in and out of the cell. Understanding how transmembrane proteins behave within the lipid membrane system will allow for a better understanding of molecular mechanisms of diseases as well as the development more targeted therapeutics. However, due to the complex nature of the cell membrane environment, it is difficult to selectively study single protein species within the whole cell system. This has driven the development of model membrane systems, which allow for the sub-division of these complex systems into simpler forms and allow for the study of individual membrane proteins. Solid supported lipid bilayers have been widely used as model systems, however they have multiple limitations, the most important being the influence of the underlying substrate on the bilayer. This can impede lipid fluidity and is particularly detrimental to mobility of reconstituted proteins as substrate-protein interactions can impede motion and even cause protein to denature.

This thesis attempts to address this by developing substrates for studying membrane proteins in a biomimetic environment where such interactions are minimized. The initial substrates, designed for optical measurements, comprise of a microcavity array substrate formed in Polydimethylsiloxane (PDMS). A method for spanning bilayers over these PDMS microcavity arrays was developed and lipid diffusion dynamics over the cavities was assessed using Fluorescence Lifetime Correlation Spectroscopy (FLCS). Importantly, diffusion coefficients for lipids over these cavities are 2 to 3 times faster than on flat PDMS, and are more akin to diffusion rates normally observed in liposomes, indicating that the bilayer is minimally influenced by the underlying substrate.

In the second part of this thesis an analogous substrate and bilayer deposition method was developed using gold substrates with the objective of using electrochemical methods to address the bilayer or trigger events within the cavity. Firstly lipid bilayers are spanned in a similar manner as developed for PDMS and the bilayer modified gold was characterised by electrochemical impedance spectroscopy (EIS). Incorporation of ion transporting molecules into the supported bilayers is also investigated by EIS. Finally a novel means of inducing electrically controlled release of reagent from inside the gold cavities to a lipid bilayer suspended across the cavity was developed using a ferrocene/cyclodextrin complex. To demonstrate this Streptavidin was released to a biotinylated lipid bilayer and its interaction with the bilayer was monitored using electrochemical impedance spectroscopy.

In Memory of my Mum Pauline.

Chapter 1

Literature Survey

2.2 Introduction

A phospholipid membrane is a semi-permeable barrier that encloses and defines the boundaries of the cell and its organelles. This plasma membrane forms the boundary between the intercellular area (cytoplasm) and the extracellular area controls what passes into and out of the cell and organelles. The plasma membrane is mainly composed of sterols, proteins and phospholipids. The phospholipids form an approximately 5 nm thick double layer in the plasma membrane into which all the other components are embedded. Plasma membrane embedded proteins mediate many key functions, such as transport across the membrane, cell adhesion and cell recognition (see Figure 1.1). The plasma membrane is a dynamic and fluid structure meaning that its component molecules are free to diffuse in the plane of the membrane. This mobility is crucial for the embedded proteins to function correctly.[1,2] Understanding how the membrane and its component proteins work is essential in order to understand their greater roles within biological processes. Studies tend to focus either on direct study of the protein of interest in cells expressing the protein or in extra-cellular studies in solution.[3,4] The former, because of the complexity of the cell environment, make it difficult to isolate the function of the protein, whereas in the latter study the protein often is in a detergent solution or truncated form of the protein to promote solubility.[5] Both approaches diminish the bio-relevance of the study. Whereas membrane bound proteins require the lipid bilayer to maintain their conformation and it is thus essential to function. Consequently, model membrane systems into which membrane proteins can be inserted and studied in an environment, which is more analogous to a cell, are an important means of studying proteins and

other components of the cell membrane away from the complexity of the cell whilst maintaining their native environment. This chapter overviews some of the models of membrane structures which have been developed and examines recent advances which have been made in such model systems as well as their limitations.

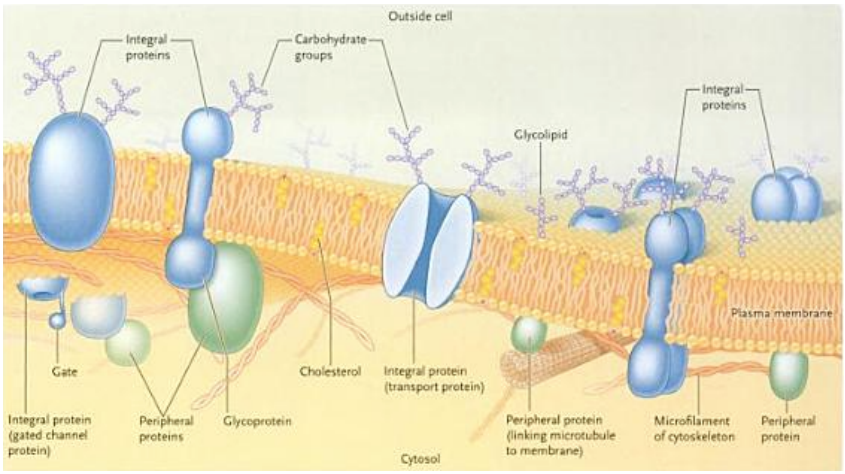

Figure 1.1 Illustration depicting the multiple components of the cell membrane. Taken from Biology the Dynamic Science. Reproduced from[6]

2.3 Components of the Cell Membrane

2.3.1 Lipids

Amiphatic lipids are the main component of the cell membrane and are responsible for the structure of the membrane. There are thousands of naturally occurring lipids, these include sphingophospholipids, glycophospholipids, and glycerophospholipids (see Figure 1.2). Glycerophospholipids are the most common lipid and are the main building blocks of the cell membrane. Most comprise a

hydrophilic head group most commonly of glycerol and a negatively charged phosphate group. They have a hydrophobic tail, which consists of two long fatty acid chains, usually between 14 to 24 carbons long. Phosphocholine (PC) is one of the most abundant lipids in animal cells, and so it is the main lipid used in the work described here. It is found naturally as egg PC or soy PC or synthetically as 1,2-dioleoyl-*sn*-glycero-3-phosphocholine (DOPC). At low concentration these phospholipids exist in monomeric form as the concentration increases the repulsive forces of neighbouring polar head groups begins to be outweighed by the self-organization of the hydrophobic tails. It is this hydrophobic-hydrophobic interaction between the tail groups of the phospholipids which causes spontaneous organisation of the lipid bilayer.[7] As the concentration increases the phospholipids self-assemble into a lipid bilayer structure, which consists of two leaflets of lipids with the hydrophobic tails oriented inwards, excluding water and creating a hydrophobic core, and the hydrophilic heads pointing out into the aqueous solution.[8]

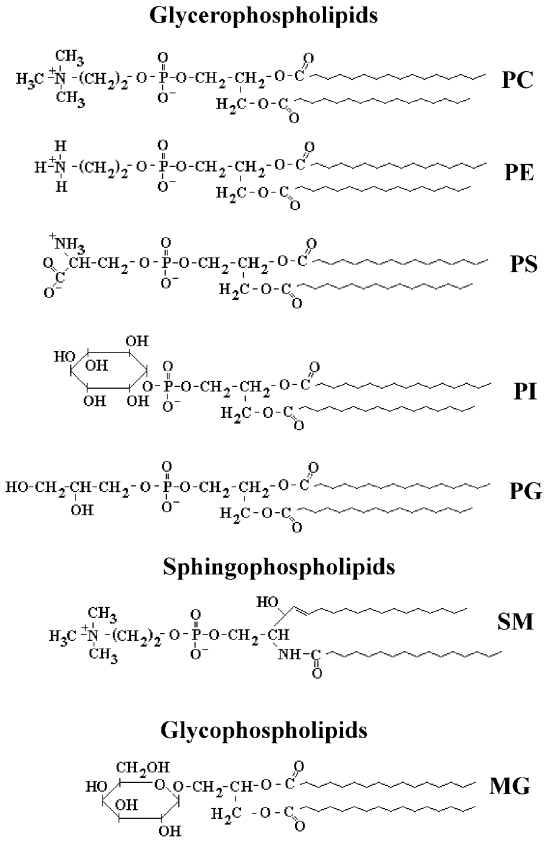

Figure 1.2 Structure of a selection of lipids present in the cell membrane. PC - Phosphatidylcholine, PE - phosphatidylethanolamine, PS – phosphatidylserine, PI – phosphatidylinositol, PG – phosphatidylglycerol, SM – sphingomyelin, MG – monogalactosyldiglyceride. *Taken from*[9]

Packing of lipids into the lipid bilayer is mainly influenced by their hydrophobic tails.[10,11] The tails are composed of two hydrocarbon chains, the length of this chain has an impact on the lipids mobility within the bilayer. The shorter the chain the easier the lipid can diffuse within the bilayer. The saturation of the hydrocarbon chains also has an impact on the lipid's diffusion. Lipids with double

bonds on their hydrocarbon chains are more fluid, but form a more ridged bilayer due to the disruption of interactions with the hydrophobic tails of neighbouring lipids. The fluid mosaic model was developed by SJ Singer and GL Nealson in 1972 and describes the fluidity in the lipid bilayer.[12]

Sphingophospholipids are another class of lipids, an example of which is sphingomyelin. Sphingomyelin is similar in structure to glycerophospholipids but have a ceramide backbone rather than a glycerol backbone. It is found in high concentration within the myelin sheath which surrounds and electrically insulates many nerve cell axons suggesting its role as an insulator.[13] Its main role however is in the formation of lipid micron domains, or lipid rafts. These are areas of the lipid bilayer which are more compact and ordered then the rest of the lipid bilayer. It is thought that sphingomyelin's higher transition temperature as well as its interactions with cholesterol are responsible for aiding in raft formation.[14]

Sterols are a non-phospholipid class of lipids which are present in natural plasma membranes. Their structural rigidity disrupts the interactions between the hydrophobic chains and thus have an effect on membrane fluidity and rigidity.[15,16] Sterols, exemplified by cholesterol, consist of a polar OH head group, a hydrophobic core consisting of rigid sterol rings and a 'floppy' carbon chain. The main sterol found in human cells is cholesterol and is in fact the main component of the plasma membrane, often comprising more than 50%. Cholesterol is mainly responsible for providing mechanical strength to the lipid bilayer and plays an important role in preventing leakiness of solutes across the membrane with the highest concentration of cholesterol located in the outer leaflet of the bilayer.[17] The sterol rigid sterol rings

provide this mechanical strength by inserting in between lipid molecules and increasing the lipid packing by 'straightening' the acyl chains. This creates what is known as the liquid ordered (l_o) phase, the extension of the acyl chains by the cholesterol increases the membrane thickness in sterol rich domains creating lipid raft. Lipid rafts are dynamic nano-scale domains and an intensively investigated research field as they are believed to be key for the activity of many raft specific proteins and their activity.[18]

The phospholipid bilayer is composed of two different leaflets however the composition of these leaflets is strikingly different. This asymmetrical organization of lipids was first discovered by Bretscher in 1972.[19] He observed that in human erythrocys cells that the outer leaflet of the bilayer consisted of phosphatidylserine, phosphatidylethanolamine, and phosphatidylinositol whereas the inner leaflet consisted of phosphatidylcholine and sphingomyelin. Glycophospholipids are carbohydrate containing lipids and proteins make up between 5 to 10 % mass of the cell membrane and occur exclusively in the extracellular membrane leaflet thanks to lipid asymmetry. Carbohydrates are usually found appended to either lipids, known as glycolipids, or proteins, known as glycoproteins. Glycolipids and glycoproteins are thought to help protect the plasma membrane from harsh conditions (such as pH and harsh enzymes)[20] and charged glycolipids are important in controlling ion concentration at the membrane surface. The main function of glycolipids however is in cell recognition where carbohydrate binding proteins, or lectins, bind to both glycolipids and glycoproteins.[21]

2.3.2 Membrane Proteins

A typical plasma membrane is made up of 50 % proteins by weight, i.e. one protein molecule for every fifty lipid molecules.[22] Membrane proteins can be organized according to the way in which they interact with the membrane as illustrated in Figure 1.3 below. Some proteins are amphipathic in nature and have a hydrophobic region, which interacts with the hydrophobic core of the plasma membrane. This results in a protein which traverses the lipid bilayer with its hydrophobic core traversing the membrane and its hydrophilic regions oriented at the aqueous extracellular and plasma regions and are referred to as transmembrane proteins Some of these proteins traverse the bilayer only once, form example integrin or GP proteins, (illustration 1 in figure 1.3), whereas others traverse the membrane multiple times, such as bacteriorhodopsin (illustration 2 in figure 1.3).

Other proteins associate with either the intracellular or extracellular region only and interface with only with one leaflet of the plasma membrane (illustration 3 and 4 in figure 1.3). This is usually achieved via an α-helix expressed on the protein surface or a covalently attached lipid chain. Proteins can also associate themselves to either face of the plasma membrane by non-covalent bonds. These proteins are known as peripheral proteins and can be released from the membrane by subtle changes in pH or ionic concentration.[2]

Cell adhesion is another key function mediated by membrane proteins[23]. Cell adhesion is crucial for maintaining the 3D architecture of groups of cells into tissues. An example of this are cadherins, which are a group of transmembrane proteins

responsible for mediating cell adhesions. They act as both receptor and ligand on the cell surface and are diverse, i.e. there are many different types of cadherins, which are specific to one another. This allows them to mediate monotypic adhesion of cells and therefore makes them a key component for selective cell-cell adhesion. Another example is the integrin family, integrins consist of two non-covalently associated transmembrane glycoproteins, which form a heterodimer with the bulk of the glycoprotein excising in the extracellular region. Integrins are responsible adhesion of the cells to the extracellular matrix and one another. As with cadherins, integrins exist in many varieties and are therefore collectively responsible for many adhesion mechanisms.[24]

Membrane proteins also act as receptors for cell signalling on the cell surface, they contain a receptor on their extracellular portion to which a signalling molecule binds to. This causes a signalling process to occur in the intracellular portion of the protein, which can lead to a change in the behaviour of the cell, examples of the process include gene regulation, ion channel gating and metabolic pathway regulation.

These proteins have many different functions and modes of action. One of their major roles is in cargo transport across the impermeable plasma membrane which will be discussed in detail in the next section.

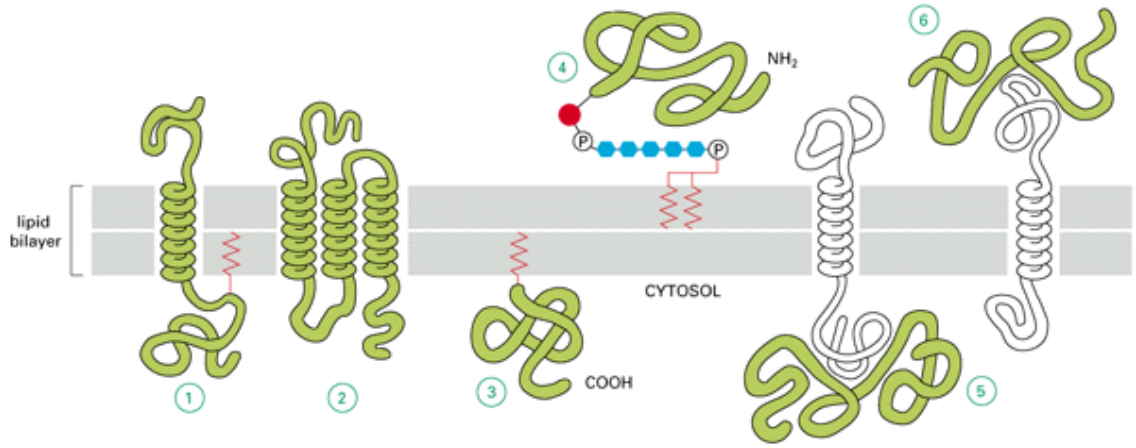

Figure 1.3 Representation of various ways proteins can associate with the plasma membrane. 1 and 2 represent trans membrane proteins, 3 and 4 represent lipid anchored integral proteins and 5 and 6 represent peripheral proteins. Image reproduced from[2]

2.3.3 Transport Across the Cell Membranes

Membrane proteins are diverse in function but can be broadly divided into 3 main categories, which are illustrated in Figure 1.4 below, these include transporters and ion channels, anchors or cell adhesion proteins and receptors.

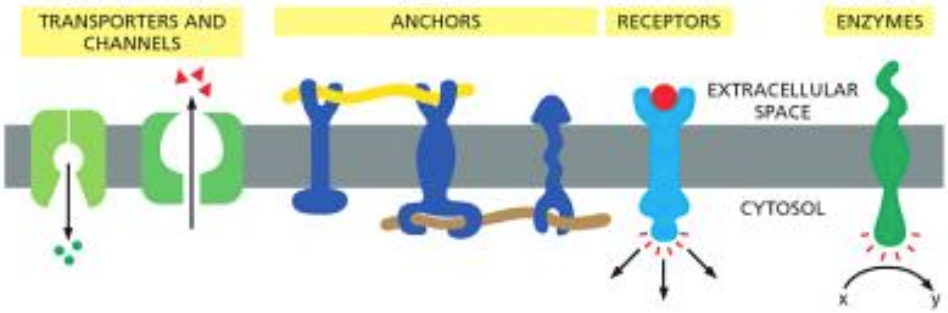

Figure 1.4 Examples of membrane proteins and there functions. *Taken from Essential Cell Biology, Fourth Edition.*[25]

Transport proteins function to allow specific species across the cell membrane. All such proteins are integral proteins and they can be classified as either channels or carriers. Transport across the membrane is mainly controlled by transport proteins however some gasses, such as O_2 and CO_2, as well as small uncharged polar molecules can cross the bilayer by passive diffusion.[2]

Ion channel proteins are responsible for transporting ions across the membrane down their concentration or potential gradient as this process is spontaneous and does not warrant the use of energy. However, some channel proteins can transport material against a chemical gradient if coupled to another energy producing process. Ion Channel proteins typically form β-barrel structures within the lipid bilayer, which generate water filled channels that traverse the cell membrane. The size of these pores is tightly controlled by the protein and this dictates the size of the ion that can pass, thus giving the ion channel its selectivity.[26,27]

Carriers tend to carry molecules and ions across the cell membrane and can categorised as active or electrochemical potential driven transporters. ATP-powered pumps are an example of an active carrier protein, they function by facilitating the movement of small molecules and ions across the membrane against a chemical gradient or electrical gradient. This process requires the expenditure of energy, which is provided to the protein by the hydrolysis of ATP to ADP. Examples of such transporters include the plasma membrane calcium ATPase pump (PMCA pump) which is responsible for maintaining the low concentration of Ca^+ within the cytoplasm of human cells[28] and the Na^+-K^+-ATPase which is responsible for maintaining normal levels of sodium and potassium ions within the cytoplasm.[29]

Ionophores are a classification of carrier molecules that are driven by the electrochemical potential across the call membrane. Ionophores can be protein or small hydrophobic molecules that are soluble within the lipid membrane. Valinomycin is an example of one of these molecules, it is a ring shaped polymer[30] which that transports K^+ ions across the lipid bilayer, down its electrochemical gradient. Ionophores can be further divided into 3 groups, uniporters, antiporters and synporters. Uniporters carry a single solute from one side of the membrane to the other usually down an ionic gradient. Examples include Valinomycin, which transports K^+ across the membrane[31] and Gramicidin which transports Na^+.[32] Antiporters carry two solutes across the membrane in different directions, such as Nigericin which moves K^+ ions across the membrane in exchange for H^+.[33] Where as synporters carry the solutes across in the same direction. Antiporters and symporters employ a mechanism known as secondary active transport to drive ion movement. This occurs where diffusion of one molecule down its concentration gradient powers the transport of another molecule against its concentration gradient.

2.4 Model Lipid Bilayers

Model membrane systems have been developed to create model systems to understand lipid behaviour with bilayers to understand membrane transport and, ligand receptor interactions[34] where the receptor is a membrane bound protein which requires a membrane environment to support its native structure.

2.4.1 Lipid Vesicles:

One of the earliest membrane models is the liposome. They were first discovered by Dr Alec Bangham in 1964 when he imaged gram negative stained phospholipids using an electron microscope.[35] Liposome preparation is quite straightforward: dried lipids, typically on glass, are hydrated in a polar solvent, usually water, and spontaneously form vesicles. However, vesicles formed in this way are usually diverse in size and often contain layers of vesicles within each other; known as multilamellar vesicles (MUV's). MUV's can be readily made more uniform with a single bilayer by either sonication or by extrusion through a polycarbonate membrane. This approach typically generates 50 to 100 nm vesicles known as small unilamellar vesicles (SUV's).[36] Alternatively, liposomes can be formed by rehydrating lipids in the presence of an AC electrical field. This results in much larger liposomes with a diameter of 10 to 100 μm, known as giant unilamular vesicles (GUV's).[37] These vesicles are very useful as model membrane systems as their large size makes them amenable to optical imaging. They have proven useful for monitoring lipid dynamics[38,39,40] lipid raft formation[41,42], membrane fusion[43] as well as protein behaviour[44,45] Although GUV's are useful as model membrane systems, they are often limited to fluorescence experiments and imaging techniques, their long term stability is poor and there are limits to their composition, e.g. they cannot be prepared to be asymmetric. However some studies have used cyclodextrin to remove cholesterol from one leaflet to provide some asymmetry.[46]

2.4.2 Black Lipid Membranes:

The first planar model of the phospholipid bilayer was reported in the early 1960's by Mueller et al. and was composed of extracted brain lipids in a chloroform methanol solution, which were painted underwater over a hole of 1 mm diameter bored into a polyethylene surface. It was used to study the electrical properties of the bilayer.[47] These bilayers appear black under reflected light, which is why they are commonly referred to as black lipid membranes (BLM's). BLM's consist of a lipid multilayer over a small aperture formed on a hydrophobic material. This method involves painting an organic phospholipid solution, usually 1 to 2% lipid in n-decane, which is then placed in contact with an aqueous environment at both bilayer interfaces, an example of which is depicted in Figure 1.5 below. BLMs have been useful for the investigation of the electrical properties of the bilayer as well study of transport biomolecules such as ion channel proteins as each side of the lipid layer is in contact with water. BLM's in particular have been used to study channel forming proteins such as Gramicidin[48] and OmpF.[49] However BLM's have a number of important drawbacks; they are unstable and the methods of interrogation are usually limited to simple light techniques or electrical detection. A key drawback is that organic solvents are used during their preparation, which often leads to solvent residues being retained within the lipid layer.[50] It is also difficult to incorporate proteins and other complex biomolecules into them. Finally, due to the method of painting employed to form these structures lipid multilayers are usually the result and it is a significant challenge to control the layer thickness.[42]

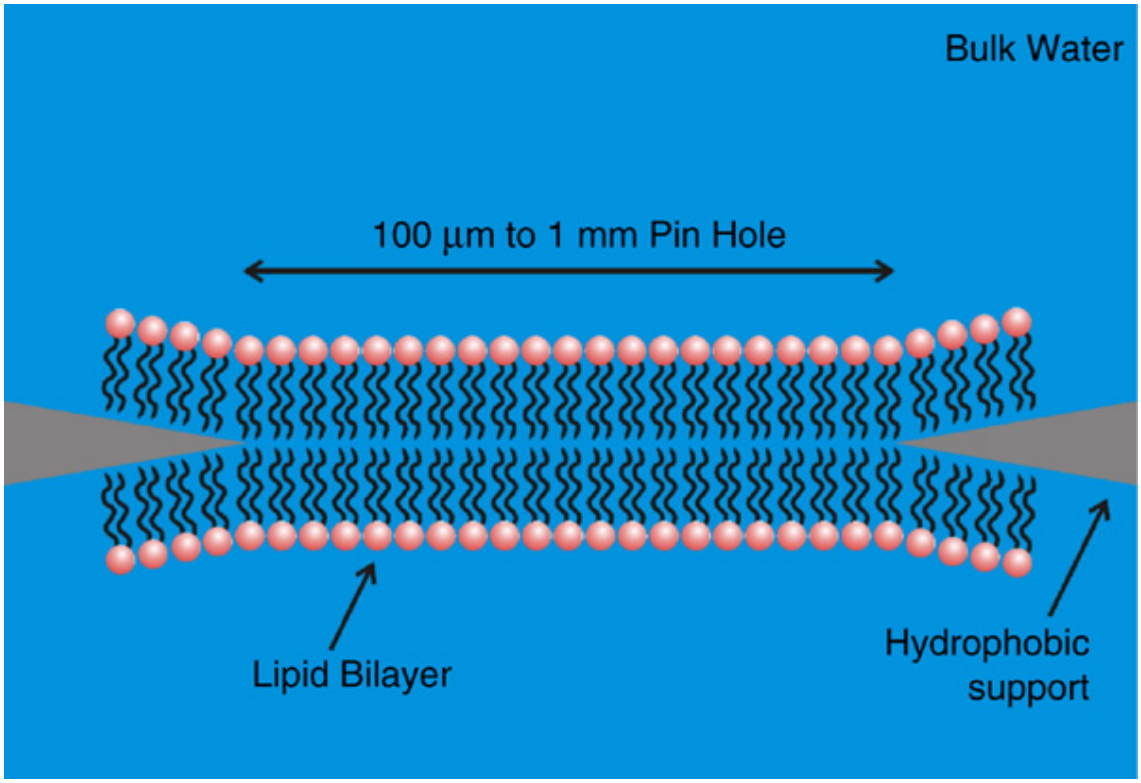

Figure 1.5 Schematic of a Black Lipid Membrane. Image reproduced from[51]

2.4.3 Supported Lipid Membranes

Twenty years on from the formation of the first black lipid membrane Tamm et al. successfully formed a stable lipid bilayer on oxidized silicon wafer; this was the first solid supported lipid bilayer.[52] Supported lipid bilayers (SLB's) have since been shown to form on a variety of substrates provided they are clean, smooth but most importantly, hydrophilic. Examples of substrates used for supported lipid bilayers include borosilicate glass[53], mica and oxidised silicone.[54]

There are three general methods for the formation of supported lipid bilayers. The first method involves the adsorption and fusion of lipid vesicles on the substrate.

SUVs have been known to spontaneously form lipid bilayers on their introduction to hydrophilic substrates (see Figure 1.6b)[55] to create supported lipid bilayers, The mechanism of vesicle disruption and bilayer formation has been widely examined.[56,57,58] When a single vesicle is adsorbed on the substrate it remains intact, however the adsorption of further vesicles onto the surface causes deformations in the vesicles, which causes it to rupture on the surface. Next, more vesicles adsorb and rupture in the same way, which creates a bilayer patch. This bilayer patch in turn adds further stress to any other adsorbed vesicles and further increases the rupturing of vesicles adsorbed on the substrate. This process continues until a supported lipid bilayer is formed on the substrate.[59]

A second method of forming supported lipid bilayers involves the transfer of a lipid monolayer from an air-water interface by the Langmuir- Blodgett technique (Figure 1.6 A) which will be described further in a later section. Briefly, the substrate is quickly dipped into the air/water interface then slowly withdrawn in the process depositing a monolayer of lipid onto the substrate. This is followed by the Langmuir-Schaefer method, which involves horizontally dipping the substrate with the monolayer into the interface to create the upper leaflet (Figure 1.6 C). However when looking at more complex bilayer systems which may include proteins, the Langmuir-Blodgett/Langmuir-Schafer method is useful as it requires the proteins to be exposed to air in the air/water interface for prolonged periods of time which may cause them to denature.

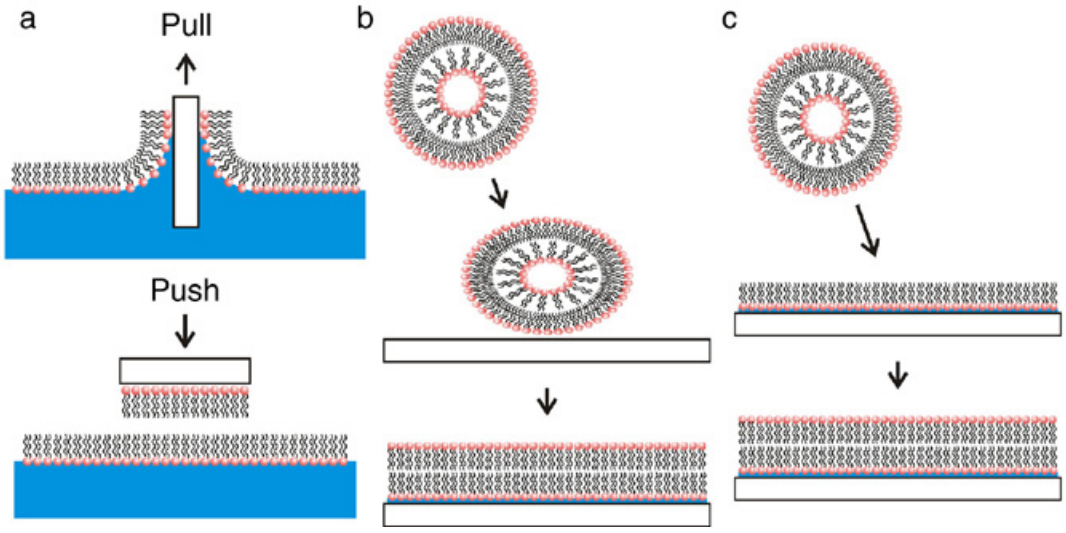

Figure 1.6 Schematics showing methods of forming supported lipid bilayers. a) The Langmuir-Blodgett/Langmuir- Schafer Method: deposition of an underlying lipid monolayer on the substrate using the Langmuir-Blodgett method followed by the formation of a second layer by horizontally dipping the substrate. b) Vesicle fusion method: the addition of unilamellar vesicles to a hydrophilic substrate and their spontaneous formation of a lipid bilayer c) Langmuir-Blodgett/Vesicle Fusion method: deposition of an underlying lipid monolayer on the substrate using the Langmuir-Blodgett method followed by the addition of unilamellar vesicles which fuse and form the upper leaflet. Image reproduced from[51]

The final method, which has been exploited in this work, involves a combination of the first two methods. Firstly, a monolayer is formed on the substrate via the Langmuir-Blodgett technique. This monolayer forms the lower leaflet of the bilayer onto which vesicles can adsorb and fuse onto, forming the upper leaflet and completing the bilayer (Figure 1.6 c). Langmuir-Blodgett vesicle fusion, can be used

to incorporate proteins as it is relatively straightforward to introduce proteins into vesicles using detergent removal via dialysis,[60] this means that vesicles with proteins incorporated into them can either be fused directly onto substrates or onto a phospholipid monolayer deposited using the Langmuir-Blodgett technique. Like the LB method a significant advantage of this approach is that the composition of the membrane is flexible and can be built to include biomimetic asymmetry into the structure.

The major advantage supported lipid bilayers have over black lipid membranes is that they are considerably more stable over time, particularly when maintained contact with aqueous media. Recent studies have examined ways of improving already impressive stability by modifying the bilayer with PEG groups to increase their stability in air.[61] Supported lipid bilayers are also far more amenable to interrogative techniques than black lipid membranes, such as atomic force microscopy,[62] quartz crystal microbalance[63] and photo physical and spectroscopic methods,[64] allowing for deeper understanding of their properties.

Substrate selection is key when forming supported lipid bilayers, as the properties of the substrate can have a profound effect on the properties of the resulting supported bilayer. For example the hydrophobicity of the substrate will influence the thickness of the water layer between the lipid bilayer and the surface of the substrate, the thickness of this layer will in turn have an impact on the fluidity of the lipids in the bilayer.[65] Ionic strength and pH have also been shown to have an effect on the mechanical properties of bilayers composed of zwitterionic lipids.[66] One of the most common substrates used for formation of supported lipid bilayers is glass. Glass is

ideal as it is naturally hydrophilic and, in most cases, only requires cleaning prior to bilayer formation. Many studies of supported bilayers have been carried out on glass, including the study of diffusion of behaviour of pegylated lipids on ozone treated glass[67] and the effect of etching glass on bilayer formation.[68] Polymer materials, such as polydimethylsiloxane (PDMS) are also an attractive material for supported lipid bilayers due to its low cost, biocompatibility and it is processability and its compatibility with light methods, as it has low reflectivity and fluorescence background. One major disadvantage of PDMS is that it is naturally hydrophobic meaning it requires modification prior to bilayer formation. It has been demonstrated that patterned bilayers can be formed on PDMS by placing a TEM grid on the substrate during plasma treatment, when vesicles are added to the surface bilayers are seen to only form on the plasma treated areas of the PDMS.[69,70] Bilayers have been shown to form by vesicle fusion on plasma treated PDMS micro-channels which have been used for ligand binding studies.[71]

Gold is also another attractive substrate for supported lipid bilayers;[72,7374] although it is hydrophobic it can be easily modified by self–assembled monolayer formation to render it hydrophilic. Another method for forming supported lipid bilayers on gold is to use thiolated lipids to form a monolayer on the surface, onto which vesicles can be fused onto to form a bilayer.[75] As gold is a useful electrode material comparison between the different methods of forming bilayers on gold has been made using Electrochemical Impedance Spectroscopy (EIS).[32,76] Using gold as the substrate for bilayer support opens for possibilities for sensor design using electrochemical detection methods.[77,78] However, a drawback of gold is that it is not

optically transparent, and indeed is a very reflective surface making it challenging to work with for optical methods, particularly as described in this thesis for application in single molecule methods. Gold can also quench emission from fluorophores and this can take effect from distances as far as about 20 nm from the substrate through energy transfer which can also be a drawback when working with interfacial films.

2.4.4 Polymer cushioned lipid bilayers:

Although versatile and stable, one of the major drawbacks of supported lipid bilayers is the undesirable membrane-substrate interaction they enable. As mentioned previously the properties of the substrate, for example its hydrophilicity, can have an impact on the behaviour of the lipids in particular their diffusion. That the surface has such an impact is due to the proximity of the lower leaflet of the bilayer to the substrate. In a hydrophilic substrate such as glass there is typically only a 5 nm thick layer of water between the substrate and the lipid bilayer,[79] although this is enough to allow the lipids within the bilayer to diffuse, it is not sufficient to fully decouple the movement of the proximal leaflet from the underlying surface. This becomes an even more important issue when membrane proteins are incorporated into SLB's, especially those with large extra-membrane portions. Frictional interactions prevent protein from diffusing in such substrates and depending on the size of the membrane aqueous contacting region, the protein will sit improperly in the membrane. Depending on the strength of interaction with the substrate such interactions can cause non-specific and steric hindrance which would cause the protein to be inactive.[80]

There has been much focus recently on trying to overcome lipid substrate and protein substrate interactions in SLBs, typically by trying to increase the distance between the bilayer and the substrate. This has been addressed by using polymer spacers, or cushions, between the substrate and the bilayer to decouple the bilayer from the substrate and limit lipid and protein interactions with the substrate. Many different materials have been employed as polymer cushions. Si/SiO_2 has been covalently functionalised with dextrin to act as a hydrophilic cushion for dimyristoylphosphatidylcholine (DMPC) bilayers containing 20 mol % Cholesterol which were shown to be stable over 7 days.[81] Cellulose has also been used as a cushion for bilayers on ITO composed of DMPC, Cholesterol, and dihexadecyldimethylammonium bromide (DHADAB). The bilayers, from , electrochemical impedance spectroscopy exhibited resistance values of 0.44 MΩ and had good mechanical stability which extended over several days. Incorporation of the ion channel protein Gramicidin into these bilayers was also investigated as well as its activity in different ions.[82] Chitosan on ITO has also been used to form DMPC/Cholesterol bilayers.[83]

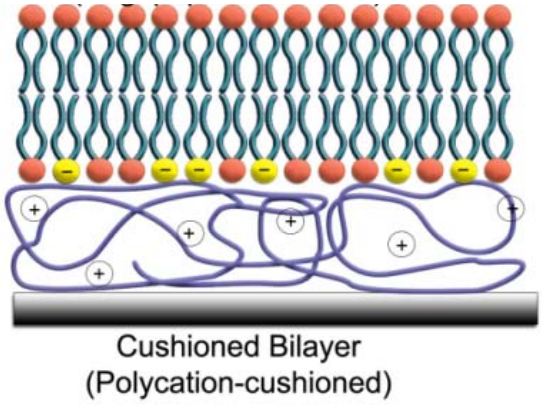

Figure 1.7 Schematic representation of a polymer cushioned supported bilayer. Image reproduced from[84]

Although cushioning has been successful in increasing the distance between the bilayer and the substrate. It has been found that strong interaction still exists between the bilayer and the polymer cushion. In the cases of the cushioned bilayers described above stable DMPC bilayers where formed when they contained cholesterol, however pure DMPC bilayers where found not to be as stable as SLBs. This is thought to be due to the interplay of electrostatic interactions and repulsive forces between the dextrin and the lipid bilayer, the presence of cholesterol is thought to increase the electrostatic forces and stabilise the bilayer. Cushion supported lipid bilayers also have little effect on the diffusion usually having diffusion coefficients around 2.5 $\mu m^2/s$ as measured by FLCS, similar to that observed form lipids on substrates without polymer cushions.[85] This implies that the polymer cushion does not have the ability to limit the lipid substrates interactions. This and the fact that these systems are limited in the lipid composition that they can use suggests that they would not be suitable for creating diverse model membrane systems.

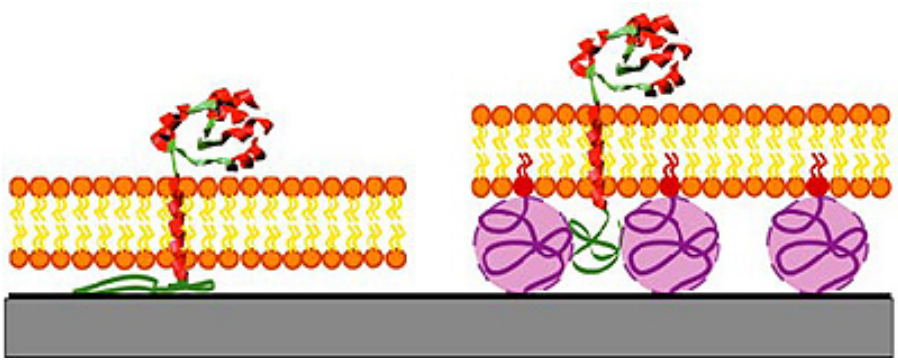

Figure 1.8 Schematic representation of a suppoterd lipid bilayer containing a trans membrane protein with a tethered polymer support (right) and without (left). Image reproduced from[86]

Another related approach is to covalently tether the lipid to the polymer support, although electrostatic forces are still required to promote association of the polymer support with the substrate, it eliminates the electrostatic forces with the lipid bilayer overcoming some of the stability issues that arise with more traditional polymer cushions (see Figure 1.8). One way this has been done is by incorporation of PEG modified DOPE lipids into the lipid bilayer on glass and quartz. This resulted in lipid diffusion of around 2.4 $\mu m^2/s$ at 4 mol % of DOPE-PEG however when the concentration of PEG is increased the lipid diffusion coefficient decreased.[87] Other work with PEG tethered bilayers measured the diffusion of two membrane proteins, Cytochrome C (D = 1.32 $\mu m^2/s$)and Annexin V (D = 0.30 $\mu m^2/s$) incorporated into POPC bilayers, they also found a slower component in there diffusion studies, which was caused by the protein interacting with the polymer support.[86] This is a clear indication that even though this approach is successful in limiting the proteins

interaction with the substrate, the use of polymeric supports causes a new set of undesirable interactions. Other work attempted to pacify the substrate by firstly adsorbing BSA before the formation of the PEG modified lipid bilayer. Although this succeeded in increasing the mobile fraction of Annexin V to 35% with a diffusion coefficient of 2.0 $\mu m^2/s$ it did not completely eliminate the protein interactions with the polymer cushion as 65% of the protein remained immobile.[88]

Another approach is to create a tether between some lipids in the lower leaflet of the bilayer and the substrate (see Figure 1.9). Lipids have been modified with thiol groups to allow them to self-assemble on gold substrates[89,90] and with silane groups to allow self-assembly on silicon.[91] Although this achieves the same effect as polymer cushioning it limits the available substrates which can be used. This in turn places limitations on the techniques which can be used to interrogate the lipid bilayer and any incorporated membrane proteins. However, some work has been done to prepare substrates which allow for multiple methods of interrogation of the lipid bilayer. For example, a study showed the use of optical wavelength lightmode spectroscopy and electrochemical impedance spectroscopy to interrogate the formation of melittin pores in a polymer cushioned bilayer.[92]

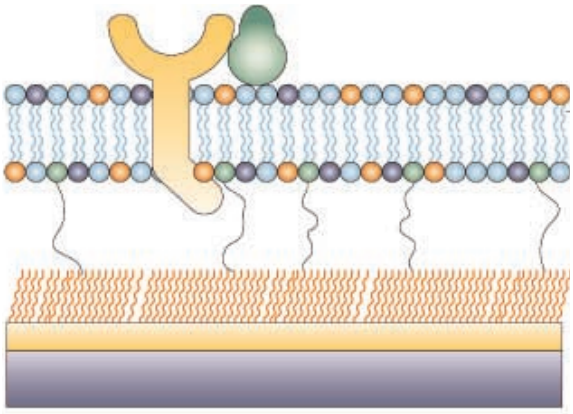

Figure 1.9 Schematic showing supported lipid bilayer tethered to a gold substrate. Image reproduced from [84]

Overall, although there has been much progress in development of model lipid membranes which promote biomimetic fluidity of all membrane species a number of issue remain such as;

- Lipid/protein substrate interactions prevent normal diffusion and protein function.
- For membrane proteins, insufficient depth of aqueous well to accommodate protein which causes improper association of the protein into the bilayer
- The inability to address both leaflets of the lipid bilayer independently, which is key in the investigation of proteins with intra- and extra-cellular binding site.
- Limitation as to the method of interrogation which is dependent on the substrate used.

There is a clear need for the development of new substrates which can successfully limit lipid-substrate and protein-substrate interactions without compromising the bilayers stability and integrity. Currently work is being driven towards suspending the lipid bilayer over nanocavity substrates. This can increase the aqueous layer beneath the lipid bilayer and in turn decouple the bilayer from the substrate without the need for cushions or tethers. However, to date this work seems has been limited to small sized, usually micro sized, and seems to have a minimal effect on the lipids and may be too small to allow for the incorporation of membrane protein at sufficient concentration or without causing protein-substrate interactions e.g. at pore edges. A more in-depth literature review of these substrates can be found in the introduction of chapter 2.

2.5 Background to Methods used for Fabrication and Characterisation of Supported Lipid Bilayer

Outlined below are the background theory behind the operation of the key methods used to fabricate substrates and study them in this thesis.

2.5.1 Langmuir-Blodgett Trough:

The Langmuir-Blodgett method uses the amphillic properties of surfactant molecules which causes them to self-assemble as a monolayer on an air/water interface. The mechanism was first proposed by Agnes Pockles in 1892 and further developed by Irving Langmuir in 1917[93] and later used as a means to transfer

monolayers from the trough onto a surface by Katherine Blodgett.[94] Phospholipids are amphilies and when added to the surface of water they spread as an insoluble monolayer, also known as a Langmuir monolayer. The accumulation of this monolayer at the air/water interface lowers the surface tension of water. Surface tension is measured in terms of surface pressure (Π), which is the difference between the surface tension with no monolayer (Υ_0) and the surface tension with monolayer (Υ).

$$\Pi = \Upsilon_0 - \Upsilon$$

The surface pressure is measured by a Wilhelmy plate and is plotted against surface area to give a pressure-area isotherm, A typical isotherm is shown below in figure 1.10 and shows a number of distinct regions of phases. These regions can provide information on the condition of the monolayer on the interface. The first phase, known as the gas phase, is where the monolayer exists in a gaseous state. In this state the molecules spread out and fill the entire area of the trough, limiting their interaction with one another. Upon compression of the monolayer the molecules begin to interact with one another and enter the liquid-expanded state (L_1). Upon further compression the intramolecular interactions become stronger and the monolayer enters the liquid-condensed phase (L_2). Finally, after enough successive compressions a compact ordered monolayer is formed on the interface and the monolayer is said to be in the solid phase (S). If any further compressions are preformed while the monolayer is in the S phase the monolayer will collapse into a three dimensional structure, which is observed by a rapid decrease in the surface pressure.

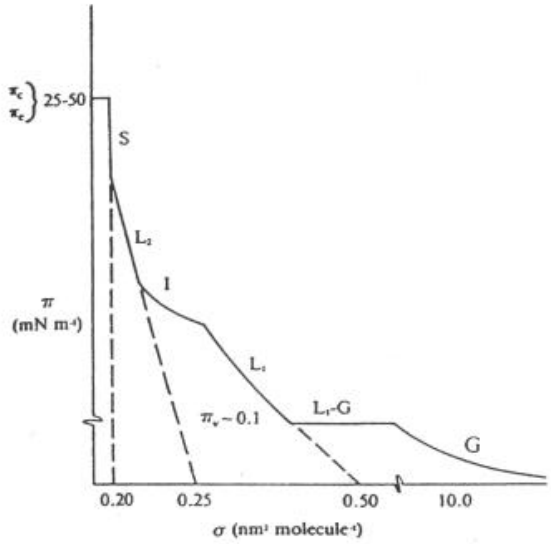

A)

Gas Liquid Solid

B)

Figure 1.10 A) Schematic representation of a pressure-area isotherm and B) a representation of the gas liquid and solid phases for a monolayer. Image reproduced from[95]

Once the monolayer is in the solid phase the surface pressure is then high enough to ensure sufficient intermolecular interactions so that the layer can be transferred intact to a surface. To transfer a monolayer onto a surface the pressure of the monolayer on the air/water interface is held constant, at the solid phase. The substrate is then dipped quickly into the interface and withdrawn slowly depositing a monolayer in the process. The orientation of the monolayer depends on the surface

wettability (see Figure 1.11), if the substrate is hydrophilic then the polar region of the monolayer will be attracted to the surface and the monolayer will be transferred when the substrate is withdrawn. However, if the substrate is hydrophobic then the hydrophobic region will be attracted to the substrate and the monolayer will be transferred when the sample is dipped into the interface.

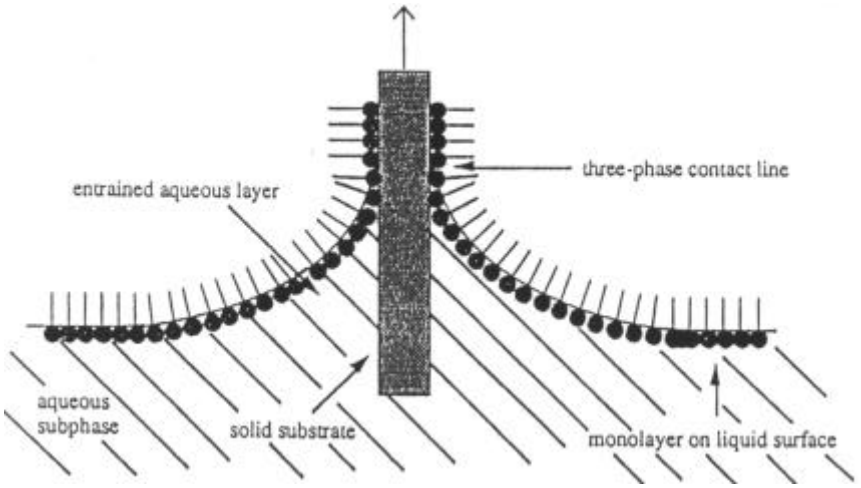

Figure 1.11 Schematic representation of monolayer transfer to a hydrophilic substrate. Image reproduced from[81]

2.5.2 Confocal Imaging Microscope

Traditional wide field fluorescence microscopy involves illumination of a large area of the sample with the excitation light and collection of the fluorescence image along with unfocused background. Confocal microscopy limits this background unfocused contribution by exciting the sample at one focused point only.[96] This focused point is obtained by passing the excitation light through an aperture and then

focusing through an objective lens (see Figure 1.12). This gives a small, diffraction limited excitation volume, known as the confocal volume. Scattered laser light as well as the fluorescent light is collected by the objective lens and passed through a dichroic mirror. The dichroic mirror allows excitation light to pass through and reflects fluorescent light. The light is then passed through a pinhole, which eliminates the out-of-focus light, prior to reaching the detector. This also increases the depth resolution, or z-resolution, however signal intensity is decreased.

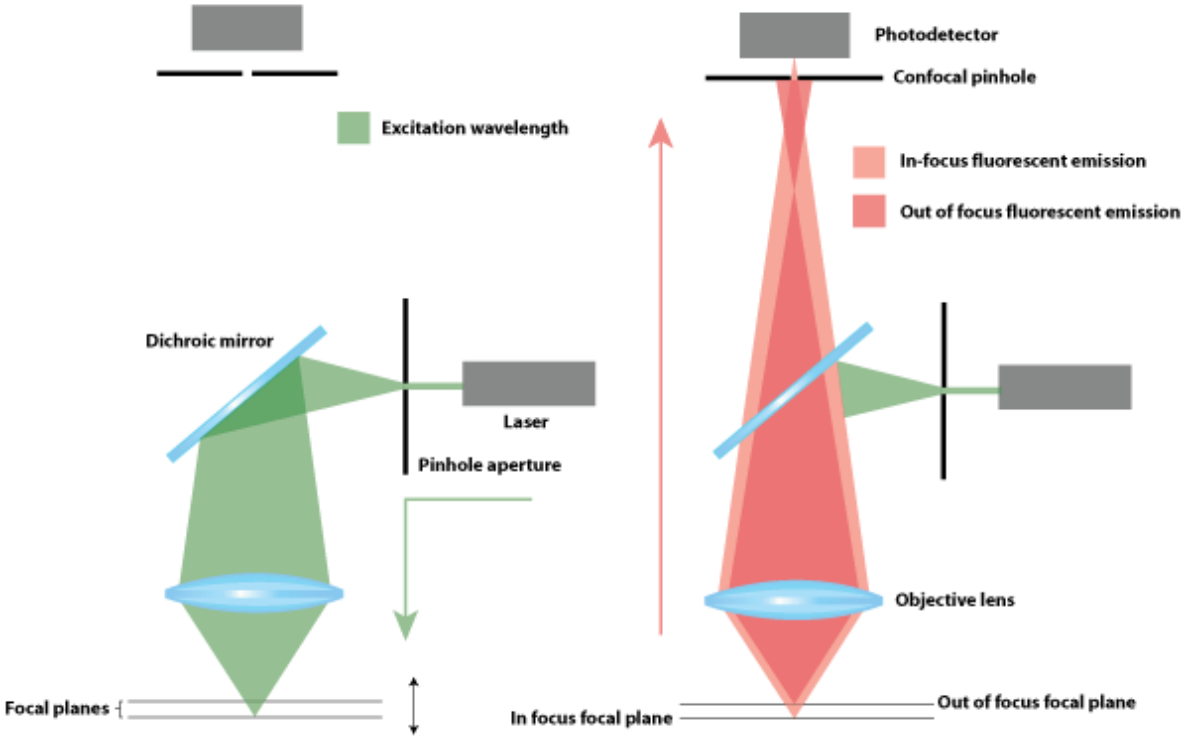

Figure 1.12 Schematic representation of a confocal set up.

2.5.3 Fluorescence Correlation Spectroscopy

Fluorescence Correlation Spectroscopy (FCS) is a single molecule method which monitors the fluctuations of the emission intensity of a fluorphore.[97,98] The observation volume is a confocal volume of approximately 1 femtoliter. Fluorphores travel into and out of this region causing small fluctuations in the emission intensity (see Figure 1.13 below). The method works best at low fluorophore concentrations, ideally with one fluorescent molecule in the observation volume. The fewer fluorophores present, the greater the amplitude of intensity fluctuation.

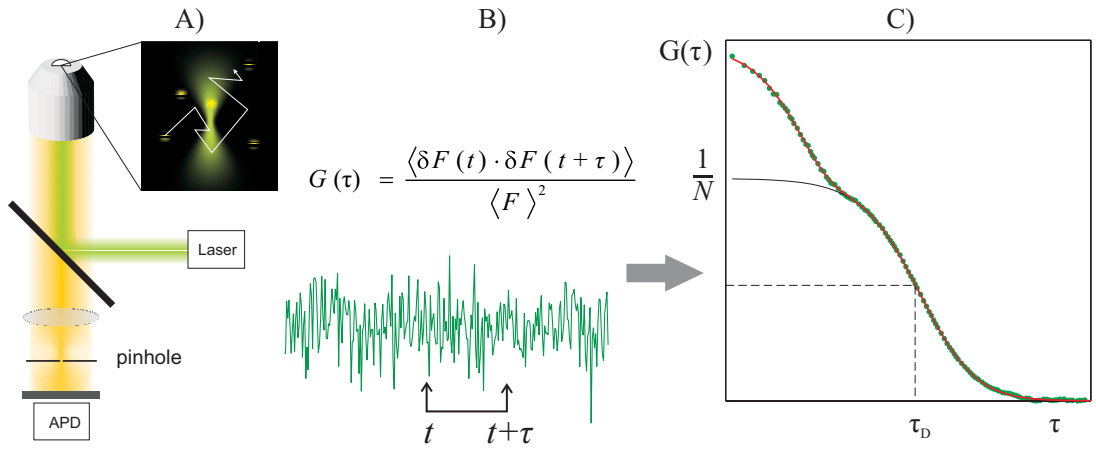

Figure 1.13 Schematic of FCS measurements showing a fluorescent particle diffusion into and out of the focus volume which results in a fluorescence signal which is then converted into a correlation curve. Reproduced from[99]

The fluorescence intensity fluctuations are autocorrelated by comparing the intensity fluctuations at time, F(t), and the intensity fluctuations after a delay time F(t + τ) with the average intensity $\langle F \rangle$ using the equations below.

$$\delta F(t) = \langle F \rangle - F(t) \qquad \text{(Equation 1.1)}$$

$$\delta F(t+\tau) = \langle F \rangle - F(t+\tau) \qquad \text{(Equation 1.2)}$$

These values can then be put into the equation below to give the correlation curve G(t) and the shape of this function provides information on the time-scale of these fluctuations.

$$G(t) = \frac{\langle \delta F(t) \delta F(t+\tau) \rangle}{\langle F \rangle^2} \qquad \text{(Equation 1.3)}$$

As mentioned these fluctuations are mainly caused by diffusion of fluorescent molecules into and out of the observation volume but can also be due to photochemical processes, like intersystem crossing into a non-fluorescent triplet state. These processes can be distinguished by their time-scale; diffusion processes usually occur in milliseconds to seconds whereas photochemical processes are longer. Diffusion of a 2 dimensional system, like a lipid bilayer, can be extracted by fitting the autocorrelation function to the following equation:

$$G(\tau) = 1 + \frac{1}{N} \frac{1}{1+(\tau/\tau_D)^{\alpha}} \qquad \text{(Equation 1.4)}$$

Where N is the average number of fluorescent particles in the observation volume, α is the anomalous exponent and τ is the diffusion time. N and τ_D are

extracted from the experimental data and can be used to find the diffusion coefficient using the equation below, once the radius of the observation volume (ω) is known.[100]

$$D = \frac{\omega^2}{4\tau_D} \qquad \text{(Equation 1.5)}$$

The width of the observation volume can be determined in one of two ways. The first method involves imaging sub-resolution fluorescent beads (100 nm in diameter), the radius of the observation volume (ω) can be obtained by imaging a bead in the xy direction and fitting to a 2 dimensional Gaussian fit. The height, of the observation volume (k) can also be obtained in a similar way by imaging in an xz direction. Both the observation radius and the eccentricity can then be used to calculate the observation volume. The second method involves measuring the autocorrelation function of a solution of dye with a known diffusion coefficient. The measured autocorrelation function can then be fitted using the known diffusion coefficient for the dye from which ω_0 and k can be extracted.

One limitation of FCS is that the detected signal is a combination of the contributions of all signals within the sample. Using a combination of FCS and time correlated single photon counting (TCSPC) one can separate out the different FCS contributions. This can be achieved if each component has a distinct unvarying lifetime component. For example, if two fluorescent compounds, A and B, have each different lifetime kinetics and where 60 % of the signal comes from compound A.

After each pulse the the emitted photon is binned into channels (i) and gives the curve D(i) (figure 1.14). This curve is a superposition of the contributions of A and

B, if the decay of one contributor is known (usually by measuring one compound on its own) then it can be used to obtain the other by deconvolving the histogram. When calculating ACF's in FCS each photon contributes equally to the final ACF. In FLCS the TCSPC histogram is used to assign weighting, from compound A and B, to each photon channel (see Figure 1.12). This gives two filters, $f_a(i)$ which when applied to the data gives the ACF form compound A and $f_b(i)$ which would give the ACF for compound B. This can also be a useful tool for eliminating any background scattering from the substrate.

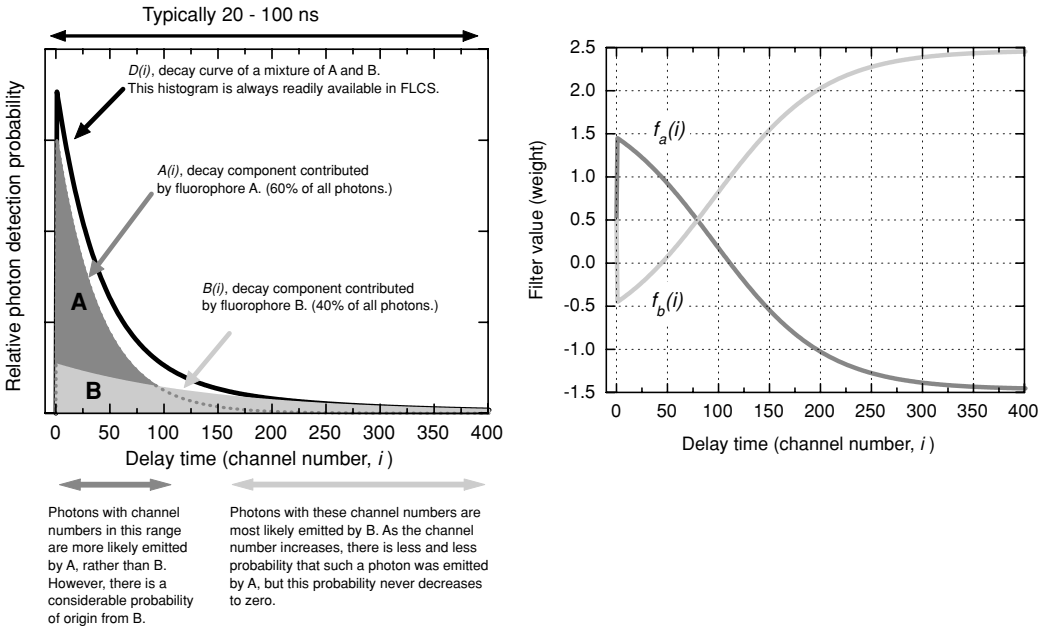

Figure 1.14 Left: example of a TCSPC histogram obtained from a sample containing two fluorescent compounds. Right FLCS filter functions calculated from the TCSPC histogram. Images reproduced from[101]

Although FCS is useful for measuring the diffusion of individual molecules it does have some limitations when attempting to measure the change in diffusion caused by molecules interacting with one another. The Saffman-Delbruk equation describes the lateral diffusion (D_L) of a molecule, such as a protein, in a bilayer:

$$D_L = \frac{k_B T}{4\pi\eta h}\left(\ln\frac{\eta h}{\eta_W a} - \gamma\right) \qquad \text{(Equation 1.6)}$$

where k_B is the Boltzmann constant, T is the absolute temperature, η is the viscosity of the bilayer, η_W is the viscosity of the surrounding aqueous phase and γ is Euler's constant. The molecule in the bilayer is treated as a cylinder of radius, a spanning the bilayer of thickness, h. This equation shows an exponential relationship between the molecule's radius and its diffusion. This means that FCS allows for the characterisation of binding of small fluorescent ligands to large molecules but it would be very difficult to measure the effect this binding may have on the diffusion of the acceptor molecule within a lipid bilayer. Nevertheless, FCS is still a very powerful, non-destructive technique for the investigation of lipid and protein dynamics within lipid bilayers. It allows for the measurement of diffusion of single lipid molecules usually within a femtoliter volume, in comparison to other techniques like fluorescence recovery after photobleaching (FRAP) which works destructively and is an ensemble method.

2.5.4 Electrochemical Impedance Spectroscopy

Resistance is a measure of an electrical circuit's ability to resist the flow of electrical current. It is defined by Ohm's law, where E is potential and I is current:

$$R = \frac{E}{I} \qquad \text{(Equation 1.7)}$$

Ohm's law describes an ideal resistor, one that obeys Ohm's law at all current and voltage. An ideal resistor exhibits resistance that is independent of applied AC frequency such that AC current and voltage signals passed through such a resistor are in phase. However, this is not the case in more complex systems, such as supported lipid bilayers where a phase separation exists between applied AC voltage and current reflecting the impedance of the system. Electrochemical impedance allows for the measuring of resistance which is not restricted by the same simplifications as Ohm's law. Impedance is measured by applying an AC potential to an electrochemical cell and studying the AC current response. In EIS a small AC potential is applied to the cell to give a pseudo-linear response. As the AC potential signal is a sinusoidal function, if the potential is pseudo-linear, the current response should also be a sinusoidal function at the same frequency but shifted in phase, as shown in Figure 1.15.

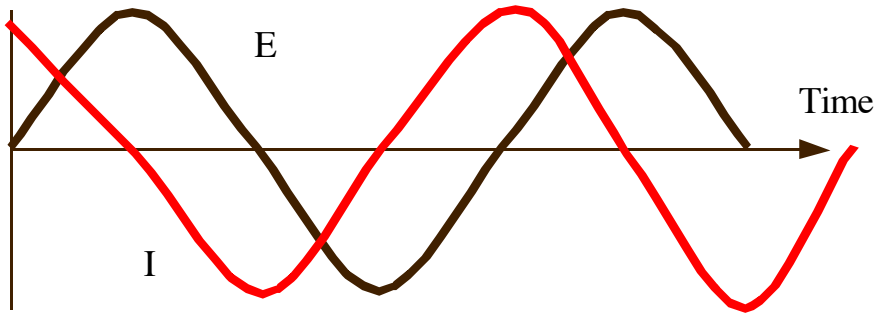

Figure 1.15 examples of an impedance potential waveform (E) and current response waveform (I).

Therefore, electrochemical impedance describes the phase relationship between the potential, of excitation waveform (equation 1.8 below) and the current, or response waveform (equation 1.9 below). This allows impedance to be represented as Z(w) (see equation 1.10 below), where the Cartesian coordinates can be defined (see equation 1.10).

$$E(\omega) = Eexp(j\omega t) \qquad \text{(Equation 1.8)}$$

$$I(\omega) = Iexp(j\omega t - \phi) \qquad \text{(Equation 1.9)}$$

$$Z(\omega) = \frac{E}{I} = Z_0 \exp(j\phi) = Z_0(cosj + jsin\phi) = Re[Z(\omega)] + jIm[z(\omega)]$$

(Equation 1.10)

Impedance spectroscopic data can be plotted in a number of different formats each of which has its advantages depending on the system of interest. The main format used in this report is the Nyquist plot. Nyquist plots Im[Z(w)] vs Im[Z(re)] (see Figure 1.16 below). Each point on the plot represents the real and imaginary components of

the impedance at a given frequency. The length of the vector, from 0 to any point gives the total impedance |Z| and the angle of this vector gives the phase angle. This form of representation can be useful for extracting information on the bilayers resistance and visual inspection of the Nyquist plot can provide immediate insight into changes to overall impedance of a film in response to a perturbation. Another widely employed way to present impedance data is the Bode plot (see Figure 1.17) which plots log frequency vs. phase shift. Unlike the Nyquist plot, the Bode plot explicitly shows frequency information.

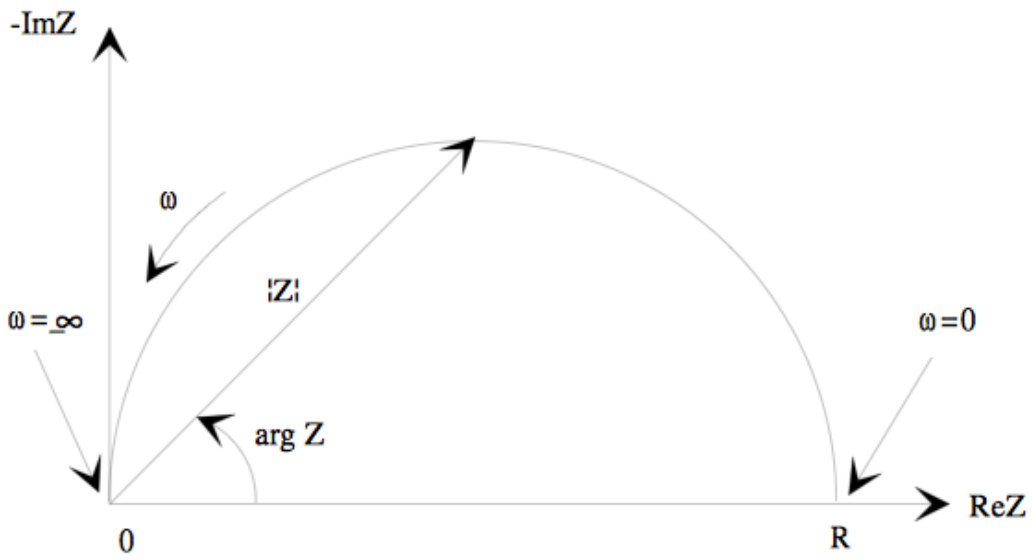

Figure 1.16 Example of a Nyquist plot, which plots ImZ Vs. ReZ

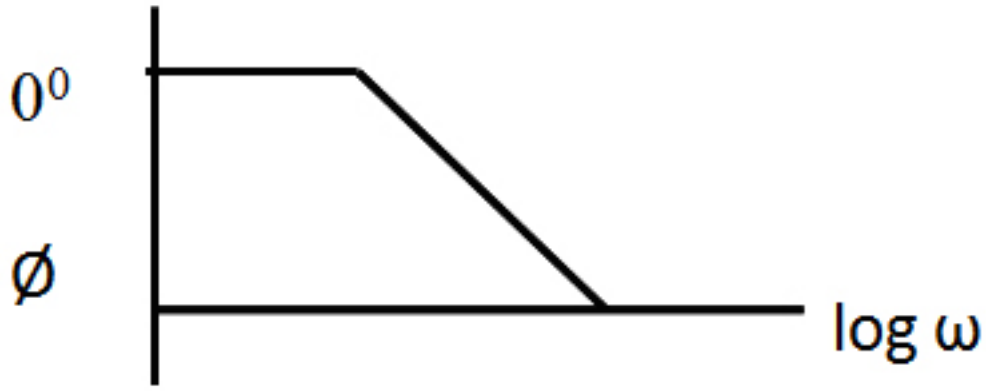

Figure 1.17 Example of a Bode plot, which plots log frequency verses phase shift.

Quantitative information on resistance and capacitance of bilayers can be obtained by fitting the impedance data to an equivalence circuit model (ECM). This allows for the extraction of electrical and dialectical properties of the system. It is important to understand the physical elements, and their electrical properties, within the system being studied in order to select the correct ECM. Figure 1.18 shows a typical ECM used for fitting impedance spectra of supported lipid bilayers. [48,102,103,76] It contains a resistor corresponding to the solution resistance (R_{sol}), and a resistor and compositor in parallel which correspond to the resistance and the capacitance of the lipid bilayer (R_{bl}, C_{bl}). The model also has a capacitor for the electronic double layer (C_{dl}) that exists between the electrode and the surrounding electrolyte.

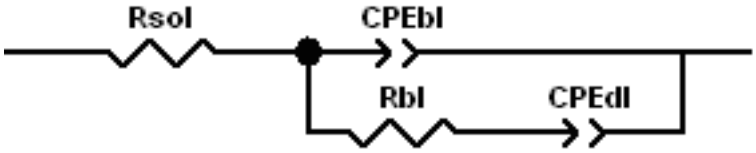

Figure 1.18 Typical equivalent circuit model (ECM) used for fitting Impedance spectra of supported lipid bilayers.

EIS has been extensively used to assess the electrical properties of supported lipid bilayers. For example, Steinem et al have used impedance to assess the different approaches to forming supported lipid bilayers and the properties of the bilayers formed.[75] In particular EIS has been used to study the properties of ion channel proteins in supported lipid bilayers. In most cases the above ECM has been used, for example in the study of Valinomycin in planar bilayers[104] as well as tethered lipid membranes on gold electrodes,[105,106] and over porous alumina.[48] Impedance has also been used to monitor the formation of ion channel pores. Gramicidin D pores in black lipid membranes on gold covered porous alumina substrates.[48,107] In this case a Warburg diffusion element is added to the ECM to account for the mass transport processes at the membrane interface caused by the formation of a pore in the lipid bilayer. A more detailed review of lipid bilayers using EIS can be found in the introduction to chapter 3

2.6 Conclusions

Chapter 1 has described with the current state of the art in model lipid membrane systems. Model membranes have and continue to be applied to many important research questions spanning fundamental biophysics to issues of the pharmacetucial industry i.e. from lipid dynamics, investigating drug membrane interactions, the study of protein ligand interactions and protein dynamics. Although many advances made using solid supported bilayers which can incorporate membrane proteins, there is still a long way to go to creating stable cell membrane mimics that offer stability, reproducibility and sophistication required to mimic faithfully key aspects of the plasma membrane.

This thesis aims to develop substrates which can be used to develop model membrane systems in which membrane proteins can be studied. This will be achieved by using microcavity substrates over which supported lipid bilayers will be spanned. It is hoped that by spanning the bilayer across these cavities that the lipid substrate interactions, and subsequently the lipid protein interactions, will be limited. Two different types of substrates will be investigated, PDMS substrates for development of fluorescent measurements and gold for the development of electrochemical measurements.

Chapter 2

Planar and Microcavity Supported Lipid Bilayers on PDMS Substrates.

2.1 Introduction

The cell membrane is a complex structure which contains hundreds of lipids and membrane proteins which are responsible for a wide range of cellular processes, from cell signalling, to transport of material in and out of the cell. Understanding how membrane associated proteins and lipids behave within their native membrane environment will enable a better understanding of disease states as well as the development of more targeted therapeutics.

However, due to the complex nature of cells and their heterogeneity, it is difficult to isolate the behaviour of selected proteins within a whole cell system. A more facile approach is to use model membrane systems, which may allow study of the unit function of the membrane associated components away from the complexity of the living cell.

One such model is the Supported Lipid Bilayers (SLB's), which are typically formed from a lipid bilayer on a planar hydrophilic substrate, such as glass, by fusion of lipid vesicles, lipid painting or using a Langmuir-Blodgett trough. Such films have been shown to successfully form on many hydrophilic surfaces. Lateral diffusion of the lipids within these bilayers is maintained due to the presence of a hydration layer, approximately 5 nm thick, between the substrate and the bilayer. This layer is thick enough to prevent the lipids from interacting strongly with the underlying surface, although their diffusion coefficient is typically half that of lipids in liposomes. However, when a transmembrane protein is introduced into an SLB (and there are relatively few examples reported) this layer is typically insufficient to prevent the

protein from interacting with the substrate resulting in protein immobility and decreased activity due to steric hindrance. Some groups have attempted to decrease the protein substrate interactions by increasing the distance between the bilayer's lower leaflet and the substrate. This has been achieved, for example, by incorporating pegylated lipids into vesicles or by using lipids tethered to the substrate. However, this results in only a 25% mobile fraction suggesting the cellulose cushion does not fully prevent protein substrate interactions.[80] Diaz et al. used a combination of both methods; a BSA cushion and a PEG spacer to investigate the diffusion of Anexin 5, with this method they managed to successfully increase the mobile fraction of protein to 75%.[88]

Cushioned and tethered lipid bilayers partially address the problem of protein substrate interactions but do not succeed in eliminating the problem completely. One tactic currently being explored is the formation of freestanding lipid bilayers that would contain areas of the bilayer, which would not be in contact with the substrate. Bilayers have been spanned over 60 nm porous alumina substrates[108] and on silicon nitride substrates with pores ranging from 85nm to 440nm.[109] However, in both cases, the bilayer formed is a black lipid membrane, formed by painting lipids, over an aperture, from a solvent solution. Although this succeeds in forming a free standing bilayer some of the organic solvent remains in the bilayer, which will affect its diffusion, the method also makes it difficult to successfully incorporate trans membrane proteins.

Several groups have demonstrated the formation of supported lipid bilayers on porous substrates. In these approaches the area of the bilayer spanning over the pore

would be far enough away from the substrate that it would not experience lipid substrate interactions. Studies have shown successful formation of suspended lipid bilayers over nano-dimensioned pores on silicon substrates by Langmuir-Blodgett deposition[110] or by using vesicles with larger sizes than the pores to be spanned.[111] Other work has reported ruptured giant unilamular vesicles (GUV's) over porous substrates to form spanning bilayers, however, this usually results in the formation of unstable bilayer patches rather than the formation of a continuous, homogeneous bilayer.[112,113] Other approaches have included using shear flow and variations in pH to span lipid bilayers across 80 nm diameter pores, however this results in a bilayer spanning over dry cavities which is of limited biological relevance.[114] All of these methods have potential to be developed into a lipid system, which could be used to monitor the diffusional behaviour of transmembrane proteins however one disadvantage of them is that the pore sizes used are too small and would make it difficult to measure diffusional behaviour of lipids or proteins over the pores alone. In the work presented here we develop a strategy to prepare supported lipid bilayers at substrates containing aqueous filled micron-sized cavities across which lipid bilayers can be spanned, and eventually into which protein can be reconstituted and suited to measurement by FLCS to measure their diffusion.

The approach used here is to span phospholipid bilayers across aqueous filled micro-cavity array Polydimethylsiloxane (PDMS). These substrates are formed using nanosphere lithography employing 1 to 5 micron diameter polystyrene beads as a template over which the PDMS can be moulded. The pores can then be filled with aqueous solution via sonication. Lipid bilayers can then be spanned over these fluid filled cavities over deep aqueous wells, which should decouple the bilayer from the

substrate, increase lipid mobility and allow for proteins to diffuse freely without influence from the substrate. The cavity also allows for an area below the bilayer into which, for example, protein activator molecules could be deposited, to influence protein behaviour during measurement.

PDMS is a useful substrate for the investigation of supported lipid bilayers due to its low cost, optical transparency, processability and its biocompatibility. The optically transparency of PDMS is particularly important, as it has low reflection and fluorescence so was deemed a good choice for study by FLCS, which as described in chapter 1 is a single molecule method and so very prone to optical interference. However, a key challenge is that PDMS is a hydrophobic polymer and unsuited without modification for lipid bilayer support. Therefore in order to enable phospholipid bilayer assembly at its surface PDMS must first be rendered and sustained as hydrophilic at its interface.

This chapter explores methods of modification to the interface of PDMS substrates hydrophilic via modification with UV/Ozone or air Plasma. These treatments are also coupled with further treatment; chemical modification by 3-Aminopropyltrithoxysilane or adsorption of BSA to investigate approaches to slow down PDMS surface remodelling. The hydrophilicity of these treated surfaces, and how this hydrophilicity is sustained over time, is monitored using contact angle measurements to determine the optimal treatment and storage conditions of PDMS substrates for use as substrates for supported lipid bilayers.

Next, using planar PDMS, the ability of these modified substrates to support

lipid bilayers and the impact of treatment on bilayer fluidity is examined. Finally, PDMS microcavity arrays are fabricated and lipid bilayers are formed on them using vesicle fusion and a combination of Langmuir-Blodgett and vesicle fusion. These bilayers are assessed by confocal imaging and Fluorescence Lifetime Correlation Spectroscopy (FLCS) to determine if the bilayers formed are spanning the cavities and if this has the effect of increasing lipid mobility.

2.2 Experimental

2.2.1 Modification of Planar PDMS Surfaces

To investigate the effect of various surface treatments on Polydimethylsiloxane (PDMS), planar PDMS substrates where formed by mixing PDMS elastomer and curing agent (Salegard 184, Down Corning), in a 10 to 1 ratio (elastomer to curing agent). This was then poured over a glass microscope slide and then cured at 150 ºC for 1 h. The cured PDMS was allowed to cool and then carefully peeled off the microscope slide and cut into small blocks (approx. 2cm x 2 cm x 2cm).

The PDMS blocks were then either treated with UV/Ozone or Air Plasma. UV/Ozone treatment was performed with a UV/ Ozone ProCleaner (Bioforce Inc.) for 1h, while Air Plasma was performed with a Harrick PDC-002 Plasma (Harrick Plasma Inc.) cleaner for 5 minutes at 1000 mT of pressure, using air as the process gas.

The effects of further surface modifications with 3-aminopropyltriethoxysilane (APTS) and adsorption of BSA after plasma treatment were also examined. These

modifications were performed by placing the PDMS surfaces into a 1 mg/ml solution of either APTS or BSA overnight. The surfaces were then removed, rinsed with water and then dried with nitrogen. Surface contact angle of the treated PDMS were measured using a First Ten Angstroms FTA200 contact angle microscope. Measurements were taken in triplicate immediately after treatment.

2.2.2 Fabrication of PDMS Substrates for Supported Lipid Bilayers

Planar Polydimethylsiloxane PDMS substrates were formed by curing PDMS, in a 1 to 10 ratio (elastomer to curing agent), over a piece of mica approximately 100 μm thick which was glued to a glass microscope slide using Ardlite epoxy glue. The PDMS was then cured for 1 h at 150 ºC after which it could be peeled off the glass slide.

Micro-cavity PDMS substrates were formed in a similar way outlined in Figure 2.1 below. Firstly 50 μL of a 0.1% w/v solution of Polystyrene microspheres in water was deposited onto the piece of mica glued to the glass microscope slide as mentioned above. The polystyrene solution was left to evaporate overnight, after which PDMS was cured over the spheres for 1 h at 150 ºC. The PDMS was then removed from the mica and the polystyrene spheres dissolved out of the PDMS by immersing the substrate in THF for 1 h. This method was used to fabricate micro cavities using 5, 3 and 1 μm polystyrene spheres. Substrates were then sonicated for 1h in Tris Buffer (50 mM Tris, 100 mM NaCl, pH 7.4) to facilitate cavity filling.

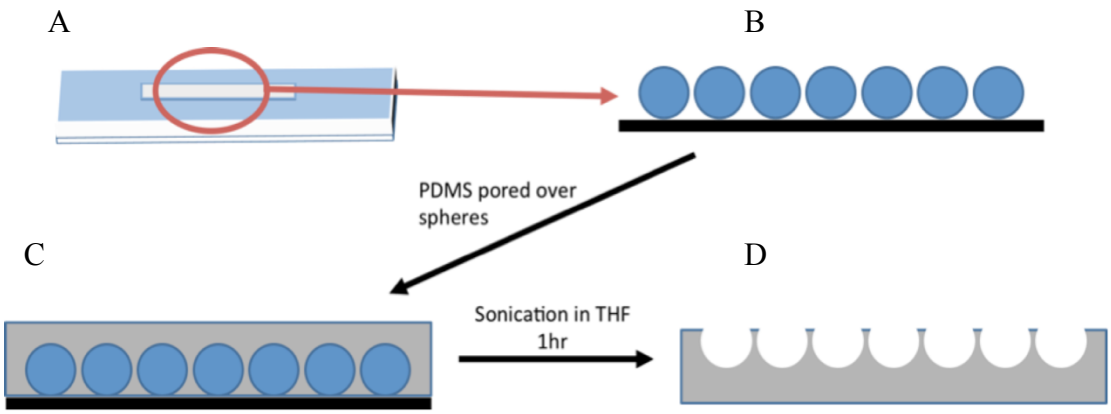

Figure 2.1: Microcavity Fabrication: A) 100 micron high piece of mica microscope slide, B) polystyrene spheres deposited on mica, C) PDMS cured over polystyrene spheres and D) Microcavity PDMS after removing polystyrene spheres with THF.

A flow cell was then created with the PDMS substrates to allow for the formation of bilayers and their examination with an inverted microscope. Firstly, two holes where punched in the PDMS, to allow for tubing attachment. The substrates were then plasma treated using a Harrick PDC-002 Plasma cleaner (Harrick Inc.). Plasma treatment was performed using air at a pressure of 1000 mT for 5 min. After which, substrates were sonicated for 1hr in Tris Buffer (50 mM Tris, 100 mM NaCl, pH 7.4) to facilitate cavity filling. The substrate was then bonded to a clean glass slides using epoxy resin. Figure 2.2 below shows a schematic of the assembled PDMS flow cell.

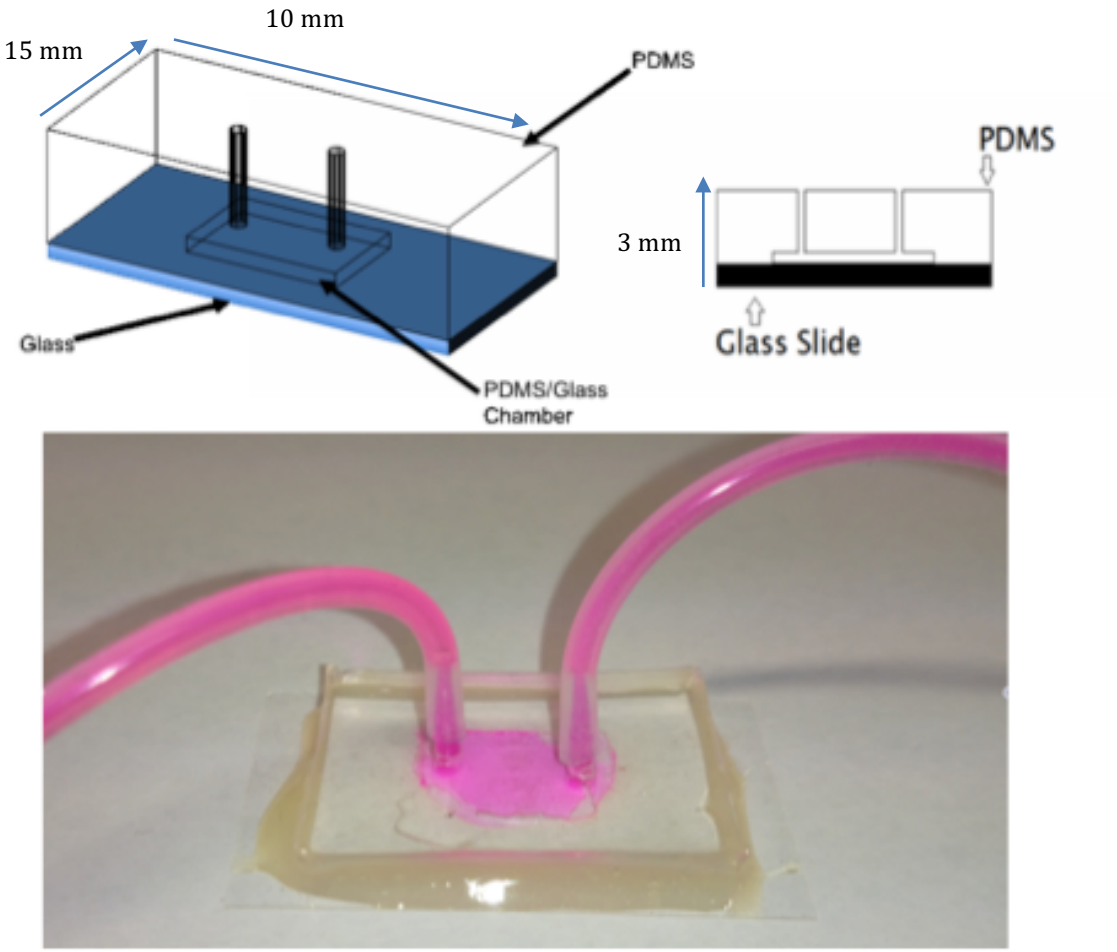

Figure 2.2: Schematic of assembled PDMS Flow Cell (above) and image of and assembled PDMS microcavity flow cell, with a solution of Rhobamine B inside it for visualisation.

2.2.3 Formation of Phospholipid Bilayers on PDMS Substrates

2.2.3.1 Planar Substrates

Bilayers composed of 1,2-dioleoyl-sn-glycero-3-phosphocholine (DOPC) were formed on planar PDMS by vesicle fusion (as depicted in figure 2.3). Small unilammelar vesicles (SUV's) were formed by taking 100 μL of DOPC (50 mg/mL in Chloroform from Avanti polar lipids Inc.) and 1 μM fluorescently tagged 1,2-dioleoyl-sn-glycero-3-phosphoethanolamine (DOPE). The solution was then dried under a gentle stream of nitrogen and then under vacuum for 30 min. The lipid solution was then rehydrated with 1 mL of Tris buffer to create vesicles. The vesicles were extruded through a 100 nm polycarbonate membrane several times to form monodisperse vesicles. These vesicles were then injected into the PDMS chamber, forming a bilayer on the PDMS and the glass surface. Vesicles where allowed to fuse for 30 mins after which the PDMS chamber was gently flushed with Tris buffer to wash away any remaining un-fused vesicles.

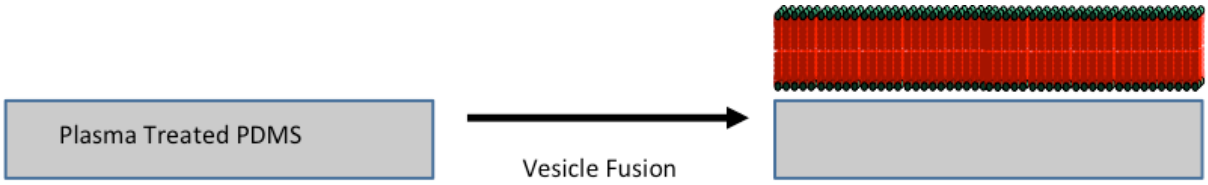

Figure 2.3: Formation of bilayers on Planar PDMS by vesicle fusion.

2.2.3.2 Cavity Substrates:

Bilayers were formed on PDMS micro-cavity substrates by first depositing a lipid monolayer onto the substrate, using the Langmuir-Blodgett (LB) technique, onto which small unilamular vesicles where then disrupted to form the bilayer (see Figure 2.4). To form the monolayer by LB, DOPC in chloroform was deposited onto the air-water interface of a NIMA 120m Langmuir-Blodgett trough (NIMA Inc.). Milli-Q water was used as the sub phase. A solution of 100 μL of a 50 mg/mL DOPE lipid labelled with Carboxyflourocene (DOPE-CF) was added at a concentration of 5 mol% for confocal images, for FLCS measurements DOPE labelled with Atto655 (DOPE-ATTO 655) was used at 1 μM. The chloroform was allowed to evaporate for 20 min after which the lipids where compressed to a surface pressure of 32 mN/m. Surface pressure was measured using a paper Wilhemy plate. The substrate was then lowered into the interface and slowly withdrawn to allow for the transfer of a monolayer onto the surface. Once the monolayer was formed, two holes were punched into the PDMS and the substrate was glued to a glass slide using epoxy glue.

Small unilamellar vesicles (SUV's) were formed, as before, with the same composition as the LB deposited monolayer. The vesicles were injected into the PDMS chamber, forming a bilayer on the PDMS micro cavities by fusion of the vesicles onto the monolayer formed previously by LB. Vesicles were allowed to fuse onto the LB monolayer for 30 min after which the PDMS chamber was flushed with Tris buffer.

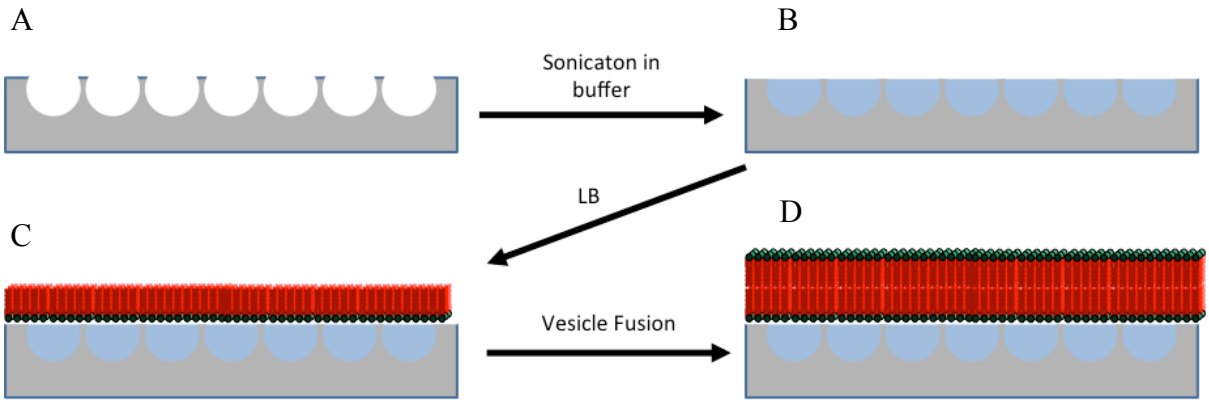

Figure 2.4: Formation of bilayers on microcavity PDMS: A) Plasma treated PDMS, B) Pre-filling of cavities with buffer, C) formation of phospholipid monolayer using Langmuir-Blodgett (LB) and D) formation of phospholipid bilayer by fusing vesicles on LB monolayer.

2.2.4 Confocal Microscopy

All confocal images were recorded using a LSM 200 (Zeiss Microscopes, Germany) with an excitation wavelength of 488 nm, fluorescence was collected using a 505 longpass filter and reflectance was collected using a 420 longpass filter. Both fluorescence and reflectance were collected simultaneously at two separate detectors. All lipid bilayers imaged were labelled with 5 mol% DOPE-CF in both leaflets of the bilayer.

2.2.5 Fluorescence Lifetime Correlation Spectroscopy

Fluorescence correlation spectroscopy measurements were conducted using a Pico Quant Micro Time 200 Fluorescence lifetime imaging microscope (PicoQuant,

Germany). Point measurements where performed using an excitation wavelength of 640 nm and measurements were performed over 300 seconds each repeated in triplicate. The resulting autocorrelation curves where fit to a 2D diffusional model, as described in Chapter 1, to determine the diffusion coefficient of the lipid label. For all FLCS measurements lipid bilayers where labelled with DOPE-Atto655 at a concentration of 1 μM.

The radius of the observation volume (ω) was obtained by performing an FLCS point measurement at a 1 μM solution of Atto655 dye for 10 min. The resulting autocorrelation function was then used to find ω using the diffusion coefficient of the dye.

2.3 Results and Discussion

The main aim here is to develop methods of modification of PDMS substrates to render them hydrophilic so as to be suitable for lipid bilayer formation. The ability of these modified substrates to support lipid bilayers and the impact of treatment on bilayer fluidity will then be examined. After this, PDMS microcavity arrays will be fabricated and lipid bilayers are formed on them using vesicle fusion and a combination of Langmuir-Blodgett and vesicle fusion. These bilayers will be assessed by confocal imaging and Fluorescence Lifetime Correlation Spectroscopy (FLCS) to determine if the bilayers formed are spanning the cavities and if this has the effect of increasing lipid mobility.

2.3.1 Contact Angle Measurements of Modified Planar PDMS Surface

PDMS is a hydrophobic polymer, the molecular structure is shown in Figure 2.5, and therefore its interface must first be rendered hydrophilic to enable it to support a lipid bilayer. Two methods were employed to render the surface of PDMS hydrophilic; treatment with an UV/Ozone plasma or treatment with air plasma. In both cases the plasma is believed to oxidize the methyl groups on the surface of the PDMS and leading to formation of a SiOx network with interfacial hydroxyl groups which render the surface hydrophilic (see figure 2.5 below).[115]

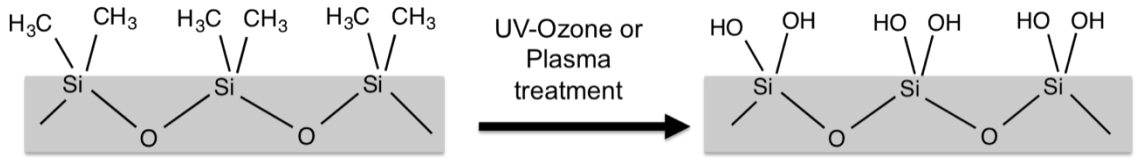

Figure 2.5: Conversion of PDMS surface groups by UV-Ozone of Plasma treatment.

Treatment of PDMS in an UV/Ozone cleaner for 1 h reduced the contact angle from 100º to 60º (as shown in Figure 2.6 below) whereas treatment with air plasma for 5 min resulted in a contact angle of 16º. This treatment renders the PDMS surface more hydrophilic than glass. As lipid vesicles are known to fuse to glass and spontaneously form lipid bilayers, it is safe to suggest that this may be the same for plasma treated PDMS given it yields the lowest water contact angle of the two approaches.

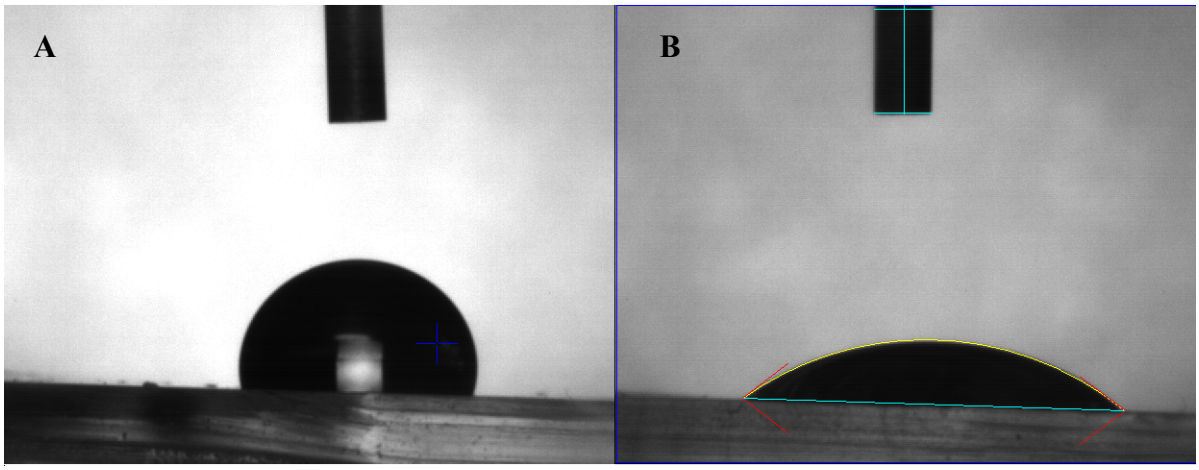

Figure 2.6: Contact angle image of a water droplet on A) untreated PDMS and B) Plasma treated PDMS

However a key issue with plasma treatment of PDMS is that as it yields only temporary modification of the surface chemistry, it has been shown that the hydrophilicity of air plasma treated PDMS can be lost over time due to low molecular weight species which migrate from the bulk PDMS to the surface and replace the newly formed hydroxyl groups, reverting the surface back to the native methyl groups.[116,117,118] Figure 2.7 shows the investigation of the recovery of contact angle for the PDMS treated as described above and found that typically plasma treated PDMS can recover its hydrophobicity within 2 h when exposed to air. However, we found that contact angle recovery can be delayed by storing the material under water, which maintains the contact angle below 60º for approximately 4 d.

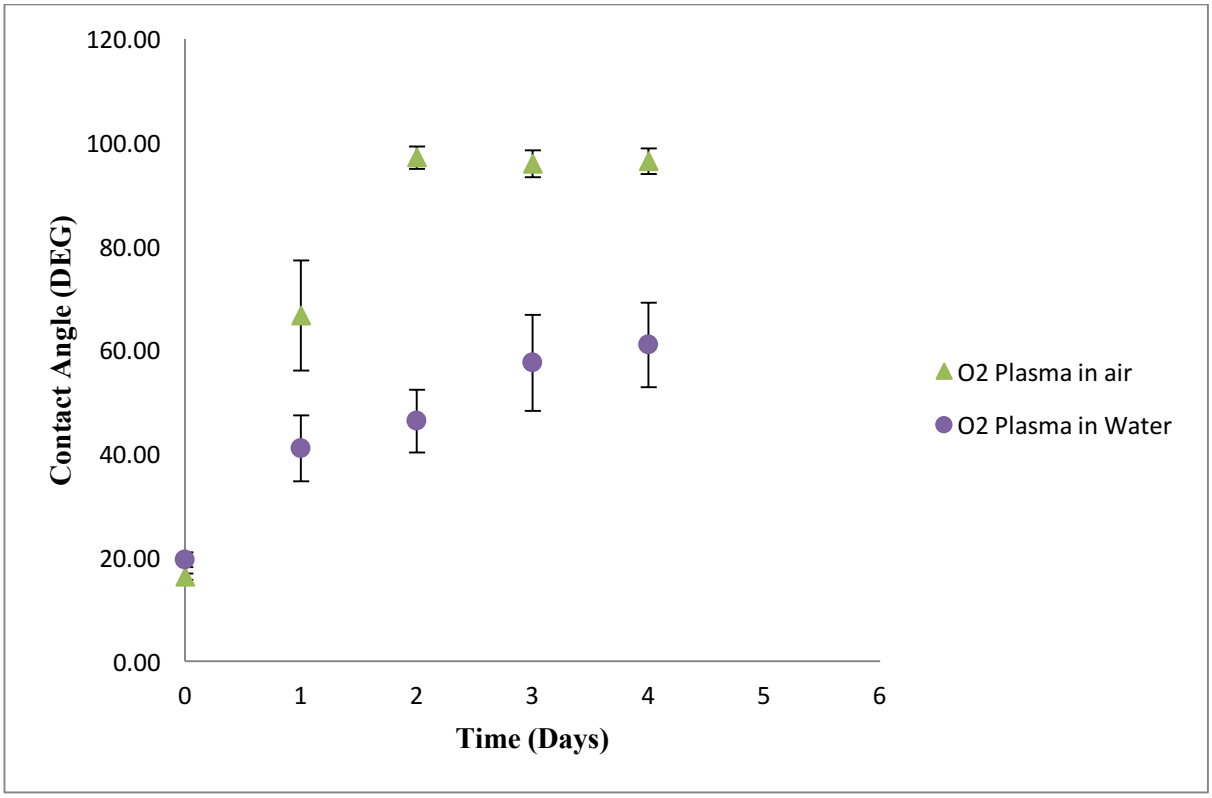

Figure 2.7: The difference in hydrophobic recovery of air plasma treated PDMS as a function of storage. Contact angle measurements were taken in triplicate once a day for 4 d. Error based on n = 5

To investigate the possibility of extending the lifetime of the hydrophilic interface in PDMS we explored alternative methods of modifying the interface. The hydroxyl groups formed on the surface of the PDMS after UV/Ozone or plasma treatment leave the surface open for further chemical modifications. Further modification of the surface may allow for the stabilisation of the PDMS's hydrophilicity. To investigate this, air plasma treated PDMS was further modified with a silane reagent, 3-aminopropyltriethoxysilane (APS), after plasma treatment was

investigated as well as adsorption of Bovine Serum Albumin (BSA) onto the PDMS surface as a means of stabilising the hydrophilicity (see figure 2.8). Treatment of plasma treated PDMS substrates in a 1 mg/mL solution of APS overnight should generate a layer of amino groups on the surface. This treatment resulted in a contact angle of 61.34° ± 3.87 which is higher than the contact angle of plasma treated PDMS. Therefore, this was not pursued further as a treatment method.

As BSA was used in a previous study for forming a double layer cushion on supported lipid bilayers,[88] modification of plasma treated PDMS surfaces by their overnight incubation in a 1 mg/mL solution of BSA protein was also investigated. BSA adsorption resulted in a contact angle of 59.02° ± 3.08, which is the same as UV/Ozone treated PDMS. This shows that further modification of plasma treated PDMS with BSA does not greatly improve the hydrophobicity of PDMS over Plasma treated PDMS.

Air plasma treatment of PDMS surfaces yielded in a contact angle of 15.93° ± 0.07, over just 5 min treatment. Therefore, air plasma results in formation of super hydrophilic (contact angle less than 20°) surfaces. It has been shown previously that superhydrophillic surfaces are excellent for bilayer formation with high lipid mobility.[59] As neither APS nor BSA treatment of oxidised PDMS attained a contact angle as low as that achieved after air plasma treatment, neither was deemed a useful alternative method to air plasma, even though this treatment is not stable it can be slowed down by storage under water.[119]

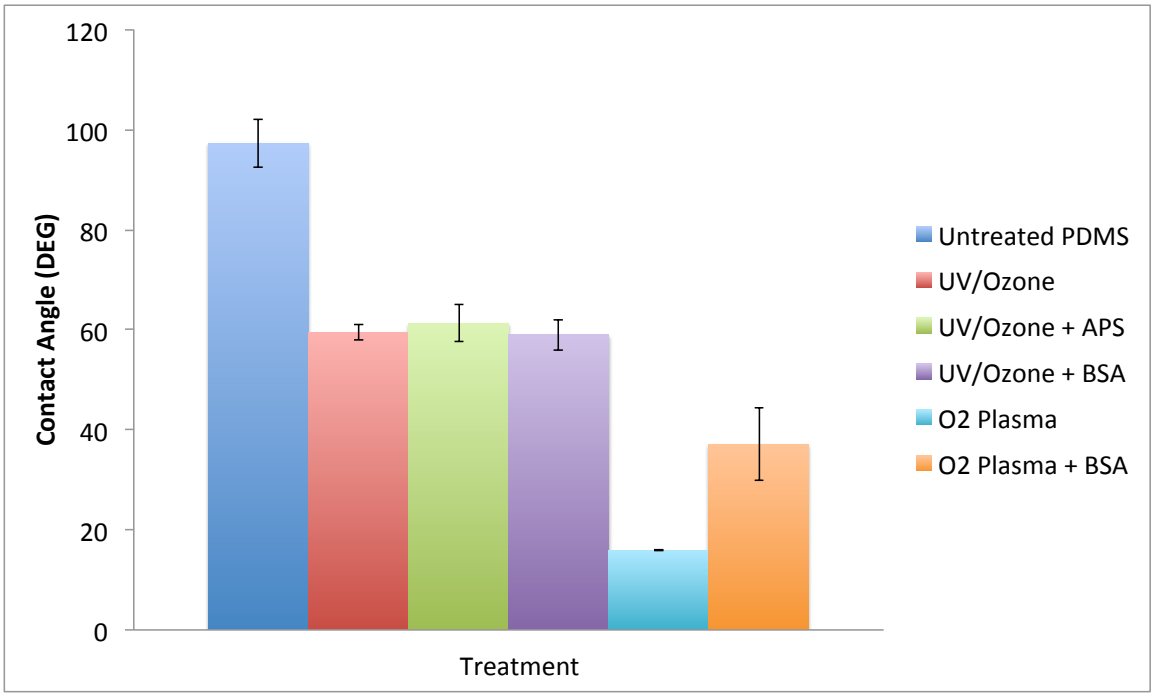

Figure 2.8: Bar chart showing contact angles (with water) for various treatments of planar PDMS error bars based on SD from n = 3.

2.3.2 Formation and Mobility of Supported Bilayers on Planar PDMS

The lateral diffusion coefficient of lipids in a supported lipid bilayer is dependent on the properties of the substrate. In general, the more hydrophilic the substrates, the more fluidic the bilayer.[57] This is due to the increasing thickness of the aqueous layer between the bilayer and the substrate with increasing hydrophilicity which improves the mobility of the lipids within bilayer. The fluidity of supported lipid bilayers of different compositions on Air plasma treated PDMS was investigated using Fluorescence Lifetime Correlation Spectroscopy (FLCS) to measure the diffusion coefficient of fluorescently labelled lipid. Bilayers where formed on air

Plasma treated PDMS by injection of small unilamular vesicles (SUV's) composed of 1,2-dioleoyl-sn-glycero-3-phosphocholine (DOPC) and 1 μM 1,2-dioleoyl-sn-glycero-3-phosphoethanolamine-ATTO655 fluorescent lipid (DOPE-ATTO655), this gave a molar ratio of 1:100,000 dye to lipid which is ideal for FLCS measurements. The SUV's where injected into a flow cell constructed from air plasma treated PDMS and a glass microscope slide (see figure 19 below). This spontaneously formed a bilayer on the lower glass surface as well as the upper plasma treated PDMS surface.

Three different lipid bilayer compositions where formed on the air plasma treated PDMS substrates to establish their versatility for measuring diffusion coefficients in supported lipid bilayers of different compositions. The lipid compositions used were; DOPC alone, 1,2-dimyristoyl-sn-glycero-3-phosphocholine alone (DMPC) and Egg L-α-phosphatidylcholine alone (EggPC). For all compositions, the bilayers were formed as described above and fluorescently labelled by including 1 mol% of DOPE-ATTO655 into the lipid composition. Fluorescent Lifetime Images (FLIM) were collected for each bilayer composition on the plasma treated PDMS surfaces. The images shown in figure 2.9 and clearly show the formation of a continuous and uniform fluorescence across the PDMS surface, which is consistent with formation of supported lipid bilayer

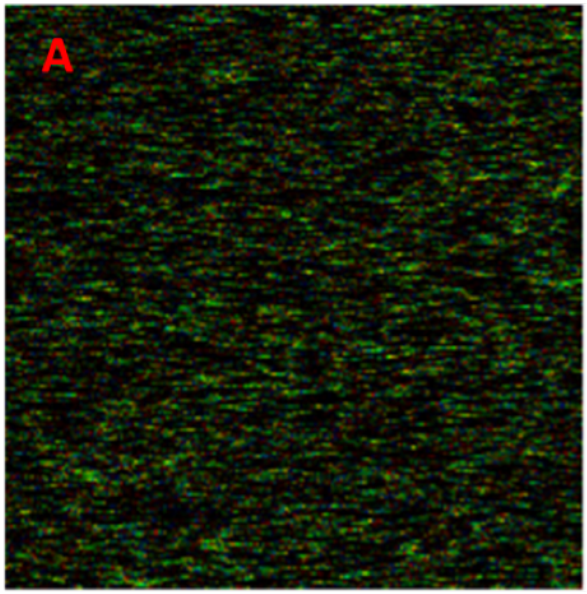

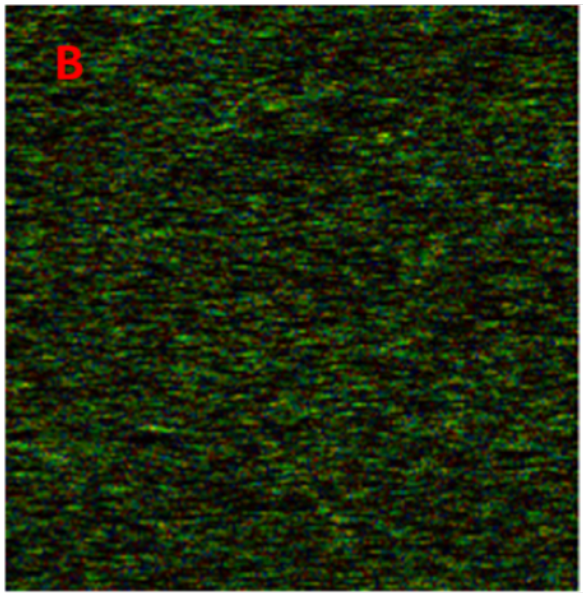

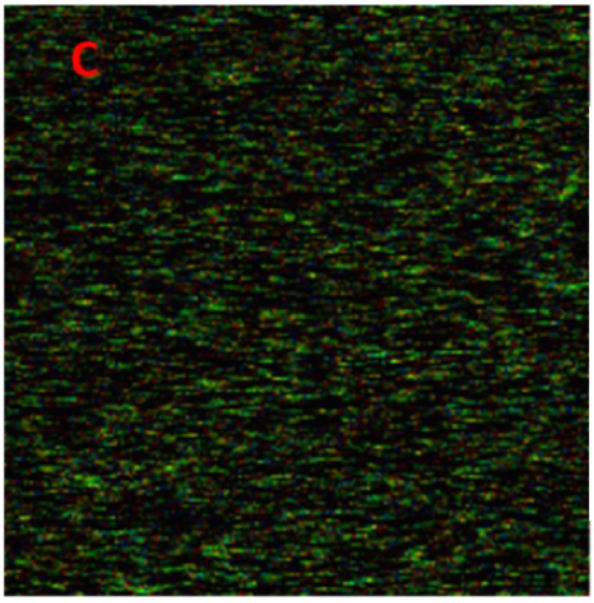

Sample	Florescence Intensity
A	3,977,317
B	4,514,448
C	3,926,605

Figure 2.9: 80 µm x 80 µm FLIM images of phospholipid bilayers on air plasma treated PDMS. Bilayers are composed of; A) DOPC, B) DMPC and C) EggPC. All bilayers are labelled with 1mol% DOPE-ATTO655 and use an excitation laser of 640 nm, fluorescence was collected with a 640 nm long pass filter for all images. The inset table showed the fluorescence intensity of each image measured using ImageJ software.

The lateral diffusion of each supported lipid bilayer composition on glass and PDMS were then measured and compared using Fluorescence Lifetime Correlation Spectroscopy (FLCS). This was done by performing point measurements for 300 sec in triplicate for each composition at the SLBs on PDMS and the glass surfaces. The location of the bilayer was obtained by scanning in the z-direction until the highest fluorescence intensity was obtained. The resulting autocorrelation functions are shown in figure 2.10 and were fitted to the following 2D diffusional model:

$$G(\tau) = 1 + \frac{1}{N} \frac{1}{1+(\tau/\tau_D)^{\alpha}} \qquad \text{(Equation 2.1)}$$

where N is the average number of fluorescent molecules in the observational volume, τ_D is the diffusion time. α is the anomalous exponent, which describes the mode of diffusion i.e.: the closer α is to 1 the more Brownian the diffusion. τ_D can extracted by fitting the experimental data and can be used to find the diffusion coefficient (D) using the equation below, once the observation volume (ω) is known[56] (see section 2.2.6 for detail on how ω was obtained).

$$D = \frac{\omega^2}{4\tau_D} \qquad \text{(Equation 2.2)}$$

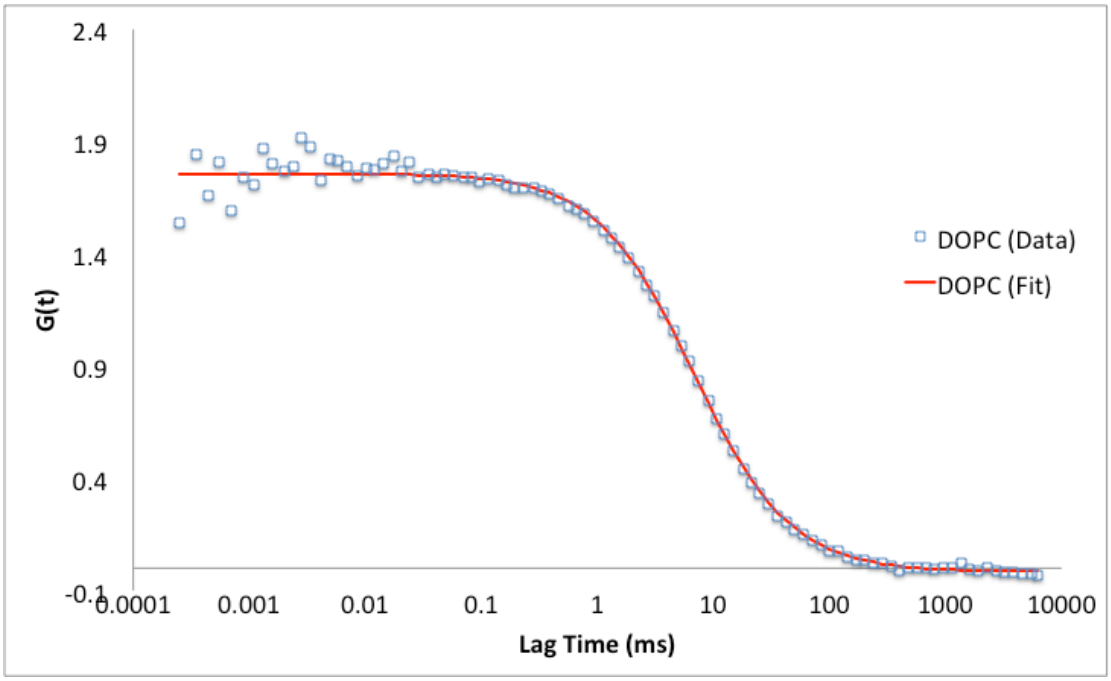
2.4
1.9
1.4
0.9
0.4
-0.1
G(t)
0.0001
0.001
0.01
0.1
1
10
100
1000
10000
Lag Time (ms)
DOPC (Data)
DOPC (Fit)

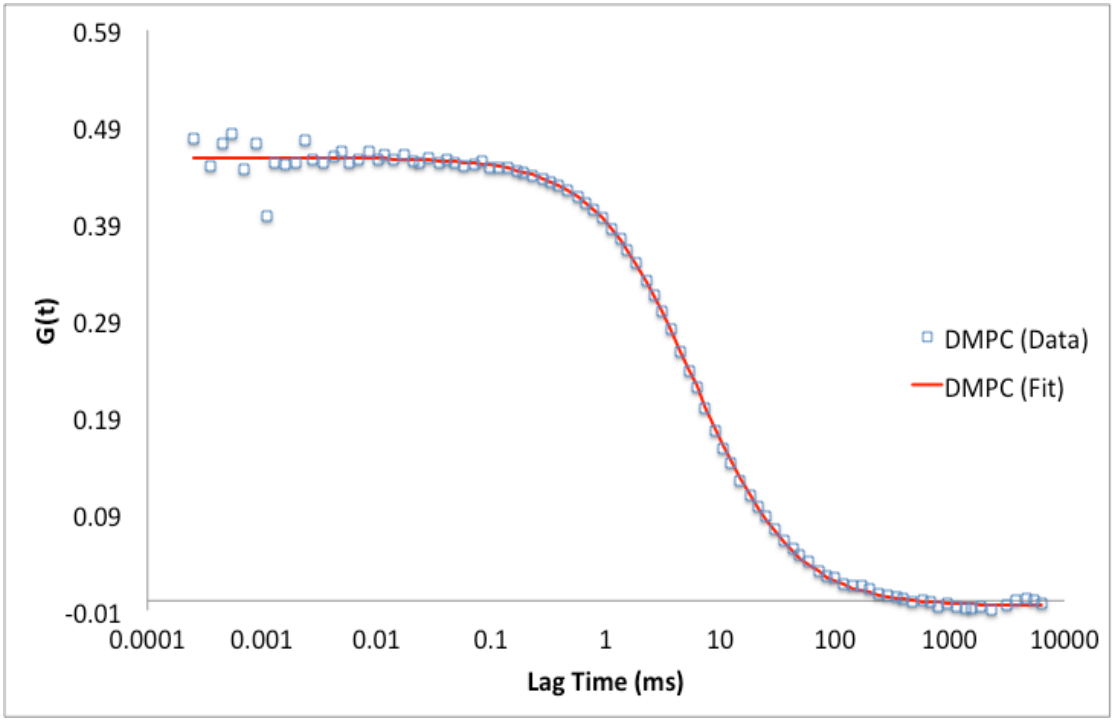
0.59
0.49
0.39
0.29
0.19
0.09
-0.01
G(t)
0.0001
0.001
0.01
0.1
1
10
100
1000
10000
Lag Time (ms)
DMPC (Data)
DMPC (Fit)

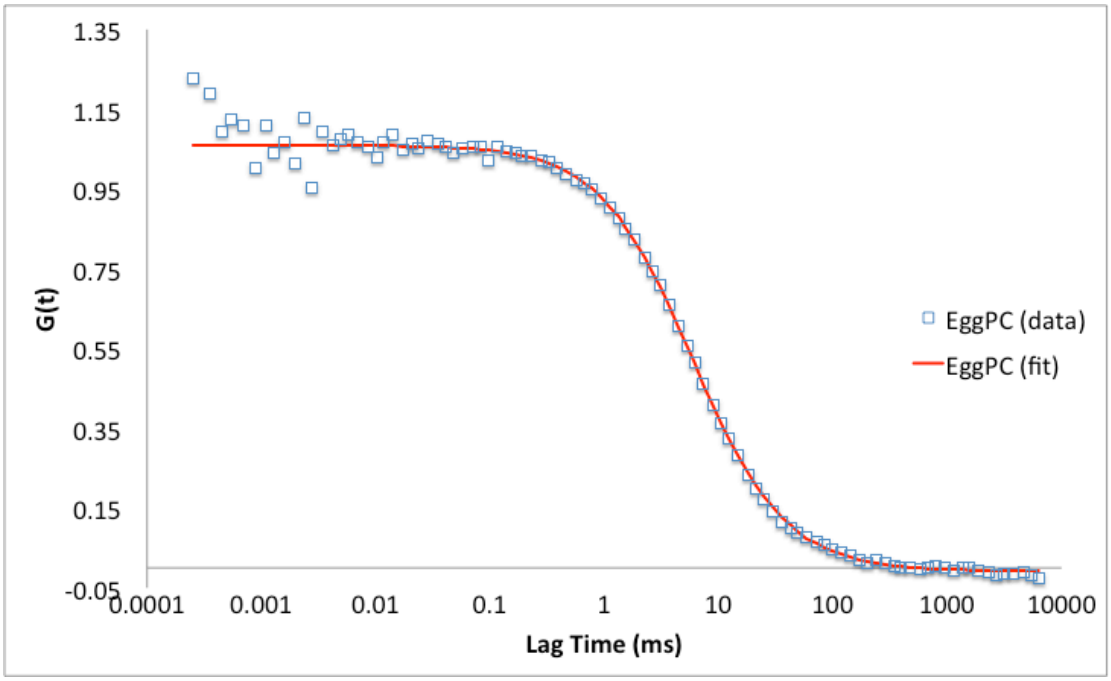

Figure 2.10: FLCS autocorrelation function for DOPC, DMPC and EggPC bilayers. All bilayers where labelled with 5 nM of DOPE-Atto655, fitted to 2D diffusion model. Fluorescent fluctuations at a single point on the PDMS surface where recorded for 300 sec. The excitation laser wavelength was at 640 nm and the fluorescence was collected with a 640 nm long pass filter.

Table 2.1: Diffusion Coefficients of various lipid compositions on glass and air plasma treated PDMS obtained by FLCS

Lipid Composition	Diffusion Coefficient Glass ($\mu m^2/s$)	α	Diffusion Coefficient Plasma Treated PDMS ($\mu m^2/s$)	α
DOPC	3.57 ± 0.14	1.04 ± 0.01	4.37 ± 0.12	1.02± 0.04
DMPC	4.37 ± 0.11	1.01 ± 0.01	4.85 ± 0.02	1.01 ± 0.01
EggPC	3.84 ± 0.32	1.06 ± 0.02	4.80 ± 0.10	1.04 ± 0.03

The above compositions where chosen as they are the widely studied compositions used for supported lipid bilayers.[65,120,121] The diffusion coefficients for each composition and substrate, are shown in table 2.1 above, and showed consistently faster diffusion on the PDMS surface when compared to the glass surface. However all are comparable to literature values of about 4.2 $\mu m^2/s$ obtained for DOPC and 5.5 $\mu m^2/s$ obtained for DMPC on glass substrates.[67,122] The ACFs of each composition fitted well to the 2 dimensional model and returned α values very close to 1 indicating Brownian lipid diffusion. Overall, the ability of the air plasma treated PDMS to disrupt and support a homogeneous lipid bilayer across multiple compositions is clear from the imaging and FLCS results. The high fluidity of each lipid composition, which exceeds that of the same SLB on a glass supports indicates that oxidized PDMS substrates are at least as suitable, as glass which is almost universally used for diffusional studies of supported lipid bilayers using FLCS.

2.3.3 Spanning Phospholipid Bilayers on PDMS Micro Cavities

Having established the suitability of air plasma treated PDMS to support SLBs, we then moved on to the application of microcavities in this material as substrates for MSLBs. Two methods were explored to span lipid bilayers across air plasma treated PDMS microcavities, vesicle disruption and a Langmuir Blodgett/vesicle fusion method.

The first method was the direct fusion of Small Unilamular Vesicles (SUV's), at the aqueous filled interface of the array as demonstrated before by Mallon *et al*.[123] However in this study, which was on gold cavities the diameter of the pores was just 850 nm. This aqueous prefilling was shown to be essential for spanning bilayers in these cavity sizes. PDMS microcavity substrates were formed by curing PDMS over a dried layer of 5 micron polystyrene spheres which had been deposited onto a piece of mica glued to a glass microscope slide as described in section 2.2.2. The microcavity array was then plasma treated for 5 min at 1000 mT pressure of air and then sonicated in Tris NaCl for 30 min to pre-fill the cavities with buffer. Small unilminar vesicles (SUV's) 100 nm in diameter composed of DOPC with 5 mol % DOPE-Carboxyflorescine (DOPE-CF) were formed as mentioned before (section 2.2.3). The fluorescent SUV's were then injected onto the PDMS microcavities, spontaneously forming bilayers on the PDMS. The bilayers were then examined by confocal microscopy to determine if the bilayers were spanning the cavities. However, as seen in figure 2.11, for cavity sizes used in this study, the bilayers formed did not span over the cavities but rather conformed to the interior walls of the cavity. This resulted in a bright ring of fluorescence around the cavity. The intensity of the edges

due to the fact that the confocal z-plane is elongated and so the fluorescence from the cavity walls which are encompassed within the volume appear brighter. This is also evident from the z-scan image below. The inability to span cavity dimensions of 2 to 5 microns by this method is thought to be due to the diameter of SUV's which are significantly smaller than the diameter of the cavity opening, allowing them to enter and fill the cavity.

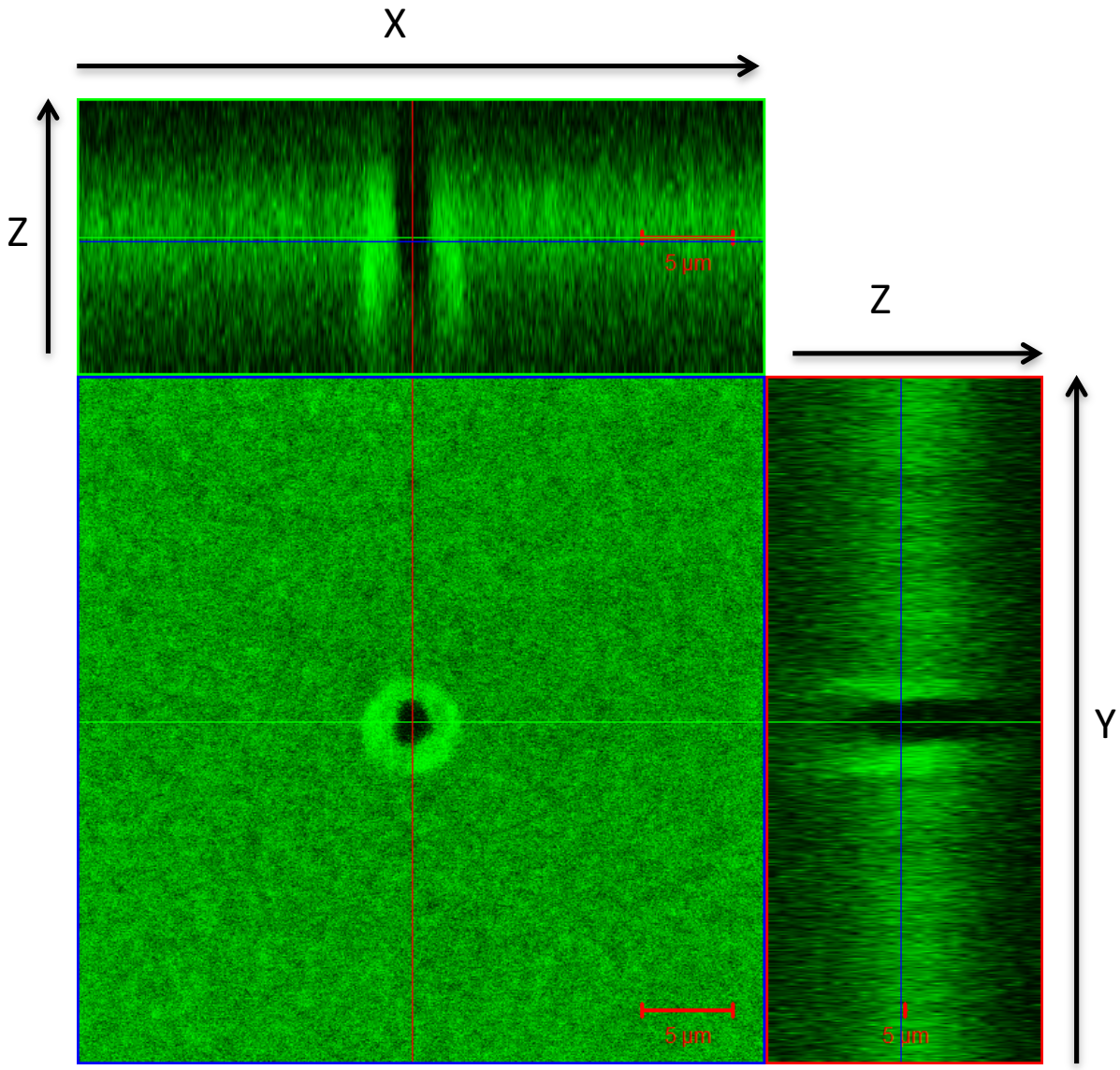

Figure 2.11: Z-stack confocal imaging of bilayer DOPC bilayer containing 5 mol % DOPE-Carboxyflorescine label on 5 micron diameter cavities in PDMS. Excitation wavelength was at 488 nm; fluorescence was collected using a 505 long pass filter.

The alternative method was then explored which involved the deposition of a Langmuir-Blodgett (LB) monolayer onto plasma treated PDMS microcavities, which were pre-filled with Tris NaCl buffer. The LB deposited monolayer was composed of DOPC with 1 mol% DOPE-CF, to allow for imaging with confocal microscopy. SUV's containing the same composition as before where then fused onto the monolayer. As figure 2.12 shows, this method proved effective in forming bilayers spanning microcavities at aqueous filled microcavities ranging from 1 μm to 5 μm diameter. Critically, confocal fluorescence imaging of theses bilayers showed that the bilayer was only spanning cavities that were successfully pre-filled with buffer.

The PDMS arrays have an important advantage; There is a significant refractive index difference between PDMS ($n \approx 1.45$) and the buffer ($n \approx 1.33$) and due to the spherical porous nature of the cavities, the incident laser light scatters strongly at the positions of the filled cavities and results in significantly brighter spots in the reflectance image than the unfilled cavities or the planar regions of the PDMS. This is a very useful characteristic which allows for accurately and precisely locating pores with suspended lipid bilayers.

It is clear from the reflectance images that not all cavities are filled with buffer after sonication and that the degree of filling appears to decrease with increased cavity diameter. Unlike gold which we found very effectively fills with buffer, in PDMS, this is presumably because of the hydrophobicity of this medium and difficulty in plasma treatment of the cavities areas. It is clear from the fluorescence images for 3 and 5 micron cavities that the bilayer exclusively spans over cavities that are pre-filled, whereas it coats the interior of the cavities that are unfilled. However, in the case of 1

micron cavities shown here there appears to be no aqueous filling according to the reflectance image, yet a homogeneous fluorescence indicates that the bilayer appears to be spanning. It would appear that the aqueous support in the fluid filled cavities is necessary for the Langmuir-Blodgett monolayer to assemble across the cavity in cavities exceeding 1 micron diameter. Whereas LB is capable of forming continuous monolayers over smaller cavities that are not aqueous filled. For the larger pore sizes, occasional pores which are not filled do not present an issue in the FLCS measurement since these measurements are conducted on a cavity by cavity basis and as described, it is easy to identify which cavities are not filled.

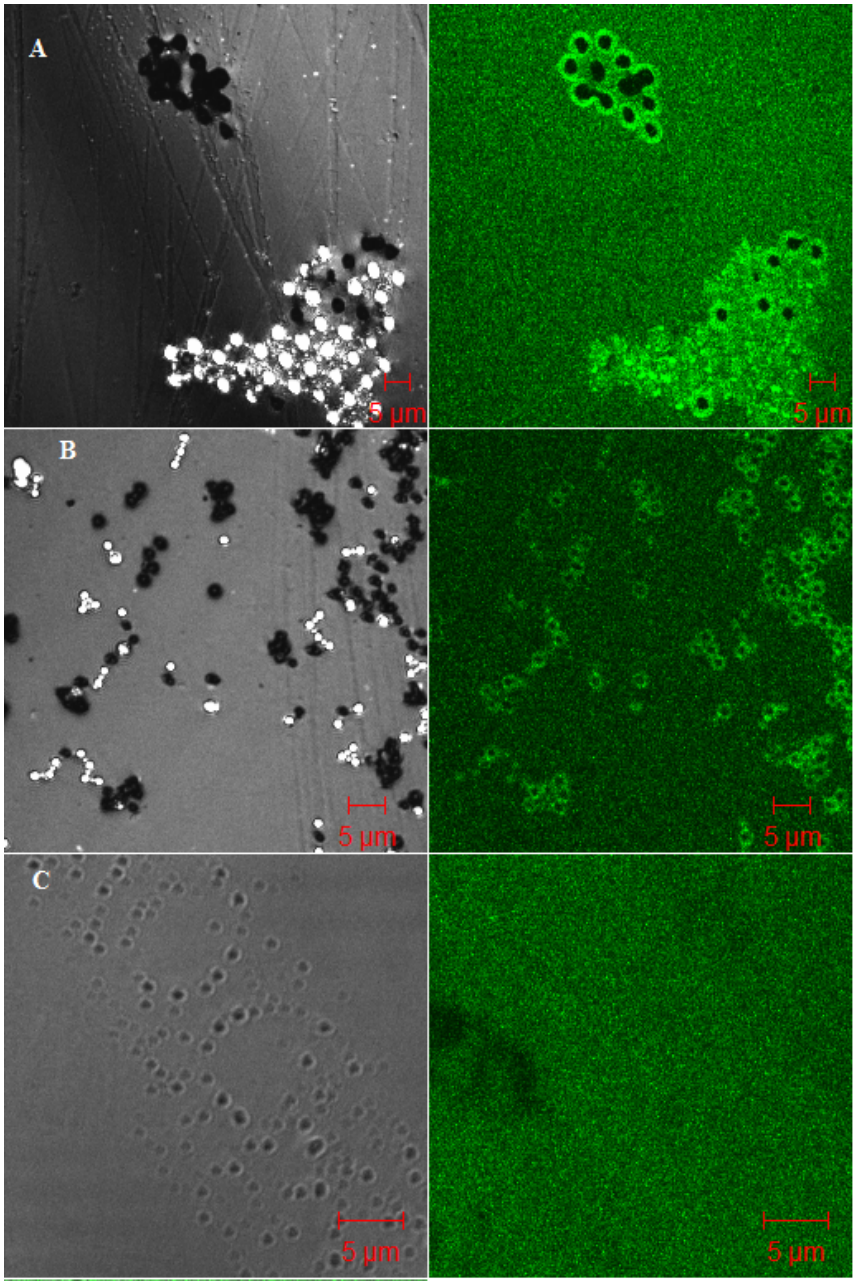

Figure 2.12 Confocal Images, with reflectance on the left and fluorescence on the right, of cavities made with A) 5 micron, B) 2 micron and C) 1 micron polystyrene spheres. Excitation wavelength was 488 nm, fluorescence was collected using a 505 longpass filter and reflectance was collected using a 420 longpass filter. Both fluorescence and reflectance where collected at the same time using two different channels. In all cases the bilayer was composed of DOPC with 10 mol% DOPE-CF

2.3.4 Diffusion Studies of Supported Bilayers on PDMS Micro Cavities

Lipid diffusion at cavity substrates was examined using FLCS. Point measurements were taken, in triplicate, on planar areas as well as directly over cavities across all diameter substrates studied. The autocorrelation functions where fit to the same 2D diffusion model described above (equation 2.1). It was observed that the diffusion of lipids on flat areas were 4.1 ± 0.1 $\mu m^2/s$ with an α value of approximately 1 i.e. = 0.997 ± 0.002 for all cavity sizes, which agrees well with the data described for planar plasma treated PDMS cited above. However, interestingly, diffusion coefficients for lipid above cavities were found to be two to three times faster than lipids on flat areas the data are presented in table 2.2.

Table 2.2: Diffusion values measured by FLCS for DOPC bilayer labelled with 1 mol% DOPE-Atto655 over various sized PDMS cavities. The data below for each cavity size comes from the measurement of 3 separate samples, in each sample at least 3 separate cavities were measured.

Cavity Size (µm)	Diffusion Coefficient ($\mu m^2/s$)	α
5	11.2 ± 0.4	0.992 ± 0.002
3	10.2 ± 0.6	0.989 ± 0.004
1	7.1 ± 0.3	1.012 ± 0.004
Planar	4.1 ± 0.1	0.997 ± 0.002

These fast diffusion values over cavities are attributed to the depth of the underlining wells environment provided by buffer filled cavities. The bilayer experiences a bulk aqueous environment at both interfaces leading to a lipid bilayer, which is effectively free standing above the cavities with an aqueous interface at each side. This effectively decouples the lipids from the surface and allows them to diffuse freely in 2 dimensions with minimal influence from the underlying substrate. The diffusion of the DOPC lipid bilayer measured over 1 μm diameter cavities is comparable to lipid diffusion measured in Giant Unilamellar Vesicles (GUV's) which has been measured as 7.8 $\mu m^2/s$.[120] Interestingly, the results also show that the diameter of the cavity influenced the diffusion coefficient observed. The origin of this effect is not clear, it may originate from the curvature of the bilayer, which may be greater at wider diameter apertures. This has been demonstrated by AFM for DMPA/DMPC bilayers on silicon pores ranging 300 nm to 1 micron, though not for apertures as large as described here.[91] Alternatively it may be influence of lipid diffusion from planar regions of the array, in smaller pore sizes precisely locating exciting laser volume in the centre of the cavity may not be achieved and some contribution from planar lipid diffusion may be contributing to the ACF. Overall however, the data above shows that the lipid diffusion is significantly faster over cavities, which is an indication that there is minimal influence on the lipids from the substrate; it was logical to assume the same would apply for transmembrane proteins and indeed as subsequent work on these platforms demonstrated, reconstituted membrane proteins diffuse 100% over the cavity regions.[124]

2.4 Conclusions

A number of methods for treating PDMS to improve its hydrophilicity were explored in order to enable lipid bilayer formation at PDMS supports and to promote stability of the bilayer once formed. It was found that the most efficient way to improve hydrophilicity is to treat the PDMS with air plasma. Supported lipid bilayers of various compositions were demonstrated to for at the air plasma treated PDMS substrates. Homogenous SLBs were formed on PDMS using vesicle fusion and lipid diffusion in these assemblies is slightly better than on glass. The diffusion coefficients of the lipid bilayers across these platforms were higher than those of analogous compositions on glass.

This work also demonstrated a new method for forming freestanding lipid bilayers over PDMS microcavity arrays with pore dimensions ranging from 1 to 5 μm diameter using a combination of the Langmuir-Blodgett and vesicle fusion. We have measured the diffusion coefficients of lipids over these cavities and shown that they are 2 to 3 times faster than on planar PDMS, and very similar to diffusion coefficients of lipids in free-standing liposomes confirming that these substrates are potentially valuable for diffusional studies of trans membrane proteins. Indeed, in separate work, the cavities were subsequently employed for study of a range of membrane proteins where they were found to both reconstitute efficiently and exhibit mobility only observed previously in liposomes.[103]

Chapter 3

Characterization of Suspended Lipid Bilayers on Gold Microcavity Substrates.

3.1 Introduction

Artificial models of biological membrane can provide valuable insight into the behaviour of the membranes lipids and associated proteins and sugars by mimicking key facets of the cell membrane structure decoupled from the challenging complexity and redundancy of the living cell. The lipid membrane is a semipermeable barrier, largely impermeable to large and aqueous soluble molecules and ions. Transport across the cell membrane is highly regulated and ion transport is assisted by membrane proteins, usually ion channels, and others lipid soluble carrier molecules. Such ionophores are lipid soluble molecules, which passively transport ions down the concentration gradient.

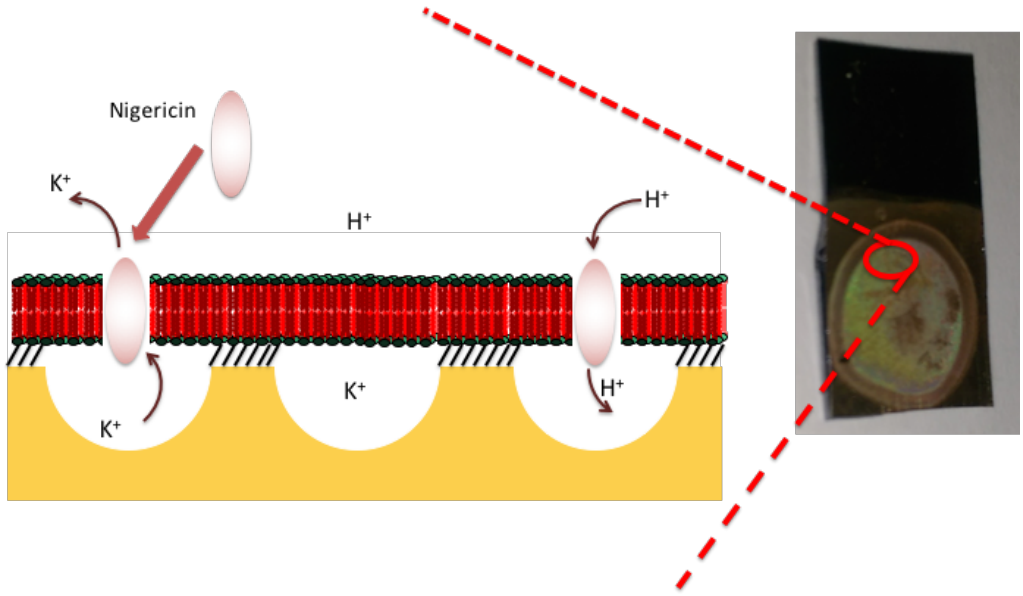

Figure 3.1 Schematic of ionophore transport across a lipid bilayer spanning gold microcavities.

A number of model systems have been used to investigate ion carriers in lipid membranes. Black lipid membranes (BLM's), formed where phospholipid in organic media is painted across an aperture at a structure which is then placed into an aqueous solution so that there is an aqueous interface at both bilayer sides. BLMs have been widely applied to the investigation of the electrical properties of the bilayer including the study of channel forming proteins Gramicidin[48] and OmpF[49] as well as Valinomycin, which is a uniporter of K^+ ions.[125] However, BLMs have a number of drawbacks which reduce their versatility and biorelevance. Painting the film from organic solvent frequently results in formation of lipid multilayers, rather than bilayers, and yields layers which incorporate organic solvent residue.[50] In general, they exhibit very poor stability,[126] it is also difficult to incorporate proteins and other complex biomolecules into BLMs.

As described in chapter 1, supported lipid bilayers (SLB's) overcome many of the limitations of BLM's. The have increased stability usually lasting for days rather than hours. SLB formation is usually by vesicle fusion, or Langmuir-Blodgett method, or a combination of the two. These methods are less restrictive on the lipid compositions than painting, and are organic solvent-free, so amenable to incorporation of membrane proteins. However, a key drawback of SLBs is the bilayer's proximity to the supporting substrate, which can cause protein substrate interactions that affect protein diffusion and activity. Unlike BLMs this proximity to the substrate also greatly limits the depth of the aqueous environment below the bilayer meaning that the ionic concentration can only be controlled from one side of the bilayer. Other approaches to the study of ion channels have included the study of phospholipid

monolayers at mercury electrodes.[127,128] The key advantages of mercury as a platform for lipid mono and bilayers is its fluidity which yields an electrochemically addressable and defect-free surface on which the mono or bilayers are assembled; it has enabled very accurate impedance models, and is highly sensitive to ion transport and for screening of membrane-molecular interactions.[129] Tethered bilayer lipid membranes (t-BLM's) have also been employed in recent years to study ion transport across the membrane.[130] They, like SLB's, overcome some of the issues posed by BLM's, like stability, ensuring a true bilayer is forming, and solvent residue. However, they still suffer from lipid substrate interactions and often involve using thiolated lipids for the leaflet of the bilayer that is closest to the substrate. In addition, they do not provide the opportunity to independently control the ionic reservoir below the lipid bilayer.[105]

Related studies by our group previously demonstrated that aqueous filled gold nanocavities supported mobile lipid bilayers formed from vesicle disruption across 800 nm diameter cavities.[123] This work advances this development to progress to larger sized gold cavities to facilitate EIS studies at gold electrode structures. This work exploits the cavity arrays to build DOPC bilayers to study ion transport behaviour of two ionophores, Valinomycin which is a K^+ uniporter and Nigericin which is a K^+/H^+ antiporter, into microcavity spanning lipid bilayers, and investigate the effect of introducing anionic gradients across the lipid bilayer. In doing so we exploit a key advantage of the cavity nature of the structure; its capacity to be fluid filled, which allows us to build bilayers at two aqueous interfaces with distinct ionic strengths. We confirm the bilayer has formed and is mobile using fluorescence

microscope and exploit Electrochemical Impedance Spectroscopy (EIS) to investigate the electrical properties of the resulting microcavity supported lipid bilayers as a function of ionophore and ionic gradient.

3.2 Experimental

3.2.1 Fabrication of Gold Microcavity Substrates

Gold microcavity substrates were prepared by cleaning 1 cm x 2 cm pieces of gold silicon wafer (AMS biotechnology) with ethanol and drying with nitrogen. Half of the wafer was then covered with Teflon tape leaving a 2 cm x 1 cm area of wafer exposed. Next 200 μL of a 0.5% (w/w) solution of 2.88 micron Polystyrene spheres was deposited onto the wafer and allowed to dry at room temperature overnight.

Gold was then electrochemically deposited onto the wafer, through the gold templating spheres using a commercially available electroplating solution (Technic Inc.). The electroplating solution was degassed with nitrogen for 20 min prior to electroplating. Electroplating was carried out on a CH660 potentiostat (CH Instruments Inc.) using a standard 3 electrode set up which consisted of an Ag/AgCl reference electrode, a platinum counter and the wafer as the working electrode. The electroplating was performed at an applied potential of -0.95 V until a charge of 0.7 C was obtained on the working electrode. It should be noted, however, that these conditions work for the electroplating solution used in this work, however when a new solution is used it was found that these conditions needed to be optimised again.

Following electrodeposition, the substrates were rinsed with DI water to remove any remaining electroplating solution and were then sonicated for 1 h in THF to remove the polystyrene spheres. This yielded substrates with ordered arrays of cavities of approximately 2.88 micron diameter.

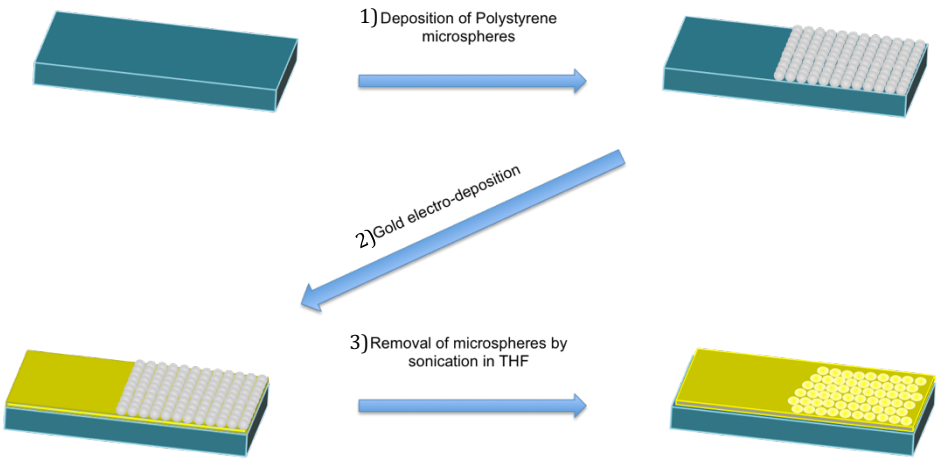

Figure 3.2 Overview of steps involved in gold microcavity array preperation. 1) 2.88 μm PS spheres are dropcast on to a silicon wafer which has a layer of vapor deposited gold. 2) Gold is electrochemicaly grown. 3) PS spheres are remover by sonication in THF.

3.2.2 Characterisation of Gold Microcavity Substrates by Cyclic Voltammetry

The electro-active surface areas of the gold microcavity electrodes were measured by cyclic voltammetry. The voltammogram of 4 microcavity electrodes were measured in a degassed solution containing 0.1 mM of potassium ferricyanide and 1 M potassium chloride in water. All four electrodes were measured over a potential window from 0 to + 600 mV (vs. Ag/AgCl) at scan rates of 20, 40, 60, 80, 100, 120, 150 and 200 mV/s. The peak current was taken for each scan rate to give a

plot of (scan rate)$^{1/2}$ vs. peak current. These plots were then applied to the Randles-Slevik equation to calculate the electro-active area of the microcavity electrodes.

3.2.3 Formation of Suspended Lipid Bilayers on Gold Microcavity Substrates

To build phospholipid bilayers on the gold microcavity array, the substrates were rendered hydrophilic by first modifying the top surface of the array with a mercaptoethanol self-assembled monolayer by immersing the substrates in a 1 mM solution of 2-mercaptoethanol overnight. The SAM modified substrates were then rinsed with ethanol and dried with nitrogen.

To fill the cavities, the substrates were sonicated for 1 h in Tris buffer. This is an important step, as it is necessary to sonicate to properly fill the cavities, as discussed previously.[112] After sonication, the lipid bilayers were formed using a combination of Langmuir-Blodgett to form the proximal leaflet followed by vesicle fusion to form the distal leaflet, as described for microcavity PDMS in section 2.3.

3.2.4 *Fluorescence Lifetime Correlation Spectroscopy of Suspended Lipid Bilayers on Gold Microcavity Substrates*

Fluorescence correlation spectroscopy measurements were conducted using a Pico Quant Micro Time 200 Fluorescence lifetime imaging microscope. Point measurements were performed using an excitation wavelength of 532 nm and measurements were performed over 300 sec each repeated in triplicate. The resulting

autocorrelation curves where fit to a 2D diffusional model to determine the diffusion coefficient of the lipid label. For all FLCS measurements lipid bilayers were labelled with 2-(4,4-Difluoro-5,7-Dimethyl-4-Bora-3a,4a-Diaza-s-Indacene-3-Pentanoyl)-1-Hexadecanoyl-sn-Glycero-3-Phosphocholine (β-BODIPY-C5-HPC) at a concentration of 1 nM. The location of the bilayer was obtained by scanning in the z-direction until the highest fluorescence intensity was obtained

The radius of the observation volume (ω) was obtained by performing an FLCS point measurement at a 1 μM solution of Atto655 dye for 10 min. The resulting autocorrelation function was then fitted using the diffusion coefficient of the dye to find ω as described previously in chapter 2.

3.2.5 Incorporation of Ionophores into Microcavity Suspended Lipid Bilayers

The ionophores, Nigericin and Valinomycin, were incorporated into DOPC bilayers suspended over gold microcavities by incubating the DOPC bilayer on gold in a Tris NaCl solution containing 0.5 % (V/V) of ethanol and 10 μM of the selected ionophore. The substrates were incubated with the ionophore solution for 1 h at 20^{o}C after which it was gently rinsed in Tris NaCl to remove any of the ionophore that was not associated with the bilayer.

3.2.6 Electrochemical Impedance Spectroscopy

Electrochemical impedance was performed using a CH660A potentiostat (CH Instruments). A standard 3-electrode set up was employed which consisted of an Ag/AgCl reference electrode a platinum counter electrode and the microcavity array as the working electrode. The impedance was measured over a frequency range of 100,000 Hz to 0.01 Hz with an AC modulation amplitude of 0.005 V at a potential bias of 0 V (vs Ag/AgCl). All measurements where run in a glass cell (approximate volume of 15 mL) in Tris NaCl buffer at pH 7.4.

3.3 Results and Discussion

3.3.1 Characterization by Scanning Electron Microscopy

Gold microcavity arrays were formed by electroplating gold through 2.88 micron polystyrene spheres. Templating spheres were deposited onto gold sputtered silicon wafers with (See section 3.1.1 for further details). A number of trial experiments had to be performed to optimise the conditions required for deposition. It is important to note that these conditions are required to be re-optimised when using a new electrodeposition solution. A representative example of the i-t curve obtained during gold electrochemical deposition is shown in figure 3.3 below. After electroplating, the polystyrene spheres were removed from the substrates by sonication in THF for 30 min. Figure 3.4 shows an SEM image of the cavities formed and reveals the close packed spherical pore arrangement. Image analysis was carried

out using ImageJ software and the cavity diameter distribution was obtained, which is shown in Figure 3.5. The figure shows that the cavities are uniform and monodisperse with a size distribution of 2.69 ± 0.06 microns. The total surface area of the electrode can also be estimated using the SEM images, assuming that each cavity is hemispherical and that all cavities have a diameter of 2.88 microns. This results in an estimated surface area of a 1 cm^2 electrode of 1.94 cm^2.

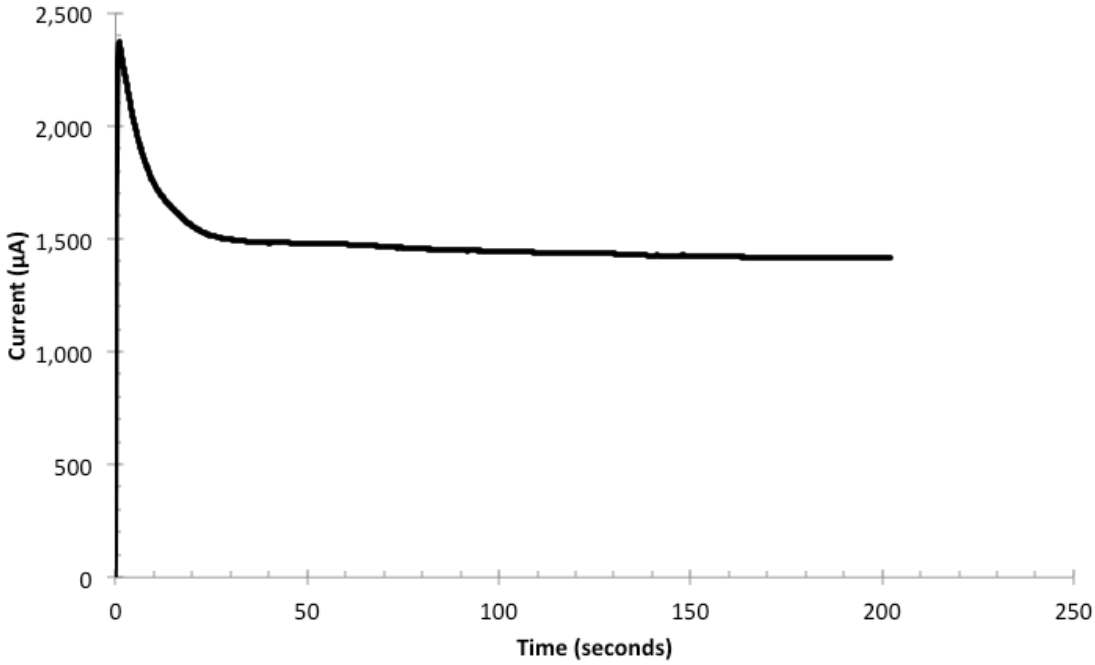

Figure 3.3 A representative example of the characteristic i-t curve observed during the electrodeposition of gold onto a wafer with 2.88 micron PS spheres present.

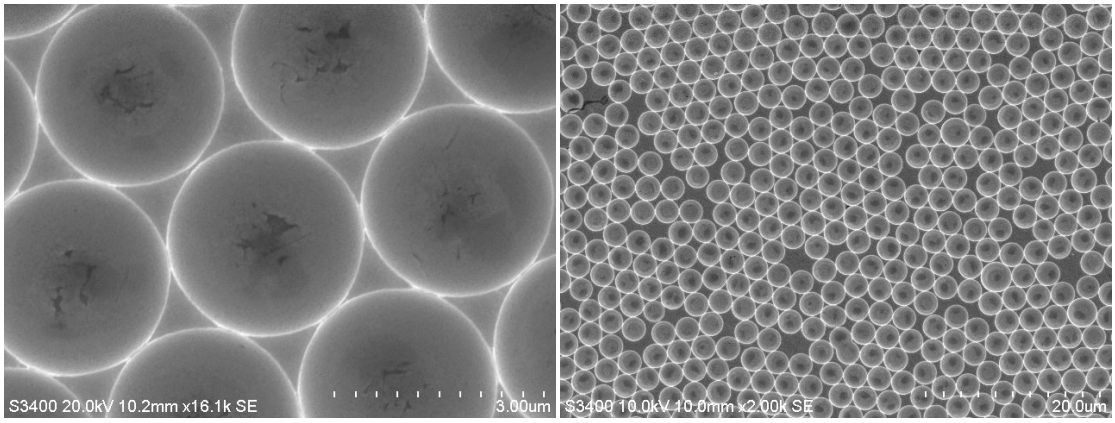

Figure 3.4 SEM images of gold microcavities formed from i-t curve above under the same conditions electro deposition of gold using 2.88 µm diameter polystyrene spheres as templates.

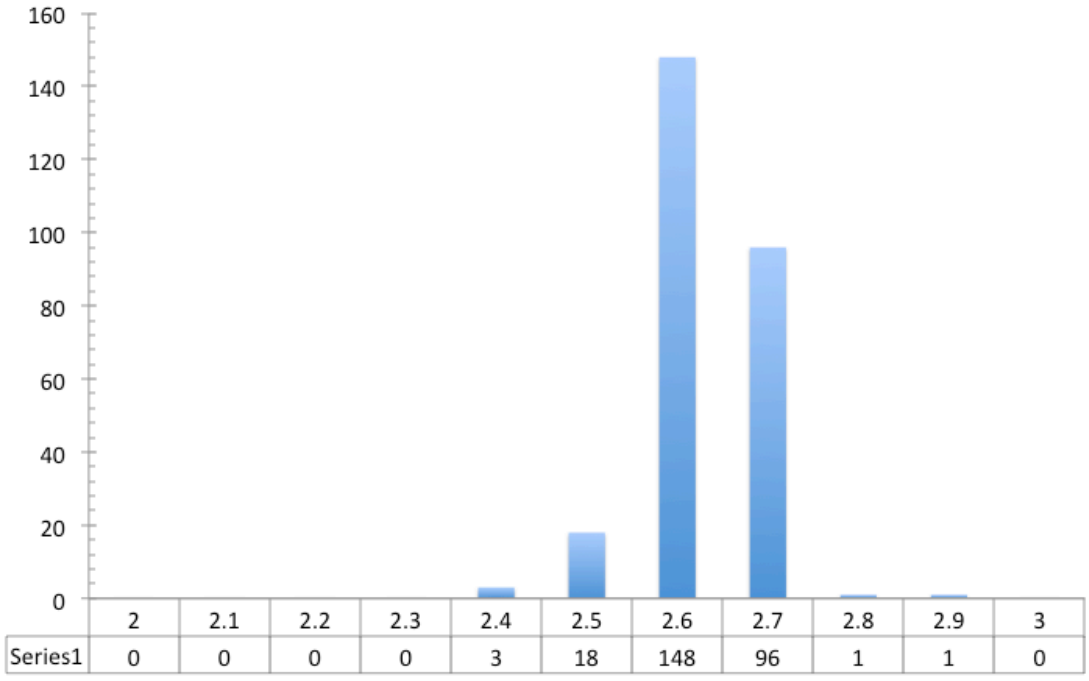

Figure 3.5 Size distribution for gold cavities formed using 2.88 micron PS spheres which produces cavities of diameter 2.69 ± 0.06 µm.

3.3.2 Characterization of Gold Microcavities by Cyclic Voltammetry

In order to accurately quantify the resistance and capacitance of bilayer systems on gold microcavities by impedance it is essential to know the electroactive area of the electrode. In order to establish this, three gold micro cavities were prepared as described previously; the spheres were removed with THF resulting in 2.69 micron diameter aperatured cavities as shown above. Cyclic voltammetry was carried on 0.1 mM potassium ferricyanide in 1 M KCl. The potential was scanned from 0 to 0.80 V, using the cavity array electrodes as the working electrode, and the CVs were collected at various scan rates. The Randles-Sevcik (equation 3.1) was applied to the scan rate dependent data by plotting i_p versus $v^{1/2}$, where i_p is peak current, n is the number of electrons transferred, F is Faradays constant, A is area of the electrode in cm^2, D is the diffusion coefficient for potassium ferricyanide (7.09 x 10^{-6} cm^2/s), C is the concentration of potassium ferricyanide used in mol/cm^3 and v is the scan rate in V/s.

$$i_p = 0.4463\ \mathrm{nFAC}\left(\frac{nFvD}{RT}\right)^{\frac{1}{2}} \qquad \text{(Equation 3.1)}$$

A representative plot of $(\text{scan rate})^{1/2}$ vs. peak current for a microcavity array substrate along with the linear fit to the is shown in (see Figure 3.6).

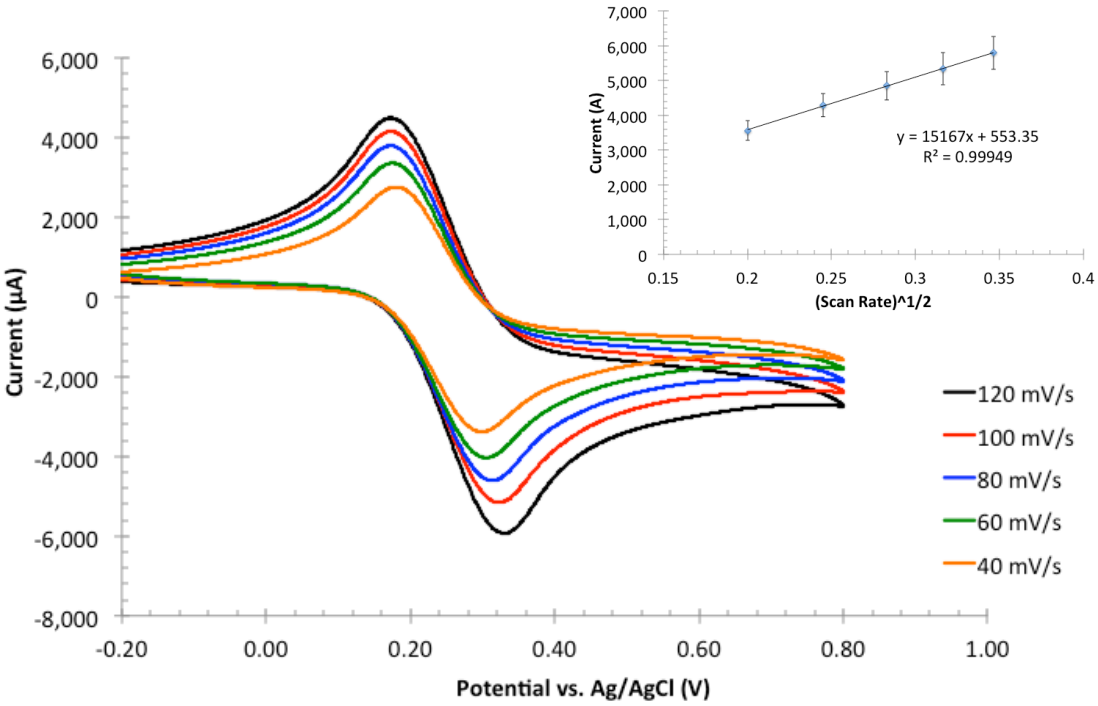

Figure 3.6 An example cyclic voltammogram of one gold microcavity measured in 10 mM $K_4[Fe(CN)_6]$ and 1 M KCl as the supporting electrolyte at 120, 100, 80, 60 and 40 mV/s. Insert shows plots of $\sqrt{}$Scan Rate Vs. oxidation peak current. The current plotted here is the average oxidation peak current of 3 different untreated Gold microcavity electrodes (vs Ag/AgCl).

The slope of plot in figure 3.6 was fit to the Randles-Sevcik equation (Equation 3.1) and the electro-active area of each electrode was determined and is shown in Table 3.1. From the data in Table 3.1 it is evident that the electroactive area of each of the independently prepared arrays is very similar. This is important as its speaks to the reproducibility of the fabrication method, particularly given the complexity of the arrayed structure and possibility for forming planar defect regions which will alter the surface area An average area of these three electrodes was calculated to be 2.12 cm^2 with a deviation of ± 0.20 cm^2. This small deviation between the electrodes means it

is acceptable to assume that any gold cavity array made using 2.88 micron spheres will have an approximate surface area of 2.12 cm^2. Interestingly, there is also good agreement between this value and the surface area of 1.94 cm^2 calculated using the SEM images. It is important to note that the system descried here does not seem to completely follow the Randles-Sevcik equation. This is apparent in the plot of i_p versus $v^{1/2}$ in Figure 3.6 where the intercept of the trend line is not zero. This means that it may not be accurately depicting the true surface area of the cavity arrays but rather the top surface of the cavities.

Table 3.1 Electroactive area determined from the Randles–Sevcik equation of three independently different gold cavity array substrates.

Electrode	Slope of Trend line	Electro-active Area (cm^2)
1	1.58×10^{-2}	2.21
2	1.35×10^{-2}	1.89
3	1.62×10^{-2}	2.27
Average		2.12± 0.28

3.3.3 Selective surface modification of the Arrays:

The gold microcavity array preparation and selective top surface modification was carried out according to a protocol previously described by our group[131] and was necessary to increase the hydrophilicity of the gold. Our group previously that lipid bilayer is readily supported across aqueous filled gold cavities of 800 nm diameter.

Therefore, initially we attempted to form bilayers across aqueous filled but unmodified gold arrays. However, we found for the larger dimensioned pores >1 micron diameter the bilayer did not span uniformly across the array, ie. there was always a fraction of the pores that the bilayer coated or that did not fill effectively, and the stability of the MSLB is lower, reflected in EIS signal that, unlike the data presented here, drifted over time.

Because of the uniformity of coverage required for EIS measurements it was necessary to modify the top surface of the array is necessary to ensure the lipid bilayer coats the electrode homogenously and effectively spans the cavities uniformly.

The top surface of the gold microcavities was selectively modified with mercaptoethanol (ME). This was accomplished by placing the cavities in a 1 mM solution of ME, in ethanol, for 24 h following electrodeposition, but before removal of the templating PS spheres from the array. It has been shown previously that leaving the PS spheres in place during SAM formation blocks monolayer assembly at the interior of the cavity ensuring only the top surface of the array is modified.[113] After treatment the cavities were sonicated in THF to remove the PS spheres. Mercaptoethanol is known to reduce the contact angle of gold[132] therefore,

modification with ME was carried out was to make the surface of the gold suitably hydrophilic to ensure bilayer formation across the cavities. Figure 3.8 shows the contact angle measurements of an untreated microcavity array and one after treatment with ME. In both cases the substrates where sonicated in buffer for 1 h to ensure cavity filling. The contact angle shows a reduction from 80° to 25° after ME treatment and could be a result of the increased hydrophilicity of the surface due to the OH groups now present on the gold surface as a result of the ME monolayer. The contact angle for ME treated cavities is lower than the reported values for planar ME treated gold[132] therefore, it can be concluded the cavities are water filling with ME on the surface so that 90 % of the contacting surface is actually water, hence the lower than expected contact angle. It could also be possible that the modification of the gold with ME actually enables the cavities to fill with aqueous solution, meaning that this modification would be key to ensuring the aqueous filling, which is key to bilayers spanning over the cavities.

CV's of the gold cavities were next measured in 10 mM potassium ferricyanide to investigate the effect of this surface treatment on the electrochemistry of the electrode. Figure 3.7 shows the CV's of three individual microcavity arrays, one where the top surface was selectively modified, one where the entire surface had been modified and one, which was not treated. The CV of cavities treated with ME is similar to the CV of bare gold microcavities as the ME is a short chain thiol and has a minimum effect on blocking electron transfer from the electrode.[133] There is no change to the peak potentials, although there is slight increase in the peak current but this most likely due to the differences in surface area between the three samples. The majority

of the surface area of the gold electrodes is derived from the cavities and has been shown by SEM to be approximately 90 % of the overall surface area, so modification of the top surface alone would only account for 10 % of the total electrode area and would not be expected to significantly change the electroactive area.

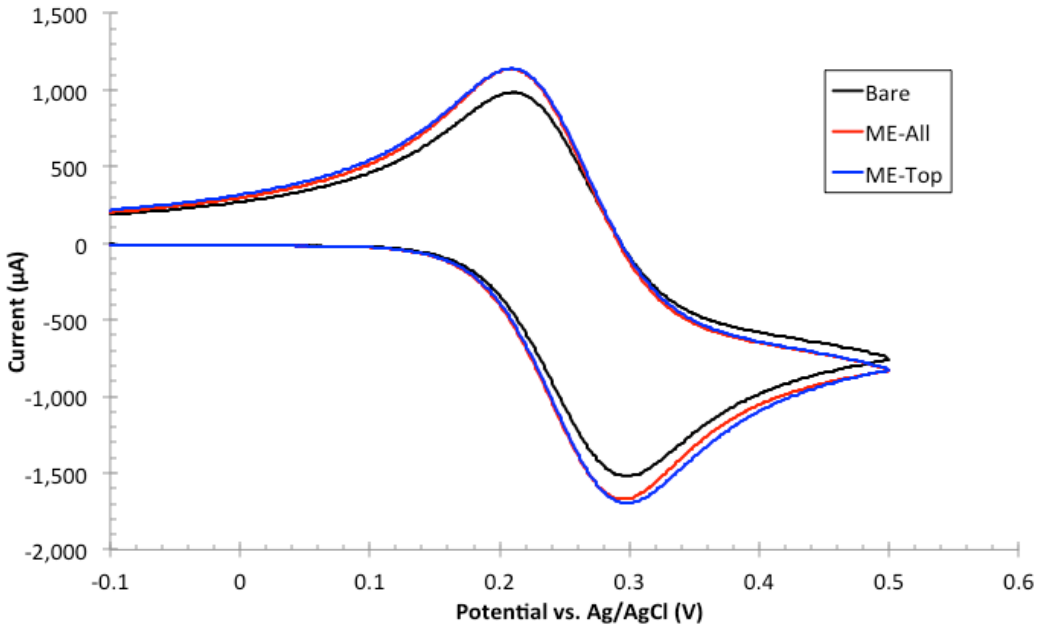

Figure 3.7 Cyclic voltammograms of bare gold microcavity, cavities treated with ME everywhere and cavities selectively treated with ME on the top surface. All electrodes where measured using a standard 3 electrode set up in 10 mM $K_4[Fe(CN)_6]$ and 1 M KCl as the supporting electrolyte and measured from -0.1 to 0.5 V (vs. Ag/AgCl) at a scan rate of 50 mV/s.

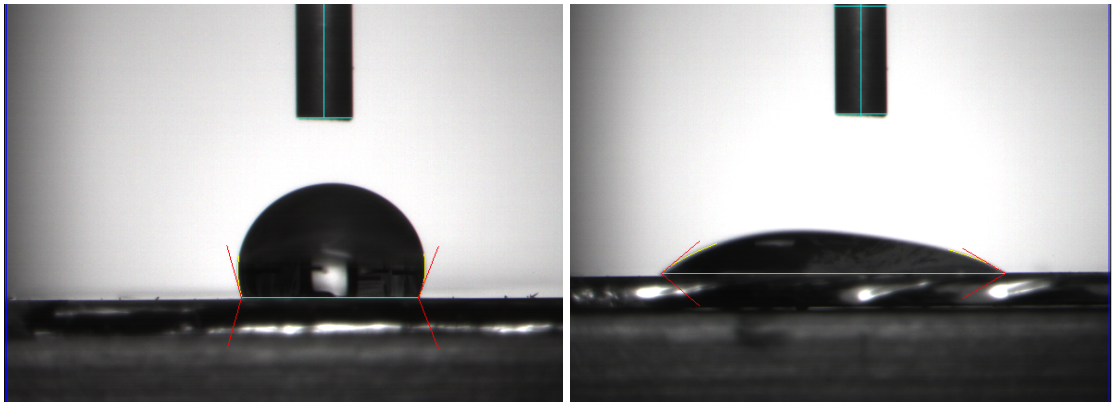

Figure 3.8 Contact angle measurements of untreated gold (left) microcavities formed using 2.88 micron PS, and the same cavities after treatment with ME for 24 h (right).

3.3.4 Diffusional Studies of Suspended Lipid Bilayers on Gold Microcavity Substrates

Fluorescence imaging was used to confirm that the lipid bilayer spanned across the gold array electrode uniformly and fluorescence lifetime correlation spectroscopy (FLCS) was used to confirm that a lipid bilayer had formed at the gold microcavity array, to confirm that the bilayer is spanning across the aqueous filled cavity apertures and that it is fluid.

As shown previously, lipid diffusion over an aqueous filled microcavity prepared from a 2.88 μm template in PDMS was over 2 times faster than on planar PDMS (See Chapter 2). It is therefore anticipated that there will be a comparable diffusion rate here over the cavity in the gold array compared with the gold interface.

To facilitate FLCS studies, the DOPC bilayers were labelled with 1 nM β-BODIPY-C5-HPC, which roughly corresponds to a molecular ratio of label to lipid of

1:100 000.

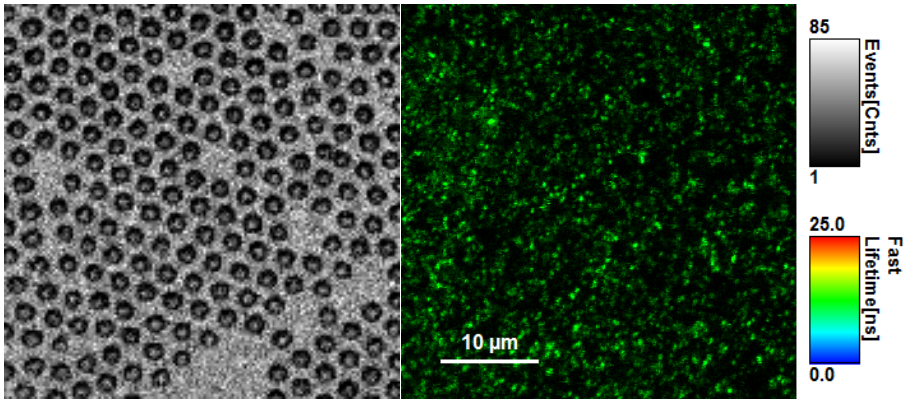

Figure 3.9 Reflectance (left) and FLIM image of a DOPC bilayer spanning gold micro cavities formed using 2.88 micron PS spheres. The bilayer was labelled with 1 nM β-BODIPY-C5-HPC images where taken with a 523 nm laser and are 40 x 40 micron in size.

Figure 3.9 shows white light reflectance (left) and fluorescence lifetime images (right) taken from a lipid bilayer modified gold cavity array. The continuous nature of the lipid luminescence, as seen in the fluorescence image, is first confirmation that the bilayer is spanning the gold microcavity array. It was shown in chapter 2 that in instances where the bilayer is not spanning, i.e. where rather it is conforming to the walls of the cavity array, a luminescence pattern is observed from the array that matches the cavity pattern with intense luminescence spots originating from the walls of the cavity.[134] In gold, in particular, the contributions from reflection and plasmonic enhancement can lead to very high intensities from the cavity where the bilayer is not spanning.[123] Critically, there is no evidence of patterned fluorescence from the cavities in the FLIM image shown in Figure 3.9. Instead, the fluorescence is homogeneous

across the array consistent with a continuous bilayer spanning across the array. The probe used here is β-BODIPY-C5-HPC. It is a tail labelled lipid (see Figure 3.10 for structure), was have found to be somewhat prone to aggregation when incorporated into a lipid bilayer supported at a planar surface. This can be attributed to steric distortion to the bilayer due to the probes orientation within the hydrophobic core which cannot be accommodated above on solid supported surfaces. However, because of its emission lifetime and wavelength, this probe was the only one which allowed the monitoring at the low level of labelling FLCS demands against background interference from laser reflectance and scatter from the gold surface.[134]

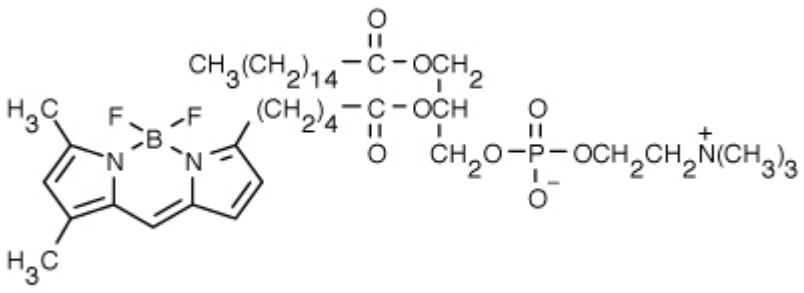

Figure 3.10 Structure of β-BODIPY-C5-HPC

Although of limited use as a topographical tool compared to SEM, the reflectance images are nonetheless valuable in aiding precise location of the pore apertures from the planar regions of the array. This, along with z-scanning, allows the accurate locating of the bilayer over the pore, permitting collection selectively of autocorrelation function data from bilayer spanning each region in Figure 3.9. The arrayed nature of the lipid modified substrate also means we can make multiple

independent measurements at a single substrate to build robust statistics for measurements. Point measurements of the fluorescence intensity fluctuations were collected for 180 sec to obtain Autocorrelation Functions (ACF's). Each point measurement was taken 3 times on each different substrate.

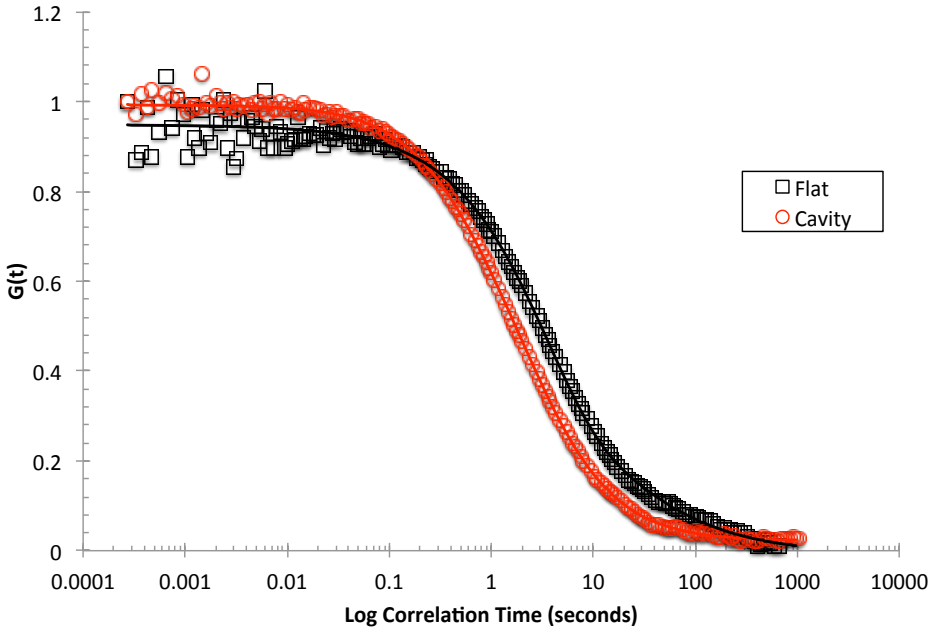

Figure 3.11 Representative FLCS correlation curves for a DOPC bilayer labelled with β-BODIBY-C5-HPC (1 x 10^{-9} mol) suspended across aqueous buffer (tris NaCl and pH 7.4) filled mercaptoethanol treated gold microcavity arrays, formed using 2.88 micron diameter PS spheres. □ indicates a ACF collected on a flat region of the array ○ indicates an ACF collected from bilayer spanning over a cavity. The solid lines show the fit of the model equation 1 used to obtain the diffusion coefficients. All points were taken for 180 seconds using a 532 nm laser as the excitation source.

The ACF's (see Figure 3.11) were fit to the 2-dimensional model (as described in Chapter 2) to obtain the lateral diffusion coefficients of the lipids at each region.

The lateral diffusion coefficient obtained for the DOPC lipid bilayer supported on planar regions of the gold array were determined to be 2.91 ± 1.29 $\mu m^2 s^{-1}$ with an α of 0.92 ± 0.22 which is comparable to other supported lipid bilayers on gold.[135] This value is marginally slower than the lipid diffusion coefficient reported for comparable bilayers composed of DOPC supported on glass substrates measured by FLCS.[64] The anomalous exponent is slightly lower than the value of 1 expected for purely Brownian motion. The lower anomalous exponent is attributed, as described above to the steric effect of tail labelling of the lipid which causes a barrier to diffusion at planar surfaces. Conversely, the diffusion coefficient for labelled lipid within the bilayer spanning the aqueous filled cavities was found to be 12.58 ± 0.28 $\mu m^2 s^{-1}$ with an α value of 1.03 ± 0.02, consistent with Brownian motion. This diffusion coefficient is consistent with the values for lipid diffusion over the aqueous filled cavities in PDMS, as discussed in Chapter 2. That it is substrate independent is consistent with lipid diffusion at a double aqueous interface, i.e. confirming that the lipid bilayer is successfully spanning an aqueous interface in all cases. The anomalous parameter of 1 indicates the labelled lipid is diffusing normally over the cavity. This is because the distortion of the bilayer due to the steric effect of the probe can be accommodated over water and there is no barrier to diffusion. The small increase in diffusion coefficient observed here compared with the PDMS cavities discussed in Chapter 2, is attributed to the fact that the gold cavity apertures are larger than those on PDMS and as previously reported, the aperture has an impact on the observed diffusion rate.

3.3.5 Characterisation of Suspended Lipid Bilayers by Electrochemical Impedance Spectroscopy.

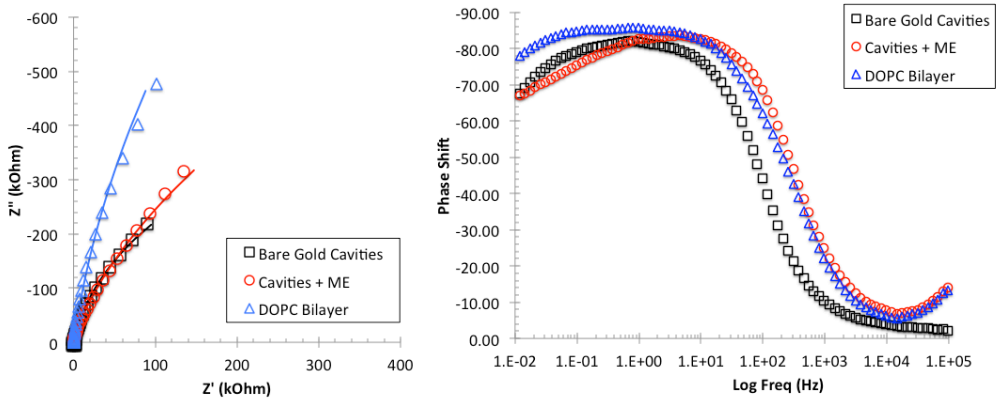

Figure 3.12 Nyquist (Left hand side) and Bode (right hand side) plots showing the change in impedance of aqueous filled microcavity electrodes following modification with mercaptoethanol (ME) and after spanning of a DOPC bilayer over the microcavities. All measurements were carried out using a standard 3-electrode set up at the OCP (vs Ag/AgCl) using AC amplitude of 0.01 V with a frequency range of 1 MHz to 0.01 Hz.

Non-faradaic impedance spectroscopy was employed to characterize the gold microcavity arrays before and after their treatment with mercaptoethanol (ME) and following assembly of the DOPC bilayer at the fluid filled arrays. Figure 3.12 above shows a typical Nyquist plot (Z'' vs Z') and Bode plot collected for a 1 cm^2 gold microcavity electrode before and after bilayer formation. The Bode plots the phase shift against frequency and consists of an area of low phase shift (at > 1 kHz), which corresponds to the solution resistance, after which there is an increase in the phase shift (at 1 kHz to 5 Hz), which corresponds to the capacitive behaviour of the system

and the final part with a phase shift between - 80 and - 70, which corresponds to the resistance of the system (bellow 5 Hz). The Bode plot shows a change in the impedance after modification with ME and after formation of the lipid bilayer. The Nyquist plot provides more information and shows the relationship between the real and imaginary component of the complex impedance and consists of an intercept on the real axis (Z') at high frequency, which corresponds to the solution resistance and contributions from the connections to the electrode. As frequency decreases we see the beginning of a semi-circular arc from high to low frequencies, which corresponds to the capacitive and resistive properties of the electrode. In order to extract the electrical properties of the bilayer it is necessary to fit the obtained data to an equivalent circuit. The most common model applied to EIS data of lipid bilayers supported on planar electrodes is shown in Scheme 3.1. It consists of a resistor element corresponding to the solution resistance (R_{sol}) in series with a capacitor in parallel with a resistor, which corresponds to the capacitance and resistance of the lipid bilayer ($R_{bl}|C_{bl}$). The circuit uses a Constant Phase Elements (CPE) instead of pure capacitors to account for the inhomogeneity of the lipid bilayer. The impedance of a CPE is given by $Z_{CPE} = Q\text{-}1(j\omega)\text{-}\alpha$ where Q is the magnitude of the capacitance of the CPE, ω is the angular frequency, and α is a real number between 1 and 0 (the closer α gets to 1 the more ideal the capacitive behaviour of the CPE). The circuit also contains a capacitor element to compensate for the double layer capacitance (CPEdl).

This model was initially applied to the MSLBs but, unsurprisingly, provided a poor fit to the data obtained for suspended lipid bilayers on gold microcavity electrodes. It was considered that this might be due the increased inhomogeneity of

the lipid bilayer, as the resistance and capacitance at the aqueous suspended lipids might be expected to be lower to those at the planar regions of the array. In order to compensate for these two dissimilar surfaces another parallel resistor and capacitor element was added to the circuit (see Scheme 3.1). Although this model seemed to be a closer fit to the measured data, the values obtained for the resistance and capacitance of the bilayer did not make physical sense. For example, the resistance and capacitance values returned for the bilayer where abnormally high and the quality of the fit returned was still relatively poor, usually with chi squared values no lower than 1×10^{-2}. It is also apparent from the measured spectra that there is a lack of a second domain within the frequency range measured, which one might expect to observe if inhomogeneities in the lipid bilayer where present over the cavities.

Finally, a model was chosen that is a modification of the classical model (Scheme 3.3) which accounts for additional resistance on the electrode due to the cavities. The circuit consists of the solution resistance (R_{sol}) in series with a resistor and capacitor in parallel, which corresponds to the lipid bilayer on the electrode surface (R_{bl}, C_{bl}). The circuit also contains a component to compensate for the resistance of the microcavities,[136] Rcav and the double layer capacitance, Cdl.

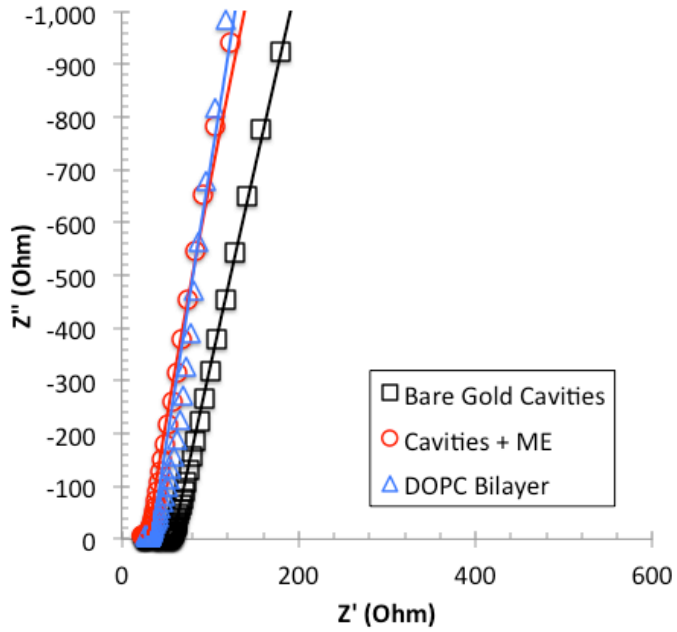

Figure 3.13 Data shown from figure 3.9 zoomed into higher frequency points and shows the impedance of aqueous filled microcavity electrodes following modification with mercaptoethanol (ME) and after spanning of a DOPC bilayer over the micro cavities. All measurements were carried out using a standard 3-electrode set up at the OCP (vs Ag/AgCl) using AC amplitude of 0.01 V with a frequency range of 1 MHz to 0.01 Hz.

The solid lines in Figure 3.12 above, show the fit of this final model to (solid line) to the experimental plots (points) using the equivalent circuit shown in Scheme 3. The fit is in very good agreement with the measured data, even across the high frequency data range (Figure 3.13) and returns χ^2 values below 3 x 10^{-3} which were consistently the lowest across all models applied. The fitted values show a decrease in the electrodes capacitance from 26.62 µF/cm^2 to 14.07 µF/cm^2 after modification of the top surface of the array with ME. This decrease in capacitance is consistent with

the formation of a self-assembled monolayer on the electrode, which increases the double layer thickness at the electrode. After formation of the DOPC bilayer the increase in resistance at the electrode is reflected in the increased arc in the Nyquist plot. This is confirmed in the fitted data, which shows an increase in the membrane resistance. Over 3 measurements on a single electrode, the average membrane resistance is 3.41 ± 0.21 MΩ. The membrane resistance observed here is comparable to values reported for tethered lipid membranes supported on a silicon oxide surface.[130] However, it is lower than values reported for BLM's. High resistance is desirable from the perspective of analytical sensitivity however BLM's, tend to exhibit poor stability, usually no more than a few hours. For example, some of the most stable BLM reported persisted for 5 h over a 128 micron pore,[137] whereas other studies shows stability of only 1 h over smaller pores.[91] BLMs are also, as described previously frequently multilayer, organic solvent containing structures, and thus have limited analogy to biomembranes. In contrast, Figure 3.14 shows the resistance of a DOPC lipid bilayer assembled across the microcavity array measured using EIS which confirms that there is no change in the bilayers resistance over 6 hours, which is a typical experimental window for our measurements (See Appendix Figure A.1 for EIS spectra). Indeed, later experiments confirmed the bilayers EIS signal are stable for at least a day.[138]

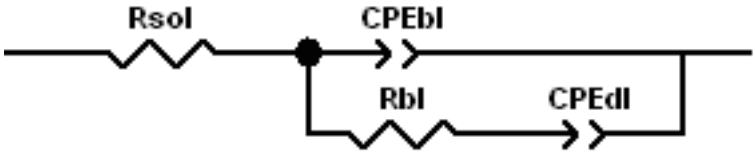

Scheme 3.1

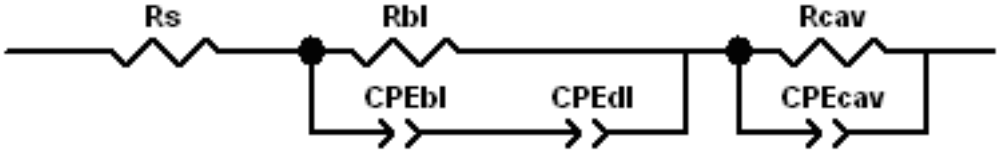

Scheme 3.2

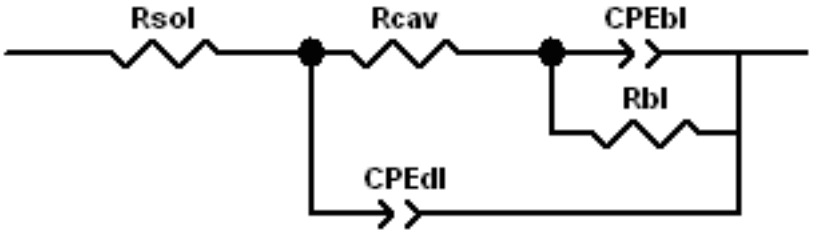

Scheme 3.3

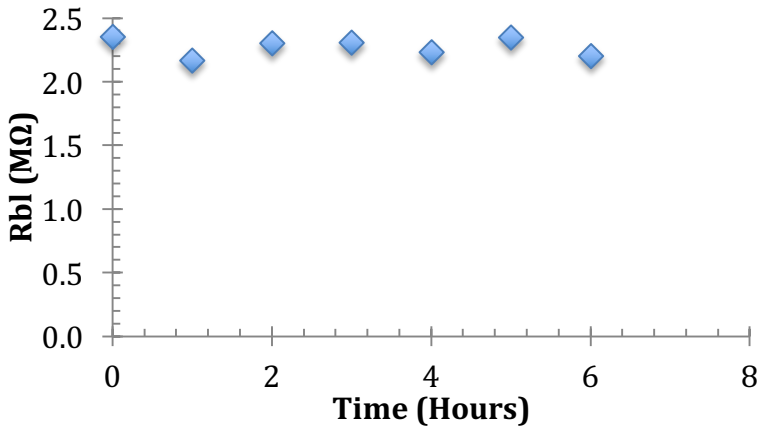

Figure 3.14 Representative R_{bl} obtained for a DOPC bilayer suspended over Tris NaCl buffer filled gold cavities. The EIS of bilayer was measured every hour for 6 h using a standard 3-electrode set up at the OCP (vs Ag/AgCl) using AC amplitude of 0.01 V with a frequency range of 1 MHz to 0.01 Hz.

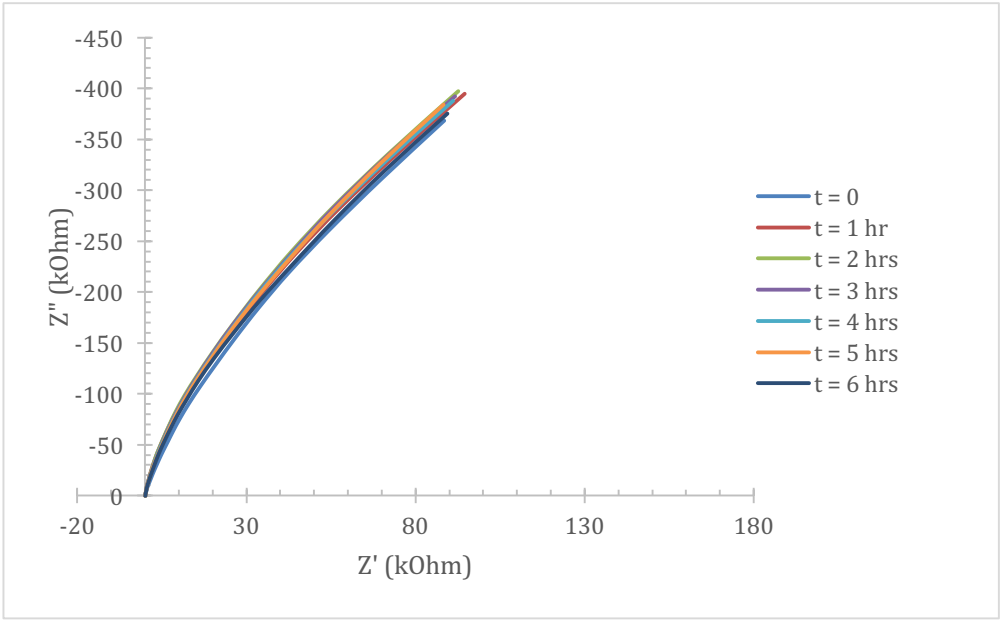

Figure 3.15 EIS measurements showing stability of a DOPC bilayer over a cavity array prepared from 2.88 micron diameter PS spheres when no gradient is present i.e. Tris NaCl on both sides of the bilayer. All measurements were conducted using a standard 3-electrode arrangement at the OCP (vs Ag/AgCl) using AC amplitude of 0.01 V with a frequency range of 1 MHz to 0.

3.3.6 Characterisation of Uniporter Ionophore in Suspended Lipid Bilayers by Electrochemical Impedance Spectroscopy

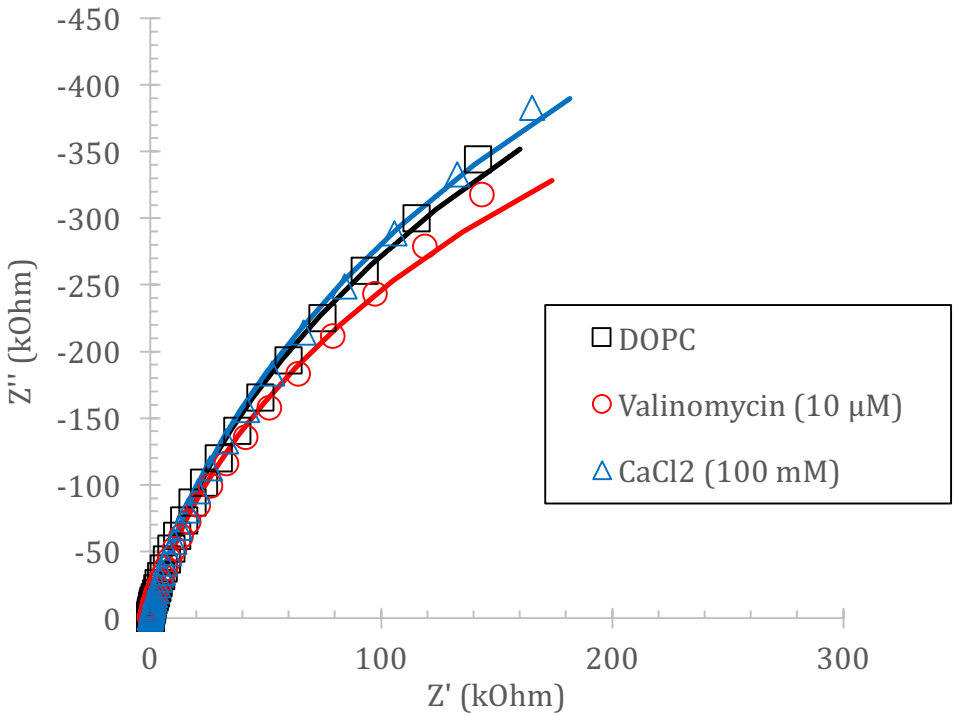

Figure 3.16 EIS measurements showing Valinomycin incorporation into a DOPC bilayer of cavity array prepared from 2.88 micron diameter PS spheres when no gradient is present i.e. Tris NaCl on both sides of the bilayer. All measurements were conducted using a standard 3-electrode arrangement at the OCP (vs Ag/AgCl) using AC amplitude of 0.01 V with a frequency range of 1 MHz to 0.01 Hz.

Table 3.2 Bilayer resistance (Rbl) obtained for DOPC bilayers suspended over 2.88 micron cavity arrays, before and after incorporation of Valinomycin, in the absence of an ionic gradient and after the addition of $CaCl_2$.

Sample		Rbl ($M\Omega cm^2$)	ΔRbl ($M\Omega cm^2$)
Sample 1	DOPC	9.39	
	Valinomycin 10 µM	8.31	- 1.08
	100 mM $CaCl_2$	9.50	+ 0.11
Sample 2	DOPC	6.57	
	Valinomycin 10 µM	5.49	- 1.08
	100 mM $CaCl_2$	6.61	+ 0.04
Sample 3	DOPC	5.87	
	Valinomycin 10 µM	4.92	- 0.95
	100 mM $CaCl_2$	5.96	+ 0.08
Average	DOPC	7.28 ± 1.86	
	Valinomycin 10 µM	6.24 ± 1.82	- 1.04 ± 0.07
	100 mM $CaCl_2$	7.36 ± 1.88	+ 0.08 ± 0.03

Given the stability and fluidity of the cavity supported bilayer arrays, it is interesting to investigate if they could be used to support and study ionophores. Ionophores are a class of transporters within the cell membrane; they range from small hydrophobic molecules that are soluble within the lipid membrane to membrane proteins. Valinomycin is an example of a small molecule transporter molecule; it is a ring shaped antibiotic peptide that inserts into and transports K^+ ions across the lipid bilayer, down its electrochemical gradient. Valinomycin transportation of K^+ ions across the lipid membrane has been well studied using EIS making it useful for testing if the lipid bilayers are suspended over gold cavities. However, it has been limited to study with black lipid membranes (BLM's),[48,105] thiolated supported lipid bilayers on gold,[139] or tethered bilayer lipid membranes (t-BLM's).[140] And, in the case of the latter examples, it is difficult to study ionic gradients as there is no aqueous well on the inner bilayer surface.

The gold microcavity arrays described here are a potentially useful alternative to BLM's and t-BLM's for study of ionophores as the large pores supporting the bilayer offer the opportunity to vary buffer composition or ionic strength at each side of the membrane. Furthermore, as described recently, microcavity supported lipid bilayers at fluid filled cavities exhibit excellent stability compared to BLM's. The bilayers here also show stability over several days, typical of the stability of solid supported lipid bilayers, but with an accessible aqueous well in contact with both the proximal and distal leaflets. The EIS data above shows the electrochemical stability of the bilayers is also excellent over a minimum of 6 hours and showed no evidence for drift in the impedance data and no change to film resistance.

Non-faradaic electrochemical impedance spectroscopy was employed to monitor the change in the resistance of the lipid bilayer on integration of the Valinomycin into the bilayer. Figure 3.16 shows the Nyquist plot for the EIS data obtained for a DOPC bilayer before and after incubation in contact with an buffered aqueous solution of 10 μM Valinomycin. We observe a clear decrease in the EIS arc indicating a decrease in the impedance. Table 3.2 Shows the values obtained for the bilayer resistance (R_{bl}) from fitting the data to the equivalence circuit shown in scheme 3.3 and is similar to one used in previous studies of Valinomycin. [105,106,130] Other reports use a modification of this model to extract further data on the kinetics of ion transport across the membrane.[141] The work presented here focuses more on the platform development and its response to changes in the bilayer therefore the simpler model was used. There is a significant deviation in the measured resistance value obtained for each substrate, which is attributed to the differences in the surface areas of each of the independently prepared samples. However, the average change in the three bilayers (ΔR_{bl}) is the same. This data shows an average decrease in the bilayer resistance of -1.04 ± 0.07 $M\Omega cm^2$ on the incorporation of Valinomycin into the bilayer. Valinomycin inclusion into the bilayer causes an increase in the dielectric permittivity of the lipid bilayer. The observed resistance change is consistent with other reports on Valinomycin integrated into SLB's.[110] Divalent cations are known to bind to and block Valinomycin due to their larger size, thus stopping the transport of K^+ across the lipid bilayer, Figure 3.16 shows that after the addition of 100 mM $CaCl_2$ the resistance returns to its original value which is further evidence for successful Valinomycin incorporation into the lipid bilayer.

The advantage of the MSLB system described here over other lipid bilayer models is that we can prefill the cavities with a different buffer to the buffer at the exterior of bilayer, i.e. an ionic gradient can be created. Figure 3.17 shows the EIS response of the same DOPC system in the presence of an ionic gradient consisting of Tris KCl (20 mM Tris, 600 mM KCl) inside the cavities and Tris NaCl outside (20 mM Tris, 150 mM NaCl). Here, a decrease in the arc of the impedance spectrum on introduction of the Valinomycin is observed indicating a decrease in film resistance after incubation in a 10 mM Valinomycin solution for 1 h. Although no gradient is present, this reduction in resistance may be due to a reorganisation of the lipid bilayer due to the incorporation of Valinomycin. The response in the presence of the gradient is amplified in comparison to measurements taken without a gradient. This is consistent with other work that shows increased activity of Valinomycin with increased concentration of K^+ in the bulk electrolyte solution.[125] The values obtained from fitting the data in Figure 3.17 to the equivalent circuit shown in Scheme 1 are shown in Table 3.3 and reveal a decrease in the bilayer resistance (R_{bl}) of -3.96 ± 0.31 $M\Omega cm^2$ in the presence of an ionic gradient compared to a decrease of only - 1.04 ± 0.07 $M\Omega cm^2$ when no gradient is present. The average membrane resistance has a large deviation, from sample to sample, due to difficulty controlling exactly the surface area and exact number of cavities on each electrode. Nonetheless, the magnitude of the change, within a single experiment, after the addition of Valinomycin is highly consistent across multiple substrates. As Valinomycin is a passive transporter of K^+, transporting it from areas of high to low K^+ concentration the decrease R_{bl} in the presence of an ionic gradient is speculated to be due to the combined effects of increased activity of the Valinomycin, along

with amplification of the resistance changes induced by the ion gradient itself due to the increase in chemical potential across the lipid bilayer.

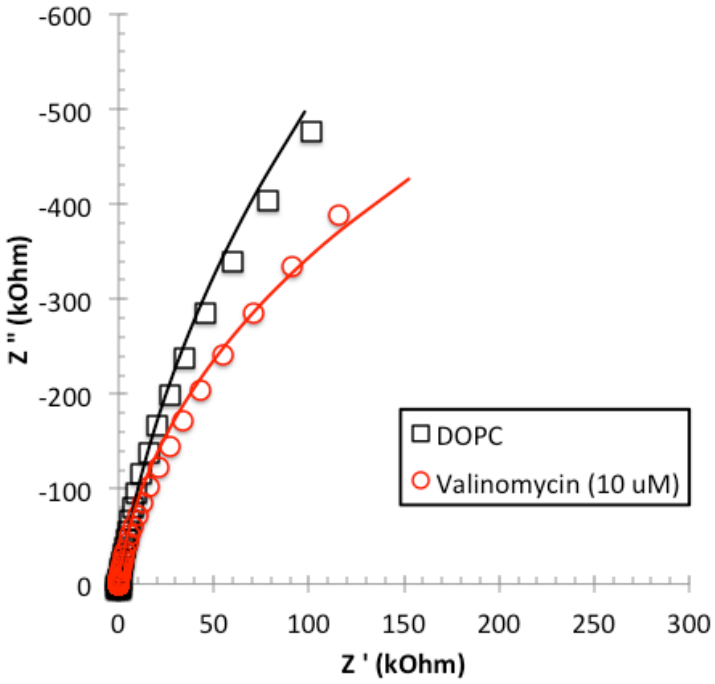

Figure 3.17 EIS measurements showing Valinomycin incorporation into a DOPC bilayer of cavity array prepared from 2.88 micron diameter PS spheres in the presence of an ionic gradient consisting of Tris KCl (20 mM Tris and 600 mM KCl) inside the cavities and Tris NaCl (20 mM Tris and 150 mM NaCl) as the bulk electrolyte solution. All measurements were conducted using a standard 3-electrode arrangement at the OCP (vs Ag/AgCl) using AC amplitude of 0.01 V with a frequency range of 1 MHz to 0.01 Hz.

Table 3.3 Bilayer resistance (Rbl) obtained for DOPC bilayers suspended over 2.88 micron cavity arrays, before and after incorporation of Valinomycin, with an ionic gradient.

Sample		Rbl (MΩcm^2)	ΔRbl (MΩ cm^2)
Sample 1	DOPC	9.20	
	Valinomycin 10 μM	5.55	-3.65
Sample 2	DOPC	8.03	
	Valinomycin 10 μM	4.07	-3.96
Sample 3	DOPC	6.57	
	Valinomycin 10 μM	2.31	-4.26
Average	DOPC	7.94 ± 1.32	
	Valinomycin 10 μM	3.98 ± 1.62	-3.96 ± 0.31

3.3.7 *Incorporation of Antiporter, Nigericin, into a Microcavity Supported Lipid Bilayer*

Ion channel proteins are typically classified into 3 categories; uniporters, antiporters and symporters. Uniporters carry a single solute from one side of the lipid membrane to the other, usually across an ionic gradient. Antiporters carry two solutes

across the membrane in opposing directions, and symporters carry two different solutes across the membrane in the same direction.

The capacity to fill the cavities and build ionic gradients across stable but fluidic bilayer structures in the microcavity arrays provides a useful opportunity to study antiporters. Nigericin, which is an antiporter of K^+ and H^+ and is widely used to manipulate the K^+/H^+ concentration within cells.[33,142,143] Nigericin has been investigated in a model electrochemically addressable black lipid membrane system.[144] In this study Steinem *et al* also released a study where they established an ionic gradient across suspended lipid bilayers and monitored the change in pH after addition on Nigericin by observing the fluorescence of pyranine, a pH sensitive flurophore.[145]

Figure 3.18 shows the EIS measured from buffer filled micro cavities supporting a DOPC bilayer, in contact with a solution of Tris NaCl (20 mM Tris, 150 mM NaCl) in which the cavities have been filled with Tris KCl (20 mM Tris, 300 mM KCl). Measurements were made before and after incubation of the MSLB with a 10 mM solution of Nigericin for 1 h at room temperature and show a clear decrease in the impedance and show a clear shift in the arc after Nigericin incorporation, indicating a decrease in the impedance. The values obtained when the data are fitted to the ECM shown in scheme 3.3 are provided in Table 3.4. As observed for Valinomycin, incorporation into the bilayer, introduction of Nigercin to the lipid bilayers induces a significant decrease in the resistance of film $\Delta R = -2.23 \pm 0.03$ $M\Omega cm^2$ after incubation of the bilayer in 10 μM Nigericin. As the cavities have been pre filled with potassium, and there is none on the other side of the bilayer, addition of Nigericin is

expected to cause an influx of protons and egress of potassium ions across the membrane. Therefore, the decrease in the bilayer's resistance is attributed to an increase in the porosity of the bilayer due to the incorporation of Nigericin transporting K^+ and H^+ ions across the membrane. This result agrees with the report by Steinem's et al who showed that the transport of H^+ ions by Nigericin, across a bilayer on porous silicon substrates only occurred in the presence of K^+ ions.[123]

Next 500 μL of citrate buffer was added to the buffer in contact with the distal bilayer interface corresponding to approximately 5 μM of H^+ ions. This should cause the formation of an H^+ gradient across the lipid bilayer and should in turn activate Nigericin's antiporting. The addition of protons to one side of the bilayers lead to a decrease in the bilayer resistance to give a further decrease of $\Delta R = -4.54 \pm 0.21$ $M\Omega cm^2$. This resistance decrease is attributed to the increase of the Valinomycin activity caused by the increase in H^+ ions due to the creation of an ionic gradient of H^+ ions on one side of the bilayer. This in turn activates the function of Nigercin in antiporting K^+ and H^+ across the membrane. A contribution originating from the ionic gradient across the film as H^+ affecting the bilayers resistance directly can be discounted as when the same experiment is repeated without Valinomycin present in the bilayer no change in impedance is observed (see Figure 3.19).

The above studies demonstrate the utility of metal cavity supported lipid bilayers substrates in studies where it is desirable to be able to independently control the composition of the aqueous environment on either side of the lipid bilayer, but in a system which is considerably more stable than BLMs. This is an important step towards creating a more biomimetic bilayer system for studying electrically controlled

membrane moieties.

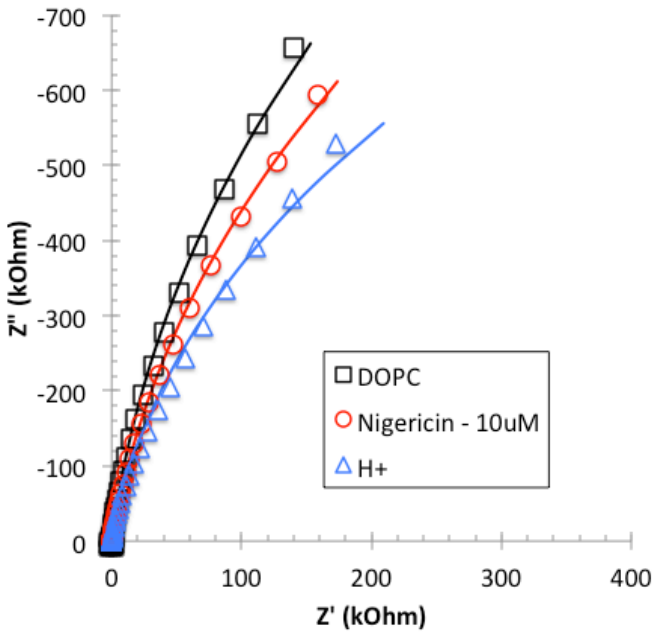

Figure 3.18 EIS measurements showing Nigericin incorporation into a DOPC bilayer of 3 µm diameter cavity array. All measurements were run using a standard 3-electrode set up at the OCP (vs Ag/AgCl) using AC amplitude of 0.01 V with a frequency range of 1 MHz to 0.01 Hz.

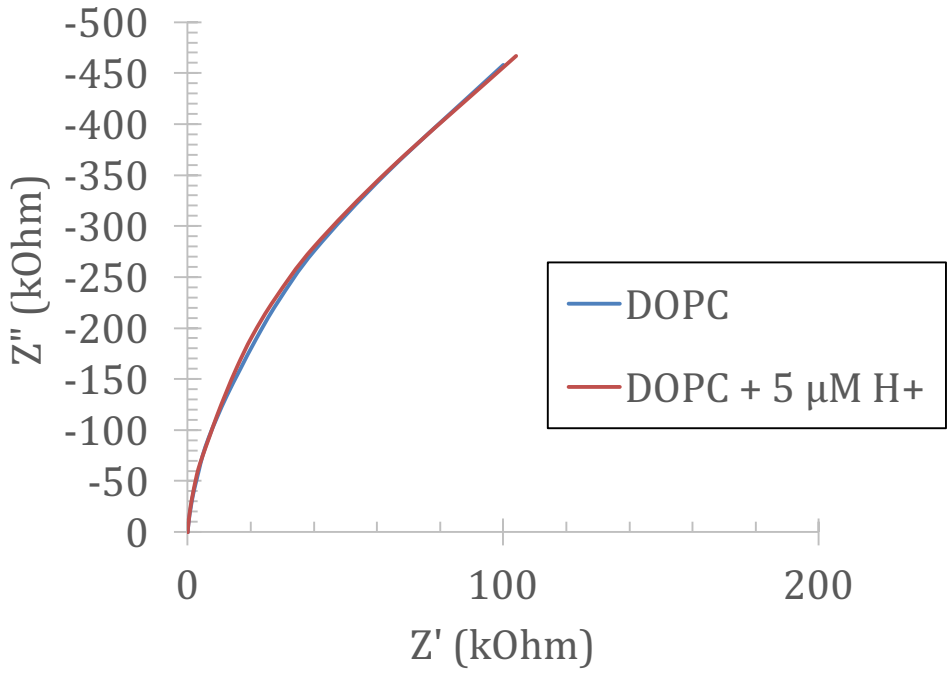

Figure 3.19 EIS measurements DOPC bilayer of 3 µm diameter cavity array before and after addition of H^+ All measurements were run using a standard 3-electrode set up at the OCP (vs Ag/AgCl) using AC amplitude of 0.01 V with a frequency range of 1 MHz to 0.01 Hz. Within experimental error, addition of H+ ions to the exterior there is no impact on the recorded film impedance.

Table 3.4 Bilayer resistance (Rbl) obtained for DOPC bilayers suspended over 2.88 micron cavity arrays, before and after incorporation of Valinomycin, and after the addition of H^+ ions The values below come from the average of 3 electrodes.

Sample		Rbl ($M\Omega cm^2$)	ΔRbl ($M\Omega cm^2$)
Sample 1	DOPC	9.67	
	Nigericin 10 µM	7.41	- 2.26
	5 µM H^+	4.90	- 4.77
Sample 2	DOPC	9.54	
	Nigericin 10 µM	7.31	- 2.23
	5 µM H^+	5.19	- 4.35
Sample 3	DOPC	8.06	
	Nigericin 10 µM	5.85	- 2.20
	5 µM H^+	3.54	- 4.52
Average	DOPC	9.09 ± 0.90	
	Nigericin 10 µM	6.86 ± 0.87	- 2.23 ± 0.03
	5 µM H^+	4.54 ± 0.88	- 4.54 ± 0.21

3.4 Conclusions

Chapter 3 describes a strategy for forming supported/suspended DOPC lipid bilayer across gold micron dimensioned spherical cavity arrays. This was achieved by selective decoration of the top surface of the array with mercaptoethanol which enabled lipid bilayer support, not possible in the absence of modification. The mercaptoethanol dramatically promoted filling and wettability of the array. EIS measurements demonstrated that stable bilayers could be formed homogenously across 1 cm^2 arrays with pores of 2.64 micron diameter apertures. FLCS was used to demonstrate stable lipid bilayers over these cavities formed and that they were fluid. The arrays showed two distinctive lipid diffusion behaviours; over planar regions of the platform the lipid diffusion coefficient was 2.91 ± 1.29 $\mu m^2 s^{-1}$, which increased to 12.58 ± 1.28 over cavities. This indicates the formation of stable free standing bilayers on substrates. The diffusion was Brownian over the cavities but sub-diffusion over planar regions due to steric perturbation of the bilayer by the tail modified lipid, which hindered diffusion over solid substrate regions. This work also demonstrated the first example of an array that can be studied by dual detection; electrochemical and optical.

EIS was used to study the lipid bilayers formed over the gold microcavity arrays and an appropriate equivalent circuit model was developed to extract the resistive values of the bilayers. The EIS data showed variations of the bilayer's resistance form sample to sample, which is thought to be a result of the variation in electrode area caused by the variation of the numbers of cavities. However, within a single sample the lipid bilayers display remarkable stability and have been shown to be stable for at least a day.

The arrays were used to investigate the incorporation of two ionophore peptides Valinomycin and Nigericin. In the case of Valinomycin the ability to create an ionic gradient by prefilling the gold microcavities with a higher concentration of KCl then on the other side of the bilayer caused a 3 fold increase in the electrical response observed with EIS. With Nigericin we showed it was possible to prefill the cavities with KCl and increase H^+ concentration on the external side of the bilayer to observe nigericen's antiporting activities with EIS.

Overall we have demonstrated a new platform for the electrochemical detection of molecular interactions with a suspended lipid bilayer. This substrate, with application of the right probe, can be used to study both EIS and fluorescence on a single substrate, which holds promise for investigation of electrically induced processes at the lipid bilayer ion and molecular transport across the lipid bilayer and possibly as a model system in the application of drug membrane interactions such as drug permeability across the membrane as well as drug interaction with protein receptors.

Chapter 4

A Strategy for Spatiotemporal control of reagent delivery to lipid bilayer.

4.1 Introduction

Chapter 2 described the application of the PDMS cavities to study of diffusion of membrane proteins reconstituted into a spanning lipid membrane.[103] This was one of the first examples of an SLB structure in which membrane protein were reconstituted and which retained full mobility. It demonstrated the value of these substrates for studying both lipids and proteins. Chapter 3 demonstrated that the cavities give a further advantage in that the buffer can be independently controlled at each lipid interface.

In this chapter we advance the arrays further by exploring the prospect of using the cavities to address independently the proximal and distal lipid bilayer. Introduction of reagent to the external leaflet is easy as we just introduce reagent to the contacting solution. However, here we explore a method of releasing a reagent from the cavity to the lower leaflet of the bilayer. Such an approach could, in principle, lead to the possibility of bidirectional modification of a protein at the bilayer, as a mimic of bidirectional signalling common in membrane proteins[146], or could be used for spatiotemporal modification of lipid or other bilayer constituent in response to a reagent release.

The gold interface allows for electrochemical addressability and an electrochemically induced release of fibrinogen from both planar gold electrodes and the interior of microcavities via reductive de-adsorption as has been reported previously[147] In the case of the cavities, this was achieved by first selectively modifying the gold cavities at the top surface with a blocking alkane thiol and then

filling the cavities with a fibrinogen solution which then spontaneously and non-specifically adsorbed at the interior of the cavity. The fibrinogen could then be reductively desorbed from the interface. However, the fibrinogen once released was found from SDS page experiments to be fragmented.[131]

This work investigates an alternative method for electrochemically induced release of a protein or other reagent from a gold surface. In this approach, direct contact between the releasable species and the interface is avoided by introducing a carrier molecule whose supramolecular interaction with a surface bound redox active moieity is altered by electrochemical switching of this species. In the case of protein or peptides in particular, this approach avoids adsorption induced denaturation of the protein but also allows us to use lower potentials to issue release. This is done by exploiting the ferrocene/β-cyclodextrin host-guest complex which is assembled at the gold cavity interface. A schematic of the approach used here is shown in Figure 4.4.

Gold electrodes were modified with ferrocenehexanethiol (Fc) monolayers (for structure see figure 4.1) onto which β-cyclodextrin (β-CD) spontaneously forms through a host-guest interaction.[148,149] Oxidizing the ferrocene destroys the complex, allowing the cyclodextrin to depart the surface. The construction of the Fc monolayer on the surface is key to controlling the destruction of this complex for example, Reinhoudt *et al* has shown that a mixed monolayer system is needed to ensure efficient oxidation of the Fc metal centre.[150] This work exploits ferrocene because it can be oxidized at low potentials and in aqueous electrolytes, which should prevent damage to both the lipid bilayer and the material to be released. The cyclodextrin used here is one functionalised with a succinyl group, this means it can be synthetically modified

with the material, e.g. protein or ligand to be delivered to the bilayer allowing for spatiotemporally controlled release.

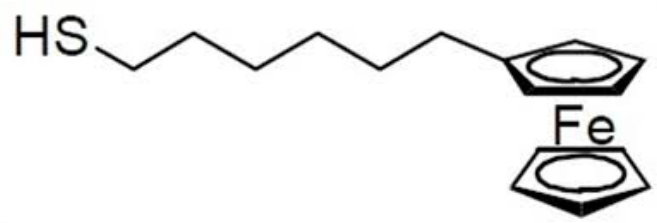

Figure 4.3 Structure of Ferrocenehexanethiol.

The formation of the host guest and the controlled release of the β-CD are interrogated here by cyclic voltammetry and electrochemical impedance spectroscopy. Specifically, the work also exploits the strong affinity of streptavidin and Biotin to demonstrate the controlled release of a streptavidin from the cavity surface to a Biotin modified spanning lipid bilayer. The interaction of the released streptavidin and the Biotin in the bilayer is monitored by electrochemical impedance spectroscopy (EIS).

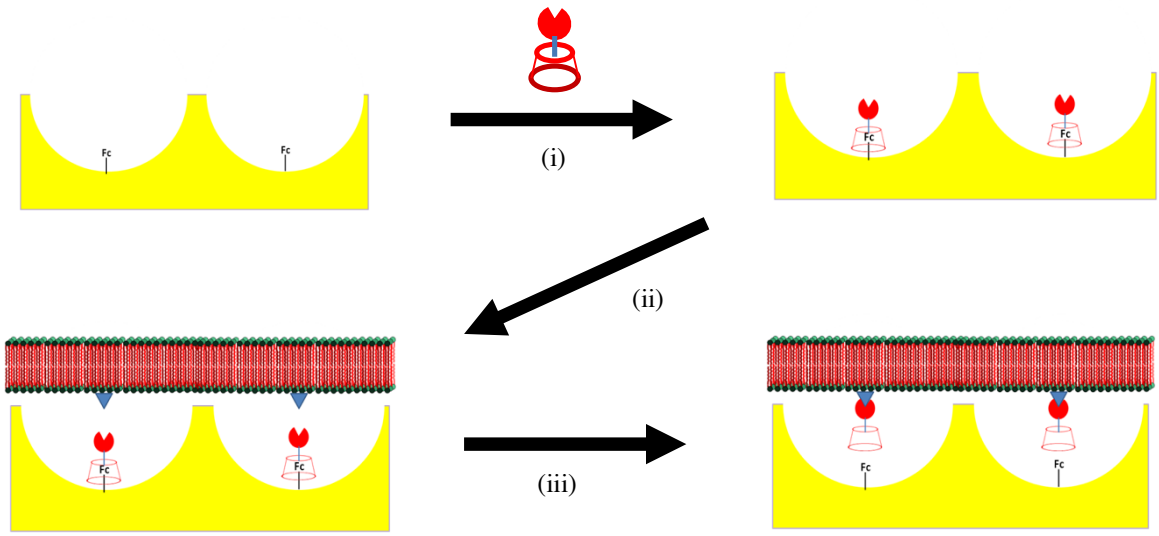

Figure 4.4 Schematic illustrating the controlled release strategy which is the focus of this chapter, for release of b-CD-Streptavidin to bilayer containing Biotin. (i) Incubation in ß-Cyclodextrin coupled to Avidin , (ii) Formation of bilayer containing Biotin over cavities (iii) Electro-release of ß-CD-Avidin to Biotin.

4.2 Experimental

4.2.1 Materials:

Silicon wafers coated with a 100 nm layer of gold on a 50 Å layer of titanium were obtained from AMS Biotechnology Inc. 2.94 μm diameter polystyrene spheres were obtained from Bangs Laboratories Inc. 1,2-dioleoyl-sn-glycero-3-phosphocholine (DOPC), 1,2-dioleoyl-sn-glycero-3-phosphoethanolamine-N-Biotinyl (DOPE-Biotin), 1,2-dioleoyl-sn-glycero-3-phospho-L-serine (DOPS) and cholesterol were all obtained from Avanti Polar Lipids Inc. Gold electro deposition solution (TG-25RTU) was obtained from Technic Inc. All other reagents were obtained from Sigma Aldrich and used as received.

4.2.2 Modification of Gold Microcavities

Gold microcavities were fabricated as described in Chapter 3. To allow for the electrorelease of cyclodextrin selectively from within the gold cavities, the top surface of the cavities was first modified with mercaptoethanol. This was achieved by placing the substrates into a 1 mM solution of mercaptoethanol overnight, prior to the removal of the polystyrene spheres with THF. After treatment the spheres were removed and

the substrate was then treated with 1 mM mercaptoethanol solution containing 20 mol% 6-(ferrocene)hexanethiol. This resulted in ferrocene inside the cavities only. The substrate was then sonicated in Tris NaCl for 30 min to aqueous fill the cavities after which they were incubated in a 0.1 mg/mL solution of cyclodextrin for 30 min to assemble. Phospholipid bilayers were then formed over these substrates after they had been washed and filled with aqueous buffer as before using Langmuir-Blodgett method and vesicle fusion.

4.2.3 Coupling of β-Cyclodextrin to Avidin.

Streptavidin was coupled to succinyl β-CD via EDC coupling following a similar previously described procedure.[151] 100 μL of a 0.62 mg (0.55 mM) solution of succinyl-β-CD dissolved in 20 mM HEPES buffer at pH 8.5 was added drop wise to 0.32 mg (1.5 mM) of EDC dissolved in 10 μL of HEPES pH 8.5. The reaction was stirred for 30 minutes after which a 1 mg/mL solution of streptavidin was added drop wise to the reaction mixture. The coupling reaction was allowed to stir overnight to yield the streptavidin - β-Cyclodextrin (β-CD-SA) complex. Figure 4.5 shows the UV absorption spectra of β-CD and β-CD-SA, an absorption peak at 280 nm which can be attributed to Streptavidin. This indicates successful coupling of streptavidin to β-CD.

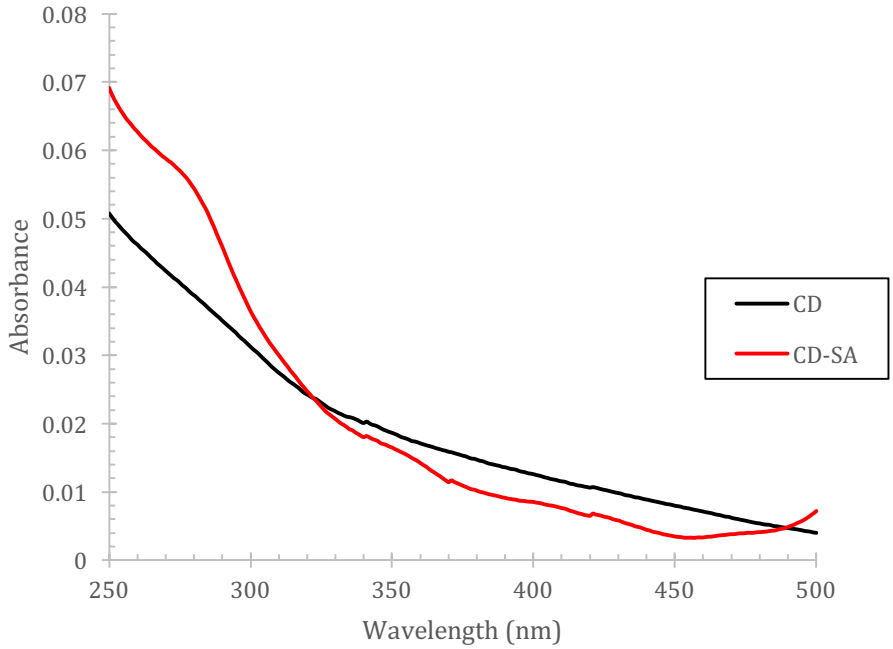

Figure 4.5 UV absorbance spectra of β-CD and β-CD-SA. Both spectra were performed in Tris NaCl at pH 7.4 and at a concentration of 1 mg/mL

4.2.4 Characterisation of Modified Gold Microcavity Substrates by Cyclic Voltammetry

Cyclic voltammetry at modified gold cavity array working electrodes was performed in Tris NaCl buffer at pH 7.4 using a 3 electrode set up comprising a Ag/AgCl reference electrode, a platinum wire as the counter electrode and the gold microcavities as the working electrode. Scans where performed from 0 to 0.7 V at a scan rate of 100 mV/s and 3 successive scans where taken for all samples.

4.2.5 Formation of Suspended Lipid Bilayers

Formation of suspended lipid bilayers was performed as in Chapter 3. All bilayers comprised of DOPC unless otherwise stated.

4.2.6 Electrochemical Impedance Spectroscopy

Electrochemical impedance was performed with a CH660A potentiostat (CH Instruments). using the 3-electrode set up as described above. The impedance was measured over a frequency range of 100000 Hz to 0.01 Hz with an AC modulation amplitude of 0.005 V at a potential bias of 0 V (vs Ag/AgCl). All measurements were performed in a glass cell of approximate volume of 15 mL in Tris NaCl buffer at pH 7.4.

4.3 Results and Discussion

4.3.1 Formation and Release of Ferrocene/β-Cyclodextrin Complex

Gold microcavity arrays were selectively functionalized with ferrocene hexanethiol (Fc) and the interstitial planar gold regions at the top of the cavity modified with 2-mercaptoethanol (ME) by firstly modifying the substrate with ME, while the PS spheres where still in the cavities, and then placing them in a solution containing Fc and ME (20:80 mol %) in ethanol for 24 h after removal of the PS spheres. It has been shown previously that when treating electrodes with ME and Fc that the Fc should be

kept below 20 % of the overall monolayer concentration to prevent neighbouring Fc molecules from interacting with one another and preventing efficient oxidation of the Fc. If the Fc concentration within the monolayer is too high when one Fc centre is oxidized, coulombic lateral interaction between Fc pairs makes the oxidation of adjacent Fc centres more difficult.[150] Therefore, here we co-adsorbed the Fc with 2-mercaptoethanol when modifying the cavity interior

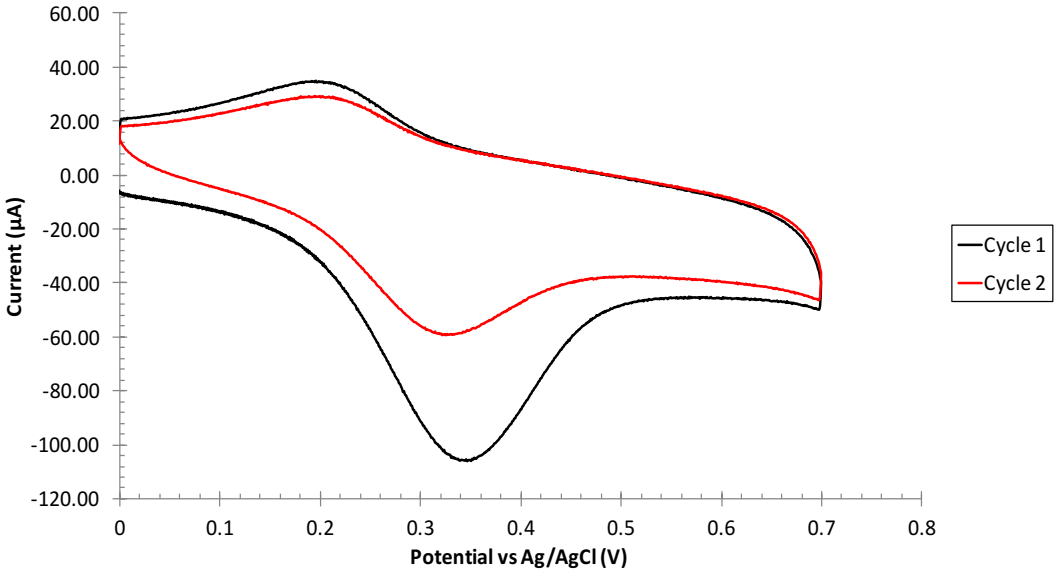

Figure 4.6 Cyclic voltammogram of microcavity array treated with mercaptoethanol on the top surface and ferrocene hexanethiol inside the cavities. The measurement was performed in Tris NaCl buffer at pH 7.4 using a standard 3 electrode set up. The scan was run from 0 to 0.7 V (vs Ag/AgCl Reference) at 100 mV/s. Two consecutive scans were run on the same electrode; the first scan is shown above in black and the second in red.

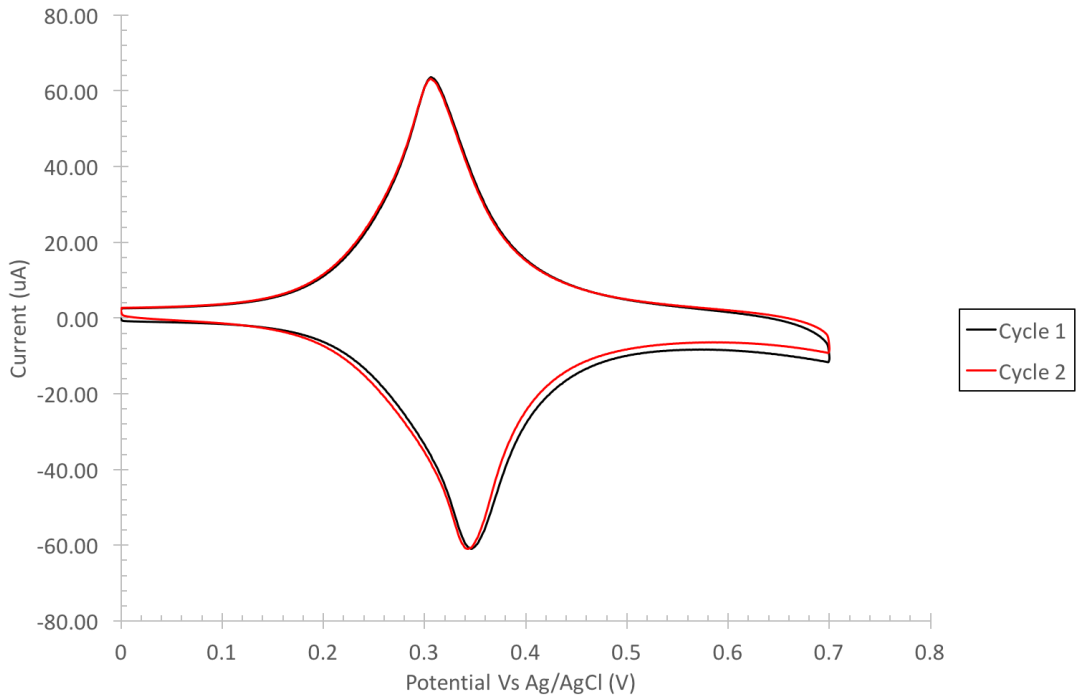

Figure 4.7 Cyclic voltammogram of microcavity array treated with mercaptoethanol on the top surface and ferrocene hexanethiol inside the cavities. The measurement was performed in Sodium Perchlorate using a standard 3 electrode set up. The scan was run from 0 to 0.7 V (vs Ag/AgCl Reference) at 100 mV/s. Two consecutive scans were run on the same electrode; the first scan is shown above in black and the second in red.

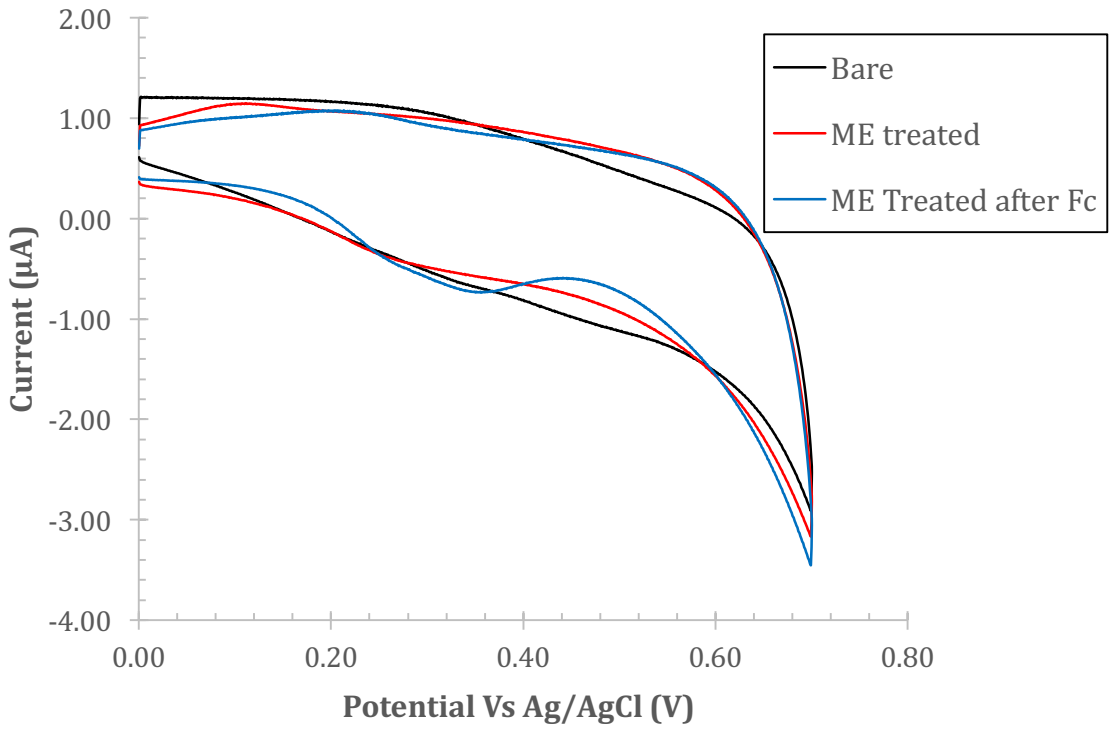

Figure 4.8 Cyclic voltammogram of untreated microcavity array (Black) and microcavity array treated with mercaptoethanol everywhere (ME) before (Red) and after (Blue) treatment in ferrocene hexanethiol (Fc). The measurement was performed in Tris NaCl buffer at pH 7.4 using a standard 3 electrode set up. The scan was run from 0 to 0.7 V (vs Ag/AgCl Reference) at 100 mV/s.

Figure 4.6 shows the cyclic voltammetry of cavities modified with ME on the top surface at a mixed monolayer of ME/Fc in the interior of the cavities which exhibits an anodic peak at approximately 350 mV attributed to the oxidation of ferrocene which is localised at the cavity interior. The oxidation process is chemically irreversible as the associated reduction peak which is observed at 200 mV has an area which integrates for approximately 85 % less than its associated oxidation. This is also

confirmed in the peak to peak separation, which is about 120 mV indicating non Nernstian behaviour. The irreversibility is made more apparent on successive scans, which shows that the relative area of the oxidative peak diminishes after the first scan. However, upon additional scans there is no further change (see Figure 4.9). The chemical irreversibility of the Fc monolayer has been noted previously and occurs for oxidation of ferrocene in the presence of Cl^- ion due to ion paring between the Fc^+ and chloride which prevents the reduction back to Fc.[152] All measurements in this work were performed in Tris NaCl buffer to ensure this process occurs and is not present when measured in Sodium Perchlorate as seen if Figure 4.7. This chemical irreversibility is key to the release mechanism as it ensures the Fc/CD recombination is avoided.

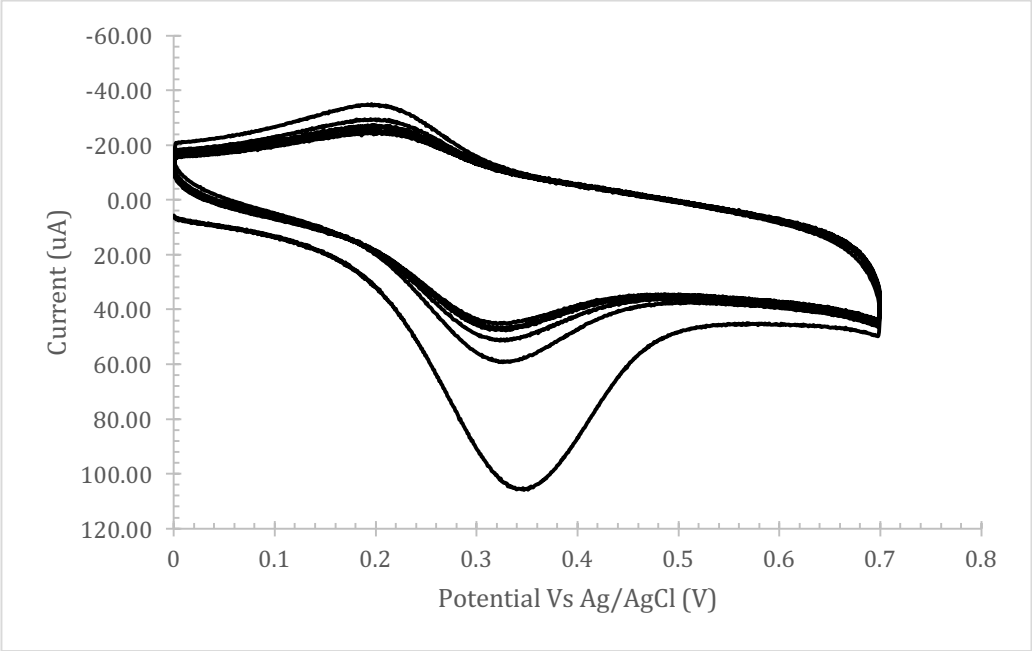

Figure 4.9 Cyclic voltammogram of microcavity array treated with mercaptoethanol on the top surface and ferrocene hexanethiol inside the cavities. The measurement was performed in Tris NaCl buffer at pH 7.4 using a standard 3 electrode set up. The scan was run from 0 to 0.7 V (vs Ag/AgCl Reference) at 100 mV/s. Five consecutive scans were run on the same electrode.

To ensure that the selective pre modification of the top surface of the electrode (according to the method described in Chapter 3) with ME was effective at preventing Fc from adsorbing onto this surface, cyclic voltammograms of ME treated cavities were compared before and after incubation in the thiolated Fc solution. CVs of bare and ME treated cavities were measured in contact with Tris NaCl at a scan rate of 100 mV/s. Within the potential window 0 to 0.7 V vs Ag/AgCl, both voltammograms are very similar albeit with a slight decrease in non-faradaic background on the ME treated electrode from the decreased capacitance of the electrode due to modification of the top surface of the array. Next the ME treated cavities were placed in a solution of 1 mM Fc in ethanol for 24 h, after which they were sonicated in ethanol for 10 min to remove any Fc that was not chemically adsorbed on the surface. The CV of the treated electrode was then measured as before. The voltammogram from this electrode is shown in Figure 4.8 and shows the appearance of an irreversible oxidation peak at around 300 mV which corresponds to the oxidation of Fc on the surface of the electrode. However, the area under peak is significantly lower when compared to the peak observed for cavities where only the top surface of the cavities is blocked with ME prior to treatment with Fc. This indicates that, although not 100 % efficient, ME is very effective at preventing Fc from binding to the electrode surface.

β-CD is known to form a host-guest complex spontaneously with ferrocene due to the hydrophobic–hydrophobic interactions between ferrocene and the interior of β-cyclodextrin.[153] When ferrocene (Fc) is oxidized it becomes positively charged ferrocenium (Fc^+) ion. This charge disrupts the ferrocene/β-cyclodextrin complex and Fc is released from the cavity. The irreversibility of the redox reaction of ferrocene

on the interior of the cavities is advantageous in this release strategy as the formation of the chloride product prevents reformation of the ferrocene/β-cyclodextrin complex, ensuring the β-CD is irreversibly released into the cavity volume where it can diffuse to lipid bilayer, see Scheme 4.1.

Scheme 4.1 Scheme of the electrochemically controlled release of β-CD.

Representative Cyclic voltammetry of the ferrocene-modified cavity array electrodes, which have been incubated in β-cyclodextrin, are shown in Figure 4.10. The initial scan shows an oxidation wave centered at about 370 mV, which has shifted anodically by 120 mV compared with ferrocene alone, unmodified by CD. The reverse process is seen as a reduction peak centered at 250 mV vs Ag/AgCl whose peak area is about 75 % lower than the associated oxidation process as described due to the chemically irreversible nature of the ferrocene oxidation. After a second scan the anodic peak potential shifts, from 370 mV to about 300 mV which is back to a potential comparable with that observed for ferrocene alone without CD inclusion and also with a 50 % decrease in the peak current. The exposure of the Fc^+ allows for the formation of an ion pair with Cl^-, as observed when no CD is present. This shift in peak potential is attributed to loss of ferrocene-CD inclusion complex and the

departure of β-CD from the surface. This behaviour is different from what has been observed in systems where no Cl^- ions are present. Without the formation of the ion pair the oxidation of Fc is completely reversible which significantly hinders the destruction of the host-guest complex.[154] These results suggest that the conditions used here would be optimum for the release of β-CD from the surface of the cavities.

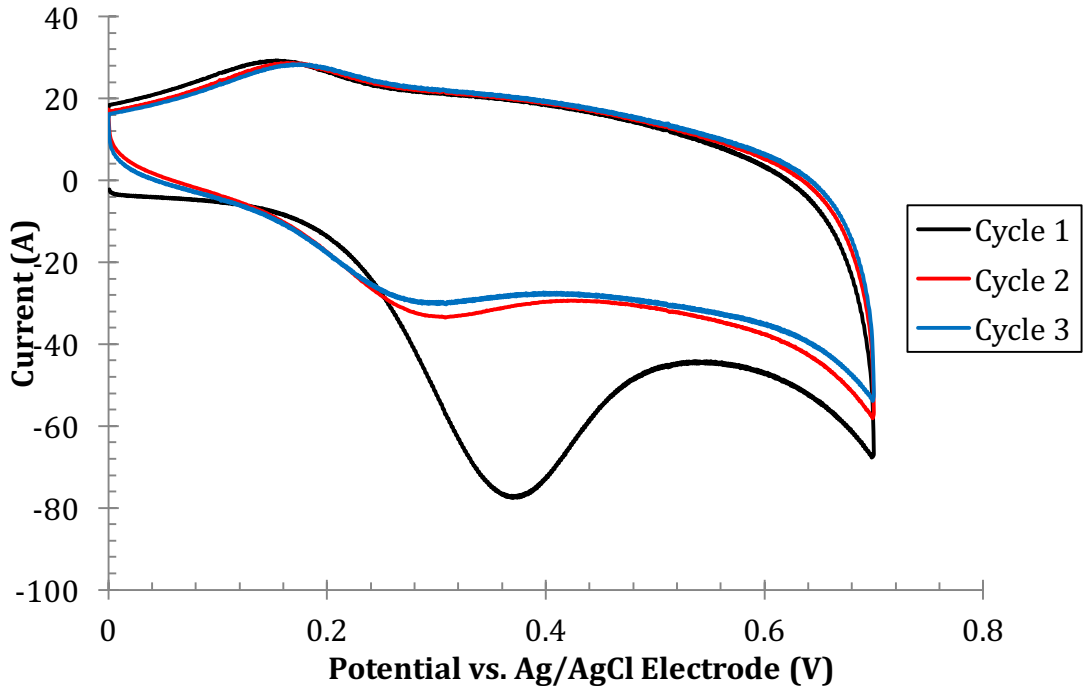

Figure 4.10 Cyclic voltammogram of release of β-CD from the microcavity array. The measurement was performed in Tris NaCl buffer at pH 7.4 using a standard 3 electrode set up. The scan was run from 0 to 0.7 V (vs Ag/AgCl Reference) at 100 mV/s. Two consecutive scans were run on the same electrode; the first scan is shown above in blue and the second in red.

The departure of β-CD from the cavities is also evident in electrochemical impedance spectroscopy data. Figure 4.12 shows the Nyquist plot before and after release of β-CD-SA from the electrode surface, by scanning from 0 to 0.7 V at a scan rate of 100 mV/s, and shows a clear shift of the impedance plot towards the real axis after release, which indicates a decrease in the impedance. This is the opposite to what is seen when the host guest complex is formed on the electrode (see Figure 2.11), which causes an increase in the impedance. These spectra where fit to the equivalent circuit model, described in chapter 3, scheme 3.3 and consisted of the electrolyte solution resistance, R_{sol}, which is in series with the resistance and capacitance of the mercaptoethanol/ferrocene monolayer on the electrode surface in parallel with each other ($R_{m,}$ C_m). The circuit also contains a component for the resistance of the microcavities, R_{cav} and the double layer capacitance, C_{dl}. As with the previous model circuit, this one also uses Constant Phase Elements (CPE) instead of pure capacitors to account for surface defects on both electrode surface, which may cause it to stray from purely capacitive behaviour.

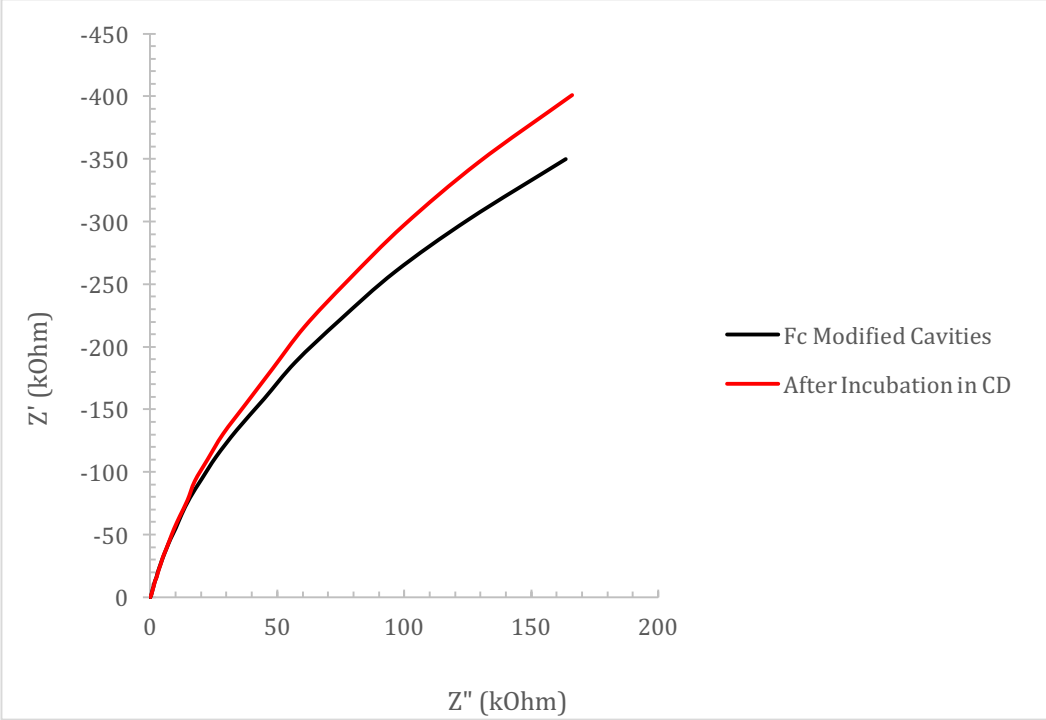

Figure 2.11 Nyquist plot of mercaptoethanol/Ferrocene treated microcavity array before (Black) and after (Red) incubation in 100 µL of β-CD. Measurements were performed at 0 V using a frequency range of 100000 to 0.01 Hz in Tris NaCl buffer at pH 7.4 using a standard 3 electrode set up consisting of a platinum counter an Ag/AgCl reference and the microcavity array as the working electrode.

The experimental and fitted data were in good agreement with one another and representative fit is shown in Figure 2.12 below. The impedance spectra of three separate electrodes was measured during electrode release and the average values obtained by fitting the EIS data to the electrical circuit are shown in Table 4.5 below. As discussed in Chapter 3, there is a significant deviation in the absolute resistance measured form cavity array electrode to cavity array electrode, primarily attributed to deviation in surface area and pore density from electrode to electrode. In order to

minimize this the average change in resistance of the sample compared to the electrode before release is used instead (ΔR_m). Over the three electrodes measured there is a reproducible decrease in the resistance of the monolayer (ΔR_m = -0.81 MΩcm^2) after the electrically controlled release of β-Cyclodextrin, which is consistent with the departure of material from the electrode surface.

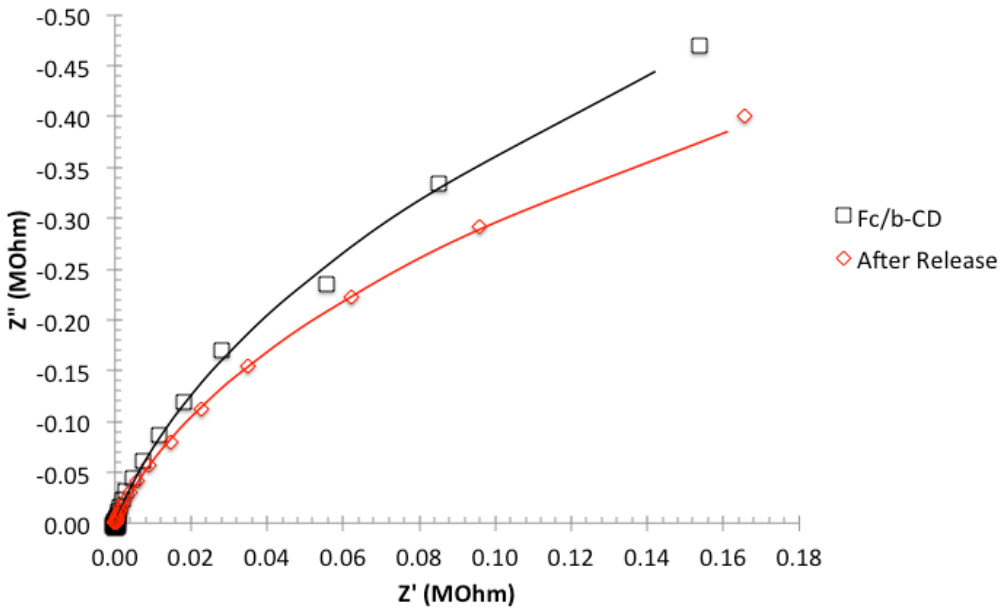

Figure 4.12 Nyquist plot of mercaptoethanol/Ferrocene treated microcavity array after incubation in 100 µL of β-CD (Black) and after electrochemical release of β-CD (Red). Measurements were performed at 0 V using a frequency range of 100000 to 0.01 Hz in Tris NaCl buffer at pH 7.4 using a standard 3 electrode set up consisting of a platinum counter an Ag/AgCl reference and the microcavity array as the working electrode.

Table 4.5 EIS values for the release of β-CD from the electrode surface. Values shown are the average value obtained from measuring 3 separate electrodes.

Sample	R_m ($M\Omega cm^2$)	ΔR_m ($M\Omega cm^2$)	R/R_0
β-CD modified	2.13 ± 0.17		
After release	1.31 ± 0.30	-0.81 ± 0.12	0.61 ± 0.01

4.3.2 Release of Streptavidin to Biotin Containing Bilayers using Ferrocene/β-Cyclodextrin Complex

To investigate if the ferrocene electrorelease method can be applied to spatiotemporal release of reagent to the lower leaflet of a suspended lipid bilayer the protein streptavidin was used to modify the CD release agent. Streptavidin is a protein that has a high affinity for Biotin with a k_d in the order of 10^{14} due to its four binding sites available for Biotin.[155] This makes the streptavidin-Biotin system a useful capture model for testing controlled release to a lipid bilayer. The approach used here is outlined schematically in Figure 4.4; succinyl-β-cyclodextrin was coupled to streptavidin via EDC coupling. Gold microcavity electrodes where modified with ME on the top surface at a mixed monolayer of ME/Fc in the interior of the cavities as before. The electrodes where then incubated in β-CD-SA for 30 min at room temperature to allow the CD-Fc assembly after which they were rinsed to eliminate any unbound CD.

A bilayer comprising of DOPC/DOPE-Biotin (90:10 mol%) was then suspended over the microcavities using the LB and fusion of vesicles containing DOPC/DOPE-Biotin described in Chapter 3. The β-CD-SA was released as before, by scanning voltage from 0 to 0.7 V at a scan rate of 100 mV as before for 3 cycles an example of which is shown in Figure 4.9 The concentration of SA released can be roughly estimated from the CV using the following equation to calculate the surface coverage of the ferrocene:

$$\Gamma = \frac{Q}{nFA}$$

where Q is the oxidation peak area, n is the number of electrons transferred (which is 1), F is Faraday's constant (9.6487 x 10^4 C/mol) and A is the electrode area which was measured as 2.12 cm^2 in Chapter 3. This gives a surface coverage of 2.59 x 10^{-10} mol/cm for the ferrocene. Assuming each ferrocene centre forms a complex with β-CD-SA it can be estimated that 0.55 nmoles of β-CD-SA is released to the bilayer above the cavity.

The impedance spectra of the electrode were measured before and following voltammetric release. The resulting EIS were fit to the equivalence circuit model as described previously (see Scheme 3.3), however, in this case R_m and C_m represent the sum resistance and capacitance of the ME/Fc monolayer on the surface of the electrode and the suspended lipid bilayer.

Figure 4.13 shows the Nyquist plot before and after release of β-CD-SA to a DOPC bilayer containing 10 mol% Biotin. A clear shift towards the imaginary axis is observed which indicates an increase in the impedance after release of β-CD-SA.

Again, because of the variation in the absolute R_{bl} values across the individually prepared substrates, the average change in the resistance compared to the bilayer before release was used (see Table 4.6). Fitting the impedance data of 3 different samples to the equivalent circuit model shows an average increase of the lipid bilayer resistance by 0.50 ± 0.09 MΩcm^2. This increase in the bilayer resistance is tentatively attributed to the binding of the streptavidin to the Biotinylated bilayer, this interaction increases the bilayer thickness and thus the capacitance. This is in contrast to a control experiment where β-CD-SA is released to a DOPC bilayer which is not Biotinylated (see Figure 4.13 and Table 4.6). In a control experiment in the absence of Biotinylation of β-CD-SA release consistently shows a decrease in the average impedance across all three experiments/substrates of of $\Delta R_{bl} = -1.88 \pm 0.63$ MΩcm^2. This decrease in the resistance we attribute to the loss of material from the interior of the cavity surface and its dissolution in the cavity buffer solution without interaction with the bilayer. CD is also known to bind to and extract lipids from lipid bilayers, [134] this may also account for the reduction in resistance observed. The magnitude of the impedance change on CD-SA release to the Biotinylated layer likely reflects combined contributions from capacitance increase due to increased layer thickness along with capacitance decrease due to loss of interfacial layer at the cavity. CD –lipid interactions are likely to be prevented in the biotyinylated layer due to the very high affinity SA has for Biotin, which will essentially traps the CD at these sites.

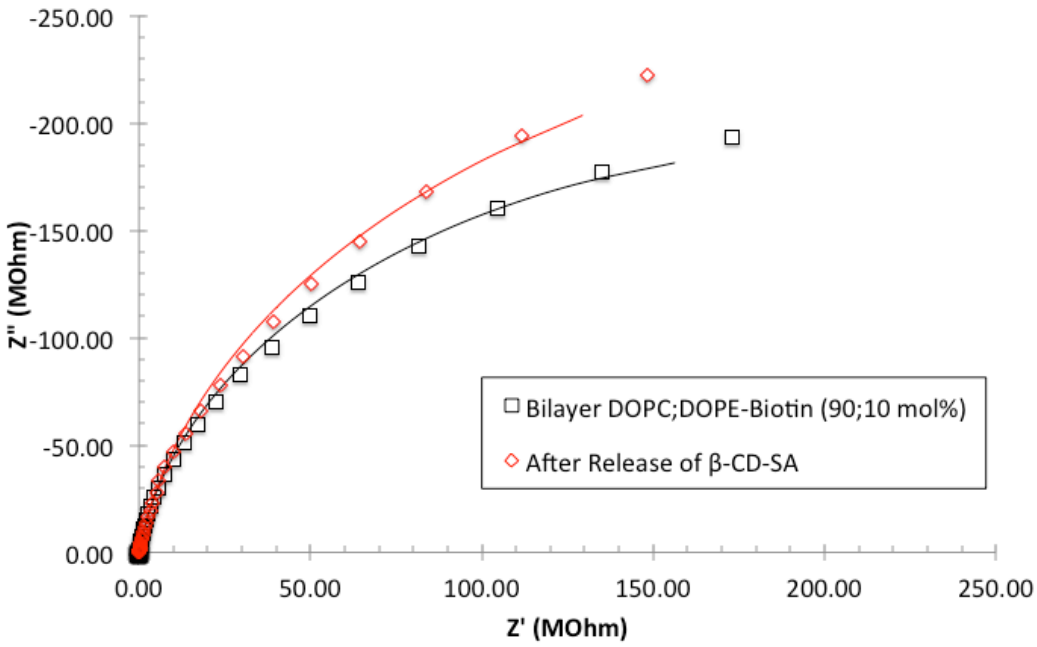

Figure 4.13 Nyquist plot of microcavity array with a DOPC; DOPE-Biotin (90; 10 mol%) bilayer before (Red) and after (Blue) the electrochemical release of β-CD-SA. Measurements were performed at 0 V using a frequency range of 100000 to 0.01 Hz in Tris NaCl buffer at pH 7.4 using a standard 3 electrode set up consisting of a platinum counter an Ag/AgCl reference and the microcavity array as the working electrode.

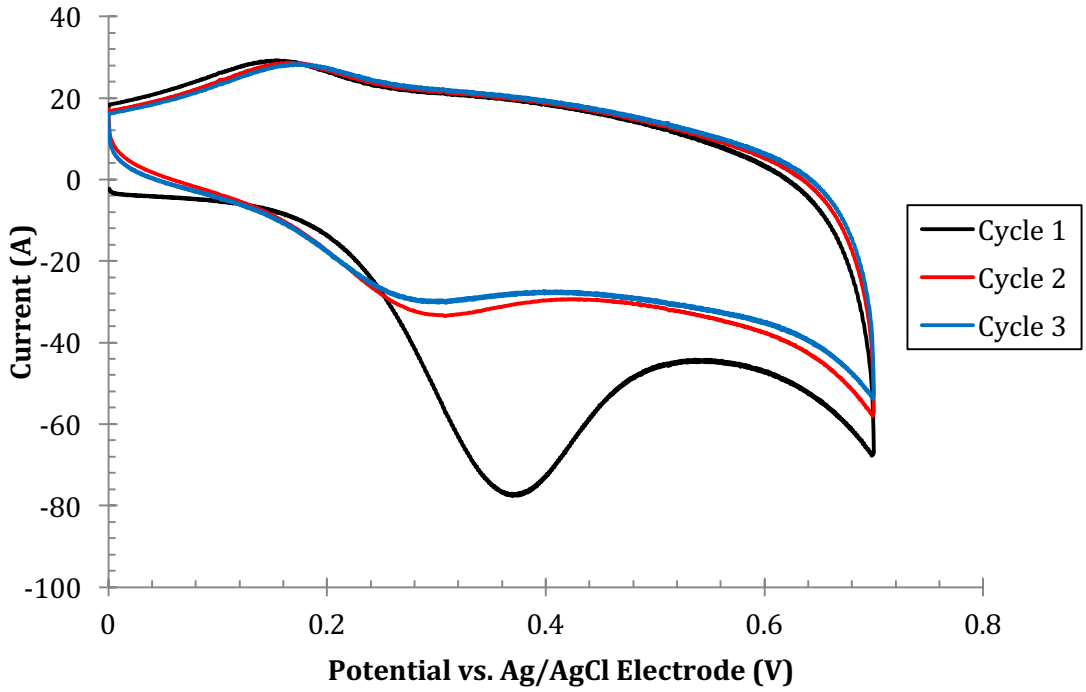

Figure 4.14 Example of CV measured during release of β-CD-SA to a lipid bilayer.

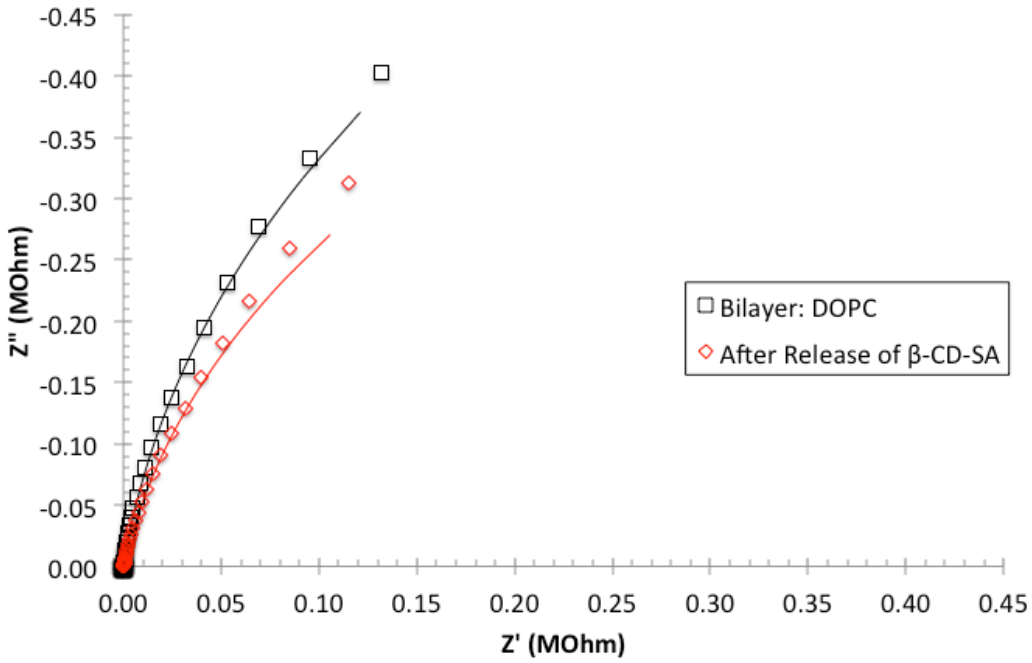

Figure 4.13 Nyquist plot of microcavity array with a DOPC bilayer before (Red) and after (Blue) the electrochemical release of β-CD-SA. Measurements were performed at 0 V using a frequency range of 100000 to 0.01 Hz in Tris NaCl buffer at pH 7.4 using a standard 3 electrode set up consisting of a platinum counter an Ag/AgCl reference and the microcavity array as the working electrode.

Table 4.6 EIS values for the release of β-CD from the electrode surface to a DOPC bilayer containing 10 mol% DOPE-Biotin. Values shown are the average value obtained from measuring 3 separate electrodes.

Sample	Rbl ($M\Omega cm^2$)	ΔRbl ($M\Omega cm^2$)	R/R_0
DOPC:Biotin	5.61 ± 1.47		
After release	3.73 ± 1.30	0.50 ± 0.09	1.10 ± 0.04
DOPC	2.65 ± 0.69		
After release	1.76 ± 0.61	-1.88 ± 0.63	0.66 ± 0.10

4.3.3 Electrorelease of ß-Cyclodextrin to Cholesterol Containing Bilayers

The results obtained in the previous section indicate that the method of releasing material from gold microcavities to a suspended lipid bilayer using ferrocene/β-Cyclodextrin host guest complex is a promising approach for spatiotemporal modification of separate bilayer leaflets. β-Cyclodextrin is well known to bind to cholesterol with a binding constant[156] of 1.7 x 10^4 M^{-1} and is known to remove cholesterol from the plasma membrane of some cells.[157] In the case of the latter, the degree of depletion is dependent on the derivative of β-CD used, concentration, temperature, incubation time, and the cell type from which the cholesterol is being removed. Methyl-β-cyclodextrins (M-β-CD) have been shown to

be the most efficient at removing cholesterol. At concentrations of 5 to 10 mM they have been shown to deplete 80 to 90 % for the total cholesterol from cellular membranes in over 2 h.[158] Although, the affinity is considerably lower than for cholesterol, CD also has affinity for lipids, for example, M-β-CD has been shown to form holes in lipid bilayers composed of DOPC and sphingomyelin (SM) which is thought to be due to the removal of lipids from the bilayer.[159] In other work by Irie *et al*[160] it was shown that β-CD has a stronger affinity for cholesterol then on DPPC and SM, whereas α-CD has a stronger affinity for DPPC then SM whereas γ-CD has an affinity on all three. Importantly for our purposes, Ohvo and Slothe have shown that a solution of 1.4 mM β-CD did not extract any DPPC lipids.[161]

A potential application of the CD release mechanism, might then be to use it as a means of spatiotemporally controlling lipid bilayer composition. This section takes a preliminary look at the impact of the electrochemical release of β-CD into the cavity of bilayer modified cavity arrays in lipid bilayers that contain cholesterol.

β-CD was electrochemically released as before from a gold microcavity electrode where the cavities had been selectively modified with ferrocene. In this instance however, the cavity supported bilayer was composed of DOPC;DOPS;Cholesterol (80:10:10 mol%) and was formed on the microcavity array as before. 10% Chol would be a common concentration to use within a lipid bilayer as a biorelevant concentration.[2] The impedance of the bilayer at the electrode was measured before and after release of the β-CD from the cavity interior surfaces and fitted to the equivalent circuit described in Chapter 3. Figure 4.14 shows representative time dependent impedance data for the CD release. In this case the average bilayer

resistance is 17.65 ± 1.17 MΩcm^2 and is much more resistive then a DOPC bilayer due to the presence of the cholesterol which causes an increase in the hydrophobic thickness of the bilayer[162] and is known to increase the resistance of supported lipid bilayers.[76]

Next the CD was released, as before, by scanning the CV from 0 to 0.70 V at a scan rate of 100 mV/s for 3 consecutive scans. The EIS of the bilayer was measured 15 minutes after the release and can be seen in Figure 4.15 and shows an initial decrease in the bilayer resistance. This can be attributed to the release of β-CD from the electrode surface and may also be due to some removal of cholesterol from the lipid bilayer. When the impedance is measured over time and there is the initial decrease in resistance, after which there is minimal change, see Figure 4., which has plotted R_{bl} normalized against the initial measurement of the bilayer before release (R/R_0). This is compared to the release of CD to a DOPC bilayer measured over the same time scale which shows minimal change in the bilayer resistance, which is shown in Figure 4.13. This may also be symmetrical nature of the lipid bilayer and the fact that only one leaflet if being addressed, meaning that only 50 % of the total cholesterol in the lipid bilayer is available for extraction. Release to a DOPC bilayer shows an initial decrease in the resistance due to the departure of CD from the cavities surface, followed by an increase in the resistance which may be attributed to the reformation of some of the Fc/CD complex inside the cavities. This suggests that the bilayer is only affected by the release of the β-CD within the first 15 minutes after release.

This is something that would have to be kept in mind if this release system was to be used for controlled release to more complex model membranes. However, it may

be useful for further monitoring the effect of removing cholesterol from lipid bilayers. In particular, it could be used to monitor the effect of cholesterol depletion on lipid dynamics such as raft formation.

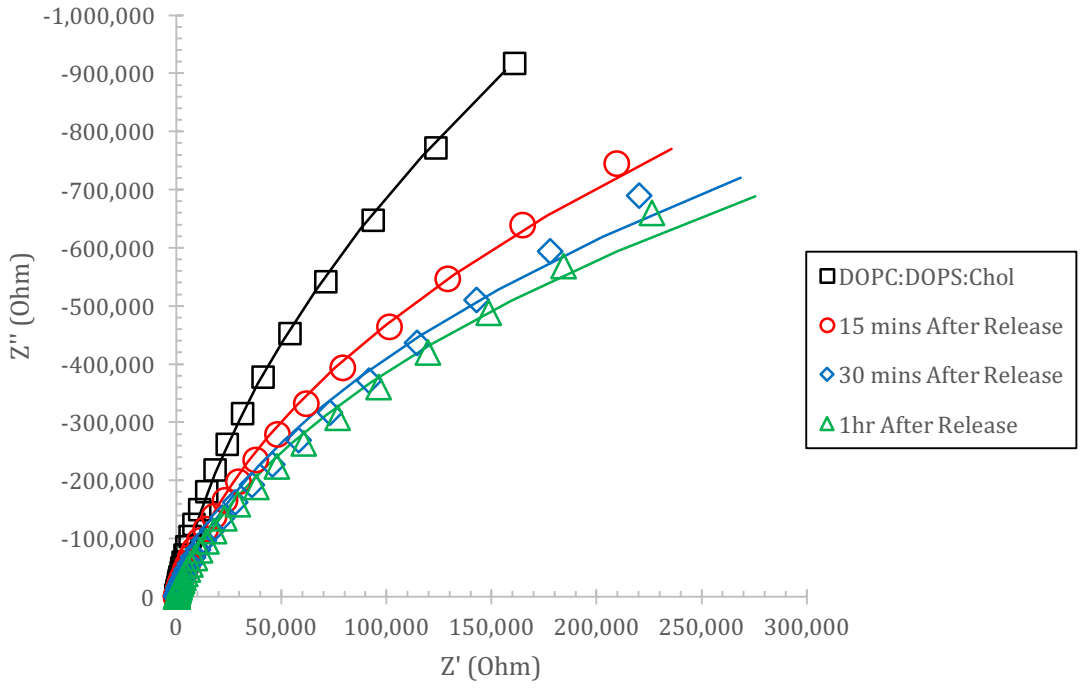

Figure 4.14 Nyquist Plot of β-CD released to Bilayer containing Cholesterol suspended over Gold microcavities. Impedance was measured before and, after release of β-CD to the cavities and after release of β-CD from the cavities. All measurements were performed in Tris NaCl buffer using a platinum counter electrode, Ag/AgCl reference and the gold cavities as the working electrode.

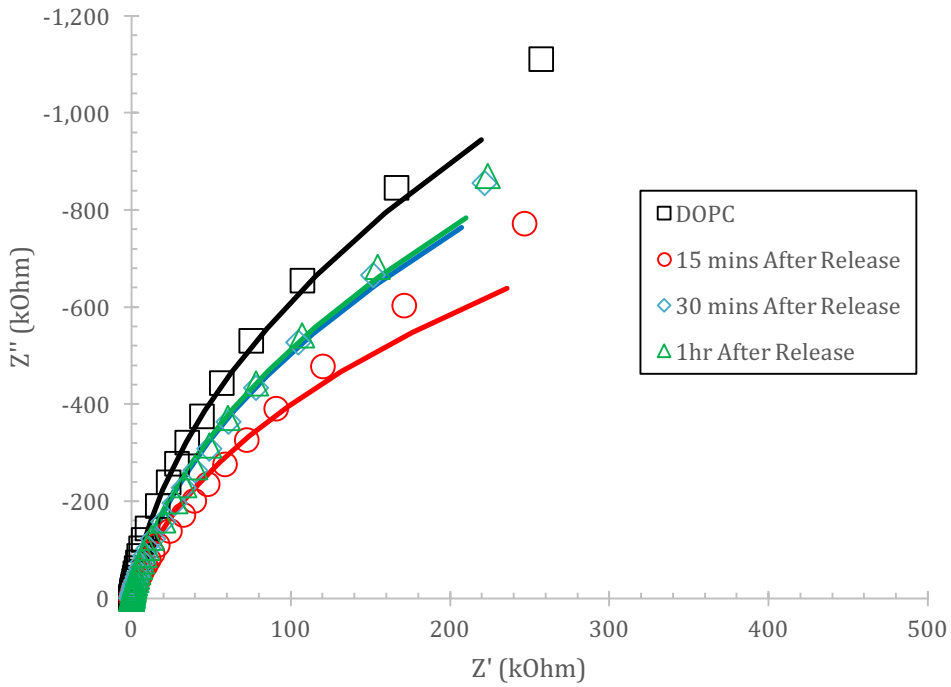

Figure 4.15 Nyquist Plot of β-CD released to a DOPC Bilayer over Gold microcavities. Impedance was measured before and, after release of β-CD to the cavities and after release of β-CD from the cavities. All measurements were performed in Tris NaCl buffer using a platinum counter electrode, Ag/AgCl reference and the gold cavities as the working electrode.

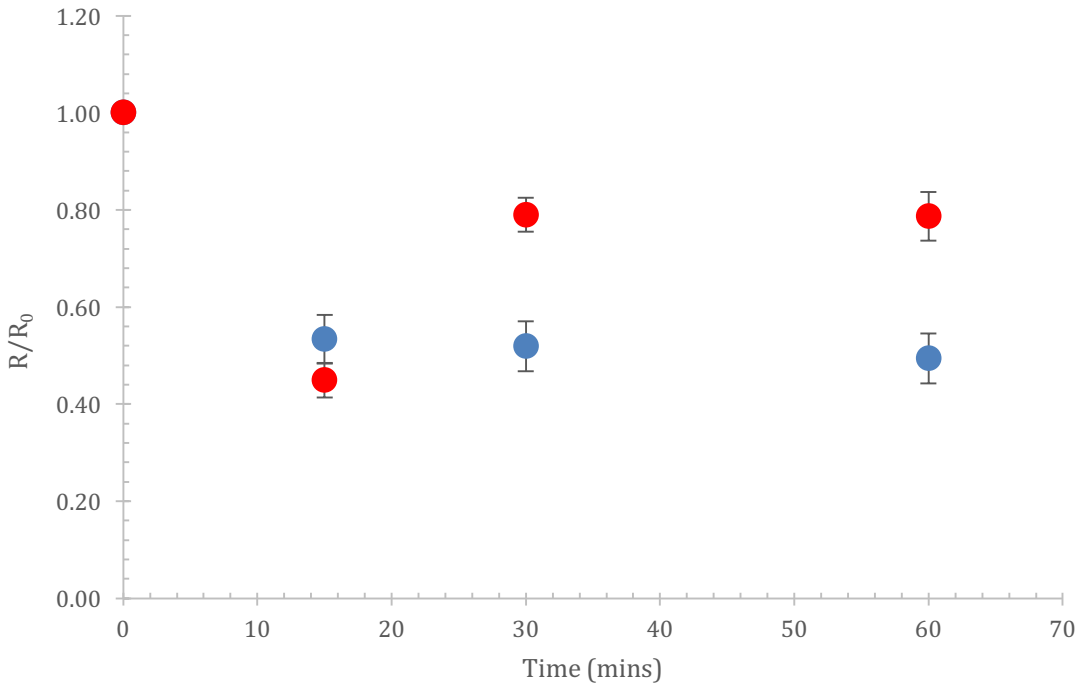

Figure 4.16 Effect of release on Rm over time after release of β-CD to a DOPC:DOPS:Chol (80:10:10 mol%) (blue) and to a DOPC bilayer (red). Results displayed are the average normalized resistance (R/R_0) of three samples.

4.4 Conclusions

Chapter 4 establishes a simple method for the controlled release of material to a lipid bilayer which does not require direct adsorption of the reagent to the electrode and uses low potentials, e.g. allowing spatiotemporal material release from the interior of a microcavity to the proximal lipid bilayer leaflet. The release mechanism was based on a reported supermolecular approach; the interruption of an interfacial ferrocene/β-Cyclodextrin host-guest complex on oxidation of the ferrocene, which was assembled selectively at the interior gold cavities with this supramolecular

structure. The formation and disruption of this supermolecular complex at the interior of the cavity was followed by voltammetry and electrochemical impedance spectroscopy in the absence of a bilayer and showed that the irreversible nature of the Fc in the presence of Cl^- ions allows for the departure of β-cyclodextrin from the cavities surface without fear of the host guest complex reforming.

The ability of the host-guest complex to release material to a lipid bilayer was demonstrated by functionalizing β-cyclodextrin with streptavidin (β-CD-SA) and releasing this to a bilayer containing Biotin. EIS showed a clear increase in the membrane resistance after the release of β-CD-SA to the bilayer which it thought to be due to the binding of SD to the Biotin in the bilayer. In a second preliminary demonstration EIS was used to study the release of of β-Cyclodextrin to a bilayer containing 10% mol/mol cholesterol. CD release caused an irreversible decrease in the resistance which is thought to be due to the removal of cholesterol from the bilayer.

The advantages of this approach are that it can be performed in a buffer solution at low potential. Also the irreversible nature of the redox process in the presence of chloride ions means that the reformation of the host-guest complex is kept to a minimum to ensure the maximum amount of material is delivered to the lipid bilayer. This is enabled by the cavity nature of the array which offers the opportunity to address both sides of a lipid bilayer independently in a temporally controlled way. This method could prove extremely useful for investigating transmembrane proteins which have binding sites on both sides of the bilayer. This method of release would allow for the activation of both sides at the same time, the lower leaflet via electrorelease and the outer leaflet via addition to the external solution.

Chapter 5

An Investigation into use of Photolithographically Prepared silicon moulds for highly reproducible templating of pore arrays.

5.1 Introduction:

Lipid bilayers have been assembled across a variety of substrates with different topographies including flat substrates, curved substrates,[163,164,165] substrates with trench like cavities[166] and substrates with cylindrical pores.[167] Supported lipid bilayers usually conform to the shape of the underlying substrate, for example uniform bilayer formation over substrates with silica nanoparticles showed the bilayer conforming to the curvature of the nanoparticles. Exceptions are sharp nanoprojections which can pierce the bilayer,[168] so radius of the curvature as well as the microscopic smoothness of the substrate is important in dictating bilayer stability. Bilayers can in some cases span over both air filled apertures and, as we have demonstrated in this work, across aqueous filled pores.

Chapter 2 described a method of forming free standing lipid bilayers over aqueous filled PDMS microcavities and chapters 3 and 4 showed the preparation of analogous arrays and their lipid bilayer assembly in gold.

In all cases the microcavity arrays where formed using micro-sphere lithography by exploiting surface assembled polystyrene spheres as templates for PDMS polymerization or as a mask for gold electrodeposition There are a number of advantages to PS sphere templating; it is a relatively easy method, and has generally good reproducibility. However, the key short coming of this approach that may limit its broader, particularly, commercial application, is that it is hard to accurately control the number of spheres deposited on the glass or gold surface to be used as the template. In most depositions there are typically defects, e.g. a planar region where a sphere has

failed to stick and form microcavities. This results in varying numbers of cavities from sample to sample, although this is not a significant issue when interrogating the sample via fluorescent techniques such as FLCS, it does have implications when using other methods like EIS as it has the effect of changing the surface area of the electrode and the relative % of planar versus cavity supported lipid bilayer on a substrate. Size dispersion of the spheres is also important and this variation and along with the fluctuation in relative planar area is the reason in chapter 3 and 4 that we use relative change in impedance rather than absolute impedance to compare the EIS across multiple substrates.

In the final part of this work an investigation into the use of an alternative method to improve reproducibility of the MSLB substrates. The objectives of this work are twofold; to investigate if use of a mould could be used to prepare reproducible arrays capable of water filling and supporting stable MSLBs, and whether the shape of the final cavity aperture affects lipid bilayer assembly.

A bilayers ability to span an aperture depends on many parameters including bilayer composition and surface functionalization,[103] but a key consideration is aperture size. In the case of spherical cavities, it is the cavity diameter which is important. Majority of work reporting lipid bilayers spanning over apertures involve spanning across nanometre dimensions, [48,163,169,170] the largest of which is 700 nm.[171] It is evident from the literature that spanning apertures of dimensions greater than this is difficult, although it is important to point out that in these reports focus on porous substrates where the pore is not fluid filled and the lipid is spanning over air. As described in Chapter 2, we observed in hydrophilic PDMS arrays that DOPC bilayers

were effective in spanning pores of 1 micron diameter. Interestingly, the depth of the pore appears also to have an impact on the bilayers ability to span the feature, with one study showing a fine balance between the diameter of the cavity and the depth.[172]

Using current methods of microlithography would allow for the formation of more uniform and reproducible samples, for example using photolithography of silicon wafers. This process is outlined in figure 5.1 and involves spin coating a photoresist polymer onto the silicon wafer, a photomask with the desired structural features is then aligned above the sample. Next UV light is focused onto the photoresist through the mask causing the photoresist to polymerise and become insoluble. The remaining photoresist can then be washed away and the exposed silicon etched to produce the desired features. However, this results in cavities with abrupt and sharp edges which may cause the bilayer to collapse into the cavity. Studies of lipid bilayers formed on sapphire substrates with sharp steps has shown that such bilayers form discontinuesly.[173]

This chapter explores the use of photolithopgrapically prepared silicon wafers which have cylindrical pillars 3 microns high which would result in apertures which are columnar in shape but with the same approximate aperture size as the arrays reported previously. The aim here is to asses the suitability of these as moulds to form PDMS substrates as an alternative strategy to PS sphere templating. In principle this approach should give us much improved batch to batch uniformity for the arrays and we are hoping will be a first step to improving manufacturability of these platforms. As PDMS is a flexible elastomer it opens the possibility to stretch these surfaces allowing for investigation of changing cavity shape enabled bilayer support.

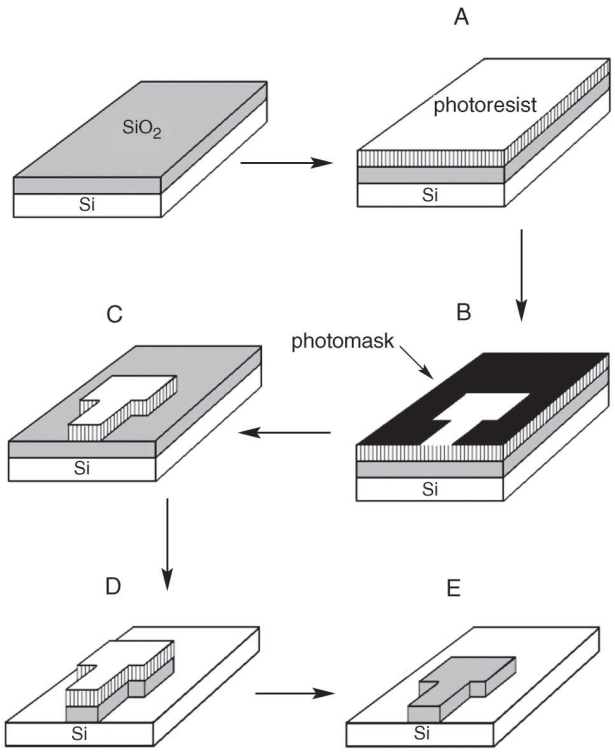

Figure 5.7 Scheme showing photolithography: A) photoresist polymer spin coated onto the silicon wafer. B) Photomask with the desired structural features is then aligned above the sample. C) UV light is focused onto the photoresist through the mask causing the photoresist to polymerise. C) The remaining photoresist can then be washed away and the exposed silicon etched to produce the desired features.

5.2 Experimental:

5.2.1 Materials:

Silicon moulds where prepared by the Tyndall National Institute in Cork, and their fabrication was funded in part through the national access program. The homemade stretching apparatus was built from pieces purchased through Thor Labs Inc. (Germany). Lipids where purchased from Avanti Lipids Inc. (Alabama, USA), and DOPE-Atto655 was purchased form Atto Tech. PDMS elastomer was purchased

from Dow Corning. All other materials where purchased from Sigma Aldrich.

5.2.2 Moulding of PDMS using Tyndall Substrates:

Silicon moulds were prepared by The Tyndall National Institute in Cork to our design specifications consisted of silicon wafers which were fabricated with cylindrical pillars of 3 μm in height. Each mould varied in pillar diameter (D) and pillar separation (S), moulds labelled D3S3 has a pillar diameter of 3 μm and a separation between the pillars of 3μm, whereas moulds labelled D2S2 had a pillar diameter of 2 μm and a separation between the pillars of 2 μm. A schematic representation of our fabrication method with the mould is shown below in Figure 5.8 for clarification. The moulds were treated with perfluorooctyl trichlorosilane (PFOCTS) by placing them in a vacuum desiccator with 2 mL of PFOCTS for 24 h in order to render the moulds hydrophobic. This was done in order to prevent the PDMS from sticking to the structures during moulding. PDMS was then mixed in a 1:10 ratio (Curing Agent: Elastomer) and poured over each mould. Next, the moulds where placed in a vacuum desiccator for 20 min to remove the air bubbles from the PDSM. Finally the moulds where placed on a hot plate at 150 °C for 15 min to cure the PDMS after which the PDMS was peeled from the moulds. Using this approach the moulds could be reused an indefinite number of times to prepare the arrays with no degradation in the reproducibility of the moulded PDMS.

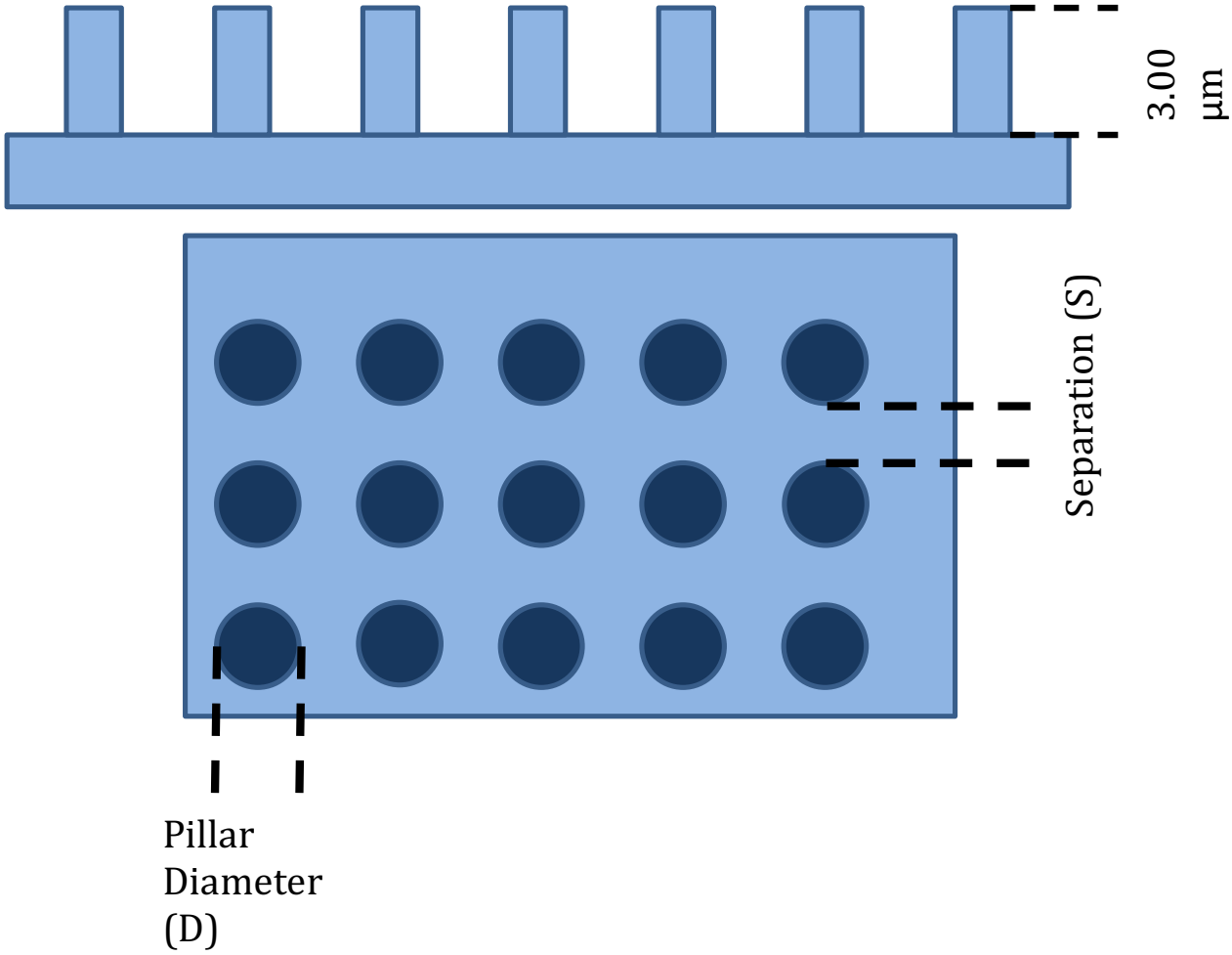

Figure 5.8 Schematic of Tyndall Substrates used to mould PDMS.

5.2.3 Stretching of PDMS:

PDMS substrates moulded from Tyndall moulds were either used directly or were stretched using the home made stretching device shown in Figure 5.10. This rack comprises of a translational stage which was controlled by a micrometer allowing precise control over the extent of stretching. Figure 5.9 shows a schematic representation of the stretching processes. All samples were stretched by 450 microns.

Epoxy glue (Araldite Rapid, Thermo Scientific) was poured onto the stretched arrays and they were adhered to a glass microscope slide whilst still in the rack to prevent the pores from recovering their shape. The glue was allowed to dry for 3 h to reach maximum hardness it was then peeled away from the PDMS to give a new copy of the stretched PDMS made from epoxy. PDMS was then mixed and poured over these moulds in the same manner as mentioned before and cured at 150 °C for 15 min to give a PDMS substrate with stretched pores.

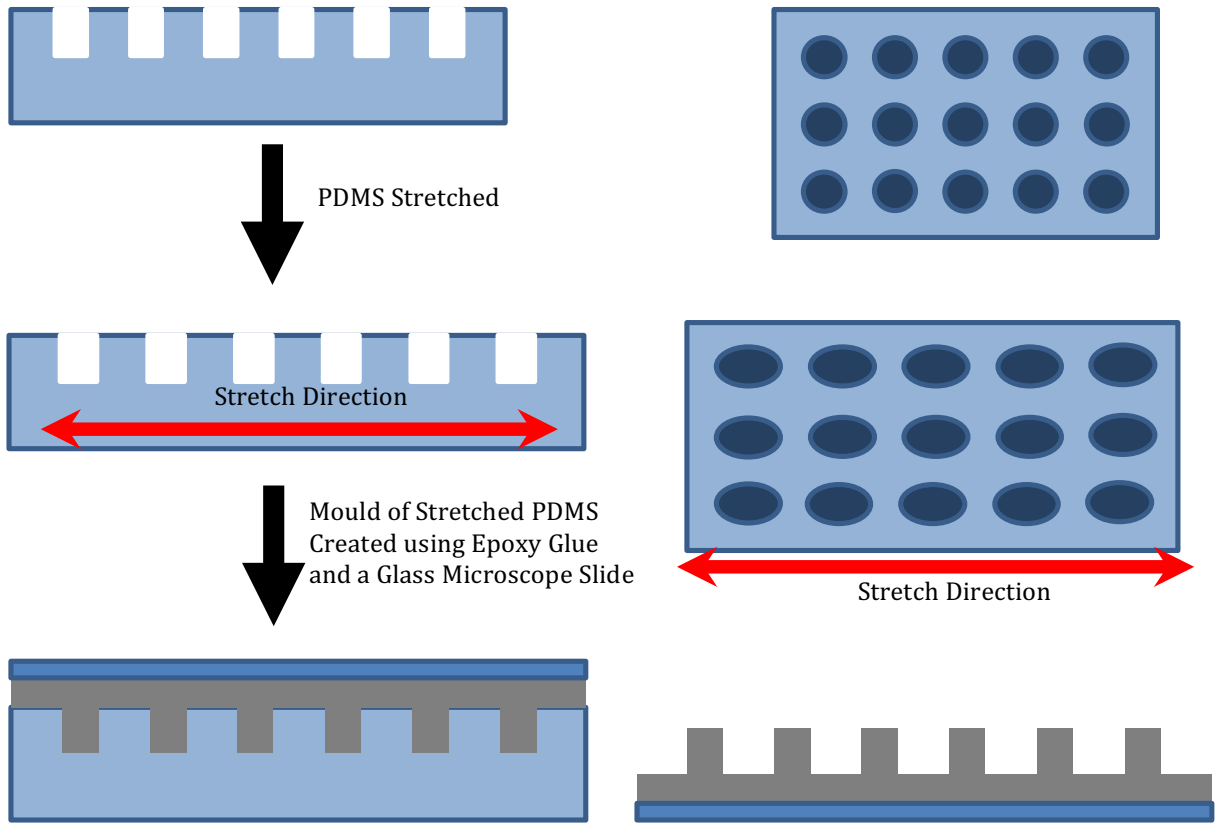

Figure 5.9 Schematic of stretching process.

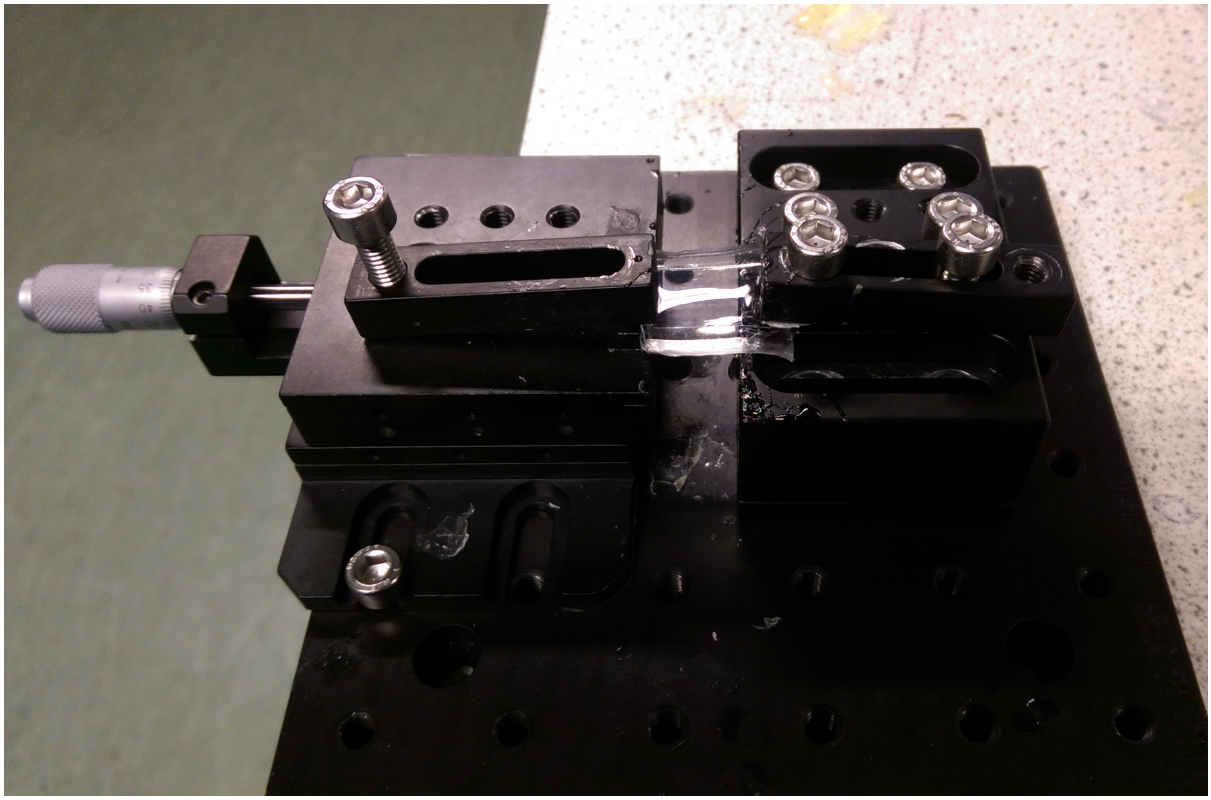

Figure 5.10 Image of device used to stretch PDMS substrates.

5.2.4 Formation of Spanning lipid bilayers over stretched substrates:

To assemble phospholipid bilayers on the PDMS substrates, the substrates were first rendered hydrophilic by treatment in a plasma cleaner, using air as the process gas at a pressure of 1000 mT for 5 min and were then sonicated for 1 h in Tris buffer to pre-fill the cavities with aqueous buffer. After sonication bilayers were formed using the combination of Langmuir-Blodgett monolayer deposition followed by vesicle fusion as described for microcavity PDMS in section 2.3. All bilayers were composed of DOPC with 1 μM DOPE-Atto655 to aid in fluorescence imaging.

5.2.5 Scanning Electron Microscopy:

SEM images where collected on a Hitachi S3400 SEM. Samples were sputter coated with gold prior to imaging to make them conducting. All images were taken using an accelerating voltage of 10 kV and a probe current of 35 μA.

5.2.6 Fluorescence Imaging:

Fluorescence images were taken using a Pico Quant Micro Time 200 microscope. The excitation wavelength used was 640 nm. The collected fluorescence was passed through a 635 long pass filter before collection.

5.3 Results and Discussion:

5.3.1 Characterisation of PDMS Direct from Tyndall Substrates:

PDMS substrates were formed using two different Tyndall moulds, one with pillar diameters of 3 μm and a separation between the pillars of 3 μm (D3S3), and one with a pillar diameter of 2 μm and a separation between the pillars of 2 μm (D2S2). It is important to note that although the aperture dimensions are very similar to the arrays described in Chapters 2 to 4, the separation between the pores, which was limited to a separation of at least a micron by the photolithographic process used by Tyndall National Institute, are much larger than for the PS sphere templating method.

Figure 5.11 and Figure 5.12 show the SEM images of the spherical aperture

samples prepared using moulds D3S3 and D2S2 and reveal uniform spherical apertures formed above cylindrical pores across the entire substrate. Analysis of the images using ImageJ software shows pore diameters of 2.44 ± 0.04 μm for D3S3 and of 1.26 ± 0.02 μm for D2S2.

Interestingly, these diameters are smaller than the diameter of the mould pillars. This may be because they are genuinely narrower, as the PDMS is stretched over the pillars during preparation and then relaxes after peeling from the mould or because the gold deposition used to generate the SEM images narrows the pore apertures.

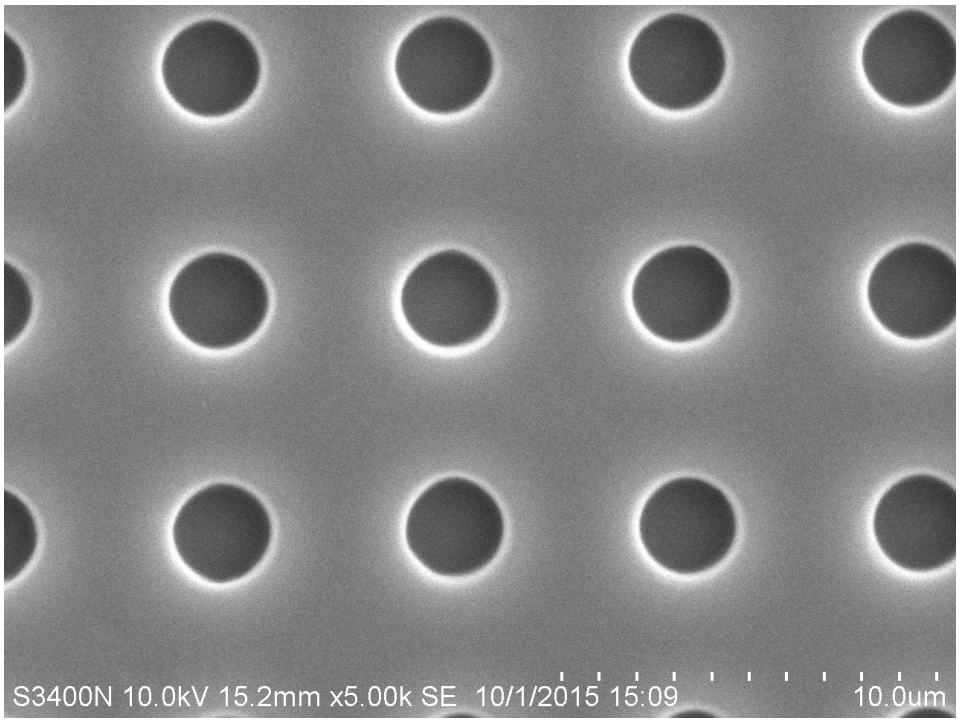

Figure 5.11 SEM image of PDMS moulded using substrate D3S3.

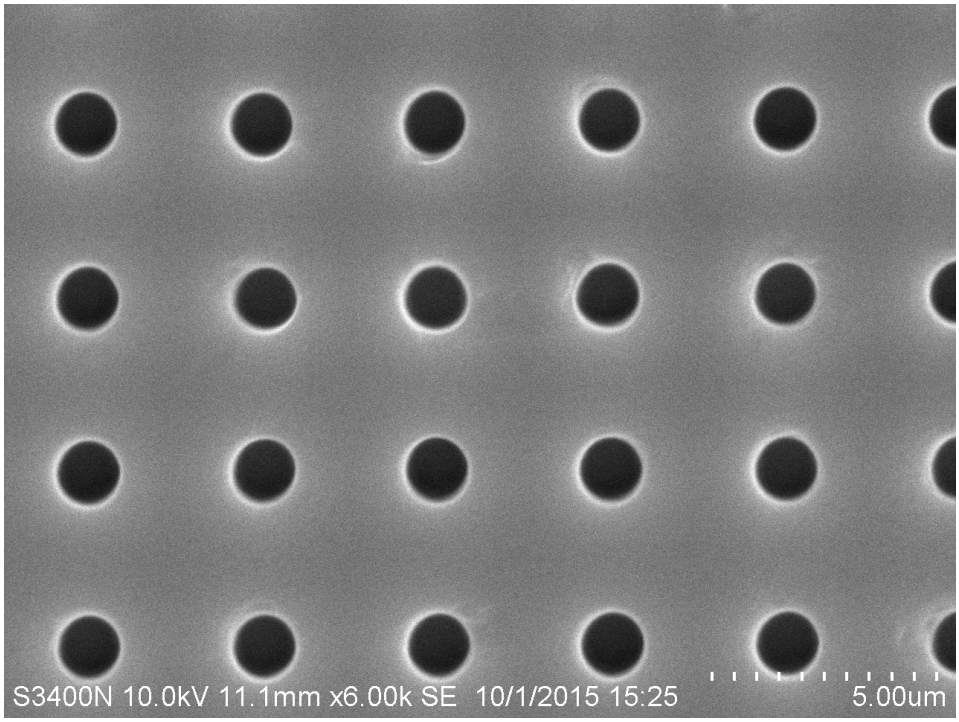

Figure 5.12 SEM image of PDMS moulded using substrate D2S2.

Importantly, though the SEM images confirm use of the mould template yields highly uniform pore sizes and the batch to batch reproducibility was excellent.

5.3.2 Fluorescence imaging of lipid bilayers on cavity substrates Direct From Tyndall Substrates

Next, supported lipid bilayers from DOPC were formed at the arrays using the same method described in Chapter 2. Firstly, the PDMS substrates where treated with air plasma for 5 min to render the substrate hydrophilic. The substrate was then for 1 h in PBS buffer in order to prefill the cavities in order to enable lipid spanning. The

lower leaflet of the bilayer was then formed using a Langmuir Blodgett trough and the upper leaflet by vesicle disruption onto the lower leaflet. In all cases the bilayer was composed of DOPC with 1 μM DOPE-Atto655 to aid in fluorescence imaging. Figure 5.13 shows a fluorescence image of a bilayer formed on a PDMS substrate formed from the D3S3 mould.

Each pore is clearly defined as a dark spot with a bright edge. As described in Chapter 2, the advantage of PDMS array is that the refractive index difference between water and polymer allows us to clearly see when a pore is filled, wherein they appear as bright spots. In this case, it looks as though the pores are not filled. As described also when we see spanning bilayer we see continuous emission from the lipid label across the array. Figure 5.7 clearly shows no spanning of the lipid bilayer and indeed as described the pores appear not to be fluid filled. Multiple attempts were made to promote filling and pore spanning, including extended plasma treatment and sonication to promote fluid filling. None of these attempts were successful and found it was impossible to span a bilayer across these substrates.

Based on the fluorescence images, which across all attempts were similar to those shown in figure 5.6, the most likely explanations for failure is that the water fails to fill the cavity. It looks from the images that it fails to fill the pore at all, but this is unlikely, nonetheless it does not appear to fill to the top edge of the pore creating a meniscus. Therefore assuming some water is present, its meniscus is too deep to support bilayer assembly. Another explanation is that the shape and depth of the cylindrical pores forms sharp edges of the pores pierce the bilayer and either prevent it spanning the pore or cause a discontinuity in the bilayer. The relatively large top

surface area available in these arrays compared with the PS sphere template cavities may also play a role. Nonetheless, whatever the cause we found these materials did not support suspended lipid bilayers.

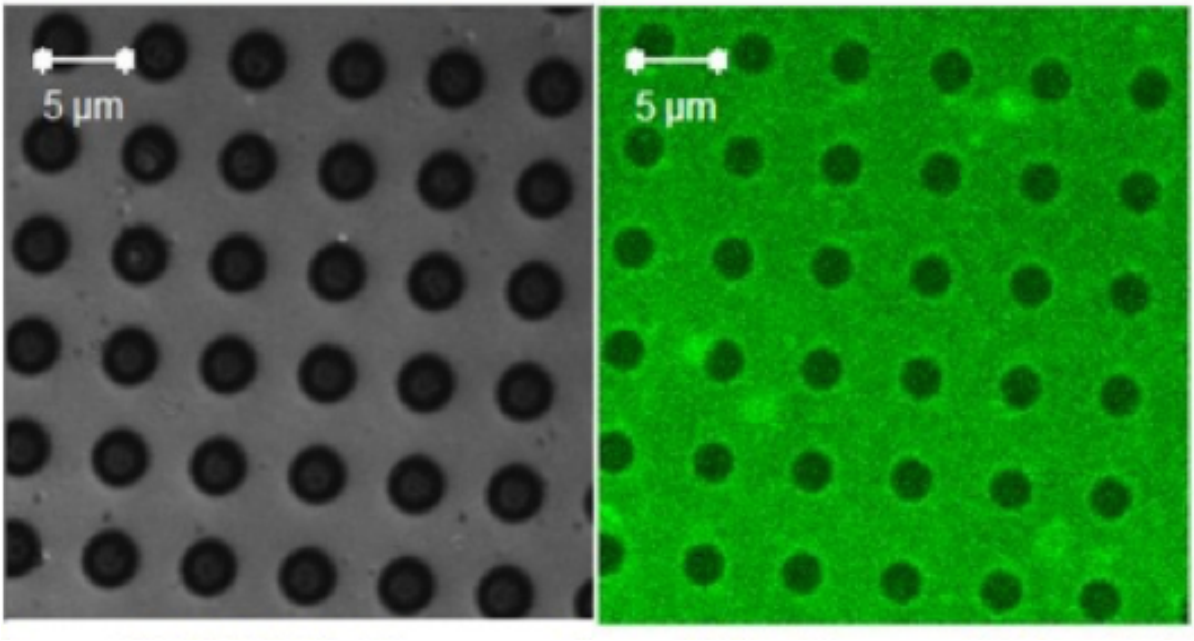

Figure 5.13 Fluorescence imaging of a DOPC bilayer labelled with DOPE-Atto655 on PDMS substrate formed from D3S3 mould.

5.3.3 Moulds made by Stretching PDMS:

We considered that the sharp edges at the pore may play a role either in bilayer disruption or in preventing filling, causing curvature of the bilayer that prevented it spanning. To investigate if we by softening the edges of the array, whilst maintaining the uniformity moulding gives us, we explored the effect of stretching the PDMS

arrays. This was achieved using the home made rack device shown in Figure 5.10 which consisted of a translational stage onto which one side of the PDMS was clamped, while the other end was clamped onto a static stand. The distance the PDMS was stretched over was controlled by a micrometer attached to the translational stage. For this study, all PDMS substrates where stretched by 450 μm.

A previously described procedure, which had been applied to small (sub micron dimensioned pores) was used to form a mould of these stretched pores by using epoxy glue.[174] After stretching, the glue was applied to the pores onto which a glass microscope slide was applied to provide a rigid backing. The glue was allowed to dry for 3 hours to achieve maximum hardness, according to the manufactures specifications, after which it was carefully peeled away form the stretched PDMS. The epoxy moulds formed were imaged by SEM and are shown below (see Figure 5.14 and Figure 5.9). These images show the formation of pillars which appear to be elongated in the direction in which the PDMs was stretched. Side images show also curvature at the base of the pillar. It was hoped such a shape would promote bilayer spanning by avoiding sharp edges at the apertures and also promoting access to plasma treatment and filling.

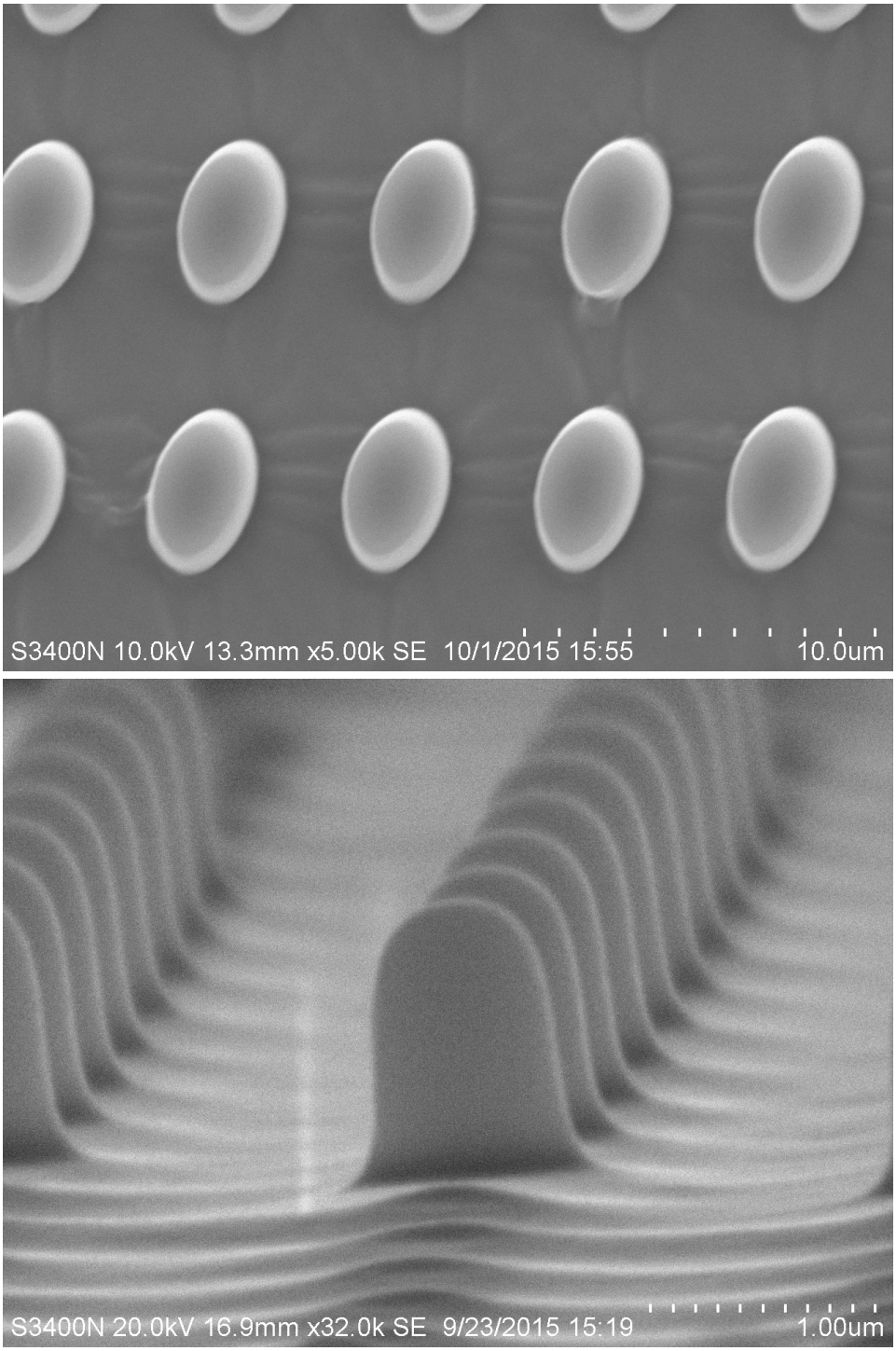

Figure 5.14 Epoxy moulds formed by stretching substrate D3S3

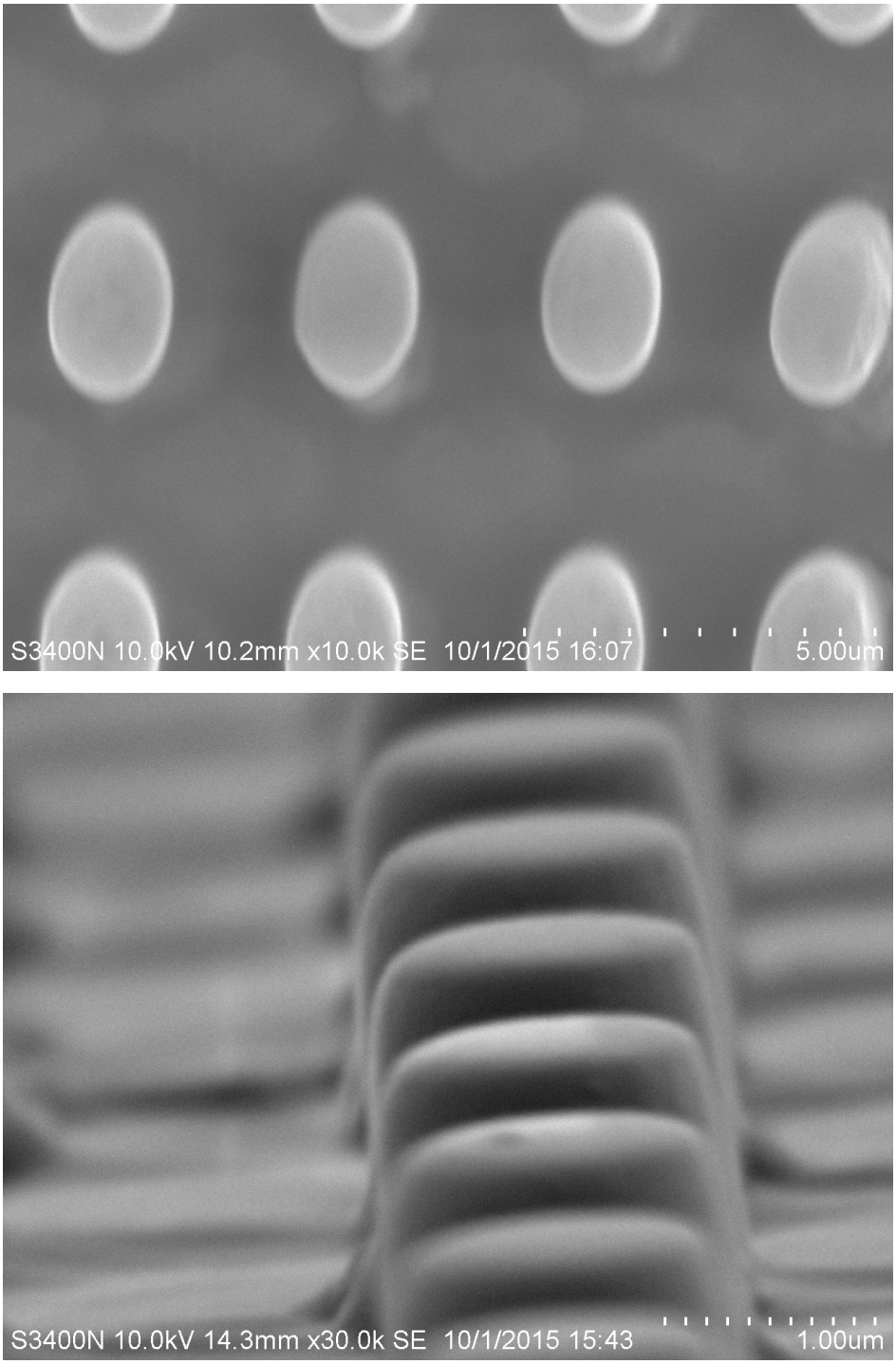

Figure 5.15 Epoxy moulds formed by stretching substrate D3S3

5.3.4 PDMS Formed from Epoxy Moulds:

PDMS was then moulded over the stretched epoxy moulds and was cured for 15 min at 150 °C, which resulted in the successful formation of PDMS substrates with stretched pores. Figure 5.16 and Figure 5.17 show representative SEM images for arrays made from the two pillar dimensions. These images also show that the curved structure observed on the base of the pillars of the epoxy moulds has transferred faithfully onto the PDMS.

The pores were characterised using ImageJ software to extract three key parameters (see Table 5.7). The circularity parameter indicates how circular the pore is, it returns a number between 1 and 0. A value of 1 would indicate a perfect circle whereas the further this member gets to 0 the more elongated the cavity therefore this parameter is useful for demonstrating the degree of deformation of the pores due to stretching. The data in Table 5.7 shows a decrease in the circularity of the pores from around 0.9 to 0.8 after stretching.

The next parameter measured is the Feret diameter comprises two parameters, the maximum Feret diameter and the minimum Feret diameter. The maximum Feret diameter is the maximum distance measured between any two points on the pores circumference giving the maximum diameter, whereas the minimum Feret diameter is the minimum distance between any two points on the pores circumference giving the minimum diameter. These two parameters provide another indication as to the extent of pore stretching. The data below in Table 5.7 shows that for the unstretched substrates the min and max Feret diameters are relatively similar, whereas after

stretching the max Feret becomes at least 1 μm bigger then the min Feret.

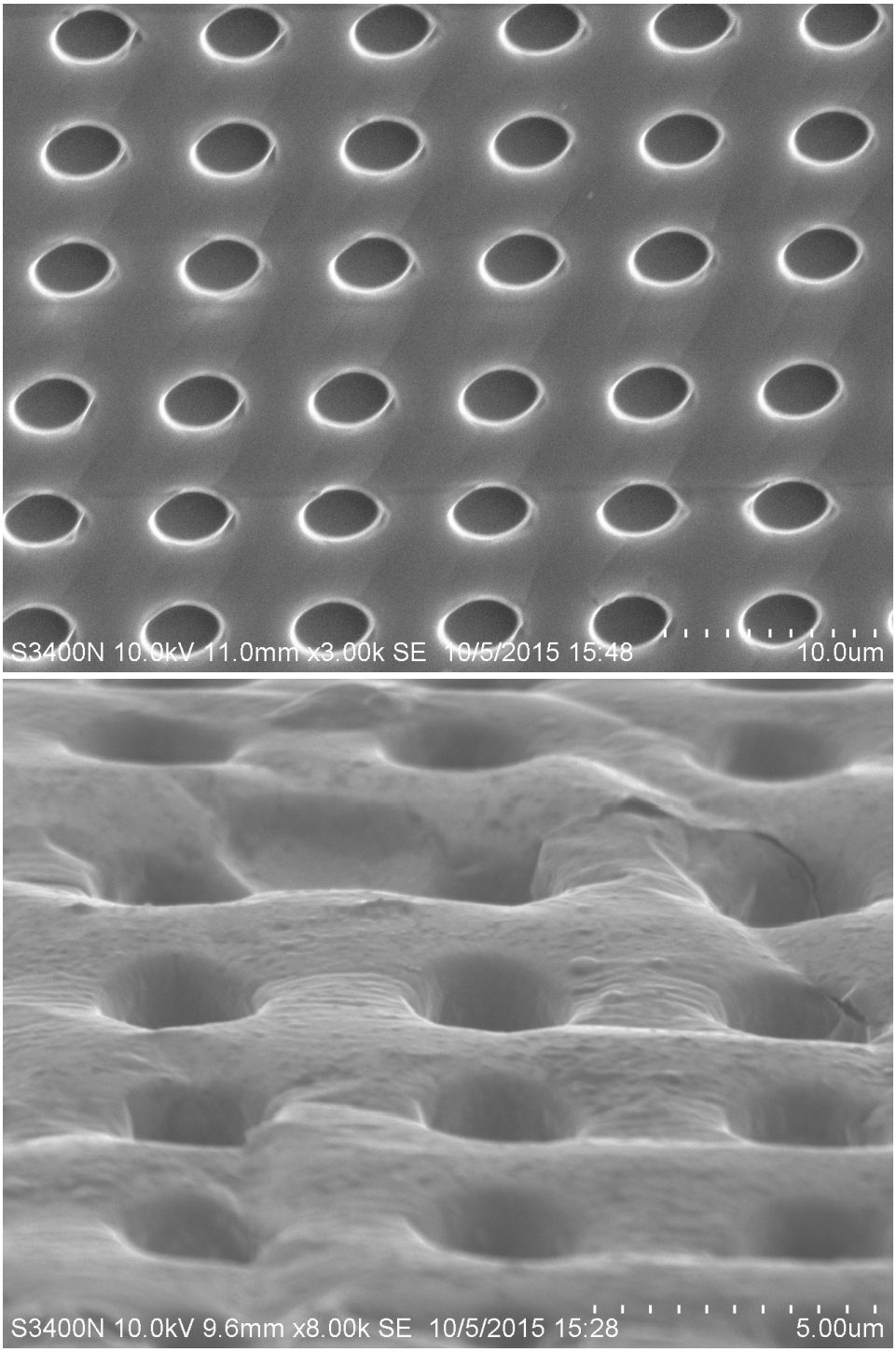

Figure 5.16 PDMS formed using epoxy molds from stretching substrate D3S3

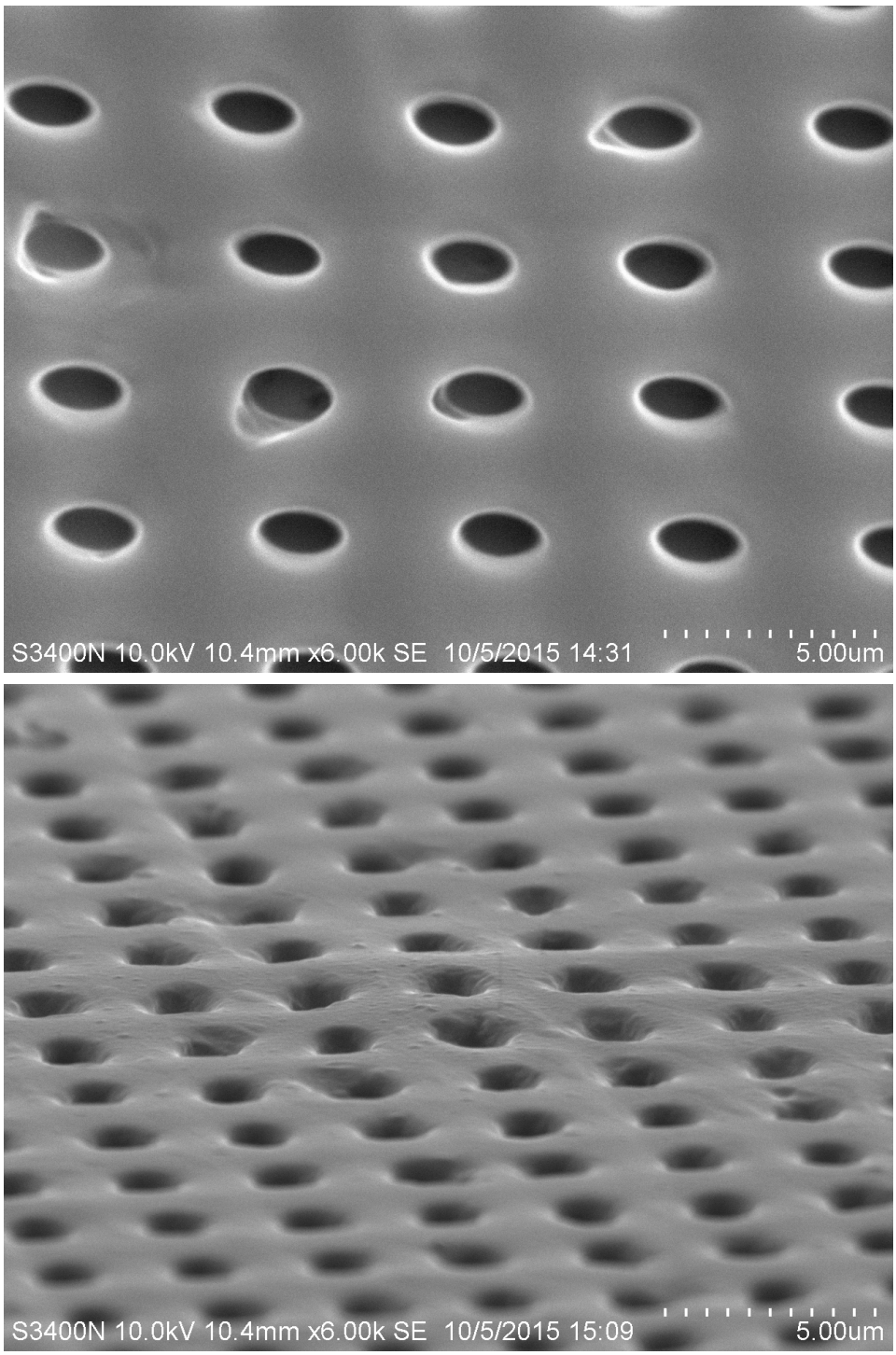

Figure 5.17 PDMS formed using epoxy molds from stretching substrate D2S2

Table 5.7 Data obtained from ImageJ for streached substrates.

Sample	*Diameter (μm)*	*Circularity*	*Max. Feret Diameter (μm)*	*Min. Feret Diameter (μm)*
D3S3	2.44 ± 0.04	0.89 ± 0.07	2.60 ± 0.03	2.45 ± 0.05
D3S3-Streched	2.65 ± 0.04	0.77 ± 0.08	3.33 ± 0.02	2.21 ± 0.04
D2S2	1.26 ± 0.02	0.94 ± 0.04	1.39 ± 0.03	1.23 ± 0.08
D2S2-Streched	1.27 ± 0.02	0.81 ± 0.05	1.83 ± 0.08	0.95 ± 0.05

5.3.5 Fluorescence imaging of lipid bilayers on stretched cavity substrates.

Attempts to prepare microcavity supported lipid bilayers were made using the same method described in Chapter 2. Firstly, the stretched PDMS substrates were treated with air plasma for 15 min to render the substrate hydrophilic. Next, the substrates were sonicated for 1 h in PBS buffer to prefill the cavities in order to aid lipid spanning. The lower leaflet of the bilayer was then formed using a Langmuir Blodgett trough and the upper leaflet by vesicle disruption onto the lower leaflet. In all cases the bilayer was composed of DOPC with 1 μM DOPE-Atto655 to aid in fluorescence imaging.

Figure 5.18 and Figure 5.19 show the fluorescence images of lipid bilayers on stretched PDMS substrates formed using moulds D3S3 and D2S2 respectively. In both cases it is clear that the bilayer is present on the planar areas in between the cavities,

however it seems that the lipid bilayers failed to span the cavities despite of the gentler edge on the cavities and instead conform to the interior of the cavities as they would for the same substrate that was not stretched. It is apparent from this result that the shape of the edge of the cavity is not the only parameter to consider when trying to form suspended lipid bilayers over cylindrical cavities. However, it may be possible that the stretching of the cavity may be preventing the retention of buffer inside the cavity prior to bilayer formation which, in Chapter 2, was shown to be key to the formation of a spanning lipid bilayer.

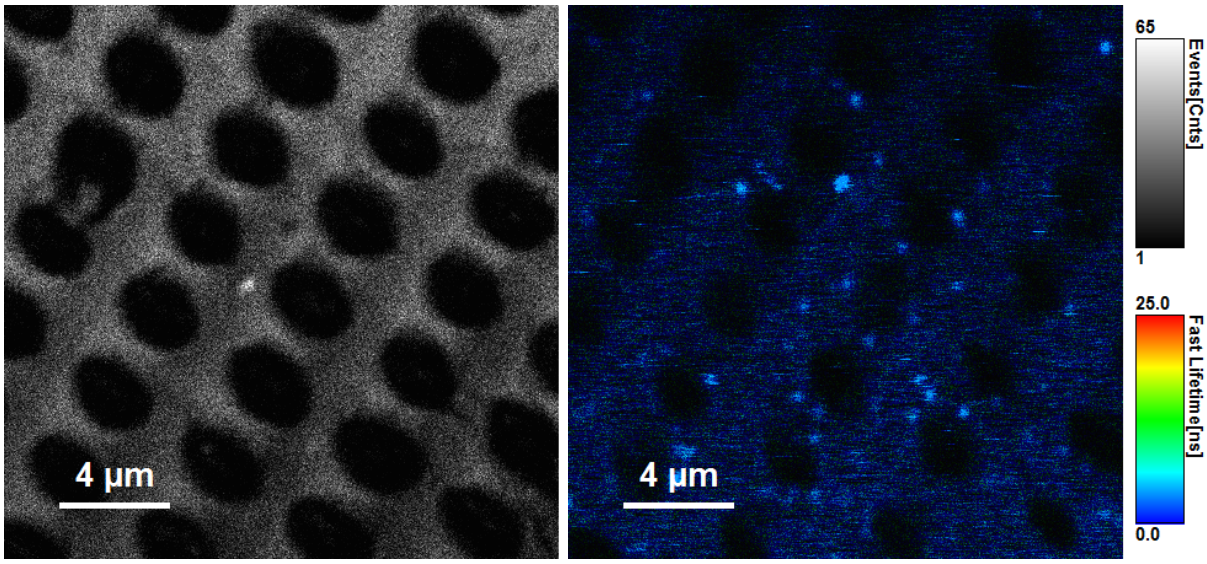

Figure 5.18 20 x 20 micron Fluorescence imaging of a DOPC bilayer labelled with DOPE-Atto655 on stretched PDMS substrate formed from D3S3 mould.

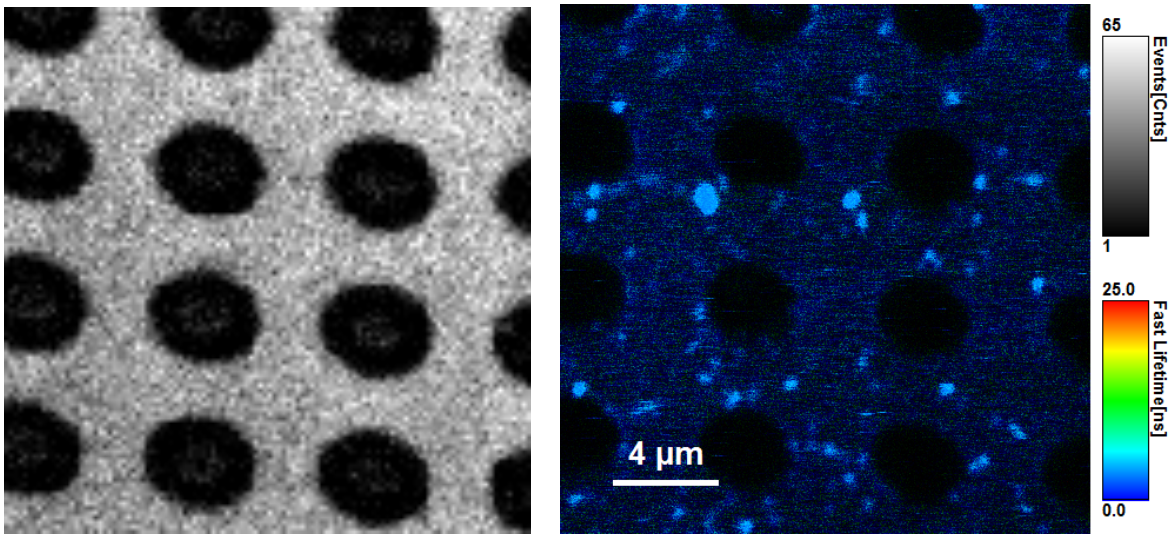

Figure 5.19 20 x 20 micron Fluorescence imaging of a DOPC bilayer labelled with DOPE-Atto655 on stretched PDMS substrate formed from D2S2 mould.

5.3.6 Effect of cavity shape on cavity filling:

To investigate if the shape of the cylindrical pore prevents prefilling of the pores, PDMS cavities formed using the D3S3 Tyndal mould and PDMS cavities formed using 3 micron polymicrospheres where both treated with air plasma for 5 min. After which they were both sonicated for 1 h in Tris NaCl buffer containing 1 µM Rhodamine B (RhB). Figure 5.20 below shows the fluorescence image taken after the prefilling of the two substrates with RhB, and clearly shows the lack of filling in the Tyndall moulded substrate. This is in comparison to the Substrate formed using PS microspheres which shows filling in both the fluorescence and the reflectance image.

This result clearly shows that the shape of the cylindrical pore does not permit retention of aqueous solution following sonication. As discussed in Chapter 2 the prefilling of the pores is key to ensuring lipid bilayer spanning. Further work will be

needed to further develop this work to find the ideal parameters necessary to form suspended lipid bilayers over these cavities. The next parameters to be consider will be surface modification of the arrays, we will move the substrates to gold and modify. What is clear overall, is that the spheres templating method produces pores, that because of their shape and the apparent effect this has on their ability to fill, they are very effective in supporting lipid membranes. If current work which is focused on improving the wettability of the moulded arrays does not work, alternative methods of forming spherical cavities in highly reproducible way will be sought.

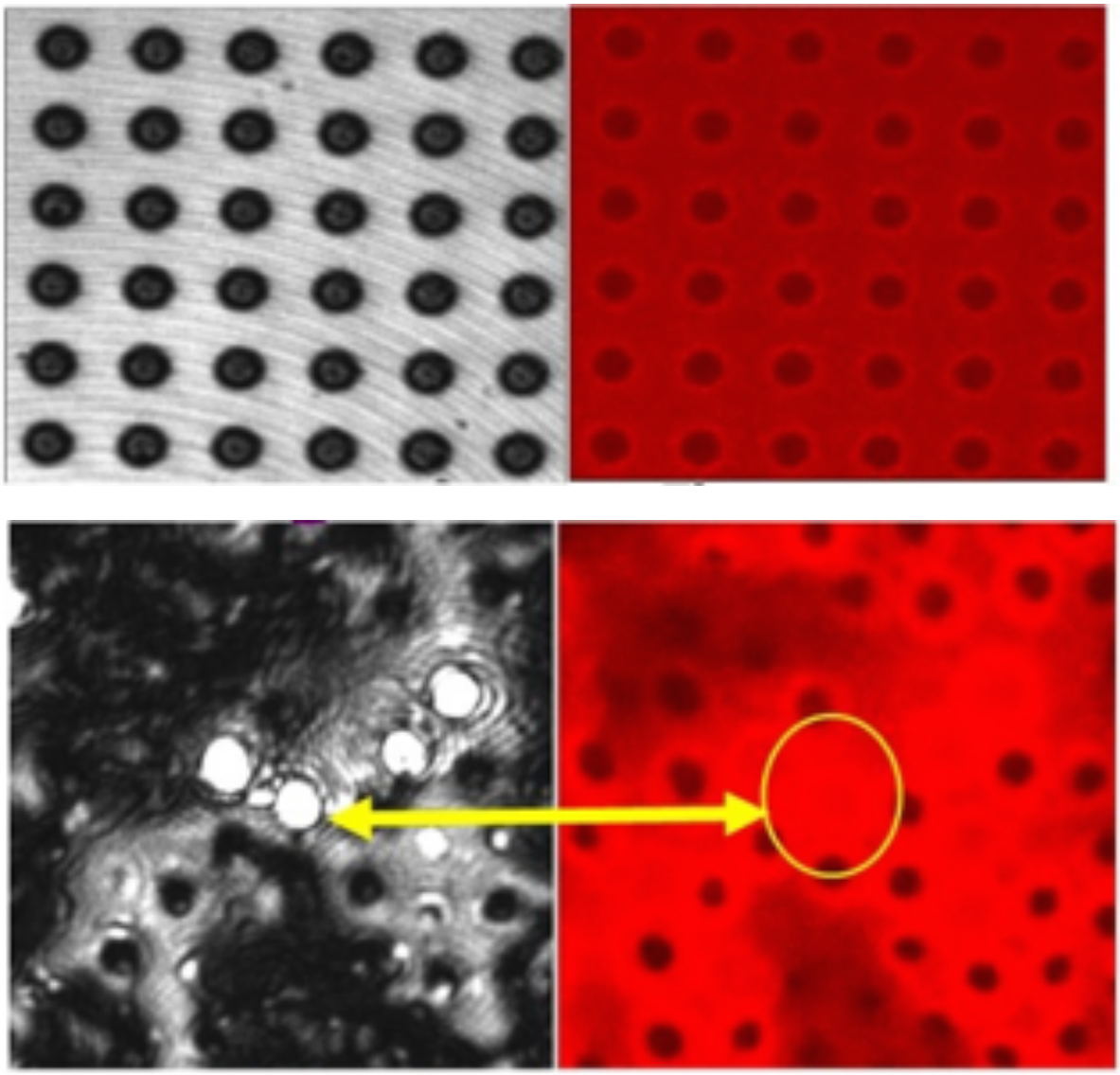

Figure 5.20 Fluorescence image of D3S3 substrate (upper) and PDMS substrate (lower) after 1 hour sonication in Tris NaCl buffer containing 1 μM Rhodamine B (RhB).

5.4 Conclusion:

This work has attempted to develop the cavity arrays discussed in Chapter 2 further by introducing a moulding method for their preparation that was anticipated would lead to improved substrates reproducibility. This has been done by designing silicon moulds (which were fabricated by Tyndall Institute, Cork which have cylindrical pillars 3 microns in height.

Templating in PDMS worked extremely well and reproducible and uniform PDMS cavity arrays were made using a molding method. However, attempts to fill and span lipid bilayers across the array apertures failed. Fluorescence imaging indicated that even with extensive plasma treatment the pores do not effectively fill, which may be an issue due to the hydrophilicity of the deep pores or the sharp edges of the substrates these columnar templates which may prevent fluid access to the plasma and the filling solution.

To address the issue of cavity shape, the substrates were stretched to make the edges of the cavity gentler and hopeful improve filling and bilayer spanning. Although SEM images show clear stretching of the cavities, and the formation of a gentler sloping edge on the cavities, the bilayers still failed to span the cavities as seen with fluorescence imaging. Indeed, we found that pores do not effectively fill with solution, even with stretching. Further work will be needed to explore further the impact on cavity morphology on a bilayers ability to span cavities.

Chapter 6

Conclusion and Future Work

6.1 Conclusion:

Supported lipid bilayers are important models for studying both fundamental biophysical parameters like lipid dynamics and membrane composition/thickness/curvature relationships but also for investigating biomedical concerns such as drug membrane interactions, the study of protein ligand interactions and protein dynamics outside of the complexity of a cell membrane.

In conventional SLBs, as described in Chapter 1, lipids and proteins within supported lipid bilayers interact with underlying substrate. These interactions prevent them from behaving as they do in the cell membrane and in the case of proteins these interactions can even cause denaturation. This thesis explored the application of polymer and metal supports for lipid membranes which contain micron dimensioned spherical pores across which lipid bilayers can span. The long term objective of this work is to create and optimise a new class of SLB; the MSLB which offers a more biomimetic environment for studying lipids and membrane associated proteins in a cell membrane model which is more biorelevant than the SLB but more versatile and stable than the liposome or BLM.

In Chapter 2 it was demonstrated that lipid bilayers of various compositions can be formed on air plasma treated PDMS using vesicle fusion. Diffusion coefficients were found at these substrates to be slightly higher than on glass, for example with DOPC lipids the diffusion on PDMS was 4.37 $\mu m^2/s$ compared to 3.57 $\mu m^2/s$ on glass. Plasma treated, hydrophilic PDMS microcavity arrays were then developed with pores ranging from 1 to 5 microns onto which bilayers where spanned, using a combination

of the Langmuir-Blodgett and vesicle fusion microns in diameter. Diffusion coefficients of lipids in bilayers at these platforms where measured over these cavities and shown that they are 2 to 3 times faster than on flat PDMS, confirming that these substrates are highly valuable for diffusional studies of lipids in which the lipid is completely decoupled from the underlying substrate. These substrates have since been applied to measure the diffusion of two proteins, Glycophorin A and Integrin $\alpha_{IIb}\beta_3$[124].

Chapter 3 dealt with the further development of microcavity supported lipid bilayers toward their application in electrochemical impedance measurements. This was achieved by forming gold microcavities with a diameter of 2.64 micron through electrodeposition using polystyrene spheres. Following DOPC bilayer deposition, by a combination of Langmuir Blodgett monolayer deposition and vesicle fusion, FLCS was used to demonstrate stable lipid bilayers over these cavities formed and that they were fluid as demonstrated for the first time by FLCS over a gold substrate. The result showed lipid diffusion of 2.91 ± 1.29 $\mu m^2 s^{-1}$ and a faster diffusion of 12.58 ± 1.28 $\mu m^2 s^{-1}$ over cavities, indicate formation of stable free standing bilayers on substrates which allow for the control of the aqueous environment on either side of the lipid bilayer like with black lipid membranes, without the instability or use of solvents. This work also demonstrated the first example of a dual system which could be and measure their electrical properties with electrochemical impedance spectroscopy (EIS).

The utility of the porous arrays was further demonstrated by investigating the incorporation of two ionophores Valinomycin and Nigericin. In the case of Valinomycin the ability to create an ionic gradient by prefilling the gold microcavities with a higher concentration of KCl then on the other side of the bilayer caused an

increase in the electrical response observed with EIS. With Nigericin this work shows it was possible to prefill the cavities with KCl and increase H^+ concentration on the other side of the bilayer to observe Nigericen's antiporting activities and result in a reduction of the bilayer resistance of -4.54 Ωcm^2 as measured with EIS.

Chapter 4 further develops the notion of electrochemical addressability in a lipid bilayer system by establishing a simple method for the controlled release of material to a lipid bilayer which does not require direct adsorption of the reagent to the electrode and uses low potentials, e.g. allowing spatiotemporal material release from the interior of a microcavity to the proximal lipid bilayer leaflet. The release mechanism was based on the interruption of an interfacial ferrocene/β-Cyclodextrin host guest complex on oxidation of the ferrocene. The assembly was built selectively at the interior gold cavities of the array by blocking the top surface with a SAM. Studies of the electrochemical behaviour of Fc were examined using CV and showed Fc's irreversible nature in the presence of Cl^- ions. This was shown to be advantageous in releasing CD from the cavity surface and minimizing the reformation of the host guest complex. The ability of host-guest complex to release material to a lipid bilayer was demonstrated by functionalizing β-Cyclodextrin with Streptavidin (β-CD-SA) and releasing this to a bilayer containing biotin. EIS showed a clear increase in the membrane resistance after the release of β-CD-SA to the bilayer which it attributed to be due to the binding of SA to the biotin in the bilayer. In a control experiment without the SA the EIS showed a decrease in the impedance due to the loss of CD-SA from the cavity surface and the absence of interaction with the bilayer. In a second preliminary set of experiments EIS was used to demonstrate that release of β-

Cyclodextrin to a bilayer containing cholesterol to see if it caused a decrease in the resistance of the film due to CD extraction. Indeed, this was observed and compared with the effect of CD release to a bilayer without cholesterol.

To improve processability of the array fabrication, we advanced to cavity array fabrication using photolithograpically prepared columnar moulds. However, although these materials provide excellent reproducibility, they failed to fill or support lipid bilayer even after extensive plasma treatment or modification of the aperture shape through stretching. It seems that for now, the spherical shape created by PS templating is needed for these platforms to work

Overall we have developed advanced lipid bilayer models lipid bilayer spanning microcavity substrates where lipid/protein substrate interactions are massively reduced to provide a system which is in close relation to lipid vesicles. This has been achieved on a polymer substrate to develop a system which can monitor lipid and protein dynamics, and on a gold substrate, which can be used to monitor the electrical properties of the lipid bilayer using electrochemical impedance spectroscopy. The gold substrates have also shown promise to be used as a dual system for both electrochemical and fluorescence interrogation of the lipid bilayer and when coupled with the electrochemically controlled release could prove to be a very powerful tool for investigating the activity of transmembrane proteins that have binding sites on both sides of the lipid bilayer.

6.2 Further work

The following sections outline possible areas of improvement that could be made to the work described in Chapters 2 to 5. Further work to develop the PDMS microcavities described in Chapter 2 would involve developing a method for producing more reproducible substrates. This could be achieved by using silicon moulds, similar to the ones described in Chapter 5. Also, further development of the work in Chapter 5 might help in this by further investigating the relationship between cavity depth, width, separation and shape with a bilayers ability to span a cavity. Once this is achieved, this substrate could possibly be developed into a microfluidic chip, possibly with multiple channels containing independent bilayers which would allow for multiple experiments to be run on the same substrate.

The gold microcavity substrates suffer from a similar problem with reproducibility, however, as they are being used for electrochemical measurements this has a larger effect. The first priority with this work would be to resolve this issue, possibly by using thiolated polystyrene spheres that might self-assemble into a close packed single monolayer of spheres more reproducibly then non functionalised spheres. Next, it would be interesting to investigate the effect of functionalising the top surface of the arrays with a longer chain thiol monolayer. This would be done to try and suppress the electrochemical signal form the area of the bilayer which is not spanning the cavities. Figure 6.1 and Figure 6.2 show the cyclic voltammogram of gold microcavities treated with mercaptohexanol (MHO) and mercaptoundecanol (MUO) in 10 mM potassium ferricyanide, and show that MHO has a slight effect on the electroactivity of the cavities whereas MUO seams to completely block the

electrodes. It would be interesting to measure the EIS response and stability of these electrodes when a bilayer is spanned across them.

The EIS measurements preformed in this work involved measuring over a wide frequency range and fitting the data to an equivalent circuit model to obtain the bilayers electrochemical properties. It would be ideal to move to single frequency measurements to allow for quicker measurements of the bilayer.

Further investigation into different fluorophores for fluorescent measurements of the lipid bilayer would further open the microcavity gold platform into a dual sensing platform. If this is coupled with microfluidics as with the PDMS platform, and with single frequency EIS measurements, it could take the first step open up the platform to becoming a commercial platform for investigating of lipid bilayer models. This could be especially useful for developing a platform for the investigation of the effect of pharmaceuticals on the lipid bilayer or as a method for rapid analysis of a new drug ability to bind to a membrane receptor.

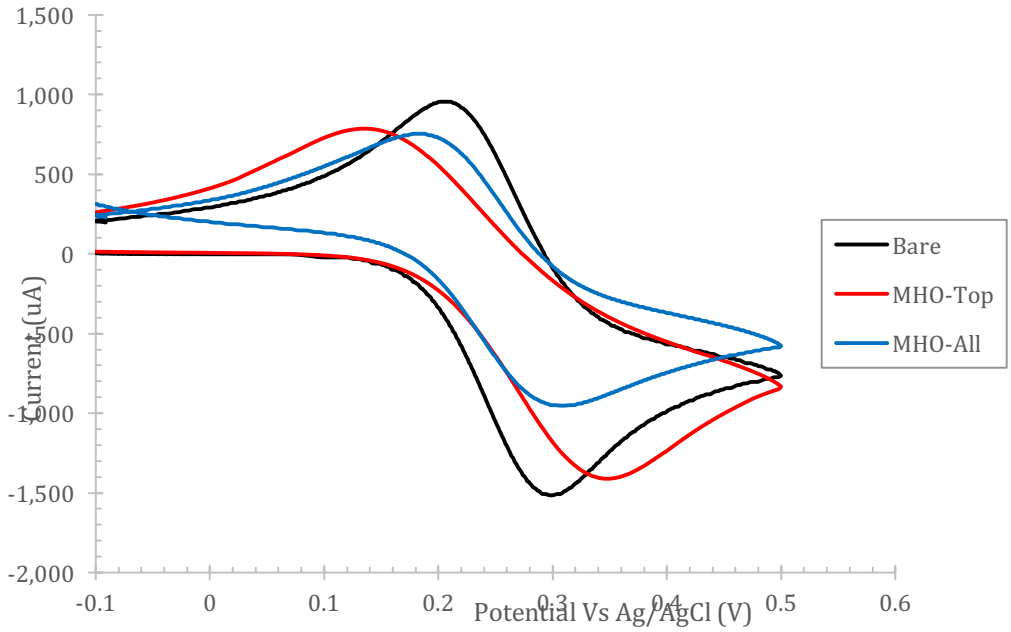

Figure 6.1 CV of mercaptohexanol (MHO) treated gold microcavities. CV's where performed in 10 mM potasium ferricynide in 1 M KCl, using a standard 3 electrode set up with an Ag/AgCl refrence, a platinum counter electrode and the gold cavities as the working. The potential was scanned from -0.1 to 0.5 V at a scan reate of 100 mV/s.

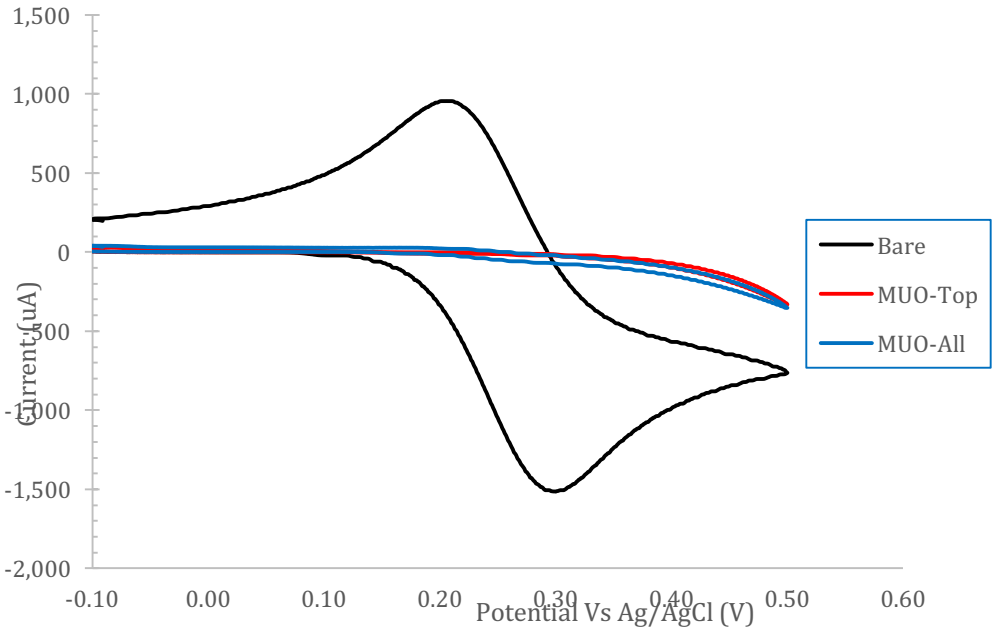

Figure 6.2 CV of mercaptoundecanol (MHO) treated gold microcavities. CV's where performed in 10 mM potasium ferricynide in 1 M KCl, using a standard 3 electrode set up with an Ag/AgCl refrence, a platinum counter electrode and the gold cavities as the working. The potential was scanned from -0.1 to 0.5 V at a scan reate of 100 mV/s.

6.3 References:

1. Yeagle, P. L. Lipid regulation of cell membrane structure and function. *FASEB J. J. Fed. Am. Soc. Exp. Biol.* **3,** 1833–42 (1989).

2. Alberts, B. *et al. Molecular Biology of the Cell*. (Garland Science, 2002).

3. Fernández, C. & Wüthrich, K. NMR solution structure determination of membrane proteins reconstituted in detergent micelles. *FEBS Lett.* **555,** 144–150 (2003).

4. Marassi, F. M. & Opella, S. J. N M R structural studies of membrane proteins. *Curr. Opin. Struct. Biol.* **8,** 640–648 (1998).

5. Sanders, C. R. & Sönnichsen, F. Solution NMR of membrane proteins: Practice and challenges. *Magn. Reson. Chem.* **44,** 24–40 (2006).

6. Russell, Wolfe, Hertz, Starr & McMillan. *Biology the Dynamic Science*. (Yolanda Cossio, 2008).

7. Tanford, C. The hydrophobic effect and the organization of living matter. *Science* **200,** 1012–1018 (1978).

8. *Biochemistry of Lipids, Lipoproteins and Membranes, 5th Eddition*. (2008).

9. Hianik, T. *Bioelectrochemistry*. (John Wiley & Sons, Ltd, 2008).

10. Rawicz, W., Olbrich, K. C., McIntosh, T., Needham, D. & Evans, E. Effect of Chain Length and Unsaturation on Elasticity of Lipid Bilayers. *Biophys. J.* **79,** 328–339 (2000).

11. Szule, J. A., Fuller, N. L. & Peter Rand, R. The Effects of Acyl Chain Length and Saturation of Diacylglycerols and Phosphatidylcholines on Membrane Monolayer Curvature. *Biophys. J.* **83,** 977–984 (2002).

12. Singer, S. J. & Nicolson, G. L. The fluid mosaic model of the structure of cell

membranes. *Science (80-.).* **175,** 720–731 (1972).

13. Voet, J. D., Voet, G. J. & Pratt, C. . *Principles of Biochemistry*. (Whiley, 2008).

14. Filippov, A., Orädd, G. & Lindblom, G. Sphingomyelin structure influences the lateral diffusion and raft formation in lipid bilayers. *Biophys. J.* **90,** 2086–2092 (2006).

15. Bloch, K. E. Sterol, Structure and Membrane Function. *Crit. Rev. Biochem. Mol. Biol.* **14,** 47–92 (1983).

16. Sharma, S. C. Implications of sterol structure for membrane lipid composition, fluidity and phospholipid asymmetry in Saccharomyces cerevisiae. *FEMS Yeast Res.* **6,** 1047–51 (2006).

17. Steltenkamp, S. *et al.* Mechanical Properties of Pore-Spanning Lipid Bilayers Probed by Atomic Force Microscopy. *Biophys. J.* **91,** 217–226 (2006).

18. Stillwell, W. *Biological Membranes From Bilayers to Rafts*. (Academic Press, 2013).

19. Bretscher, M. S. Asymmetrical Lipid Bilayer Structure for Biological Membranes. *Nature* **236,** 11–12 (1972).

20. Wertz, P. W. & Downing, D. T. Glycolipids in mammalian epidermis: structure and function in the water barrier. *Science* **217,** 1261–2 (1982).

21. Sharon, N. & Lis, H. Lectins as cell recognition molecules. *Science.* **246,** 227–234 (1989).

22. Schnaitman, C. a. Protein Composition of the Cell Wall and Cytoplasmic Membrane of Escherichia coli. *J. Bacteriol.* **104,** 890–901 (1970).

23. Gumbiner, B. M. Cell adhesion: The molecular basis of tissue architecture and morphogenesis. *Cell* **84,** 345–357 (1996).

24. Beckerle, M. C. *Cell Adhesion*. (Oxford University Press, 2001).

25. Albert, B. *et al. Essential Cell Biology*. (Garland Science, 2014).

26. Smart, O. S., Goodfellow, J. M. & Wallace, B. a. The pore dimensions of gramicidin A. *Biophys. J.* **65,** 2455–60 (1993).

27. Im, W. & Roux, B. Ion Permeation and Selectivity of OmpF Porin: A Theoretical Study Based on Molecular Dynamics, Brownian Dynamics, and Continuum Electrodiffusion Theory. *J. Mol. Biol.* **322,** 851–869 (2002).

28. Di Leva, F., Domi, T., Fedrizzi, L., Lim, D. & Carafoli, E. The plasma membrane Ca2+ ATPase of animal cells: Structure, function and regulation. *Arch. Biochem. Biophys.* **476,** 65–74 (2008).

29. Therien, a G. & Blostein, R. Mechanisms of sodium pump regulation. *Am. J. Physiol. Cell Physiol.* **279,** C541–C566 (2000).

30. Yamamoto, S., Straka, M., Watarai, H. & Bouř, P. Formation and structure of the potassium complex of valinomycin in solution studied by Raman optical activity spectroscopy. *Phys. Chem. Chem. Phys.* **12,** 11021–11032 (2010).

31. Berezin, S. K. Valinomycin as a Classical Anionophore: Mechanism and Ion Selectivity. *J. Membr. Biol.* 713–726 (2015).

32. Gritsch, S., Nollert, P., Jähnig, F. & Sackmann, E. Impedance spectroscopy of porin and gramicidin pores reconstituted into supported lipid bilayers on indium-tin-oxide electrodes. *Langmuir* **7463,** 3118–3125 (1998).

33. Margolis, L. B., Novikova I, Y. U., Rozovskaya, I. a & Skulachev, V. P. K+/H+-antiporter nigericin arrests DNA synthesis in Ehrlich ascites carcinoma cells. *Proc. Natl. Acad. Sci. U. S. A.* **86,** 6626–6629 (1989).

34. Jung, H., Robison, A. D. & Cremer, P. S. Multivalent ligand-receptor binding on supported lipid bilayers. *J. Struct. Biol.* **168,** 90–94 (2009).

35. Bangham, A. D. & Horne, R. W. Negative Staining of Phospholipids and Their Structural Modification by Surface-Active Agents as Observed in the Electron Microscope. *J. Mol. Biol.* **8,** 660–668 (1964).

36. Hope, M. ., Bally, M. B., Webb, G. & Cullis, P. R. Production of large unilamellar vesicles by a rapid extrusion procedure. Characterization of size distribution, trapped volume and ability to maintain a membrane potential. *Biochim. Biophys. Acta* **812,** 55–65 (1985).

37. Angelova, M. I. & Dimitrov, D. S. Liposome Electro formation. *Faraday Discuss. Chem. SO* **81,** 303–311 (1986).

38. Scherfeld, D., Kahya, N. & Schwille, P. Lipid dynamics and domain formation in model membranes composed of ternary mixtures of unsaturated and saturated phosphatidylcholines and cholesterol. *Biophys. J.* **85,** 3758–3768 (2003).

39. Kahya, N., Scherfeld, D., Bacia, K., Poolman, B. & Schwille, P. Probing Lipid Mobility of Raft-exhibiting Model Membranes by Fluorescence Correlation Spectroscopy. *J. Biol. Chem.* **278,** 28109–28115 (2003).

40. Kahya, N., Scherfeld, D., Bacia, K. & Schwille, P. Lipid domain formation and dynamics in giant unilamellar vesicles explored by fluorescence correlation spectroscopy. *J. Struct. Biol.* **147,** 77–89 (2004).

41. Dietrich, C. *et al.* Lipid rafts reconstituted in model membranes. *Biophys. J.* **80,** 1417–28 (2001).

42. Wesołowska, O., Michalak, K., Maniewska, J. & Hendrich, A. B. Giant unilamellar vesicles - a perfect tool to visualize phase separation and lipid rafts in model systems. *Acta Biochim. Pol.* **56,** 33–39 (2009).

43. Tanaka, T. & Yamazaki, M. Membrane fusion of giant unilamellar vesicles of neutral phospholipid membranes induced by La3+. *Langmuir* **20,** 5160–5164 (2004).

44. Kahya, N., Pécheur, E. I., de Boeij, W. P., Wiersma, D. A. & Hoekstra, D. Reconstitution of membrane proteins into giant unilamellar vesicles via peptide-induced fusion. *Biophys. J.* **81,** 1464–1474 (2001).

45. Ramadurai, S. & Holt, A. Lateral diffusion of membrane proteins. *J. Am. Chem. Soc.* **131,** 12650–6 (2009).

46. Chiantia, S., Schwille, P., Klymchenko, A. S. & London, E. Asymmetric GUVs Prepared by MβCD-Mediated Lipid Exchange: An FCS Study. *Biophys. J.* **100,** L1–L3 (2011).

47. Muller P, Rudin D.O., Tien H. Ti, W. W. C. Methods for the formation of single bimolecular lipid membranes in aqueous solution. *J. Phys. ...* **67,** 534 (1963).

48. Römer, W. & Steinem, C. Impedance analysis and single-channel recordings on nano-black lipid membranes based on porous alumina. *Biophys. J.* **86,** 955–965 (2004).

49. Schmitt, E. K., Vrouenraets, M. & Steinem, C. Channel activity of OmpF monitored in nano-BLMs. *Biophys. J.* **91,** 2163–2171 (2006).

50. Hladky, S. B. & Gruen, D. W. Thickness fluctuations in black lipid membranes. *Biophys. J.* **38,** 251–258 (1982).

51. Castellana, E. T. & Cremer, P. S. Solid supported lipid bilayers: From biophysical studies to sensor design. *Surf. Sci. Rep.* **61,** 429–444 (2006).

52. Tamm, L. K. & McConnell, H. M. Supported phospholipid bilayers. *Biophys. J.* **47,** 105–13 (1985).

53. Cremer, P. & Boxer, S. Formation and spreading of lipid bilayers on planar glass supports. *J. Phys. Chem. B* **291,** 2554–2559 (1999).

54. McKiernan, a E., Ratto, T. V & Longo, M. L. Domain growth, shapes, and topology in cationic lipid bilayers on mica by fluorescence and atomic force microscopy. *Biophys. J.* **79,** 2605–15 (2000).

55. Jass, J., Tjärnhage, T. & Puu, G. From Liposomes to Supported, Planar Bilayer Structures on Hydrophilic and Hydrophobic Surfaces: An Atomic Force Microscopy Study. *Biophys. J.* **79,** 3153–3163 (2000).

56. Keller, C. a, Glasmästar, K., Zhdanov, V. P. & Kasemo, B. Formation of supported membranes from vesicles. *Phys. Rev. Lett.* **84,** 5443–6 (2000).

57. Leonenko, Z. V., Carnini, a. & Cramb, D. T. Supported planar bilayer formation by vesicle fusion: The interaction of phospholipid vesicles with surfaces and the effect of gramicidin on bilayer properties using atomic force microscopy. *Biochim. Biophys. Acta - Biomembr.* **1509,** 131–147 (2000).

58. Keller, C. A. & Kasemo, B. Surface specific kinetics of lipid vesicle adsorption measured with a quartz crystal microbalance. *Biophys. J.* **75,** 1397–1402 (1998).

59. Richter, R. P., Bérat, R. & Brisson, A. R. Formation of solid-supported lipid bilayers: an integrated view. *Langmuir Acs J. Surfaces Colloids* **22,** 3497–3505 (2006).

60. Paternostre, M. T., Roux, M. & Rigaud, J. L. Mechanisms of membrane protein insertion into liposomes during reconstitution procedures involving the use of detergents. 1. Solubilization of large unilamellar liposomes (prepared by reverse-phase evaporation) by triton X-100, octyl glucoside, and sodium. *Biochemistry* **27,** 2668–77 (1988).

61. Albertorio, F., Diaz, A., Yang, T. & Chapa, V. Fluid and air-stable lipopolymer membranes for biosensor applications. *Langmuir* **21,** 7476–7482 (2005).

62. Reviakine, I. & Brisson, A. Formation of Supported Phospholipid Bilayers from Unilamellar Vesicles Investigated by Atomic Force Microscopy. *Langmuir* **16,** 1806–1815 (2000).

63. Richter, R. P. & Brisson, A. R. Following the formation of supported lipid bilayers on mica: a study combining AFM, QCM-D, and ellipsometry. *Biophys. J.* **88,** 3422–33 (2005).

64. Machán, R. & Hof, M. Lipid diffusion in planar membranes investigated by fluorescence correlation spectroscopy. *Biochim. Biophys. Acta* **1798,** 1377–91 (2010).

65. Seu, K. J. *et al.* Effect of surface treatment on diffusion and domain formation in supported lipid bilayers. *Biophys. J.* **92,** 2445–50 (2007).

66. Garcia-Manyes, S., Oncins, G. & Sanz, F. Effect of pH and ionic strength on phospholipid nanomechanics and on deposition process onto hydrophilic surfaces measured by AFM. *Electrochim. Acta* **51,** 5029–5036 (2006).

67. Tabarin, T., Martin, A., Forster, R. J. & Keyes, T. E. Poly-ethylene glycol induced super-diffusivity in lipid bilayer membranes. *Soft Matter* **8,** 8743 (2012).

68. Cha, T., Guo, A. & Zhu, X.-Y. Formation of supported phospholipid bilayers on molecular surfaces: role of surface charge density and electrostatic interaction. *Biophys. J.* **90,** 1270–4 (2006).

69. Hovis, J. S. & Boxer, S. G. Patterning and Composition Arrays of Supported Lipid Bilayers by Microcontact Printing. *Langmuir* **17,** 3400–3405 (2001).

70. Lenz, P., Ajo-Franklin, C. M. & Boxer, S. G. Patterned supported lipid bilayers and monolayers on poly(dimethylsiloxane). *Langmuir Acs J. Surfaces Colloids* **20,** 11092–9 (2004).

71. Yang, T., Jung, S., Mao, H. & Cremer, P. S. Fabrication of phospholipid bilayer-coated microchannels for on-chip immunoassays. *Anal. Chem.* **73,** 165–9 (2001).

72. Plant, A. L. Self-Assembled Phospholipid Alkanethiol Biomimetic Bilayers on Gold. *Langmuir* **9,** 2764–2767 (1993).

73. Munro, J. & Frank, C. In Situ Formation and Characterization of Poly (ethylene glycol)-Supported Lipid Bilayers on Gold. *Langmuir* **20,** 10567–10575 (2004).

74. Naumann, R. *et al.* Tethered lipid bilayers on ultraflat gold surfaces. *Langmuir* **19,** 5435–5443 (2003).

75. Steinem, C., Janshoff, a, Ulrich, W. P., Sieber, M. & Galla, H. J. Impedance analysis of supported lipid bilayer membranes: a scrutiny of different preparation techniques. *Biochim. Biophys. Acta* **1279,** 169–80 (1996).

76. Wiegand, G., Arribas-Layton, N., Hillebrandt, H., Sackmann, E. & Wagner, P. Electrical Properties of Supported Lipid Bilayer Membranes. *J. Phys. Chem. B* **106,** 4245–4254 (2002).

77. Tien, H. T. & Ottova, a. L. Supported planar lipid bilayers (s-BLMs) as electrochemical biosensors. *Electrochim. Acta* **43,** 3587–3610 (1998).

78. Ivnitski, D., Wilkins, E., Tien, H. T. & Ottova, a. Electrochemical biosensor based on supported planar lipid bilayers for fast detection of pathogenic bacteria. *Electrochem. commun.* **2,** 457–460 (2000).

79. Johnson, S. J. *et al.* Structure of an adsorbed dimyristoylphosphatidylcholine bilayer measured with specular reflection of neutrons. *Biophys. J.* **59,** 289–294 (1991).

80. Goennenwein, S., Tanaka, M., Hu, B., Moroder, L. & Sackmann, E. Functional incorporation of integrins into solid supported membranes on ultrathin films of cellulose: impact on adhesion. *Biophys. J.* **85,** 646–55 (2003).

81. Elender, G., Kühner, M. & Sackmann, E. Functionalisation of Si/SiO2 and glass surfaces with ultrathin dextran films and deposition of lipid bilayers. *Biosens. Bioelectron.* **11,** 565–577 (1996).

82. Hillebrandt, H., Wiegand, G., Tanaka, M. & Sackmann, E. High Electric Resistance Polymer / Lipid Composite Films on Indium - Tin - Oxide Electrodes. *Langmuir* **15,** 8451–8459 (1999).

83. Baumgart, T. & Offenhäuser, A. Polysaccharide-supported planar bilayer lipid model membranes. *Langmuir* **19,** 1730–1737 (2003).

84. Cooper, M. A. Optical biosensors in drug discovery. *Nat. Rev. Drug Discov.* **1,** 515–528 (2002).

85. Zhang, L. & Granick, S. Lipid diffusion compared in outer and inner leaflets of planar supported bilayers. *J. Chem. Phys.* **123,** 3–6 (2005).

86. Wagner, M. L. & Tamm, L. K. Tethered polymer-supported planar lipid bilayers for reconstitution of integral membrane proteins: silane-polyethyleneglycol-lipid as a cushion and covalent linker. *Biophys. J.* **79,** 1400–1414 (2000).

87. Kaufmann, S., Borisov, O., Textor, M. & Reimhult, E. Mechanical properties of mushroom and brush poly(ethylene glycol)-phospholipid membranes. *Soft Matter* **7,** 9267 (2011).

88. Diaz, A. J., Albertorio, F., Daniel, S. & Cremer, P. S. Double cushions preserve transmembrane protein mobility in supported bilayer systems. *Langmuir* **24,** 6820–6826 (2008).

89. Lang, H., Duschl, C. & Vogel, H. A new class of thiolipids for the attachment of lipid bilayers on gold surfaces. *Langmuir* **10,** 197–210 (1994).

90. Bunjes, N. *et al.* Thiopeptide-Supported Lipid Layers on Solid Substrates. *Langmuir* **13,** 6188–6194 (1997).

91. Schmidt, C., Mayer, M. & Vogel, H. A Chip-Based Biosensor for the Functional Analysis of Single Ion Channels. *Angew. Chemie* **112,** 3267–3270 (2000).

92. Sugihara, K. *et al.* Simultaneous OWLS and EIS monitoring of supported lipid bilayers with the pore forming peptide melittin. *Sensors Actuators B Chem.* **161,** 600–606 (2012).

93. Langmuir, I. The constitution and fundamental properties of solids and liquids. Part II: Liquids. *J. Am. Chem. Soc.* **39,** 1848–1906 (1917).

94. Blodgett, K. B. Films Built by Depositing Successive Monomolecular Layers on a Solid Surface. *J. Am. Chem. Soc.* **57,** 1007–1022 (1935).

95. Langmuir and Langmuir-Blodgett Films, KSV Instruments Application Note.

96. Nwaneshiudu, A. *et al.* Introduction to Confocal Microscopy. *J. Invest. Dermatol.* **132,** e3 (2012).

97. Basit, H., Lopez, S. G. & Keyes, T. E. Fluorescence correlation and lifetime correlation spectroscopy applied to the study of supported lipid bilayer models of the cell membrane. *Methods* **68,** 286–299 (2014).

98. Schwille, P. & Haustein, E. *Fluorescence Correlation Spectroscopy An Introduction to its Concepts and Applications* (2012).

99. Ries, J. & Schwille, P. Fluorescence correlation spectroscopy. *BioEssays* **34,** 361–368 (2012).

100. Buschmann, V. & Krämer, B. Quantitative FCS: Determination of the Confocal Volume by FCS and Bead Scanning with the MicroTime 200. Picoquant Application Note. (2009).

101. Kapusta, P., Patting, M., Gmbh, P. & Rüttinger, S. Fluorescence Lifetime Correlation Spectroscopy using the SymPhoTime Software : FLCS Tutorial. **6,** 13–18 (2008).

102. Heyden, V. Der, Basit, H. & Labb, P. Article de périodique (Journal article) ' Tethered Bilayer Lipid Membranes on Mixed Self- Assembled Monolayers of a Novel Anchoring Thiol : Impact of the Anchoring Thiol Density on Bilayer Formation ' Référence bibliographique Tethered Bilayer Lipid Mem. **27,** 14317–14328

103. Schmitt, E. K., Nurnabi, M., Bushby, R. J. & Steinem, C. Electrically insulating pore-suspending membranes on highly ordered porous alumina obtained from vesicle spreading. *Soft Matter* **4,** 250 (2008).

104. Alvarez, P. E., Gervasi, C. A. & Vallejo, A. E. Impedance Analysis of Ion Transport Through Supported Lipid Membranes Doped with Ionophores: A New Kinetic Approach. *J. Biol. Phys.* **33,** 421–431 (2007).

105. Raguse, B. *et al.* Tethered Lipid Bilayer Membranes: Formation and Ionic Reservoir Characterization. *Langmuir* **14,** 648–659 (1998).

106. Naumann, R., Walz, D., Schiller, S. M. & Knoll, W. Kinetics of valinomycin-mediated K+ ion transport through tethered bilayer lipid membranes. *J. Electroanal. Chem.* **550-551,** 241–252 (2003).

107. Schmitt, E. K., Weichbrodt, C. & Steinem, C. Impedance analysis of gramicidin D in pore-suspending membranes. *Soft Matter* **5,** 3347 (2009).

108. Hennesthal, C. & Steinem, C. Pore-spanning lipid bilayers visualized by scanning force microscopy. *J. Am. Chem. Soc.* **122,** 8085–8086 (2000).

109. Han, X. *et al.* Nanopore Arrays for Stable and Functional Free-Standing Lipid Bilayers. *Adv. Mater.* **19,** 4466–4470 (2007).

110. Simon, A., Girard-Egrot, A. & Sauter, F. Formation and stability of a suspended biomimetic lipid bilayer on silicon submicrometer-sized pores. *J. Colloid Interface Sci.* **308,** 337–343 (2007).

111. Kumar, K. *et al.* Formation of nanopore-spanning lipid bilayers through liposome fusion. *Langmuir* **27,** 10920–10928 (2011).

112. Kresák, S., Hianik, T. & Naumann, R. L. C. Giga-seal solvent-free bilayer lipid membranes: from single nanopores to nanopore arrays. *Soft Matter* **5,** 4021 (2009).

113. Nussio, M. R. *et al.* Nanomechanical characterization of phospholipid bilayer islands on flat and porous substrates: a force spectroscopy study. *J. Phys. Chem. B* **113,** 10339–47 (2009).

114. Jönsson, P., Jonsson, M. P. & Höök, F. Sealing of submicrometer wells by a shear-driven lipid bilayer. *Nano Lett.* **10,** 1900–6 (2010).

115. Muisiner, R. J. & Koberstein, J. T. A Room Temperature Method for the Formation of Ultrathin SiOx Films. *Polym. Mater. Sci. Eng* **77,** 653 (1997).

116. Hillborg, H. & Gedde, U. W. Hydrophobicity changes in silicone rubbers. *IEEE Trans. Dielectr. Electr. Insul.* **6,** 703–717 (1999).

117. Hillborg, H., Tomczak, N., Olàh, A., Schönherr, H. & Vancso, G. J. Nanoscale hydrophobic recovery: A chemical force microscopy study of UV/ozone-treated cross-linked poly(dimethylsiloxane). *Langmuir* **20,** 785–794 (2004).

118. Eddington, D. T., Puccinelli, J. P. & Beebe, D. J. Thermal aging and reduced hydrophobic recovery of polydimethylsiloxane. *Sensors Actuators, B Chem.* **114,** 170–172 (2006).

119. Lawton, R. a., Price, C. R., Runge, A. F., Doherty, W. J. & Saavedra, S. S. Air plasma treatment of submicron thick PDMS polymer films: Effect of oxidation time and storage conditions. *Colloids Surfaces A Physicochem. Eng. Asp.* **253,** 213–215 (2005).

120. Przybylo, M. *et al.* Lipid diffusion in giant unilamellar vesicles is more than 2 times faster than in supported phospholipid bilayers under identical conditions. *Langmuir* **22,** 9096–9 (2006).

121. Scomparin, C., Lecuyer, S., Ferreira, M., Charitat, T. & Tinland, B. Diffusion in supported lipid bilayers: Influence of substrate and preparation technique on the internal dynamics. *Eur. Phys. J. E* **28,** 211–220 (2009).

122. Benda, A., Beneš, M. & Marecek, V. How to determine diffusion coefficients in planar phospholipid systems by confocal fluorescence correlation spectroscopy. *Langmuir* **9,** 4120–4126 (2003).

123. Jose, B., Mallon, C. T., Forster, R. J., Blackledge, C. & Keyes, T. E. Lipid bilayer assembly at a gold nanocavity array. *Chem. Commun. (Camb).* **47,** 12530–2 (2011).

124. Basit, H., Maher, S., Gaul, V., Forster, R. J. & Keyes, T. E. Aqueous-filled polymer microcavity arrays: versatile and stable lipid bilayer platforms offering high lateral mobility to incorporated membrane proteins. *Analyst* **140,** 3012–3018 (2015).

125. Stark, G., Ketterer, B., Benz, R. & Läuger, P. The rate constants of valinomycin-mediated ion transport through thin lipid membranes. *Biophys. J.* **11,** 981–994 (1971).

126. Beerlink, A. *et al.* X-ray structure analysis of free-standing lipid membranes facilitated by micromachined apertures. *Langmuir* **24,** 4952–8 (2008).

127. Lindholm-Sethson, B. *et al.* Are biosensor arrays in one membrane possible? A combination of multifrequency impedance measurements and chemometrics. *Analytical and bioanalytical chemistry* **377,** 478–85 (2003).

128. Nelson, a. Conducting gramicidin channel activity in phospholipid monolayers. *Biophys. J.* **80,** 2694–703 (2001).

129. Nelson, A. Electrochemistry of mercury supported phospholipid monolayers and bilayers. *Curr. Opin. Colloid Interface Sci.* **15,** 455–466 (2010).

130. Atanasov, V. *et al.* Membrane on a chip: a functional tethered lipid bilayer membrane on silicon oxide surfaces. *Biophys. J.* **89,** 1780–1788 (2005).

131. Mallon, C. T., Jose, B., Forster, R. J. & Keyes, T. E. Protein nanopatterning and release from gold nano-cavity arrays. *Chem. Commun. (Camb).* **46,** 106–8 (2010).

132. Zhang, X. & Wang, S. Voltametric Behavior of Noradrenaline at 2-Mercaptoethanol Self-Assembled Monolayer Modified Gold Electrode and its Analytical Application. *Sensors* **3,** 61–68 (2003).

133. Weisshaar, D. E., Walczak, M. M. & Porter, M. D. Electrochemically induced transformations of monolayers formed by self-assembly of mercaptoethanol at gold. *Langmuir* **9,** 323–329 (1993).

134. Jose, B. *et al.* Emission enhancement within gold spherical nanocavity arrays. *Phys. Chem. Chem. Phys.* **11,** 10923–10933 (2009).

135. Munro, J. & Frank, C. In Situ Formation and Characterization of Poly (ethylene glycol)-Supported Lipid Bilayers on Gold *Langmuir* 10567–10575 (2004). doi:10.1021/1a048378o

136. Song, H. *et al.* Electrochemical impedance spectroscopy of porous electrodes: the e□ect of pore size distribution. *Electrochim. Acta* **44,** 3513–3519 (1999).

137. Cheng, Y. *et al.* Single ion channel sensitivity in suspended bilayers on micromachined supports. *Langmuir* **17,** 1240–1242 (2001).

138. McConnell, N. Masters Thesis. (Dublin City University, 2015).

139. Rose, L. & Jenkins, a T. a. The effect of the ionophore valinomycin on biomimetic solid supported lipid DPPTE/EPC membranes. *Bioelectrochemistry* **70,** 387–93 (2007).

140. Becucci, L., Moncelli, M. R., Naumann, R. & Guidelli, R. Potassium ion transport by valinomycin across a Hg-supported lipid bilayer. *J. Am. Chem. Soc.* **127,** 13316–13323 (2005).

141. Steinem, C., Janshoff, A., von dem Bruch, K., Goossens, J. & Galla, H.-J. Valinomycin-mediated transport of alkali cations through solid supported membranes. *Bioelectrochemistry Bioenerg.* **45,** 17–26 (1998).

142. Yapici, N. B. *et al.* Highly Stable and Sensitive Fluorescent Probes (LysoProbes) for Lysosomal Labeling and Tracking. *Sci. Rep.* **5,** 8576 (2015).

143. Plank Jr, R. H. & Rosen, B. P. Cation/Proton Antiport Systems in Escherichia coli. *J. Biol. Chem.* **255,** 3824–3825 (1980).

144. Evtodienko, V. Y., Antonenko, Y. N. & Yaguzhinsky, L. S. Increase of local hydrogen ion gradient near bilayer lipid membrane under the conditions of catalysis of proton transfer across the interface. *FEBS Lett.* **425,** 222–224 (1998).

145. Frese, D., Steltenkamp, S., Schmitz, S. & Steinem, C. In situ generation of electrochemical gradients across pore-spanning membranes. *RSC Adv.* **3,** 15752 (2013).

146. Hu, P. & Luo, B.-H. Integrin αIIbβ3 transmembrane domain separation mediates bi-directional signaling across the plasma membrane. *PLoS One* **10,** e0116208 (2015).

147. Mallon, C. T., Chaumont, C. De, Moran, N., Keyes, T. E. & Forster, R. J. Electrochemical Desorption of Fibrinogen from Gold. *Langmuir* **26,** 293–298 (2010).

148. Sabapathy, R., Bhattacharyya, S., Cleland Jr, W. & Hussey, C. Host-guest complexation in self-assembled monolayers: Inclusion of a monolayer-anchored cationic ferrocene-based guest by cyclodextrin hosts. *Langmuir* **7463,** 3797–3807 (1998).

149. Harada, A. & Takahashi, S. Preparation and properties of cyclodextrin?ferrocene inclusion complexes. *J. Chem. Soc. Chem. Commun.* 645 (1984). doi:10.1039/c39840000645

150. Auletta, T., van Veggel, F. C. J. M. & Reinhoudt, D. N. Self-Assembled Monolayers on Gold of Ferrocene-Terminated Thiols and Hydroxyalkanethiols. *Langmuir* **18,** 1288–1293 (2002).

151. Prabaharan, M. & Mano, J. F. Chitosan derivatives bearing cyclodextrin cavitiesas novel adsorbent matrices. *Carbohydr. Polym.* **63,** 153–166 (2006).

152. Uosaki, K., Sato, Y. & Kita, H. Electrochemical Characteristics of a Gold Electrode Modified with a Self -Assembled Monolayer of Ferrocenylalkanethiols. 1510–1514 (1991).

153. Hapiot, F., Tilloy, S. & Monflier, E. Cyclodextrins as supramolecular hosts for organometallic complexes. *Chem. Rev.* **106,** 767–781 (2006).

154. Mertins, O. *et al.* Further insights into hydrophobic interactions between ferrocenyl-tamoxifen drugs and non-polar molecular architectures at electrode surfaces. *J. Electroanal. Chem.* **635,** 13–19 (2009).

155. Sano, T. & Cantor, C. R. Intersubunit contacts made by tryptophan 120 with biotin are essential for both strong biotin binding and biotin-induced tighter subunit association of streptavidin. *Proc. Natl. Acad. Sci. U. S. A.* **92,** 3180–3184 (1995).

156. Breslow, R. & Zhang, B. Cholesterol recognition and binding by cyclodextrin dimers. *J. Am. Chem. Soc.* **118,** 8495–8496 (1996).

157. Kilsdonk, E. P. C. *et al.* Cellular cholesterol efflux mediated by cyclodextrins. *Journal of Biological Chemistry* **270,** 17250–17256 (1995).

158. Levitan, I., Christian, a E., Tulenko, T. N. & Rothblat, G. H. Membrane cholesterol content modulates activation of volume-regulated anion current in bovine endothelial cells. *J. Gen. Physiol.* **115,** 405–416 (2000).

159. Giocondi, M.-C., Milhiet, P. E., Dosset, P. & Grimellec, C. Le. Use of Cyclodextrin for AFM Monitoring of Model Raft Formation. *Biophys. J.* **86,** 861–869 (2004).

160. Irie, T., Fukunaga, K. & Pitha, J. Hydroxypropylcyclodextrins in parenteral use. I: Lipid dissolution and effects on lipid transfers in vitro. *J. Pharm. Sci.* **81,** 521–3 (1992).

161. Ohvo, H. & Slotte, J. P. Cyclodextrin-mediated removal of sterols from monolayers: Effects of sterol structure and phospholipids on desorption rate. *Biochemistry* **35,** 8018–8024 (1996).

162. Nezil, F. A. & Bloom, M. Combined influence of cholesterol and synthetic amphiphillic peptides upon bilayer thickness in model membranes. *Biophys. J.* **61,** 1176–1183 (1992).

163. Davis, R. W. *et al.* Nanoporous microbead supported bilayers: stability, physical characterization, and incorporation of functional transmembrane proteins. *Langmuir* **23,** 3864–3872 (2007).

164. Parthasarathy, R., Yu, C. & Groves, J. T. Curvature-modulated phase separation in lipid bilayer membranes. *Langmuir* **22,** 5095–9 (2006).

165. Sanii, B., Smith, A. M., Butti, R., Brozell, A. M. & Parikh, A. N. Bending membranes on demand: Fluid phospholipid bilayers on topographically deformable substrates. *Nano Lett.* **8,** 866–871 (2008).

166. Werner, J. H. *et al.* Formation and Dynamics of Supported Phospholipid Membranes on a Periodic Nanotextured Substrate. *Langmuir* **25,** 2986–2993 (2009).

167. Weiskopf, D., Schmitt, E. K., Klühr, M. H., Dertinger, S. K. & Steinem, C. Micro-BLMs on highly ordered porous silicon substrates: rupture process and lateral mobility. *Langmuir* **23,** 9134–9139 (2007).

168. Pogodin, S. *et al.* Biophysical model of bacterial cell interactions with nanopatterned cicada wing surfaces. *Biophys. J.* **104,** 835–840 (2013).

169. Zeineldin, R. *et al.* Using bicellar mixtures to form supported and suspended lipid bilayers on silicon chips. *Langmuir* **22,** 8163–8 (2006).

170. Claesson, M., Frost, R., Svedhem, S. & Andersson, M. Pore spanning lipid bilayers on mesoporous silica having varying pore size. *Langmuir* **27,** 8974–8982 (2011).

171. Suzuki, K. & Masuhara, H. Groove-spanning behavior of lipid membranes on microfabricated silicon substrates. *Langmuir* **21,** 6487–94 (2005).

172. Peng, P.-Y., Chiang, P.-C. & Chao, L. Controllable occurrence of free-standing lipid membranes on nanograting structured supports. *ACS Appl. Mater. Interfaces* **6,** 12261–9 (2014).

173. Isono, T., Ikeda, T. & Ogino, T. Evolution of Supported Planar Lipid Bilayers on Step-Controlled Sapphire Surfaces. *Langmuir* **26,** 9607–9611 (2010).

174. Campbell, D. J. *et al.* Replication and Compression of Surface Structures with Polydimethylsiloxane Elastomer. *J. Chem. Educ.* **76,** 537 (1999).

Analyst

PAPER

Cite this: *Analyst*, 2015, **140**, 3012

Aqueous-filled polymer microcavity arrays: versatile & stable lipid bilayer platforms offering high lateral mobility to incorporated membrane proteins†

Hajra Basit,‡ Vinnie Gaul, Sean Maher, Robert J. Forster and Tia E. Keyes*

Received 16th December 2014,
Accepted 12th March 2015

DOI: 10.1039/c4an02317j

www.rsc.org/analyst

A key prerequisite in an ideal supported lipid bilayer based cell membrane model is that the mobility of both the lipid matrix and its components are unhindered by the underlying support. This is not trivial and with the exception of liposomes, many of even the most advanced approaches, although accomplishing lipid mobility, fail to achieve complete mobility of incorporated membrane proteins. This is addressed in a novel platform comprising lipid bilayers assembled over buffer-filled, arrays of spherical cap microcavities formed from microsphere template polydimethoxysilane. Prior to bilayer assembly the PDMS is rendered hydrophilic by plasma treatment and the lipid bilayer prepared using Langmuir Blodgett assembly followed by liposome/proteoliposome fusion. Fluorescence Lifetime Correlation Spectroscopy confirmed the pore suspended lipid bilayer exhibits diffusion coefficients comparable to free-standing vesicles in solution. The bilayer modified arrays are highly reproducible and stable over days. As the bilayers are suspended over deep aqueous reservoirs, reconstituted membrane proteins experience an aqueous interface at both membrane interfaces and attain full lateral mobility. Their utility as membrane protein platforms was exemplified in two case studies with proteins of different dimensions in their extracellular and cytoplasmic domains reconstituted into DOPC lipid bilayers; Glycophorin A, and Integrin $\alpha_{IIb}\beta_3$. In both cases, the proteins exhibited 100% mobility with high lateral diffusion coefficients.

Introduction

Membrane proteins (MPs) constitute nearly one third of all human proteins and are known to orchestrate key cellular functions ranging from ion transport,[1,2] cell–cell attachment,[2] to signaling.[3] Consequently, such proteins are important targets in understanding disease progression and in pharmaceutical drug discovery. However, despite their importance, the direct *in vitro* study of membrane proteins lacks suitable high throughput screening membrane models, which can be reproducibly fabricated with controlled lipid composition, where the structural integrity and mobility of the protein is preserved upon reconstitution. A key feature of the cell membrane, vital to membrane protein function, is its inherent 2-D fluidity.[4,5] Lateral diffusion of lipids and membrane proteins within the membrane regulate the distribution of membrane components and affect many processes, such as formation of protein complexes, which are involved in signaling and the dynamic assembly/disassembly of lipid ordered and disordered domain.[6]

Artificial models of biological membranes can provide enlightening insights into the behavior of membrane lipids and associated proteins by mimicking key facets of the cell membrane structure decoupled from the challenging complexity of the living cell. However, for an artificial bilayer model for support of membrane proteins to be credible, it must exhibit the property of high lateral mobility of both lipid and protein constituents. To this end, while Supported Lipid Bilayers (SLBs) are valuable artificial bilayer models, their inherent drawback is the interaction of the bilayer with the solid substrate, which dramatically lowers the mobility of the lipids and particularly incorporated membrane proteins compared with native cell membranes or free liposomes.[7–9] Key approaches to addressing this issue include Tethered Bilayer Lipid Membranes (t-BLMs) and Cushioned Bilayer Lipid Membranes. Although t-BLMs and cushioned bilayers were shown to provide better stability to the lipid bilayers,[10] diffusion coefficients of the lipids measured were not significantly improved compared to

School of Chemical Sciences, National Centre for Sensor Research, Dublin City University, Dublin 9, Ireland. E-mail: tia.keyes@dcu.ie; Tel: +3531 7008185

†Electronic supplementary information (ESI) available: Fabrication of microcavity arrays and spanning lipid bilayers, labelling of membrane proteins and their incorporation, confocal and FLIM imaging and FLCS data. See DOI: 10.1039/c4an02317j

‡Current address: Chemistry Research Laboratory, University of Oxford.

those measured for SLBs on planar substrates.[8,11,12] In order to obtain lipid bilayers that are sufficiently decoupled from the underlying substrates, another approach is to span lipid bilayers across nano sized apertures or pores, forming Black Lipid Membranes (BLM). BLMs however, suffer poor stability due to the retention of organic solvents that are commonly used in their preparation. Moreover, the incorporation and stability of membrane proteins is severely limited owing to their unfavorable mode of preparation and the remnant solvents within the bilayer.[13–15] Several groups have demonstrated elegant approaches to solvent free methods for pore-spanning lipid bilayers. However, most such techniques function in restricted conditions such as the limited (nano-dimensioned) size of the pores and the vesicles,[16,17] application of sheer flow and pH,[18] the use of Giant Unilamellar Vesicles (GUVs)[14,19] or spanning over dry substrates, where stability is a significant issue.[20–23] While each of these methods have shed light on the behaviour of a variety of pore-spanning lipid membranes, the incorporation and manipulation of membrane proteins within artificial systems remains a challenge.

Herein, we describe a robust new supported lipid membrane model in which both lipid bilayer and reconstituted membrane proteins are highly mobile and evidently decoupled from the underlying substrate. The platform comprises lipid bilayers spanned over aqueous buffer-filled, micrometer sized hemispherical cavities formed from polystyrene sphere templated polydimethylsiloxane (PDMS) rendered hydrophilic by plasma treatment. We employ a combination of Langmuir–Blodgett and vesicle fusion techniques to obtain defect-free bilayers spanning the cavities. We demonstrate that the lipid bilayers can be reliably spanned across a range of cavity sizes prepared with templating spheres with diameters from 620 nm to 5 micrometers and that the spanning lipid bilayers remain intact, with reproducible fluidity over several days. This approach is facile, highly reproducible and importantly the cavity spanning lipid bilayer is assembled into a flow cell that can be directly mounted onto a microscope. The PDMS substrate lends itself to interference-free fluorescence studies even for, as demonstrated here, single molecule studies. Importantly, we demonstrate protocols for reconstitution of membrane proteins into these pore spanning lipid bilayers and demonstrate with two proteins with cytoplasmic or extracellular domains of different dimensions, that they diffuse freely within the lipid across the pores, with 100% mobility and with diffusion coefficients comparable to those of the proteins reconstituted into liposomes.

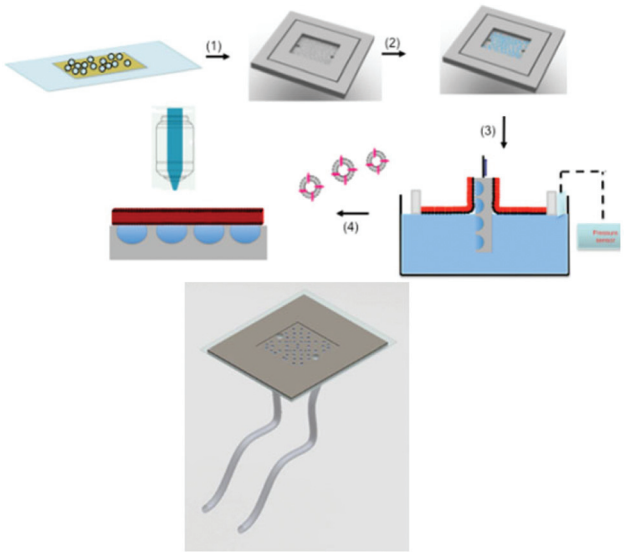

Fig. 1 Top, schematic illustration of the steps involved in the formation of free-spanning lipid bilayers over buffer-filled microcavities on PDMS. A dispersion of polystyrene spheres of selected diameter are drop casted onto a sheet of mica glued to glass and upon formation of a dry film spheres, PDMS is poured onto the glass and cured at 150 °C. In step (1) the cured PDMS is peeled off and the spheres removed by treatment with THF. In step (2), the cavities were sonicated in buffer to facilitate their filling with buffer, followed by deposition of a lipid monolayer using Langmuir Blodgett technique (3). The bilayer is finally obtained by fusion of vesicles onto the deposited monolayer (4). Bottom graphical representation of the filled cavity arrays on PDMS after their assembly in to a flow chamber.

Results and discussion

Fabrication of the microcavity arrays and spanning lipid bilayers

Fig. 1, illustrates the key steps involved in preparing the polymer cavity array and preparing the bilayer. The PDMS cavity arrays were obtained by a modification of method previously described by us.[24] Briefly, PDMS was cast onto a dried film of polystyrene spheres, of the selected diameter, formed on freshly cleaved mica, and cured. The PDMS was peeled off the mica and the spheres were removed to obtain open spherical cap cavities embedded in PDMS as described in detail in the ESI.† As described previously, this approach can be used to form extended and highly ordered 2 D arrays of microcavities, but as the focus of experiments here were at scale of tens of cavities, such arrays were not necessary and templating was restricted to small areas of the PDMS.[24]

As PDMS is hydrophobic, a critical step necessary to facilitate fluid filling and lipid membrane assembly is plasma treatment, which serves to render the substrate hydrophilic. This was reflected in the water droplet contact angle of 16° measured for planar PDMS after plasma treatment. Following plasma treatment the cavities were then filled by sonication in buffer for 30 minutes, following which, a Langmuir layer of the phospholipid (containing the appropriate dye labeled DOPE) was spread over the filled cavity array, as described in the ESI.† The flow chamber as illustrated in Fig. 1 is then constructed by adhering the edges of the hole-punched PDMS to a microscope cover slip using adhesive (ESI† for details). Phospholipid vesicles of the appropriate composition containing the dye with or without a reconstituted protein were then injected into the flow chamber to obtain the free-spanning lipid bilayers.

Lipid bilayer spanned buffer-filled cavities

Lipid bilayer spanning across aqueous filled pores in PDMS prepared from templating spheres with diameters of 602 nm, 1 μm, 2.94 μm and 5 μm were initially assessed using fluorescent confocal microscopy. Fig. 2 presents the confocal images of the fluorescently doped DOPC bilayer spread on filled cavities labelled with 1 mol% of 1,2-dioleoyl-*sn*-glycero-3-phosphoethanolamine carboxyfluorescein. There is a significant refractive index difference between PDMS ($n \approx 1.45$) and the buffer ($n \approx 1.33$) and due to the spherical porous nature of the support, the incident laser light scatters strongly at the positions of the filled cavities with the effect of making the buffer filled cavities look significantly brighter in the reflectance image than either the unfilled cavities or the planar regions of the PDMS platform, as shown in Fig. 2(a, c, e and g).

This is a very useful characteristic that is exploited for accurately and precisely locating the pores with suspended bilayers.

It is evident from the reflectance images across all cavity diameters that not all cavities fill with buffer on sonication; typically 5 to 10% of cavities are unfilled. However, interestingly, the lipid bilayer was observed to span cavities whether they were buffer filled or not if the cavity diameter was 1 μm or less. This is manifest in the confocal images shown in Fig. 2b and 2d respectively, where the reflectance image demonstrates that a number of the cavities are unfilled but a homogenous fluorescence from top of the cavity indicates that the bilayer is spanning these apertures. In contrast, for the cavities exceeding 1 μm diameter *i.e.* those made from 2.94 μm and 5 μm spheres (Fig. 2f and 2h respectively), the bilayer was observed to span exclusively across buffer filled pores. When cavities of these dimensions were not pre-filled with aqueous solution, the lipid was observed to coat the interior surface of the array. Where this occurred, it was clear in microscopy, as each unfilled, lipid coated pore showed up as intense fluorescent spots. The aqueous support in the filled pores across which the Langmuir–Blodgett monolayer assembles, is required for formation of a spanning bilayer on the larger diameter cavities. Moreover, whereas the Langmuir–Blodgett technique is capable of forming homogenous monolayers over small defects (cavities), for the larger diameter un-filled cavities the LB films formed are discontinuous, thus, when the injected vesicles are introduced they form a bilayer in the interior walls of the cavity.

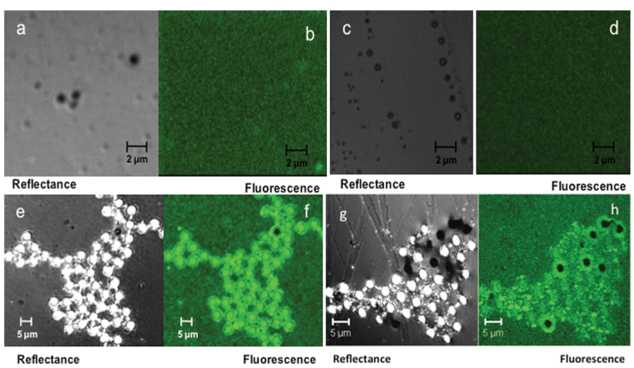

Fig. 2 Confocal imaging upon pre-filling followed by bilayer formation using LB and vesicle fusion of cavities of sizes 620 nm (a & b), 1 μm (c & d), 2.94 μm (e & f) and 5 μm (g & h). Bilayers contained 1 mol% DOPE-carboxyfluorescein as the fluorophore. The excitation wavelength was 488 nm. The fluorescence images (b, d, f and h) were collected using a 505 nm longpass filter, above 505 nm and reflectance images (a, c, e and g) were collected using a 420 nm longpass below 505 nm. Both fluorescence and reflectance images were collected simultaneously using two different channel.

In order to assess the stability of the aqueous supported lipid bilayers across the cavities, confocal fluorescence lifetime imaging was performed periodically on the supported bilayers across all the cavity sizes over a period of a week. The images showed that the lipid bilayers formed over filled cavities using the LB/vesicle fusion method were stable for a period of between 4–5 days (data not shown). This extended stability, is a significant improvement on black lipid membranes or GUVs. Furthermore, the contacting solution at the external interface of the bilayer can be repeatedly washed without causing changes to its stability.

Fluidity of cavity supported lipid bilayers

To assess the fluidity of cavity supported lipid bilayers we studied the lipid lateral diffusion coefficients of a DOPC bilayer at the arrays. The diffusion coefficient of lipid assembled over the cavity and at planar regions on the PDMS substrate were compared using Fluorescence Lifetime Correlation Spectroscopy (FLCS). The bilayers were labelled with a DOPE-Atto-655 dye at a concentration of 1 nM, which constitutes approximately a ratio of 1 : 100 000 dye : lipid.[25] To accurately identify and distinguish the bilayer at the top planar regions of the array and bilayer suspended over the cavities for the FLCS experiment, both reflectance and fluorescence images were recorded, as described in ESI.† As described above and shown in Fig. 3(a) and (b), for a 2.94 μm diameter cavity array, the reflectance images are effective guides to locating filled-cavity spanning bilayers, and once found, *z*-scanning was used to locate the bilayer from optimal emission intensity. Autocorrelation functions (ACFs) were then recorded for bilayer at each (planar and cavity) surface region. The ACFs obtained were fit to the 2-dimensional model described in eqn (1) to obtain the lateral diffusion co-efficient of DOPE-Atto655 in the bilayer.

$$G(\tau) = \frac{1}{N}\left[1 + \left(\frac{\tau}{\tau_i}\right)^{\alpha}\right]^{-1} \quad (1)$$

where, $G(\tau)$ is the autocorrelation function, N is the average number of fluorescent molecules present in the confocal volume, τ_i is the characteristic residence time, and α is the anomalous parameter which reflects the extent of deviation of the diffusion from normal or Brownian motion where $\alpha = 1$,[26] i is the index of the components. The lateral diffusion coefficient, D_L, can be obtained as $D_L = \omega^2/4\tau_i$, where, ω is the waist of the laser beam. To determine ω for each excitation

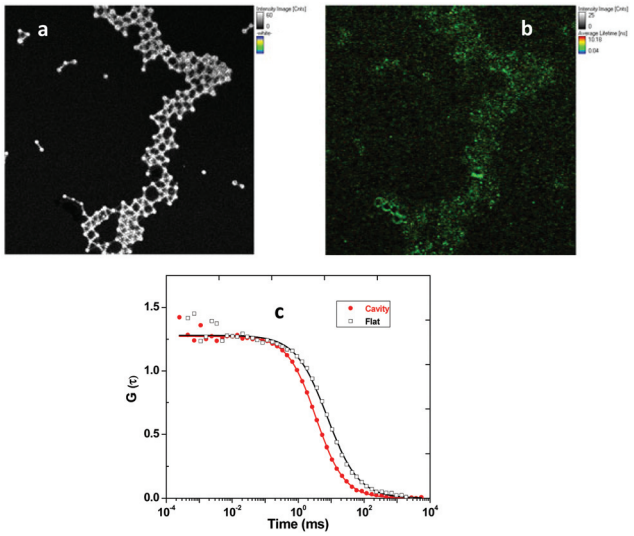

Fig. 3 (a) Reflectance and (b) FLIM images obtained for lipid spanning cavities made using 2.94 μm diameter spheres. The reflectance image allows for the identification of cavity points where FLCS should be performed. ATTO 655–DOPE at 1 nM concentration was used as the fluorophore and the image size is 80 μm × 80 μm. (c) Normalized autocorrelation function (ACF) curves measured above a single bilayer spanning cavity (red circular symbols) and on the flat regions of the supported bilayer (black rectangular symbols), measurements were acquired with 640 nm laser. The solid lines show the fits of the ACFs to eqn (1).

wavelength, a reference solution of free dye was used for which the diffusion coefficient is known. For excitation at 640 nm, the reference dye was Atto-655 in water at 25 °C and its diffusion coefficient is 426 $\mu m^2\ s^{-1}$.[9,27]

From FLCS, the diffusion co-efficient obtained for DOPE-Atto655 in the lipid bilayer supported over the planar region of the hydrophilic PDMS was found to be 4.1 ± 0.6 $\mu m^2\ s^{-1}$ with α value of approximately 1 (*i.e.* = 0.997 ± 0.002). This value, was reproducible for all the PDMS substrates independent of cavity sizes and is consistent with supported lipid bilayer diffusion previously reported on planar hydrophilic substrates.[9,28]

In contrast, the lipid diffusion coefficient for the bilayer spanning across buffer filled cavities prepared from 2.94 μm diameter spheres was determined to be 10.2 ± 0.6 $\mu m^2\ s^{-1}$ with an α value of 0.989 ± 0.004. Whereas, the diffusion coefficients of the bilayer spanning cavities made from 5 μm diameter spheres were determined to be D = 11.2 ± 0.4 $\mu m^2\ s^{-1}$ with α of 0.992 ± 0.002. *i.e.* within experimental error, the diffusion coefficients were approximately the same. The standard deviation on these values reflects replicates across 5 pores and 3 substrates of the same pore diameter. Interestingly though, the diffusion co-efficient values obtained from lipid bilayers spanning cavities made from 1 μm spheres was observed to be lower than those with larger pore diameters prepared from 2.94 μm and 5 μm diameter spheres at D = 7.1 ± 0.3 $\mu m^2\ s^{-1}$ and α at 1.012 ± 0.004.

This difference in diffusion coefficient may originate from differences in curvature of the lipid bilayer due to changes to the water meniscus, which will vary with cavity dimensions.[29] However, the key point to note here is the distinctly higher diffusion co-efficient values of the cavity spanning bilayers compared with lipid diffusion over planar PDMS regions (over 2 fold).

While such diffusion values are consistent with those reported for lipids in GUVs in solution,[30] to the best of our knowledge this is the first report of such high fluidity in a supported bilayer system. The close resemblance of the diffusion value of the cavity spanning bilayer to that observed for GUVs indicates that the lipids spread over the cavity behave similarly to free-standing vesicles owing to the aqueous reservoir within the spherical cap pore below the inner leaflet of the spanning bilayer. As pore depth is estimated to approximately 65% the diameter of the pore, *e.g.* >1.9 μm for the 2.94 μm pore, the aqueous well is sufficiently deep, even for the smallest pores sizes, that there is little chance of protein or lipid over the pore interacting with the underlying substrate.

Diffusion studies of membrane proteins incorporate in the spanning bilayers

Motivated by the evident fluidity of the bilayers suspended over cavities, we next investigated the prospect of reconstituting membrane proteins into the cavity spanning lipid bilayers. For these studies, we employed the Human Glycophorin A (GpA) protein and platelet integrin $\alpha_{IIb}\beta_3$ as model proteins. These proteins were selected because of the diversity of their structure and particularly because of the large size of their extra-membrane components. GpA is one of the best-characterized membrane proteins, it is known to span the plasma membrane, with its C-terminal end at the cytoplasmic side of the membrane, a hydrophobic region penetrating through the membrane, and its N-terminal side, which is glycosylated, exposed to the exterior of the membrane.[31] GpA forms a symmetrical homodimer and has been shown to dimerize both in detergent micelles and in membranes owing to specific interactions between the TM helices.[32–35] The radius of the transmembrane dimer is reported to be 2.6 ± 0.4 nm.[36] In the present experiments, Glycophorin A was labelled with 5-carboxytetramethylrhodamine (TAMRA) as described in the ESI.† The labeled GpA was reconstituted into DOPC vesicles labelled with DOPE-Atto 655 using the protocol described in the ESI.†[37]

The bilayer was formed by fusion of the labelled-GpA containing vesicles with DOPC monolayers formed over 2.94 μm template cavity substrates using LB deposition. As shown in Fig. 4, the fluorescence lifetime image of the resulting cavity supported lipid bilayer shows homogenous fluorescence from the TAMRA labeled GpA. Imaging at Atto655 excitation wavelength *i.e.* 640 nm, confirmed that the lipid bilayer was also uniformly formed across the substrate (data not shown). These results indicate that GpA was well incorporated within the bilayer. Interestingly, and consistent with its incorporation into the bilayer, the GpA was found to be essentially immobile over the planar regions of the PDMS substrate. This is reflected by the photobleaching in the fluorescence intensity–time curve

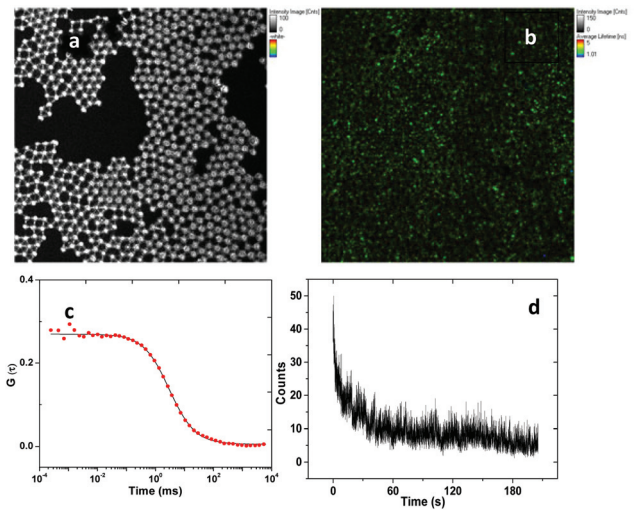

Fig. 4 Reflectance (a) and (b) fluorescence lifetime image of the Glycophorin A containing DOPC bilayer spanning a cavity made from 2.94 μm sized spheres. (c) Autocorrelation curves measured a single cavity (red circular symbols) from the arrays shown above, (d) intensity–time curve for the measurement performed on the planar region of the array. Measurements were recorded over 300 s. In all experiments the only fluorophore is Glycophorin A which is labelled with the fluorophore TAMRA, the excitation wavelength is 532 nm.

shown in Fig. 4(d) obtained from point measurements of TAMRA-GpA in the bilayer over planar PDMS. Photobleaching of the GpA TAMRA label is attributed to lack of protein lateral mobility owing to the interaction of the cytoplasmic or extracellular domains of the protein with the underlying planar PDMS. Conversely, GpA was found to be 100% mobile over the cavities and its diffusion coefficient over the cavity aperture was determined to be 7.1 ± 0.6 $\mu m^2\ s^{-1}$ with α of 0.992 ± 0.005, obtained by fitting the FCS autocorrelation curve in Fig. 4(c) using eqn (1). The lateral mobility is also seen in the intensity–time curve showing stable intensity fluctuations over the time of measurement (Fig. S3†). As expected the diffusion coefficient for the protein is considerably lower than the diffusion values for the lipid but is sufficiently high to indicate that GpA experiences little or no frictional interaction with the underlying surface.

In a previous report, the diffusion coefficient of GpA in free standing DMPC liposomes above its phase transition temperature was reported to be D_{GpA} = 4 ± 2 $\mu m^2\ s^{-1}$ using Fluorescence Recovery after Photobleaching (FRAP), whereas DMPC mobility was observed to be 5 ± 1.5 $\mu m^2\ s^{-1}$.[38] The ratio of Lipid to GpA diffusion coefficients are of the same order as that observed in our system. Such close lipid and membrane protein diffusions have so far only been observed in support free lipid bilayers such as vesicles and droplet hydrogel bilayers.[39]

The second model protein we examined was the platelet integrin protein $\alpha_{IIb}\beta_3$, which is a cell adhesion molecule consisting of a heterodimer of an alpha and beta subunit that spans the cytoplasmic membrane once. It has a large extracellular domain, (approx. 110 Å) and relatively smaller cytoplasmic tail (approx. 20 Å), though these dimensions depend on the activation status of the integrin.[40,41] The Stokes radius of intact $\alpha_{IIb}\beta_3$ Integrin in dodecyl maltoside micelles in the presence of Ca^{2+}/Mg^{2+} was determined to be 6.95 ± 0.04 nm.[42] Previous studies of $\alpha_{IIb}\beta_3$ in artificial lipid systems have focused on glass supported bilayers or polymer cushioned bilayers with mobility and diffusion assessed from fluorescence recovery after photobleaching, FRAP.[43,44] Erb *et al.* reported a diffusion co-efficient of 0.70 ± 0.06 $\mu m^2\ s^{-1}$ for $\alpha_{IIb}\beta_3$ in a bilayer on glass.[43] Whereas Goennenwein *et al.* reported no fluorescence recovery on glass, but a diffusion coefficient of 0.60 ± 0.2 $\mu m^2\ s^{-1}$ upon using a cellulose cushion.[44] In all reports, a large percentage of protein was deemed immobile. The reflectance, FLIM and FLCS studies of this protein incorporated into DOPC suspended across the 2.94 μm diameter arrays are shown in Fig. 5.

Consistent with previous reports, extensive bleaching of the Integrin Atto-655 label was observed from the bilayer at the planar regions of the PDMS cavity array, where we found majority of the integrin to be immobile. However, $\alpha_{IIb}\beta_3$ reconstituted into cavity spanning bilayers over cavities prepared from 2.94 μm diameter spheres Fig. 5(c), exhibited high mobility, with no evidence of photobleaching (Fig. S4†), and a diffusion co-efficient of 3.2 ± 0.33 $\mu m^2\ s^{-1}$ obtained from FLCS. Notably, the diffusion value correlates well with that reported for the same integrin in liposomes.[45] Crucially, no immobile fraction was identified indicating unencumbered

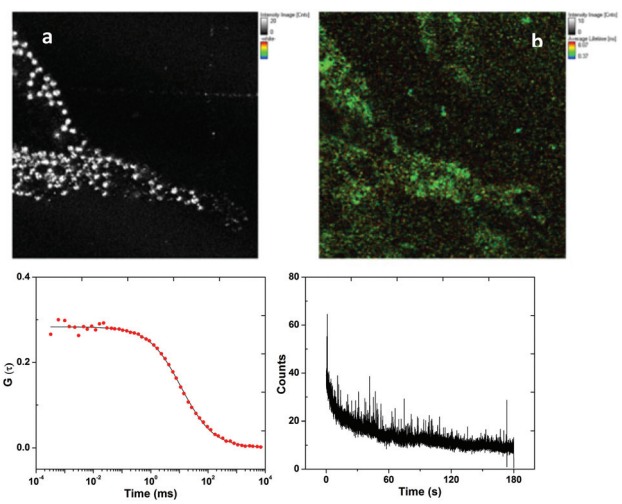

Fig. 5 (a) Reflectance image of the PDMS substrate that allows for the location of buffer filled cavities. (b) Fluorescence lifetime image of Integrin $\alpha_{IIb}\beta_3$ labelled with ATTO 655 in a DOPC lipid bilayer above the cavities shown in a. Both images are 80 × 80 μm. FLCS point measurements were performed on the labeled protein on both planar PDMS and above cavities based on the reflectance image a. (c) Autocorrelation curve for integrin $\alpha_{IIb}\beta_3$ measured above a 2.94 μm spanning cavity (red circular symbols). (d) Intensity–time curve for the measurement performed over flat regions on the supported lipid bilayer. In both measurements, the fluorophore observed is integrin $\alpha_{IIb}\beta_3$ tagged with ATTO 655. Measurements were recorded over 180 s.

lateral mobility of $\alpha_{IIb}\beta_3$ when incorporated into lipid over microcavity in this supported lipid bilayer system. Importantly, the diffusion coefficients measured for the two proteins are in good agreement with the theory suggested by Gambin *et al.*, where they propose the lateral mobility of the membrane protein to be inversely proportional to its radius ($D \propto 1/R$) according to the following equation.[46]

$$D = \frac{k_B T \lambda}{4\pi\mu h R} \quad (2)$$

where, k_B is Boltzmann constant, T is absolute temperature, h is the thickness of the bilayer, μ is the viscosity of the membrane and λ is the characteristic length, a parameter included to satisfy dimensionality.

Since, the lipid composition was identical for both proteins studied, the viscosity of the bilayers can be considered to be identical. Thus upon correlating the diffusion coefficients to their radii, we observe that D_{GpA}: $D_{\alpha_{IIb}\beta_3}$ is nearly equal to $R_{\alpha_{IIb}\beta_3}$: R_{GpA}, consistent with the theory suggested in eqn (2).

Conclusions

In summary, the results presented demonstrate that aqueous filled microcavity supported lipid bilayer arrays are potentially valuable tools for biophysical study of lipids and membrane proteins. The platforms have the versatility and stability of a supported lipid bilayer, with the fluidity of a liposome, due to the aqueous filled wells over which the bilayer is supported. A distinct feature of the described assembly is that there are no restrictions such as pH, solvent, and size of cavities or vesicles, sheer pressure *etc*. to obtain spanning lipid bilayers. The porous nature of the array offers the opportunity to vary solution at each side of the membrane. Lipid bilayer assembly onto hydrophilic PDMS substrates within a microfluidic chamber is not only extremely cost effective compared to other commonly used substrates such as Si_3N_4, SiO_2 or gold but also, because of the useful optical properties of PDMS, convenient to most microscopy platforms. In the present study we demonstrated a reliable methodology for incorporation of membrane proteins into the array, which should be broadly applicable across any membrane protein that can be reconstituted into liposomes. We demonstrated this method by incorporating two different membrane proteins into the array and confirmed high lateral mobility in both. This is a significant outcome as, currently apart from liposomes there are no effective artificial models for studying mobility of membrane proteins. Particularly important is the reconstitution of integrin into the layer as these proteins require high mobility in the cell membrane for their participation in signalling and protein recruitment. Artificial models into which such proteins can be reconstituted retaining high mobility offer exciting opportunities to better understand their behaviour.

Overall, the presented platforms offer significant promise as rational chip-based cell bilayer models and they should be amenable to broad application from fundamental biophysical studies, to pharmaceutical drug discovery.

Acknowledgements

This material is based upon work supported by the Science Foundation Ireland under grant no. [10/IN.1/B3025]. Lorcan Kent, DCU, is gratefully acknowledged for help with the drawings.

Notes and references

1 F. M. Ashcroft, *Nature*, 2006, **440**, 440–447.
2 S. J. Tucker, P. Tammaro and F. M. Ashcroft, *Ion channels and disease*, Academic Press, 1999.
3 R. Juliano, *Annu. Rev. Pharmacol. Toxicol.*, 2002, **42**, 283–323.
4 G. Espinosa, I. Lopez-Montero, F. Monroy and D. Langevin, *Proc. Natl. Acad. Sci. U. S. A.*, 2011, **108**, 6008–6013.
5 D. Marguet, P.-F. Lenne, H. Rigneault and H.-T. He, *EMBO J.*, 2006, **25**, 3446–3457.
6 J. E. Goose and M. S. P. Sansom, *PLoS Comput. Biol.*, 2013, 9.
7 M. Przybylo, J. Sýkora, J. Humpolíčková, A. Benda, A. Zan and M. Hof, *Langmuir*, 2006, **22**, 9096–9099.
8 L. Zhang and S. Granick, *J. Chem. Phys.*, 2005, **123**, 211104.
9 T. Tabarin, A. Martin, R. J. Forster and T. E. Keyes, *Soft Matter*, 2012, **8**, 8743–8751.
10 H. Basit, A. Van der Heyden, C. Gondran, B. Nysten, P. Dumy and P. Labbe, *Langmuir*, 2011, **27**, 14317–14328.
11 M. L. Wagner and L. K. Tamm, *Biophys. J.*, 2000, **79**, 1400–1414.
12 C. Rossi, E. Briand, P. Parot, M. Odorico and J. Chopineau, *J. Phys. Chem. B*, 2007, **111**, 7567–7576.
13 E. Reimhult and K. Kumar, *Trends Biotechnol.*, 2008, **26**, 82–89.
14 E. K. Schmitt, M. Nurnabi, R. J. Bushby and C. Steinem, *Soft Matter*, 2008, **4**, 250–253.
15 D. Weiskopf, E. K. Schmitt, M. H. Kluehr, S. K. Dertinger and C. Steinem, *Langmuir*, 2007, **23**, 9134–9139.
16 K. Kumar, L. Isa, A. Egner, R. Schmidt, M. Textor and E. Reimhult, *Langmuir*, 2011, **27**, 10920–10928.
17 H. Im, N. J. Wittenberg, A. Lesuffleur, N. C. Lindquist and S.-H. Oh, *Chem. Sci.*, 2010, **1**, 688–696.
18 P. Jonsson, M. P. Jonsson and F. Hook, *Nano Lett.*, 2010, **10**, 1900–1906.
19 S. Kresak, T. Hianik and R. L. C. Naumann, *Soft Matter*, 2009, **5**, 4021–4032.
20 A. Simon, A. Girard-Egrot, F. Sauter, C. Pudda, N. P. D'Hahan, L. Blum, F. Chatelain and A. Fuchs, *J. Colloid Interface Sci.*, 2007, **308**, 337–343.
21 M. R. Nussio, G. Oncins, I. Ridelis, E. Szili, J. G. Shapter, F. Sanz and N. H. Voelcker, *J. Phys. Chem. B*, 2009, **113**, 10339–10347.

22 V. C. Stimberg, J. G. Bomer, I. van Uitert, A. van den Berg and S. Le Gac, *Small*, 2013, **9**, 1076–1085.
23 C. Schmidt, M. Mayer and H. Vogel, *Angew. Chem., Int. Ed.*, 2000, **39**, 3137–3140.
24 C. T. Mallon, R. J. Forster and T. E. Keyes, *Chem. Commun.*, 2011, **47**, 7605.
25 H. Basit, S. G. Lopez and T. E. Keyes, *Methods*, 2014, **68**, 286–299.
26 C. Favard, J. Wenger, P.-F. Lenne and H. Rigneault, *Biophys. J.*, 2011, **100**, 1242–1251.
27 T. Dertinger, V. Pacheco, I. von der Hocht, R. Hartmann, I. Gregor and J. Enderlein, *ChemPhysChem*, 2007, **8**, 433–443.
28 A. Benda, M. Beneš, V. Marecek, A. Lhotský, W. T. Hermens and M. Hof, *Langmuir*, 2003, **19**, 4120–4126.
29 S.-C. J. Huang, A. B. Artyukhin, J. A. Martinez, D. J. Sirbuly, Y. Wang, J.-W. Ju, P. Stroeve and A. Noy, *Nano Lett.*, 2007, **7**, 3355–3359.
30 F. Heinemann, V. Betaneli, F. A. Thomas and P. Schwille, *Langmuir*, 2012, **28**, 13395–13404.
31 V. Anbazhagan and D. Schneider, *Biochim. Biophys. Acta, Biomembr.*, 2010, **1798**, 1899–1907.
32 H. Furthmayr and V. Marchesi, *Biochemistry*, 1976, **15**, 1137–1144.
33 M. A. Lemmon, J. M. Flanagan, H. R. Treutlein, J. Zhang and D. M. Engelman, *Biochemistry*, 1992, **31**, 12719–12725.
34 K. R. MacKenzie, J. H. Prestegard and D. M. Engelman, *Science*, 1997, **276**, 131–133.
35 L. E. Fisher, D. M. Engelman and J. N. Sturgis, *J. Mol. Biol.*, 1999, **293**, 639–651.
36 K. Mineev, E. Bocharov, P. Volynsky, M. Goncharuk, E. Tkach, Y. S. Ermolyuk, A. Schulga, V. C. I. Maslennikov, R. Efremov and A. Arseniev, *Acta Nat.*, 2011, **3**, 90.
37 E. J. J. Vanzoelen, A. J. Verkleij, R. F. A. Zwaal and L. L. M. Vandeenen, *Eur. J. Biochem.*, 1978, **86**, 539–546.
38 H. G. Kapitza, D. A. Ruppel, H. J. Galla and E. Sackmann, *Biophys. J.*, 1984, **45**, 577–587.
39 J. R. Thompson, A. J. Heron, Y. Santoso and M. I. Wallace, *Nano Lett.*, 2007, **7**, 3875–3878.
40 B. D. Adair and M. Yeager, *Proc. Natl. Acad. Sci. U. S. A.*, 2002, **99**, 14059–14064.
41 J. Bennett, B. Berger and P. Billings, *J. Thromb. Haemost.*, 2009, **7**, 200–205.
42 E. T. Eng, B. J. Smagghe, T. Walz and T. A. Springer, *J. Biol. Chem.*, 2011, **286**, 35218–35226.
43 E. M. Erb, K. Tangemann, B. Bohrmann, B. Muller and J. Engel, *Biochemistry*, 1997, **36**, 7395–7402.
44 S. Goennenwein, M. Tanaka, B. Hu, L. Moroder and E. Sackmann, *Biophys. J.*, 2003, **85**, 646–655.
45 V. Gaul, S. G. Lopez, B. R. Lentz, N. Moran, R. J. Forster and T. E. Keyes, *Integr. Biol.*, 2015, DOI: 10.1039/C5IB00003C.
46 Y. Gambin, R. Lopez-Esparza, M. Reffay, E. Sierecki, N. Gov, M. Genest, R. Hodges and W. Urbach, *Proc. Natl. Acad. Sci. U. S. A.*, 2006, **103**, 2098–2102.